Molecular Mechanisms and Transcriptional Regulation of Starvation Induced Autophagy in *Drosophila*

A thesis submitted in fulfilment of the requirements for the degree of Doctor of Philosophy in Life Sciences

DI MONACO, MARISA

School of Life Sciences, University of Warwick
Submitted October 2020

Table of Contents

List of Figures

List of Tables

ABBREVIATIONS

Ac	Actin
AMP	Adenosine 5'-Monophosphate
AMPK	AMP-activated Protein Kinase
AR	Autoradiography
Atg/*Atg*	Autophagy related protein (*Drosophila* and yeast)/gene (*Drosophila*)
ATG/*ATG*	Autophagy related protein (mammals)/gene (mammals and yeast)
ATP	Adenosine 5'-Triphosphate
BDSC	Bloomington Drosophila Stock Centre
bHLH-Zip	Basic Helix-Loop-Helix leucine Zipper
BLAST	Basic Local Alignment Search Tool
BP	Biological Process
BSA	Bovine Serum Albumin
Btd	Buttonhead
CARM1	Coactivator-associated Arginine Methyltransferase 1
CC	Cellular Component
CDS	Coding Sequence
ChIP	Chromatin Immunoprecipitation
CLEAR	Coordinated Lysosomal Expression and Regulation
CMA	Chaperone Mediated Autophagy
COBALT	Constraint-based Multiple Alignment Tool
CREBBP	Cyclic-AMP Response Element Binding protein, Binding Protein
Ct	Cycle threshold
DEPTOR	DEP containing mTOR interacting protein
DOR	Diabetes and Obesity Related gene
DRAM	Damage-Regulated-Modulator
EcR	Ecdysone Receptor
EIF4EBP1	Eukaryotic Initiation Factor 4E-Binding Protein 1
EPD	Eukaryote Promotor Database
EP300	E1A binding Protein of 300KDa
ER	Endoplasmic Reticulum
ERK2	Extracellular signal-Regulated Kinase 2
ESCRT	Endosomal Sorting Complex Required for Transport
FOXO	Forkhead Box class O
FRT	Flipase Recognition Target
Ftz	Fushi-tarazu
GAP	GTPase-Activating Protein
GNAT	GCN5-related N-acetyltransferases
GO	Gene Ontology
GSK3	Glycogen Synthase Kinase-3
GST	Glutathione S-Transferase
HATs	Histone Acetylases

HDACs	Histone Deacetylases
hMOF	human Males absent On the First
HOPs	Homotypic fusion and vacuole sorting
HORMA	Hop1, Rev7, and Mad2
HP1/2	Hydrophobic Pocket 1/2
HSC70	Heat-Shock Cognate protein 70 kDA
HX	Hexapeptode
IC	Information Content
ICM	Information Content Matrix
IF	Immunofluorescence
iLIR	Identification of LIR tool
InR	Insulin Receptor
IP	Immunoprecipitation
IRS	Insulin Receptor Substrate
Jmjd-2	Jumonji d-2
KATs	lysine (K) Acetyltransferases
KDACs	lysine (K) Deacetyltransferases
KDM4	lysine (K)-specific Demethylase 4
LAMP1/2A	Lysosomal-Associated Membrane Protein 2A
LDS	LIR Docking Site
LIR	LC3 Interacting Region
LIRm	LIR mutant
LKB1	Liver Kinase B1
LST8	Lethal with SEC13 protein 8
MEME	Multiple Em for Motif Elicitation
MF	Molecular Function
MI	Microautophagy
MITF	Microphthalmia Transcription Factor
MO25	Mouse protein 25
MTORC1/2	Target Of Rapamycin Complex 1/2
NAD	Nicotinamide Adenine Dinucleotide
NES	Nuclear Export Signal
nls	Nuclear Localisation signal
NTC	No Template Control
PAS	Phagophore Assembly Site
PBD	Protein Bank Database
PBS	Phosphate-Buffered Saline
PCR	Polymerase Chain Reaction
PE	Phosphatidylethanolamine
PFA	Paraformaldehyde
PFM	Position Frequency Matrix
PIK3	Type III PI3K
PI3K	Phosphoinositide class I 3-Kinase
PI3P	Phosphatidylinositol 3-Phosphate
PMN	Piecemeal Micoautophagy of the Nucleus
PNS	Peripheral Nervous System
PRAS40	Proline-Rich Akt Substrate of 40kDa
PSSM	Position Specific Score Matrix
PTM	Post Transcriptional Modifications
PWM	Position Weight Matrix
qPCR	Quantitative PCR

RAPTOR	Regulatory-Associated Protein subunit of mTOR
Ref(2)P	Refractory to Sigma P
RICTOR	Rapamycin Insensitive Companion of mTOR
Rpl30	Ribosomal protein L30
RT-qPCR	Reverse Transcription qPCR
RUBCN/Rubicon	Run domain Beclin-1 interacting and cysteine-rich containing protein
SAR	Selective Autophagy Receptor
SID	Selected Interaction Domain
SKP2	S-phase Kinase-associate Protein 2
SMART	Simple Modular Architecture Research Tool
SNARE	Soluble N-ethylmaleimide-sensitive factor Activating Receptor
Sqa	Spaghetti-squash Activator
SQSTM1	Sequestosome 1 (p62)
STRAD	STE-Related Adaptor
S6K	ribosomal protein Subunit 6 Kinase
TFEB	Transcription Factor EB
TFFM	Transcription Factor Flexible Model
Tm	Melting temperature
TOR	Target Of Rapamycin
TP53INP2	Tumor Protein tp53-Inducible Nuclear Protein 2
TSC	Tuberous Sclerosis Complex
TSS	Transcription Start Site
UAS	Upstream Activation Site
UBA	Ubiquitin-associated
Ub	Ubiquitin
UBD	Ubiquitin Binding Domain
Ubl	Ubiquitin-like
Ubx	Ultrabithorax
UBZ	Ubiquitin Zinc finger
UDS	Ubiquitin Docking Site
UIM	Ubiquitin Interacting Motif
VSP34	Vascular Protein 34
WT	Wild Type
xLIR	Relaxed LIR
ZIPK	Zipper-Interacting Protein Kinase
ZKSCAN3	Zinc finger transcription factors Kruppel-associated box and SCAN domain 3

ACKNOWLEDGEMENTS

Firstly, I would like to thank my PhD supervisor Professor Ioannis Nezis for giving me the opportunity to work on such an interesting and challenging project, and for providing his expert guidance throughout my 4 years at the University of Warwick. I would also like to acknowledge the support, encouragement and friendship of Dr. Anne Claire Jacomin and Dr. Stavroula Petridi, who both played such an important role in my development as a scientist. I would also like to express my gratitude towards the members of my advisory panel; Professor Kevin Moffat and Dr. Kristen Panfilio, whose alternative perspectives spurred me to keep improving and to keep asking questions. I also acknowledge the fantastic work of colleagues and collaborators of the Sequoia project; Dr. Jacomin, Dr. Petridi and Professor Alex Cameron, of the University of Warwick, and Dr. Ashish Jain and Professor Terje Johansen of the University of Tromsø.

I thank all members of the Nezis lab, from which I am lucky enough to have nurtured friendships alongside professional relationships. A special mention goes out to fellow PhD students Bhavini and Panos, who have been by my side offering their support and advice, since the beginning of our PhDs. Away from our research group I would like to acknowledge all the integral members of the School of Life Sciences at Warwick who were responsible for such a well organised department, and to the MIBTP who funded my PhD. I would also like to acknowledge the friendship and support of fellow departmental PhD students Lucy, Sahan and Talal.

I would like to thank my family for their constant love and support; my Mum and Dad, Leigh, my sisters Jessica and Alessia, my Nonni, Barbara, Uncle Carlo, Auntie Liz, and my life-long friends Luana and Daniella. I would like to especially thank my sister Sabrina, whose positivity and eagerness to help made even the toughest days in the lab that bit easier. A very special thanks also goes to Natalia, whose constant support, encouragement and interest in my work has helped me grow in character and in confidence, and whose love has made my life away from academia so happy and fulfilling.

DECLARATION

This thesis is submitted to the University of Warwick in support of my application for the degree of Doctor of Philosophy. It has been composed by the author (Marisa Di Monaco) and has not been submitted in any previous application for any degree.

Contributions: All work presented here (including data generated and data analysis) was carried out by the author except in the cases outlined below:

By Prof. Terje Johansen's group:
- Figure 3.2 (C, D)
- Figure 4.3 (A, B)
- Figure 5.4 (A, B)

By Dr. Anne-Claire Jacomin:
- Figure 3.4

By Dr. Stavroula Petridi:
- Figure 4.12

By Professor Alex Cameron
- Figure 4.4

ABSTRACT

Autophagy is a fundamental and evolutionarily conserved process, in which cytoplasmic material is degraded through the lysosomal pathway. Nutrient deprivation is one of the main stresses known to induce autophagy and is tightly regulated by autophagic machinery. However, many of these mechanisms of regulation remain to be elucidated. One of the most well studied autophagy-related proteins is Atg8a (*Drosophila* homolog to mammalian LC3), which participates in autophagosome formation and autophagy cargo selection in the cytoplasm. Despite growing evidence that LC3/Atg8a is also enriched in the nucleus, mechanisms by which it is targeted to this compartment, and the nuclear components with which it interacts with remain poorly understood. Atg8-family interacting proteins have been shown to harbour a LC3-interacting region (LIR), which is highly conserved in Eukaryotes. Bioinformatical screening for this region has provided a gateway for the identification of Atg8a-interacting proteins. Here, a novel LIR containing nuclear protein, named Sequoia, is characterised.

Following the discovery of a LIR-dependent interaction between Atg8a and Sequoia, results presented here show that *sequoia*-depletion induces autophagy in nutrient-rich conditions through the enhanced expression of autophagy genes. Harbouring a zinc-finger binding domain, Sequoia is also found to bind to promoter regions of a wide set of autophagy genes, thereby repressing their transcriptional expression. Consistent with reports that indicate that the acetylation status of Atg8-family proteins is fundamental in their ability to interact with nuclear components, we piece together a mechanism of autophagic control within the nucleus by uncovering the roles of YL-1, a member of a component of a nuclear acetyltransferase complex, and deacetylase Sir2 (mammalian homolog SIRT1). Taken together, results here suggest a mechanism for the regulatory control of autophagy genes by transcription factor Sequoia and Atg8a, highlighting the importance of acetylation events in the induction of autophagy under starvation condition. Furthermore, we also uncover a potential role of dDOR (mammalian homolog DOR/ TP53INP2) and its ubiquitin-interacting motif in the cellular redistribution of Atg8a.

CHAPTER 1. INTRODUCTION

1.1 A Brief Introduction to Autophagy

'Autophagy', a term derived from the Greek words auto- (self) and phagy- (eating), was first coined by Belgian biochemist and Nobel laureate Christian de Duve, in 1963[1], and represents an evolutionary conserved process of cellular self-degradation which plays a significant role in the maintenance of cellular homeostasis.

Autophagy begins with an isolation membrane known as a phagophore. The phagophore is likely derived from lipid bilayer contributed by the ER (Endoplasmic Reticulum) and/or the trans-Golgi and endosomes [2,3]. It functions to expand and engulf intra-cellular cargo, such as protein aggregates, organelles and ribosomes, thereby sequestering them in a double-membraned, spherical structure referred to as an autophagosome[4]. Once the autophagosome is mature, the outer membrane of the autophagosome will fuse with the lysosomal membrane, with the product of this fusion referred to as an autolysosome. Exposed to the acidic lumen and resident hydrolases of the lysosome, the autophagosome inner membrane and, subsequently, the autophagic cargo are degraded[5]. The resulting component parts are exported back into the cytoplasm through lysosomal permeases for use by the cell in biosynthetic processes and for metabolism[4]. Autophagy can therefore be considered as a cellular 'recycling function' which promotes energy efficiency through ATP (Adenosine 5'-Triphosphate) generation and mediates damage control by removing non-functional proteins and organelles [6,7].

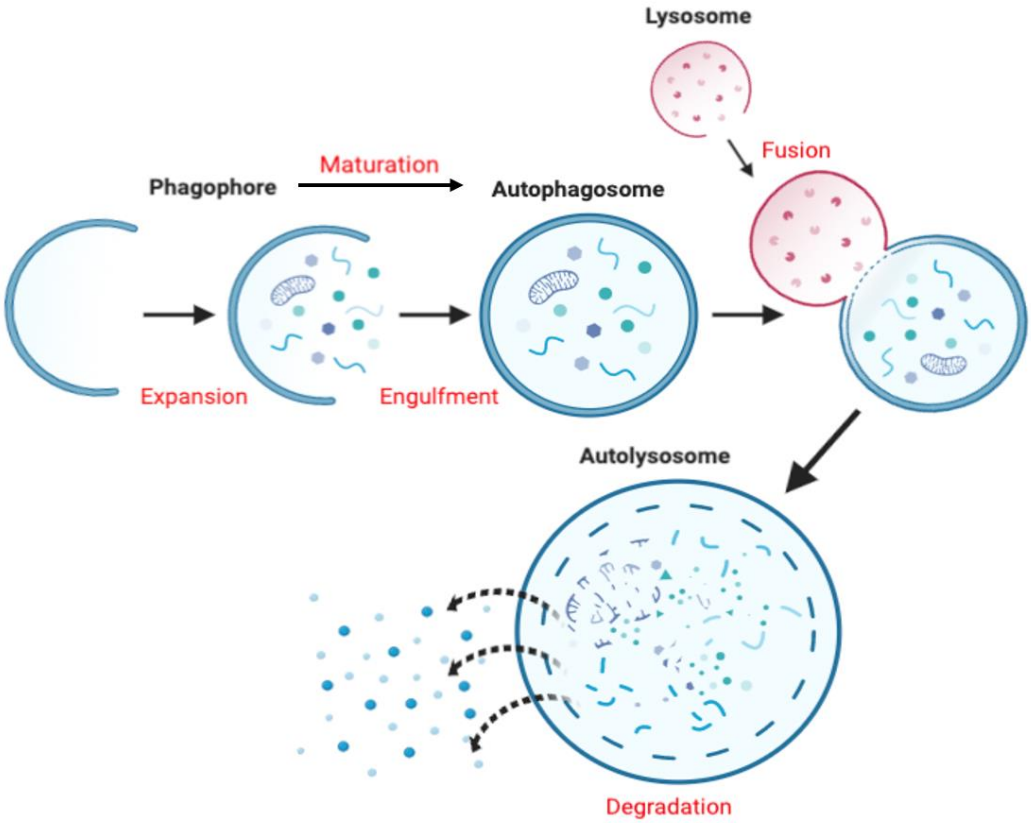

Figure 1.1 The Basic Mechanism of Autophagy: Autophagosome Formation, Maturation and Fusion with the Lysosome. Intra-cellular cargo is sequestered by an isolation membrane known as a phagophore, which functions to expand and fuse with itself to form an autophagosome. This double membraned structure fuses with the lysosome resulting in the formation of an autolysosome; thereby promoting the degradation of the loaded cargo which are subsequently exported into the cytoplasm to act as cellular resources.

1.1.1 Rising Through History

Christian de Duve, of the Rockfeller Universuty and Universite Catholique de Louvain in Belgium, first used the conceptual term 'Autophagy' at a symposium on lysosomes in 1963[8]. His work was based on observations of mitochondrial degradation and the degradation of other intra-cellular structures within the lysosome of rats, in response to an intraperitoneal injection of the pancreatic hormone, glucagon[1]. With an interest in uncovering the link between autophagosomes and cellular degradation, de Duve based much of his research on that of Thomas Ashford and Keith Porter. Published in 1962, they were first to observe that the

addition of glucagon was found to increase the number of lysosomes in rat liver cells, causing them to translocate to the centre of the cells[9]. de Duve later went on to win the Nobel Prize in Physiology or Medicine in 1974 for his discoveries concerning the structural and functional organisation of a cell.

In the decades following the emergence of this new cellular phenomenon, the biochemistry which underpinned autophagy remained largely unknown. This led to a low but steady production in the number of new articles appearing in journals exploring the field, since the first publications reporting on autophagy in the 1960's. However, the emergence of some landmark discoveries sparked a renewed interest into the field and led to an exponential increase in the number of articles being published within the last 15 years (Fig. 1.2).

One of the biggest pioneers in the field has undoubtedly been Dr. Yoshinori Ohsumi, who is responsible for first identifying the basic mechanisms which activate autophagy in yeast. The key discoveries made by Oshumi at the University of Tokyo and later at the National Institute for Basic Biology in Okazaki, Japan, were the identification and characterization of the core autophagy genes and proteins that govern the formation of the autophagosome. In 1993, alongside his collaborator Miki Tsukada, Ohsumi reported on fifteen genes responsible for driving autophagy in yeast; which would later come to be known as *ATG* genes[10]. Later in 2001, this time alongside Kuninori Suzuki, Oshumi described how autophagy related proteins assemble in a hierarchical fashion at the perivaculor PAS (Phagophore Assembly Site), where the autophagosome is produced from the phagophore in the yeast cell[11]. Importantly these discoveries uncovered that the core autophagy machinery is highly conserved in eukaryotes. Further to this, the functional expansion of the *ATG* gene family, and the multiple sites of autophagosome formation in the cytosol, were both discovered to be hallmarks of the mammalian autophagy process[12]. Oshumi's work served as a catalyst in field, leading to an explosive increase in new knowledge. Importantly, this wave begun to unpick the relationship between autophagic processes and human health and disease. Oshumi's contribution to this rapidly growing field meant that he followed in the footsteps of de Duve and earnt the Noble Prize in Physiology or Medicine in October 2016, further spurring an invested interest in the research area.

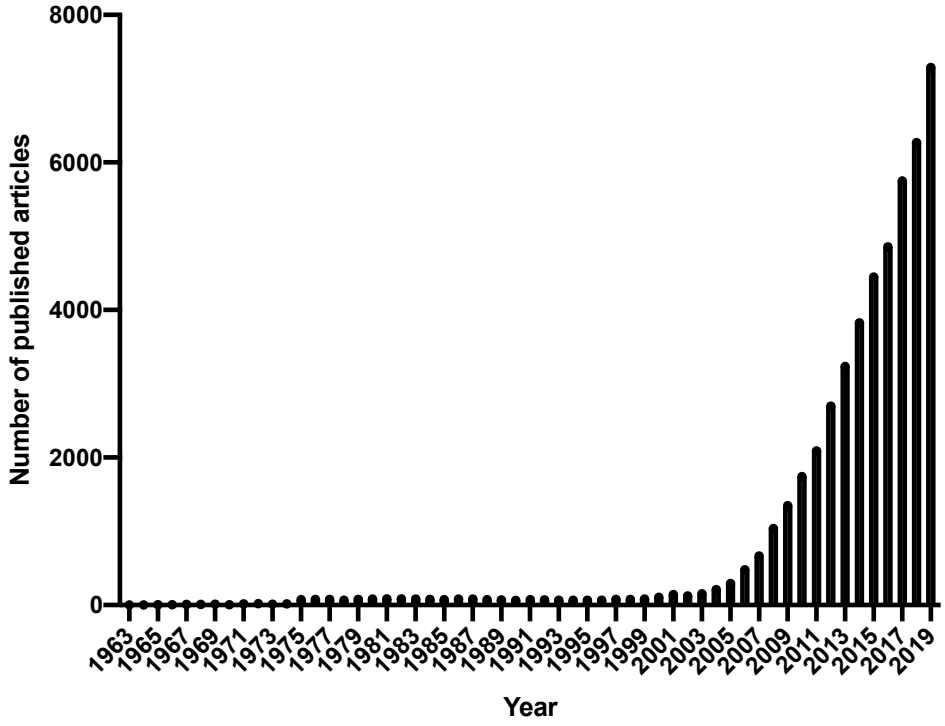

Figure 1.2 The Exponential Rise in Autophagy Articles Published in the Last 15 years. Since 1963, when records begun on research into the field of autophagy, there has been a steady increase in the number of articles published each year. In the last 15 years however, there has seen to be an exponential increase in these publications as a result of landmark discoveries sparking a heightened interest in the field. *Data accurate of 09/04/2020, sourced from PubMed.gov.*

1.2 *Drosophila melanogaster* as a Model Organism

1.2.1 The life cycle and genetics of *Drosophila melanogaster*

Due to its short life cycle, small body size and ability to produce a large number of progeny over a relatively short period of time, *Drosophila melanogaster* (*Drosophila*), or more commonly referred to as the fruit fly, has proven to be an excellent model organism in the study various of cellular processes. In particular, *Drosophila* development provides a useful system to investigate the relationship between nutrients, growth and development. Its development from embryo to adult lasts approximately 10 days in the laboratory, at 25°C; with embryogenesis lasting a single day, the three larval feeding stages- first, second and third instar stage- span 5 days combined, and the transformation from pupa to adult, known as metamorphosis, taking between 3.5 to 4.5 days[13]

(Fig. 1.3). Another attractive feature of working with *Drosophila* is that the cost of maintenance attached to the organism is very low in comparison to vertebrate organisms.

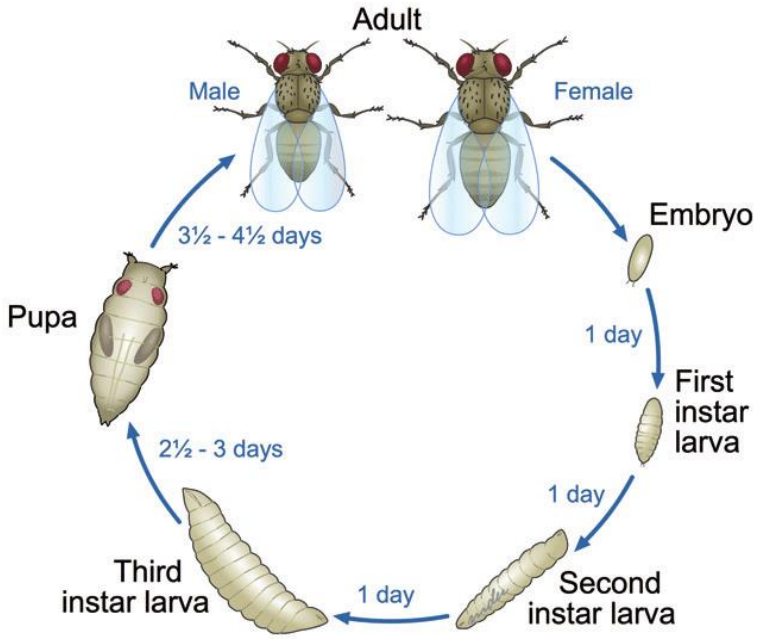

Figure 1.3 The Development Cycle of *Drosophila Melanogaster*.
The first stage of development, embryogenesis, is a fast process completed 24 hours after fertilization of the oocyte by the male sperm. There are three larval stages (3 instars) which take altogether around 5 days. During larval growth, most cell types are already differentiated and functional. Therefore, many biological questions can be addressed during the larval stages. The pupal stage begins after the encapsulation of the third instar larva, lasting approximately 4 days. Here, many larval structures are lysed, and new structures are formed. Adult flies emerge upon eclosion of the pupal case, and have a lifespan of around 30 days, although this is temperature dependant. Females are capable of laying up to 100 eggs per day, generating large progenies, thus making *Drosophila* an excellent genetic model which are very easily propagated in laboratory conditions.

Drosophila is encoded by approximately 13,600 genes located on only 4 pairs of chromosomes, in comparison to the 27,000 genes across 23 chromosomes, which constitute humans[14]. Given its genetic simplicity, *Drosophila* can easily be manipulated, with a number of strategies available to generate mutant or transgenic lines. Mobile genetic elements, known as transposons, provide one of the most common tools for genetic manipulation; with appropriately located transposons capable of causing loss-of-function in target genes, null alleles and also serve as vehicles to insert transgenes[15,16]. Additionally, genetic manipulations utilise phiC31 integrase-mediate targeted insertion, FLP/FRT recombination and the UAS/Gal4 system, all of which will be described in more detail in Chapter 2. Somatic recombination is also easily achieved, and allows for the

comparison of genetically modified; mutant, knockdown or overexpression, cells to be compared to an un-manipulated neighbouring cell in the same tissue, of the same mosaic animal[17]. Given the genetic plasticity of the organism, *Drosophila* is unsurprisingly ideal for large scale RNAi and mutant screening[18].

The simplicity of the *Drosophila* blueprint is especially appealing given that many of its genes and processes are conserved between other organisms, most notably humans. In fact, genome sequencing[14] has revealed that 75% of human disease genes can be found in flies[19], thus much of the research conducted in the organism is translatable.

1.2.2 The use of *Drosophila* to study starvation induced autophagy

Using the fruit fly as a genetically modifiable model organism, it is possible to investigate how the process of autophagy is regulated. Many reviews describing various techniques for studying autophagy in *Drosophila* have previously been published[20,21]. Notably, in 2008 a guidelines paper aimed at providing a comprehensive overview of all the assays that can be used across higher eukaryotes, including *Drosophila*, presented a consensus view of the entire research community[22]. While the application of methods may differ slightly between flies and other eukaryotes, due to high percentage of conserved autophagy related genes across higher eukaryotic organisms, the interpretation of results will always follow the same logic[23].

As cells use autophagy to generate materials and energy, it essentially acts as a cellular response to stresses such as nutrient scarcity. In order to induce this type of autophagy within the animal, larvae must be collected in the 'pre-wandering' phase of the third instar stage. The importance of studying stress-induced autophagy at this precise life-cycle stage is owed to *Drosophila* being an holometabolous insect, which means that the larval stages are followed by a non-motile life stage (first prepupa and then pupa) in which the whole body is reorganised[17]. Mid-way through the third instar stage, an increase in the moulting hormone ecdysone triggers a behavioural change in the larva which causes them 'wander' out of the food in search for a dry place to pupariate[24]. This marks the beginning of metamorphosis where larval tissues undergo histolysis while diploid cells proliferate and differentiate to form the adult organs[17]. These cells use ecdysone-induced developmental autophagy as a preparative phase of programmed cell death to free up stored biomass to be utilised by diploid cells as a nutrient and energy source during metamorphosis[24–26].

Therefore, autophagy likely plays an important role during metamorphosis, which is essentially a developmentally programmed 5-day starvation period. Given this developmentally triggered type of autophagy in *Drosophila,* it is crucial to target larvae in the pre-wandering stage in studies, which are concerned in studying the induction of autophagy via extracellular cues such as starvation.

Starvation-induced autophagy can be studied in the fat body of *Drosophila*; a tissue which is similar to human adipose tissue[24,27]. Here, autophagy can be induced by subjecting larvae to a nutrient depleted environment, typically a 20% sucrose[1] solution is used[22]. The advantage of using sucrose as opposed to water is that the density of the solution is a lot higher, allowing the larvae to float on the surface thus reducing the risk of drowning. Under these conditions, autophagy is induced within 1-1.5 hours, with the maximum number of autophagic structures peaking at around 3–5 hours in the fat body[27]. Of course, tissues other than the fat body, such as the midgut, also respond to starvation or ecdysone production[24]. However, the fat body is often chosen due to its accessibility, which results in the ability to carry out dissections quickly and precisely in order to generate a lot of sample tissue in a short amount of time. The fat body is also a monolayered tissue, making it easier to observe. This is particularly useful for imaging as it allows for precise observation of target protein localisation within clones.

1.3 Autophagy Classification

Owing to the main function of autophagy being that of providing nutrients to cellular functions during periods of cellular stress and deprivation, it was previously perceived to be a non-specific process which degraded material in bulk. However, it is now viewed as an adaptive process which reacts in the response to a number of cellular stresses including nutrient deprivation, infection, hypoxia and growth factor depletion[28]. It has also be uncovered that the process of autophagy acts as a major cytoprotective system by selectively eliminating potentially harmful cytosolic material such as protein aggregates, damaged organelles and bacteria[29]. It is responsible for a number of important functions including, promotion of cellular senescence and cell surface antigen presentation, protection against genome instability, and prevention of necrosis[30].

[1] Sucrose is a disaccharide made up of 50% glucose and 50% fructose and is broken down rapidly into its constituent parts.

Accordingly, autophagic activity is seen to modulate many pathologies, from bacterial and viral infections to cancer and neurodegeneration, and more recently in obesity[7,30,31].

When referring to the term 'autophagy', it must be noted that this is often describes the most well studied subtype: macroautophagy. However, there are three sub-types of autophagy: macroautophagy, MI (Microautophagy) and CMA (Chaperone-Mediated Autophagy), which take place dependent on the manner in which the cargo reaches and enters the lysosome (Fig. 1.4).

While each is morphologically distinct, all three culminate in the delivery of cargo to the lysosome for degradation and recycling (Fig 1.4). During MI, invaginations or protrusions of the lysosomal membrane are used to capture cargo and uptake occurs directly at the limiting membrane of the lysosome and can include intact organelles. CMA differs from MI in that it does not use membranous structures to sequester cargo, but instead uses chaperones to identify cargo proteins that contain a particular pentapeptide motif; these substrates are then unfolded and translocated individually directly across the lysosomal membrane. In contrast to MI and CMA, macroautophagy involves sequestration of the cargo away from the lysosome. In this case, *de novo* synthesis of the double-membrane autophagosome are used to sequester cargo and subsequently transport it to the lysosome.

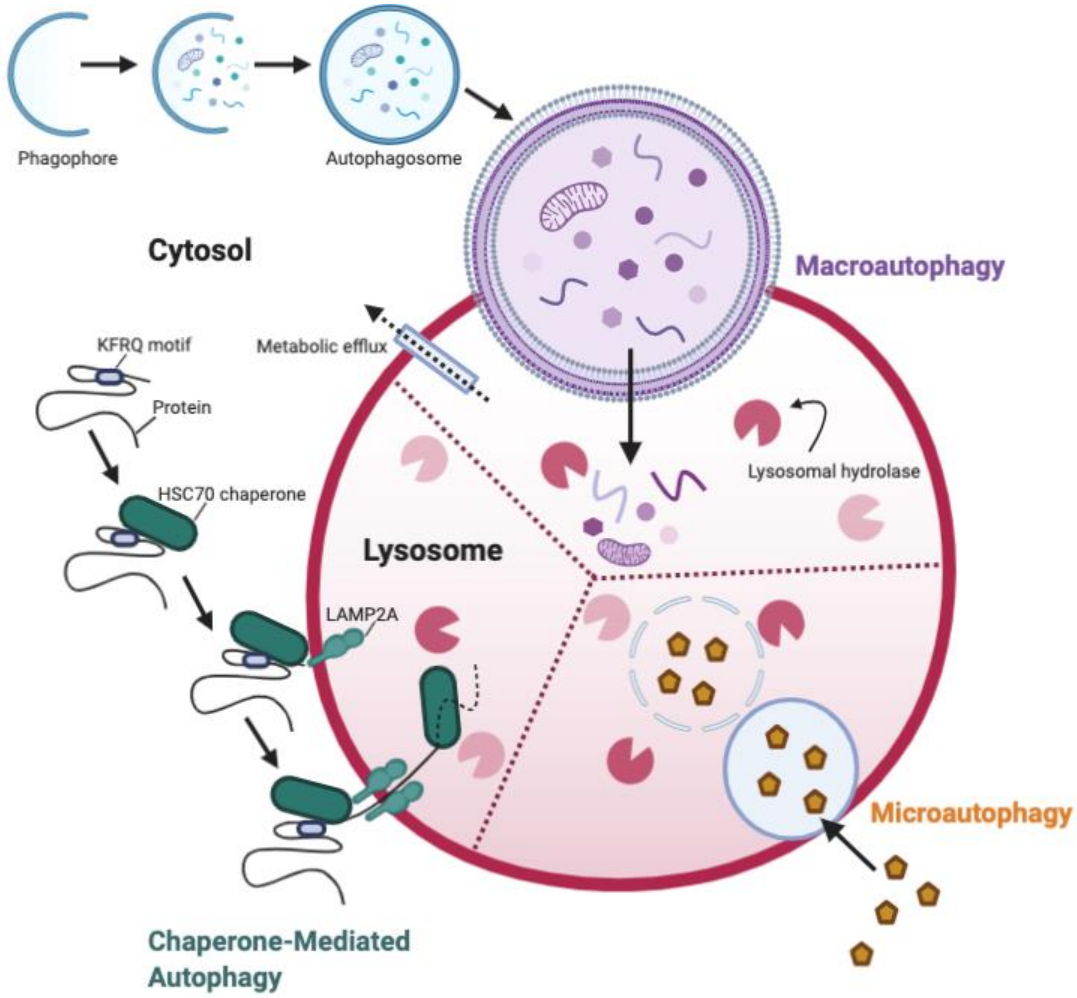

Figure 1.4 The Three Autophagy Sub-Types.

Autophagy is subdivided into three categories depending on the nature of the cargo and how it reaches the lysosome. During macroautophagy cytosolic components are sequestered by a membrane structure, called the phagophore. The cargo is delivered by specialised proteins, called selective autophagy receptors. The phagophore fuses to become a double-membrane vesicle, called an autophagosome. During maturation autophagosomes will merge with lysosomes, releasing their cargo. In CMA, the cargo is selectively transported into the lysosome without any vesicles. HSC70 recognises the KFRQ motif and facilitates the translocation of single peptides into the lysosome through the LAMP2A receptor. Microautophagy is the process whereby cytoplasmic cargo is directly engulfed by the lysosome.

1.3.1 Macroautophagy

As macroautophagy is considered as the major type of autophagy, it has been studied most extensively relative to CMA and MI. The basic mechanisms of macroautophagy are shown in Figure 1.1, with extensive details presented on this process in the following sections. As macroautophagy is explored exclusively in this thesis, from herein it will be referred to as 'autophagy'.

1.3.2 Chaperone-Mediated Autophagy

Through the process of CMA, cytosolic material can enter the lysosome for degradation via a protein translocation system at the lysosomal membrane[32]. Only proteins which are amenable to unfolding can enter the lysosome via this process which bears similarities to protein transport systems utilised by mitochondria or the ER[32]. Interestingly, the discovery of this particular process gave the first evidence that the overarching phenomenon of autophagy could function selectively, as it revealed that only a subset of cytosolic proteins could be recognised by HSC70 (Heat-Shock Cognate protein 70 kDA) and subsequently selected for degradation by CMA[33]. The pentapeptide KFERQ, was established as the motif which is necessary and sufficient to target proteins for lysosomal degradation via CMA[34].

CMA starts with the binding of HSC70 to the KFERQ consensus motif in the substrate proteins, thus targeting them to the lysosomal membrane[35]. Here the selected substrates bind to the cytosolic tail of LAMP2A (Lysosomal-Associated Membrane Protein 2A), which in this case acts as a receptor. This induces multimerization of LAMP2A, which leads to the subsequent unfolding and translocation of the substrates into the lysosomal lumen, one-by-one[36]. Along with the multimerization of LAMP2A, a form of HSC70 residing in the lysosomal lumen is also required for this process to be sucessful[37]. This has been deemed likely to facilitate the 'pulling' of the protein into the lysosomal lumen or to prevent it from translocating back into the cytosplam[38]. Upon entering the lysosomal lumen, the selected substrates undergo rapid degradation.

It is important for the cell to regulate the synthesis and degradation of LAMP2A in order to regulate the amount available to bind to substrates. Concurrently, the abundance of LAMP2A has been shown to directly correlate to the activity of CMA[37]. Many receptors involved in autophagy are found to be evolutionary conserved from yeast to mammals, however LAMP2A which is a splice variant of the gene *lamp2*, appears late in evolution[36], and is absent from yeast, fungi and worms[39]. In *Drosophila*, a gene with homology to mammalian *lamp2* has been identified with a C-terminus that is homologous with LAMP2C, however there is no evidence of splicing. The LAMP2A exon has thus far only been documented in birds and mammals[39].

Maximal activation of CMA is found in response to stressors which impact the nutrient status of the cell, such as glucose starvation. Under this form of stress, autophagy is initially activated within thirty minutes of starvation, however if conditions persists for longer than ten hours, cells

have been found to switch preferentially to CMA[40,41]. Interchangeability between autophagy and CMA is evident through a compensational relationship, with blockage of CMA in most cell types seen to be counteracted by the up-regulation of autophagy[42], and conversely *in vivo*[2] studies have shown cells to respond to the inhibition of autophagy by constitutively activating CMA[43].

1.3.3 Microautophagy

In comparison to both CMA and autophagy, the molecular machinery which governs MI is remarkably diverse[44]. Differentiated by three categories: Type 1: lysosomal protrusion, Type 2: lysosomal invagination, and Type 3: endosomal invagination; these subtypes of MI have all been observed in a number of organisms.

Lysosomal protrusion in mammalian cells was first reported by de Duve in a pioneering electron microscope experiment, in which the extension and engulfment of part of the lysosomal membrane was observed to enwrap a 'micro' segment of the cytoplasm, thereby engulfing a number of organells[45]. This mechanism strongly suggested turnover of the loaded components inside the lysosome, with reports showing a correlation between the observed frequencies of lysosomes whose protrusions sequestered cytoplasmic proportions, and the basal-protein turnover rates within rat liver cells[46]. However, the intricacies behind this process still remain largely unknown. In plants cells, it has been demonstrated that in *Arabidopsis thaliana* and *Eustoma grandiorum*, aggregated compounds are directly engulfed by extensions of the vacuolar membrane, before being transported into the vacuolar lumen[47]. This process was shown to function independently of Atg5[48], an indispensable cog in the functions of autophagy, thereby clearly distinguishing this process of MI from that of macroautophagy. Electron microscopy of yeast cells subjected to various changes in media composition, have been observed to harbour morphologically similar membranes to those described in higher eukaryotic cells; with protrusions of the vacuolar membrane functioning to sequester peroxisomes[49]. Vac8 and Atg18 have both been identified as proteins required for this process[50].

The lysosomal invagination process can loosely be described as the ability of the vacuolar membrane to form a large tubular invagination from which vesicles bud off into the lumen of the organelle. This process has largely been characterised in yeast cells; with target organelles of

[2] *In vivo* studies are those which are performed or shown to take place in a living organism, or within cells or tissue extracted from the organism.

this pathway including the cytoplasm[51], ER[52], portions of the nucleus ((PMN; Piecemeal Micoautophagy of the Nucleus))[53], mitochondria[54] and lipid droplets[55]. Across these, tubular invagination of the vacuolar membrane has been reported to be partially dependant on *ATG* genes products[56], ESCRT (Endosomal Sorting Complex Required for Transport) machinery[57] and the formation of a microdomain architecture[50]. In mammalian cells, MI invagination processes have been found to be dependent on the small GTPase Rab7[58].

Endosomal invagination has been identified and studied in *Drosophila*, yeast and murine cells. The membrane dynamics of this particular subtype of MI rely heavily on the ESCRT machinery to generate intraluminal vesicles, called the MVB (Multivesicular Body) pathway[50]. Additionally, endosomal invagination employs a number of selective adaptors proteins which function to selectively recruit cytosolic proteins onto the endosomal surface. Nbr1 represents one of the main adaptor protein in mammalian macroautophagic processes[29]. Hsc70 represents a protein which was originally identified as a key player in CMA. Intriguingly, although *Drosophila* seem to lack the functioning of CMA, the MI process of endosomal invagination seems to be well conserved in the species, and HSC70 has been uncovered to play an instrumental role in the process[59]. Here, HSC70-4 is responsible for membrane-deforming activity which is needed for protein turnover via MI. Furthermore, inhibition of the nutrient signalling pathway has been shown to induces endosomal invagination in the *Drosophila* fat body under nutrient rich conditions; a process mediated by ESCRT complex components and autophagy genes *Atg1* and *Atg13*[60].

1.4 The Regulation of Autophagy by Glucose

As basal autophagy levels are very low, an efficient mechanism is required to induce sufficient levels of autophagy in organisms which are put under stress by extracellular cues. Glucose deprivation, one of the main stresses known to induce autophagy, is tightly regulated by the serine/threonine protein kinase AMPK (AMP-activated Protein Kinase) and its inhibition of TORC1 (Target Of Rapamycin Complex 1)[61]. Here we will focus on the signalling pathways by which environmental glucose directly regulate.

1.4.1 Activation of AMPK

AMPK is an evolutionarily conserved protein kinase that acts as an energy sensor in cells and plays a key role in the upregulation of catabolism and inactivation of anabolism. It is composed of a catalytic (α) sub-unit and two regulatory (β and γ) subunits[62] (Fig 1.5). In mammals, multiple genes encode each of the aforementioned subunits, enabling the formation of a number of unique heterotrimeric complexes (α_{1-2}, β_{1-2}, and γ_{1-3})[63]. In *Drosophila*, a single gene encodes each subunit, however the functionally critical amino acids in these subunits are either conserved, or found to be replaced by biochemically similar residues[63].

Under conditions of glucose deprivation, intracellular ATP levels decline whilst AMP (Adenosine 5'-Monophosphate) levels increase; encouraging the preferential binding of AMP to the tandem repeats of the crystathionine-β-synthase domains in the AMPK γ-subunit[62]. The binding of AMP to AMPK functions to activate the kinase via three complementary mechanisms (Fig 1.5): (1) AMP-binding promotes the phosphorylation of AMPK at Thr172 by the LKB1 (Liver Kinase B1) complex; a major evolutionary conserved kinase which is responsible for phosphorylating the AMPK activation loop under conditions of energy stress across metazoans[64]. Cytosolic LKB1 functions to form a complex with STRAD (STE-Related Adaptor) and MO25 (Mouse protein 25), thereby increasing its kinase activity and enabling it to activate AMPK[65]. (2) When AMP binds AMPK, it results in a conformational change in the protein kinase which results in the inability of its Thr172 residue to become dephosphorylated; thus, rendering it continuously active[66]. And finally (3) the binding of AMP to the γ-subunits of AMPK has been shown to cause allosteric activation of the complex[67]. All the aforementioned modes of activation are not mutually exclusive and occur concordantly and are antagonized by ATP binding (Fig 1.5).

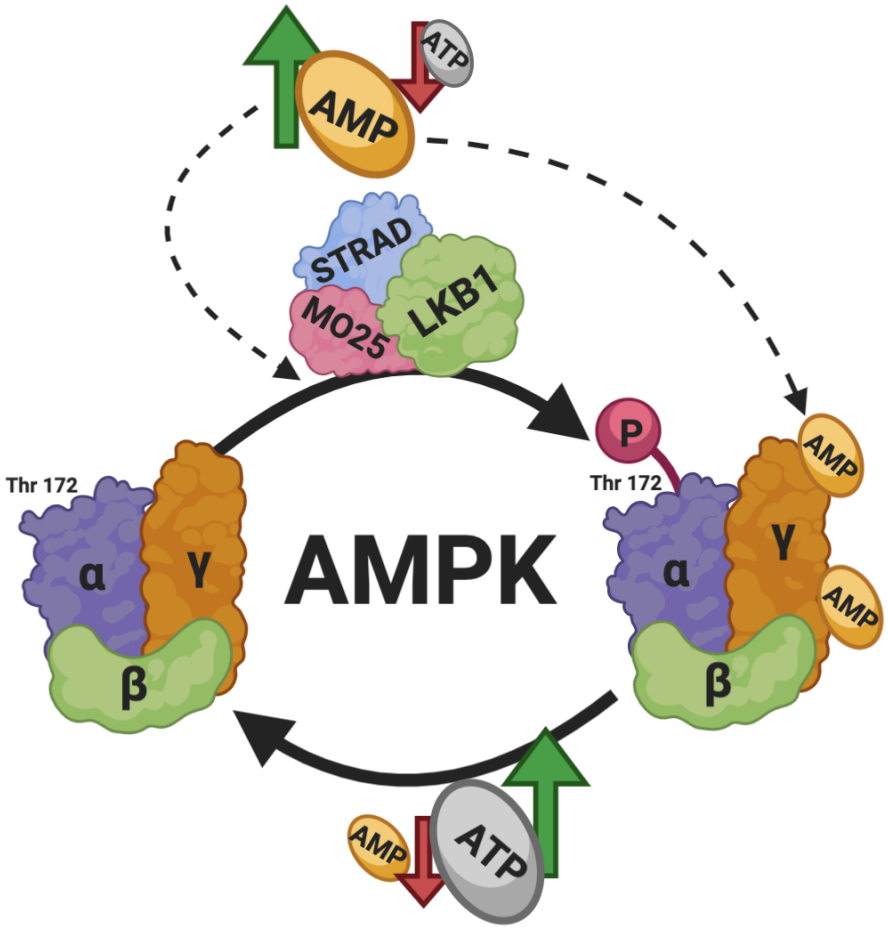

Figure 1.5 Activation of AMPK.
The AMPK protein kinase is comprised of three subunits: α, β and γ. As a result of nutrient depletion, intracellular levels of ATP decrease, whilst AMP levels increase. This change in concentration encourages the preferential binding of AMP to the γ-subunit of AMPK. This in turn initiates phosphorylation of Thr172 on the α-subunit; a reaction catalysed by the LKB1-MO25-STRAD complex. These events are antagonised by ATP, in that when nutrients are resupplied, AMPK returns to its inactive form.

The amino acids which mediate the binding of AMP at the allosteric activation site and the dephosphorylation inhibition site in AMPK γ_1, and are conserved in *Drosophila*[68]. Adult *Drosophila* with reduced AMPK function are highly susceptible to the effects of starvation, with persistent starvation behaviours and altered metabolism recorded as a result[69]. Behaviours observed in flies with reduced AMPK function included lower locomotor levels in unstressed conditions and hyperactivity in starvation conditions, which is considered an adaptive response to encourage foraging[69]. These starvation-induced behavioural responses are conserved throughout the Metazoa. Furthermore, AMPK mutant flies displayed starvation-like lipid accumulation patterns in metabolically key liver-like cells, oenocytes, even under fed conditions, whilst

oxygen consumption levels in these flies revealed metabolic rates which were significantly greater than in WT (Wild Type) flies[69].

The expression of LKB1 and the AMPK-dependant effects of LKB1 signalling are conserved in *Drosophila*[63]; further meriting its use as a model for the investigation of cellular nutrient responsive mechanisms. Furthermore, one of the best studied AMPK substrates, acetyl CoA carboxylase, is also found to be conserved in *Drosophila*[63] and, has been shown to have important implications in the regulation of lipid metabolism[70] and the autophagy promoting transcription factor TFEB (Transcription Factor EB)[71].

1.4.2 AMPK- TOR signalling

In glucose depleted conditions, the activation of AMPK can induce autophagic processes by two different mechanisms: firstly, through inhibition of the TOR protein kinase complex, and secondly via the direct phosphorylation of ULK1/Atg1 (Fig. 1.6). Both events are not mutually exclusive and ultimately implicate the function of ULK1/Atg1, as TOR also functions to inhibit ULK1/Atg1 via phosphorylation. The action of ULK1/Atg1 is fundamental in driving the formation of autophagosomes and will be discussed in greater detail in section 1.5.3.

1.4.2.1 TOR

TOR (mTOR and dTOR will be used herein when exclusively referring to mammals and *Drosophila* respectively), a member of the phosphoinositide kinase-related family, is a highly conserved serine/threonine nutrient-responsive kinase, which is capable of integrating signals from many stimuli including amino acids, glucose levels, oxygen, growth factors, and stress to coordinate cell growth and maintain metabolic homeostasis in all eukartyotes[72]. mTOR was first identified as a substrate for rapamycin; a macrocyclic lactone known to inhibit the proliferation of mammalian cells[72]. There are two types of mTOR complexes; mTORC1 and mTORC2, however only the former is sensitive to rapamycin. Both complexes have been revealed to have different composition and functional properties; mTORC1 is composed of three core subunits: mTOR, mLST8 (Mammalian Lethal with SEC13 protein 8) and RAPTOR (Regulatory-Associated Protein subunit of mTOR) (Fig 1.6). In addition to this, it has two inhibitory subunits known as PRAS40 (Proline-Rich Akt Substrate of 40kDa) and DEPTOR (DEP containing mTOR interacting protein). Differences in the composition of mTORC2 are evident in the presences of RICTOR (Rapamycin Insensitive Companion of mTOR) as opposed to

RAPTOR, and the additional regulatory subunits Protor1/2 and Sin1[73] (Fig 1.6). All the components of TORC1 and TORC2 are highly conserved in eukaryotes with dTOR, dRAPTOR and CG3004 (homolog of mLST8) all present in *Drosophila*[72].

An early step in the activation of autophagy in eukaryotes is the induction of the ULK1/Atg1; a kinase which drives the formation of autophagosomes. Under nutrient replete conditions, TORC1 primarily functions to phosphorylate ULK1/Atg1, thereby preventing its activation by AMPK (Section 1.4.3) and subsequent induction of autophagy[74]. Accordingly, the inactivation of Torc1 in yeast, via mutation or rapamycin treatment, has been shown to induce autophagy even in the presence of nutrients[75]. mTORC1 also functions to regulate translation of the downstream targets via the phosphorylation of p70(S6K) (p70 ribosomal protein Subunit 6 Kinase), S6K1 (ribosomal protein subunit 6 kinase 1) and EIF4EBP1 (Eukaryotic Initiation Factor 4E-Binding Protein 1)[73]; all of which implicate the induction of autophagy in response to a diverse range of stimuli. These include growth factors, oxygen, growth factors and amino acids[73]. The function of RAPTOR is to "bridge" the kinase domain of mTORC1 to that of its downstream substrates, thereby controlling the regulation of metabolic processes[72].

Genetic studies in *Drosophila* and mammalian cells have revealed TORC1 and TORC2 signalling to be regulated by the products of the genes TSC1 and TSC2[76] (Tuberous Sclerosis Complex) (Table 1.1). The TSC1-TSC2 complex, shows GTP enzyme activity and can hydrolyse GTP to inactivate the small GTPase Rheb, which is an activator of TOR, thereby having an overall inhibitory effect of TOR signalling[77]. Loss of TSC1 or TSC2 therefore leads to hyper-activation of TOR (Fig 1.6). A diverse range of stress signals are known to converge on the TSC1-TSC2 complex in order to regulate TOR signalling in both mammalian and *Drosophila* cells[78].

1.4.2.2 AMPK inhibits mTOR/Tor to promote autophagy via ULK1/Atg1

In glucose depletion conditions AMPK is activated, presumably via LKB1 and high AMP concentrations, enabling it to inhibit the activity of mTORC1. This can be achieved by AMPK-mediated phosphorylation of TSC2 at its Thr1271 and Ser792 residues[76]. This in turn promotes the GAP (GTPase-Activating Protein) activity of the TSC1 and TSC2 complexes which catalyse the transformation of Rheb-GTP to an inactive Rheb-GDP state, with mTORC1 subsequently being rendered inactive[79]. Accordingly, in LKB1-deficient mammalian cells it has been shown that mTOR signalling is hyperactivated[64]. Whilst in *Drosophila*, autophagy has been shown to be supressed in dTSC1 and dTSC2 mutants[27]. Inversely under starvation conditions, the activity of

mTORC1 is decreased, thus promoting the interaction between ULK1 and AMPK, and the subsequent recruitment of the ULK1 complex which drives autophagosome formation[80].

A second mode of action sees AMPK directly phosphorylate the Ser227 and Ser792 sites of the mTORC1 subunit RAPTOR[76]. This subsequently hinders the binding of RAPTOR to mTOR, thus halting the recruitment of mTOR substrates, resulting in the inhibition of the mTOR pathway. Simultaneously, the inhibitory cap mTOR places upon ULK1 via phosphorylation of its Ser758 residue is lifted. As this region is located within the region in which AMPK binds ULK1[74], this enables ULK1 to bind to AMPK directly[81]. AMPK is able to phosphorylate ULK1 across multiple sites reported in mammals[76,81,82]. The result of AMPK phosphorylation on ULK1 leads to its conformational change, promoting the recruitment of the ULK1 complex components ATG13, ATG101 and FIP200; thereby increasing the activity and stability of the ULK1 kinase[74]. The yeast homolog of AMPK, Snf1, is also suggested to promote autophagy through its regulation of the Atg1 complex[83]; however unlike AMPK it is AMP-independent[84].

A screen for mutants which fail to induce autophagy of the fat body of *Drosophila* larvae, revealed the homolog of the mammalian AMPK -γ subunit, SNFAγ, to be amongst these mutants[85]. It was shown that overexpression of SNFAγ resulted in the partial rescue of autophagy mutants via Atg1 and Atg13, however the exact mechanisms by which it governs these respective Atg proteins, in the context of starvation induced autophagy, remains elusive. It is however strongly suggested by these results, and the AMP-dependant activation of SNFAγ[63], that it does function in a similar way to its mammalian homology AMPK[85]. The tissue specific relationship between Atg1 and AMPK in the activation of autophagy has been shown in *Drosophila*, with the upregulation of Atg1 necessary and sufficient to induce AMPK-activity driven autophagy in both the brain and intestinal epithelium[86].

A body of evidence exists reporting on the bidirectional regulation of AMPK/mTORC1 and ULK1. In the case of starvation, activated ULK1 has been shown to phosphorylate AMPK, resulting in its downregulation[87]. In nutrient rich conditions, ULK1 is also suggested to phosphorylate Raptor, with implications on its ability to associate with mTORC1 substrates and the overall activity of the mTORC1 kinase[81]. Given this, AMPK, ULK1 and mTORC1 can be considered to form a signalling triad, which function in a transient feedback manner to fine tune energy and nutrient responses in different cellular context, thus ensuring a dynamic balance of autophagy.

1.4.2.3 PI3K-TOR signalling

While mTORC1 regulates an umbrella of factors involved in cell growth and metabolism, mTORC2 primarily functions to phosphorylate and activate Akt, a key effector of InR (Insulin Related)/ PI3K (Phosphoinositide class I 3-Kinase) signalling pathway[73]. The mSin1 domain of mTORC2 has been shown to contain a phosphoinositide-binding region, which is critical for the insulin dependent activity of mTOR2[73]. Autophagy is suppressed by components of the InR/ PI3K pathway, which lies up- stream of both mTOR1 and mTORC2; with mTOR activity increased by the presence of growth factors which in turn leads to the promotion of cell growth through the phosphorylation and activation of S6K[88]. In *Drosophila,* dTOR signalling by its upstream regulator PI3K has been shown to be necessary and sufficient in supressing nutrient deplete-induced autophagy in the larval fat body; with the activity of S6K shown to negatively correlate with induction[27]. In this setting, dTSC1 and dTSC2 act together to inhibit dTOR, which mediates a signalling pathway that couples amino acid availability to S6K, translation initiation, and growth[89]. Concurrently, overexpression of dTSC1 or dTSC2, or mutations in dTOR or its downstream target dS6K, result in the inhibition of autophagy, reduced cell size, growth rate[27], and the longevity phenotype[90].

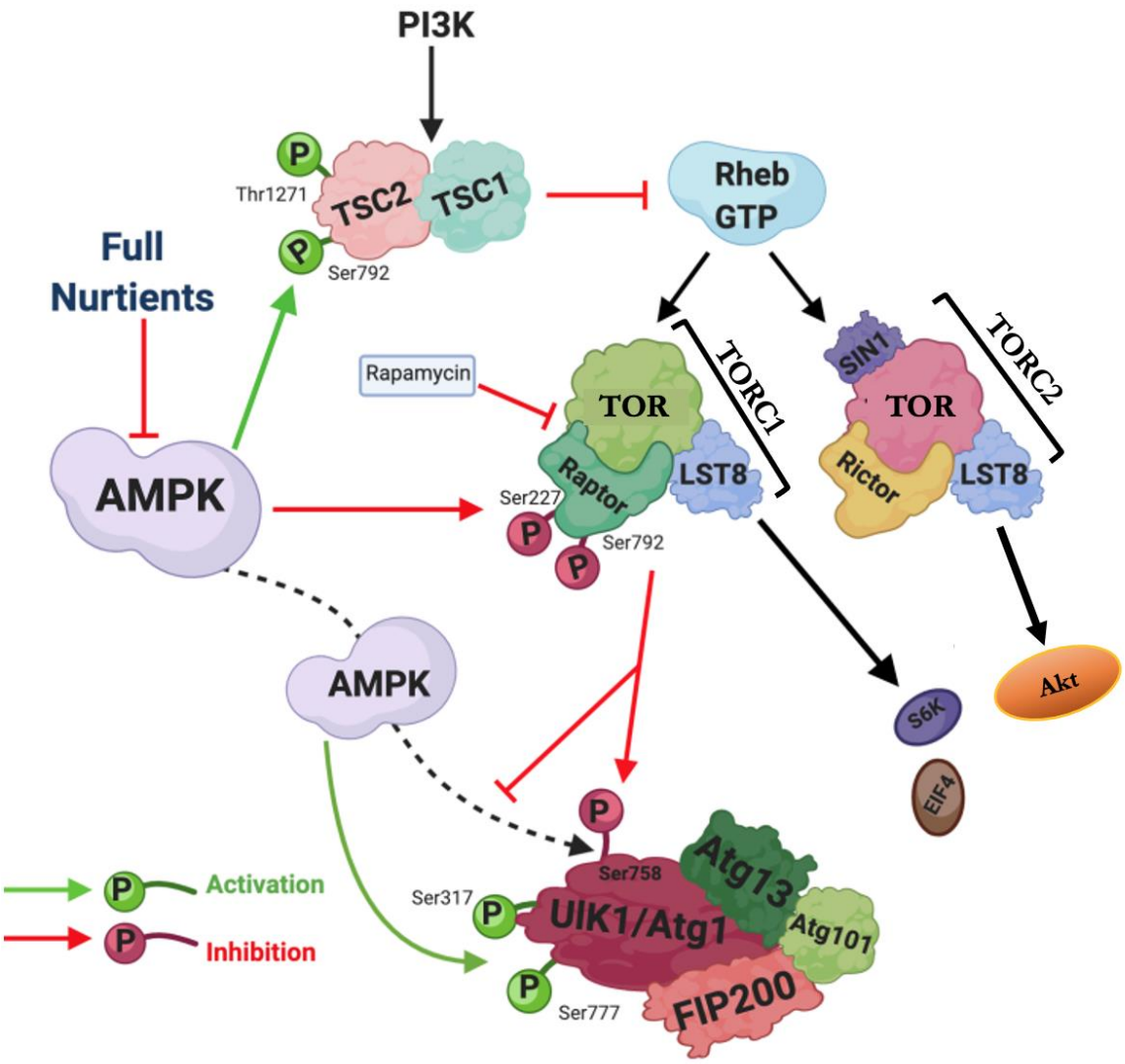

Figure 1.6 The Regulation of Starvation Induced Autophagy by AMPK and TOR.

There are two types of TOR complexes; TORC1 and TORC2, composed of three core subunits: TOR, LST8 and RAPTOR in TORC1 and RICTOR in TORC2. TORC2 also contains a SIN1, which primarily functions on the PI3K pathway, with downstream targets including Akt. TORC1 is inhibited by rapamycin. TORC1-AMPK are involved in cellular response to nutrient levels. When nutrient levels are sufficient AMPK is inactive and the TORC1 complex is activated. TORC1 phosphorylates ULK1 on Ser 758 to prevent its interaction with AMPK. When cellular nutrient levels are limited, AMPK is activated and mTORC1 is inhibited through the phosphorylation of TCS2 and RAPTOR. Phosphorylation of Ser758 is decreased and ULK1/Atg1 can interact with and be phosphorylated by AMPK on Ser317 and Ser777. Once activated the AMPK-phosphorylated Ulk1/Atg1 complex (formed with Atg13, Atg101 and FIP200) can activate autophagy. Downstream targets of TORC1 also include S6K and EIF4.

As well as its action on mTORC1 and ULK1, activated AMPK promotes autophagy directly by phosphorylating autophagy-related proteins in PIK3C3/VPS34 complexes or indirectly by

regulating the expression of autophagy-related genes downstream of transcription factors such as FOXO3, TFEB, and BRD4. All of which will be discussed in later relevant sections.

1.4.3 AMPK regulates SIRT1 activity

Loss of silencing mating loci in yeast led to the discovery of a gene named *Sir2* (Silent Information Regulator 2), which encodes a NAD^+ (Nicotinamide Adenine Dinucleotide) - dependant histone deacetylase[91]. The *sir* genes in yeast were determinants of life span in mother cells, with *sir2* responsible for promoting longetivity[92]. Homologs of the encoded protein have since been found throughout prokaryotes and eukaryotes[91]. Consistent with findings in yeast, the *Drosophila* homolog of Sir2 has been implicated in longevity by calorific restriction, with an extra copy of *sir2* shown to increase life span by 18-50%[93].

SIRT1, a class III NAD^+ dependant histone/protein deacetylase, constitutes one of seven, and the most closely related mammalian homolog of Sir2. SIRT1, has also been has been shown to be required for the response to calorific restriction in mice, with null mutations of *sirt1* found to ineffectively utilise digested food[91]; thus confirming the evolutionary conserved importance of SIRT1 in the regulation of energy metabolism.

The biochemical activation of sirtuins is directly linked to the energetic and redox status of the cells, measured by levels of NAD^+[94]. During calorific restriction, NAD^+ levels become elevated and the expression and deacetylation activity of SIRT1 has been found to be significantly enhanced[95]. Further investigation under a calorie deficit revealed that AMPK enhances SIRT1 activity by increasing the cellular levels of NAD^+[96]. This increase in SIRT1 activity results in the subsequent deacetylation and modulation of FOXO (Forkhead Box class O) transcription factors: FOXO1 and FOXO3 in mouse skeletal muscles[96]. The activity of FOXO transcription factors is essential in the induction of autophagy and cell survival (section 1.7.2); with the discovery of their AMPK-induced/SIRT1-mediated deacetylation revealing why many of the biological effects of AMPK and SIRT1 converge on energy metabolism[96]. Furthermore, the role of SIRT1 in the modulation of nutrient and energy sensing was strengthened in the discovery of its ability to associate with TSC2, in an interaction which inhibits mTORC1 signalling[78].

In a perpetuating cycle LKB1 is deacetylated by SIRT1 at Lys48, which concordantly promotes its cytoplasmic localisation and interaction with STRAD and MO25, thus increasing its kinase

activity[95]. This results in the phosphorylation and activation of AMPK in nutrient depleted conditions[95,97]. Whether other members of the sirtuin family regulate the activity of AMPK remains unknown, however it is conceivable that perhaps SIRT2, another deacetylase class III member (Table 1.2), could potentially have a role in its regulation given its shared ability with SIRT1 to deacetylate FOXO1[98]. Logically, sirtuins have important implications in the regulation of starvation induced autophagy and will be discussed in more detail in later sections.

1.5 The Molecular Machinery of Autophagy

1.5.1 Autophagy-Related Genes and Proteins: The Core Machinery

As a result of multiple genetic screenings carried out in yeast since the 1990's, over thirty different genes have been identified to govern various stages of the autophagy pathway[10]. In order to keep track of the various gene products, researchers working in the area decided to adopt a unified gene and protein nomenclature: '*ATG'* and 'Atg', respectively, which stands for 'autophagy-related'[99]. Many of these identified genes are found to be conserved between yeast, *Drosophila* and mammals. From herein, *Drosophila* genes will be stated in italic lower case: '*Atg',* and their encoded proteins also in lower case: 'Atg'. In reference to mammalian systems, these will be stated in capitals: '*ATG'* and 'ATG', for genes and proteins respectively. Table 1.1 presents a summary of *Drosophila Atg* encoded and core proteins, highlighting the particular stage in the pathway to which they are associated to.

Table 1.1 The Core Autophagy Proteins in *Drosophila*. The core autophagy machinery is well conserved throughout the animal kingdom. Here presented alongside *Drosophila* Atg protein, are the mammalian homologs.

***Drosophila* protein**	**Mammalian homologue**	**Core Protein Activity/Function**
Nutrient signalling pathway		
Rheb	Rheb	Ras small GTPase family[27]
dTSC1, dTSC2	TSC1, TSC2 (also referred to as Hamartin and Tuberin)	GTPase-activating protein[27], TOR signalling regulator[100]

TOR	mTOR	PIK-family Ser/Thr protein kinase[27]
SNFAγ	AMPK (γ-subunit)	Inhibition of TOR/phosphorylation of Atg1[74,80,96]
Autophagosome Induction		
Atg1	ULK1	Serine/threonine kinase involved in initiation of isolation membrane[27,101]
Atg13	ATG13	Component of Atg1 complex[101]
Atg17	FIP200/RB1CC1	Component of Atg1 complex[102]
Atg101	ATG101	Component of Atg1 complex[103]
Autophagosome nucleation		
Vsp34	VSP34 (PI3K class III/PIK3)	Initiates elongation of the pre-autophagosomal membrane[104]
Atg6	BECLIN1	Component of VPS34 complex, Serine/threonine protein kinase[27,105]
Atg14	ATG14	Component of VPS34 complex[106]
UVRAG	UVRAG	Component of VPS34 complex[106] (ATG14 and UVRAG are mutually exclusive VSP34 subunits[107])
Vsp15	VSP15	Component of VPS34 complex[108]

Rubicon	RUBCN	Component of VPS34 complex[109]
Autophagosome expansion		
Atg8a, Atg8b	GABARAP, GABARAPL1/2, LC3A, LC3B, LC3B2, LC3C GATE16, MAP1LC3A/B	Ubiquitin-like protein which conjugates with phosphatidylethanolamine (PE) and localises to the isolation membrane[27,105]
Atg3	ATG3	E2-like enzyme, conjugates Atg8[27,105]
Atg4	ATG4A, ATG4B, ATG4C, ATG4D	Cysteine protease, cleaves C-terminal elements of Atg8[110]
Atg5	ATG5	Conjugates Atg12[27,111]
Atg7	ATG7	E1-like enzyme, involved in the conjugation of Atg8 and Atg12[27,105]
Atg10	ATG10	E2-like enzyme, conjugates Atg12[112]
Atg12	ATG12	Ubiquitin-like protein that conjugates with Atg5, participates in Atg8 lipidation[27]
Atg16	ATG16L1, ATG16L2	Interacts with Atg5-Atg12 complex, mediates the formation of atg8 lipidation[113,114]
PAS complex		
Atg18a, Atg18b	WIPI1, WIPI2, WIPI3, WIPI4	PI3P binding[27,111] , Transport of Atg9 from PAS[115]
Atg2	ATG2A, ATG2B	Atg18-interacting protein[27,111], Transport of Atg9 from PAS[115]

Atg9	ATG9A, ATG9B	Transmembrane protein that supplies membrane material for autophagosome formation[116]

1.5.2 Autophagy Induction: Activation of the ULK1/Atg1 complex

Initiation of phagophore formation begins when the ULK1/Atg1 kinase complex is activated; an event which corresponds to the translocation of the complex to a discrete location on the ER (although other locations have been suggested), marked by the presence of ATG9/Atg9[117]. This section will discuss how the important event of ULK1/Atg1 complex activation is governed in response to nutrient availability across yeast, *Drosophila* and mammalian cells.

As in mammalian cells, TOR integrates information from multiple upstream pathways to further increase net cell growth by actively repressing autophagy via phosphorylation and inhibition of Atg1 in both *Drosophila* and yeast[31]. As described in section 1.4.3, mammalian AMPK functions to inhibit mTOR; firstly, through phosphorylation of mTCS2 which subsequently renders Rheb, the major regulator of TOR, inactive; and secondly, via direct phosphorylation of its scaffold sub-unit Raptor[76]. However, the exact mechanisms by which SNFAγ and Snf1, the *Drosophila* and yeast homologs of AMPK, mediate autophagy are yet to be fully elucidated. On the contrary, evidence strongly suggests that these homologs are likely to function in a similar way and thus SNFAγ and Snf1 are considered possible negative regulators of TOR in their respective species[85].

It must be noted that in the context of starvation-induced autophagy, the roles of TOR and the Atg1 complex in *Drosophila,* have been determined in the larval fat body[27]. Here, during starvation conditions, TOR inhibition results in the loss of Atg1 phosphorylation, which in turn activates the initiation complex, consisting of Atg1, Atg13, Atg17 and Atg101 in *Drosophila.* Under nutrient deplete conditions, loss of TOR-mediated phosphorylation allows Atg1 to undergo autophosphorylation and to drive hyper-phosphorylation of Atg13[101]. This shift in activity is directly mediated by the scaffold protein Atg17 (homolog to mammalian RB1CC1/FIP200), which is crucial for the kinase activity of Atg1[102] and regulation of autophagy through its ability to form a complex with Atg1 and Atg13[118]. Atg101 is a component of the

Atg1 complex which is present in most higher eukaryotes, except for in yeast; resulting it in being far less studied than its fellow complex members[119]. Recently however, the crystal structure of the Atg13-Atg101 complex has been determined and found to stabilise Atg1 and Atg13 within the initiation complex, as well as facilitating the recruitment of downstream substrates. Thus providing evidence that Atg101 is essential for starvation induced autophagy in *Drosophila*[120] and mammalian cells[121].

In *Drosophila* and mammalian cells Atg1/ULK1 and Atg13/ATG13 are phosphorylated by both (m)TORC1 and Atg1/ULK1 in full nutrient conditions[121,122], and Atg1/ULK1 in starved conditions[123] (Fig. 1.7). In yeast, TORC1 functions exclusively to hyper-phosphorylate Atg13 in full nutrient conditions, whilst Atg1 is auto-phosphorylated in starved conditions (Fig 1.7)[124]. In the case of *Drosophila*, Atg1 is more sensitive to dTORC1 signalling in fed conditions, whereas phosphorylation of Atg13 is highest under starved condition, where Atg1 activity is elevated[61]. The observation that Atg13 is phosphorylated by both (m/d)TORC1 and Atg1 in fed conditions has led to the suggestion that phosphorylation by one of these kinases serves as a priming event for the actions of the other[123]. Intriguingly however, there is conflicting evidence that Atg13 acts upstream and downstream of Atg1. An upstream role is hinted at by observations that Atg13 is able to localise to autophagosomes independent of Atg1, and in its ability to activate Atg1[123]. Conversely, Atg13 has been implied to act as a substrate for Atg1-dependant phosphorylation which raises the possibility that Atg13 may also act to transduce signals downstream of Atg1[123]. Furthermore, evidence suggests that Atg13 plays an analogous role in regards to mTOR-signalling, in that it has the ability to switch between states of promoting and inhibiting autophagy, thereby sharpening its response to changes in nutrients conditions[123]. Atg1 has also has been reported to directly phosphorylate mTORC1, acting as a negative feedback mechanism to inhibit cell growth and further enhance autophagy induction[111,122]. This suggests that autophagy induction may require a balanced ratio of Atg1 and Atg13, and disruption of this balance by overexpression of either protein may lead to autophagic deficiency[61].

Several studies across species have identified ULK1/Atg1 as the central target of (m/d)TORC1 in directing the formation of autophagosomes, with loss of ULK1/Atg1 resulting in the loss of autophagosome formation[27,101,124]. However, there are some key differences in how basal autophagy is maintained between yeast and other higher eukaryotes. For example, in contrast to the phosphorylation seen in mammals, and hyper-phosphorylation seen in *Drosophila,* under

starvation conditions; Atg13 is dephosphorylated in yeast allowing it to bind with a higher affinity Atg1 and induce autophagy[124]. It is likely that phosphorylation of Atg13 is dependent more on TORC1 in yeast, and to a greater extent on Atg1 in *Drosophila*[31]. Interestingly, it was well established for quite some time that dephosphorylation of Atg13 was required for its interaction with Atg1 in yeast, which led to a model in which Atg13 binds to Atg1, exclusively in starvation conditions[124]. However, the function of Atg1 has recently been discovered to require the binding of Atg13 under full nutrient conditions in yeast cells [125], with its binding affinity regulated by nutrient signalling [126]. Furthermore, the Atg1 core complex differs slightly in yeast to that of *Drosophila* and mammals, with the core complex consisting of Atg1, Atg13, Atg17-Atg29-Atg31 and Atg11 (Fig 1.7). Atg17-Atg29-Atg31 and Atg11 constitute the two scaffold proteins in this complex, with no reported homologs of Atg29 or Atg31 in *Drosophila* or mammalian cells[127]. Starvation, and inhibition of TORC1, allows for the binding of Atg13 and Atg17, which goes on to form a stable complex with Atg29 and Atg31[128]. Under nutrient rich conditions Atg1 and TORC1 are able to physically bind in mammalian and *Drosophila* cells[101], however no such interaction is reported in yeast.

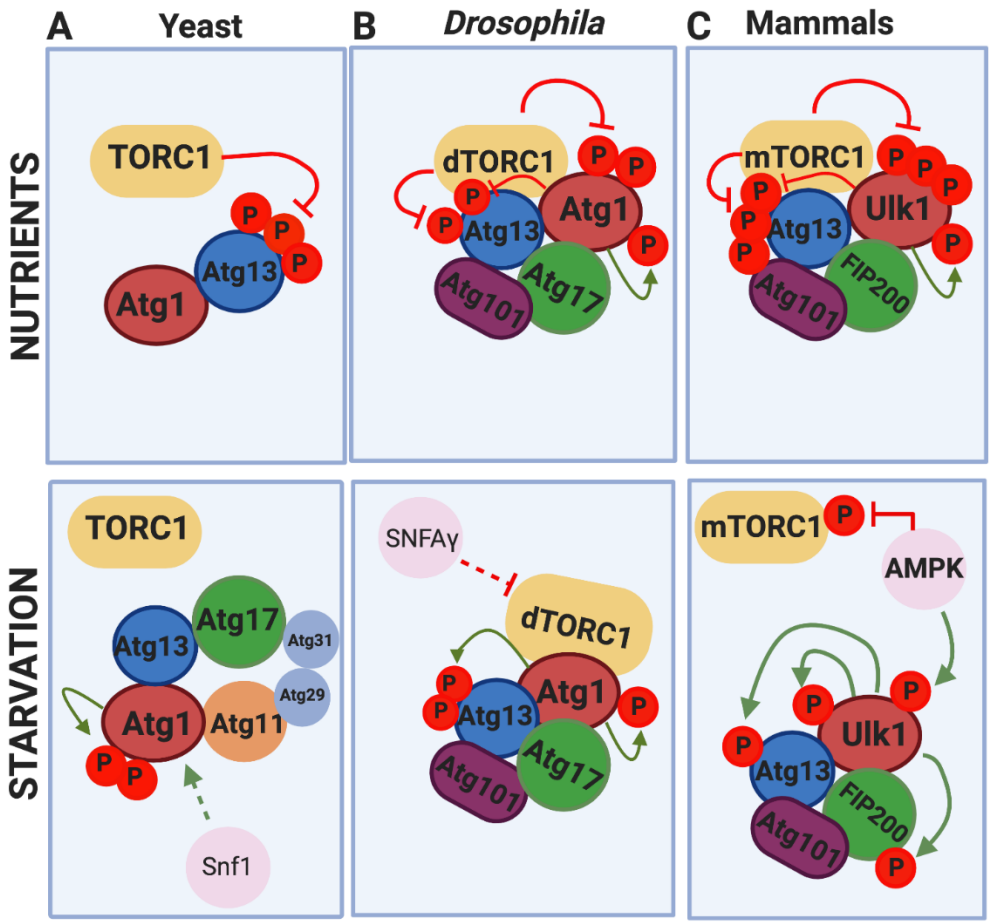

Figure 1.7 Regulation of ULK1/Atg1 complex in yeast, *Drosophila* and mammals. (A) Under nutrient rich conditions, activated TORC1 inhibits autophagy induction in yeast through the direct phosphorylation of Atg13. Inactivation of TORC1 in starvation conditions, results in dephosphorylation of Atg13, leading to scaffold recruitment (Atg17–Atg29–Atg31 and Atg11) and formation of the active kinase complex. Snf1, the yeast ortholog of mammalian AMPK, is presumed likely to regulate the activation of Atg1[83]. (B) Under nutrient rich conditions, dTORC1 functions to phosphorylate both Atg1 and Atg13. In a starved environment, these sites are dephosphorylated. Here Atg1 kinase activity is elevated, leading to an increased autophosphorylation, and phosphorylation of Atg13. SnfAγ, the *Drosophila* ortholog of the mammalian AMPK gamma subunit, a known inducer of autophagy, is likely to inhibit the function of dTORC1 in a similar fashion to that seen in its mammalian counterpart. (C) Similar to *Drosophila*, the mammalian ULK1 complex shows little change in composition in response to nutrient status, however mTOR has higher affinity for the Atg1 complex under fed conditions. ULK1 and Atg13 are both substrates of mTOR and Ulk1 in fed conditions, as in their *Drosophila* counterparts. Starvation leads to decreased phosphorylation of Atg13 due to lower mTOR activity as well as higher Atg1-dependent phosphorylation of FIP200[129]. An alternative mechanism in mammalian cells is apparent in which AMPK functions to phosphorylate ULK1, thereby activating it. AMPK also activates the ULK1 complex indirectly through the inactivation of mTORC1 via phosphorylation.

1.5.3 How does Atg1/ULK1 complex activity facilitate the induction of autophagy?

The assembly of the Atg1/ULK1 complex constitutes the most upstream stage of autophagy and has been found to have two distinct roles in the induction of autophagy. Firstly as a scaffold for the kinase-independent recruitment of downstream Atg proteins to the PAS[12]. Various sources have been proposed to be the origin of the autophagosomal membrane, including the ER[2], Golgi complex and mitochondria[3]. In mammalian cells recruitment of the VSP34 (Vascular Protein 34) complex by the ULK1 complex has been reported; with ATG101 shown to directly bind the PI3K domain[130], and the ULK1 complex shown to bind ATG14, a VSP34 subunit[131]. Recruitment at the ER has been reported to generate structures called omegosomes, which are highly conserved and shown to drive the recruitment of PI3P (Phosphatidylinositol 3-Phosphate), thus driving a change in lipid composition to form the phagophore[132]. Similarly, in *Drosophila,* TOR/Atg1 signalling has also been shown to mediate the starvation-induced recruitment of PI3P to nascent autophagosomes through recruitment of the Vsp34 complex[108]. Furthermore, upon the newly forming phagophore ATG101 plays an important role in WIPI recruitment, although a direct interaction has not been shown[133]. The recruitment of the ATG12-ATG5-ATG16 complex to the isolation membrane is regulated by FIP200[134], and dependant on PI3P produced by PI3K complex I[135,136]. Secondly the ULK1 complex is responsible for the kinase-dependant function in autophagosome formation, which is mediated by the phosphorylation of downstream substrates: BECLIN-1[137], ATG14[131], VPS34[138]; all of which are members of the VP3S4 complex. ULK1 has also been shown to phosphorylate AMBRA-1 upon stavation[139], which functions to interact with and activate BECLIN-1, which in turn activates the VPS34 complex.

An important role of the ULK1 complex subunits FIP200, ULK1 and ATG13 , is their ability to bind to Atg8-family proteins which decorate the nascent autophagosomal membranes[140]. ULK1 complex subunits have thus been found to contain an LC3 interacting region (LIR), which mediate their interaction with Atg8, with a strong preference for GABARAP. Importantly in the case of ULK1, it's LIR motif is required for starvation induced association with autophagosomes[125,140]. Similarly, in yeast and *Drosophila* Atg1 interact with their respective Atg8 proteins, demonstrating the evolutionary conservation interaction[140]. These results provide evidence that suggests that Atg8 acts as a scaffold for the recruitment of ULK1/Atg1 at the phagophore, whereby it can contribute to the formation of the autophagosome.

Atg1 and ULK1 have both been shown to regulate the actin motor protein myosin II in the induction of autophagy upon starvation[141]. In *Drosophila*, Atg1 directly phosphorylates and activates the myosin light-chain kinas Sqa (Spaghetti-squash Activator). ULK1 was also found to have the same effect on the mammalian homolog of Sqa, ZIPK (Zipper-Interacting Protein Kinase). Deletion of myosin II, Sqa and ZIPK resulted in compromised autophagosome formation in a starved setting. Interestingly, the same study found that ZIPK and myosin II had a critical role in cellular responses to nutrient deprivation through its promotion of ATG9 membrane trafficking during the early stages of autophagosome formation[141]. This is a similar regulatory process as seen with Atg1 in yeast, where Atg1 and Atg17 mediate the cycling of Atg9 from peripheral structures to the PAS[142]. Further to this, ATG13 functions to form a scaffold at the PAS via its C-terminal disordered region, which subsequently recruits ATG9 vesicles via its N-terminal HORMA (from Hop1, Rev7, and Mad2) domain, where they become part of the autophagosomal membrane[143].

1.5.4 Atg8-family proteins and the role of ubiquitin

It must be noted that many of the processes conducted by autophagy are tightly regulated by ubiquitin (Ub); a small regulatory protein which is remarkably found in the majority of tissues in eukaryotic organisms. Ubiquitination is an ATP-dependent enzymatic process that involves the covalent conjugate of the highly conserved 8 kDa Ub peptide to lysine residues of a target protein[144]. The ubiquitination reaction requires three classes of enzyme: ubiquitin-activating enzymes (E1), ubiquitin-conjugating enzymes (E2), and substrate-specific ubiquitin ligases (E3). Both Atg8-family and Atg12 constitute Ubl proteins which are essential to the process of autophagosome nucleation and expansion, which points towards common ancestry roots between the core autophagy and ubiquitination machinery.

The Atg8 gene family encode ubiquitin-like proteins that share a similar structure consisting of two amino-terminal α helices and a ubiquitin-like core[145]. Mammals have many Atg8-family paralogues (Table1.1) ; with *Drosophila* Atg8a showing most similarity to the γ-aminobutyric acid receptor-associated protein, GABARAP[145]. Along with Atg8a, Atg8b represents the other *Drosophila* Atg8-family protein; both of which localise to autophagic structures[27]. Atg8a is highly expressed in all tissues, whereas Atg8b only shows strong expression in the testis[146], therefore most assays rely on Atg8a.

Atg8-family proteins are of particular interest for those who study autophagic processes as they have become established as an important marker for the induction of autophagy[22]. As lipidated Atg8 (known as Atg8-II) undergo a unique ubiquitin-like conjugation to PE (Phosphatidylethanolamine) on the autophagic membrane, it is possible to visualise the presence of these structures by using tagged reporters or by immunostaining using antibodies against endogenous proteins[147]. Similarly to yeast and mammalians, the Atg8 conjugative system in *Drosophila* is first processed by the cysteine protease Atg4 which functions to cleave the C-terminal arginine of Atg8 (referred to as Atg8-I in unconjugated form) to reveal a glycine residue[112]. The E1 enzyme Atg7 functions to activate Atg8 transferring it to the E2 enzyme Atg3 (also known as Aut1 in *Drosophila*)[112]. Facilitated by the Atg12-Atg5-Atg16 complex in an E3-like manner, Atg8-family proteins are conjugated to the lipid target PE via an amide bond[148], yielding Atg8-II (section 1.5.5.3). The resulting modified protein is now capable of anchoring itself to either side of phospholipid membrane of the phagophore via its lipid moiety[149,150]. When the phagophore matures into an autophagosome, a proportion of Atg8 is trapped inside and is eventually degraded[149]. Importantly, this process is essential for the formation of the autophagosome, and allows for substrate uptake upon binding to several autophagy receptors[151].

It must be noted that Atg8-like proteins are not exclusively responsible for the formation of autophagosomes, as classically thought. They also contribute to autophagosome extension and closure around large substrates, fusion of autophagosomes and lysosomes, and degradation of the inner autophagosomal membranes[152,153]. Notably, the lipidation of Atg8 determines the size of the autophagosome, which may result from its ability to determine membrane curvature[154]. Furthermore, it has been made apparent that the absence of Atg8 across species does not affect the function of the other core machinery, however it does seem to greatly reduce the efficiency of the process[155]. Away from its cytosolic responsibilities, Atg8-family proteins have been reported to reside in the nucleus[156–159]. Much of its nuclear functioning remain unclear and will be discussed in more detail in section 1.9.

1.5.5 Autophagosome Formation

In contrast to other processes of vesicle formation in endomembrane trafficking, the double-membraned autophagosome assembles at the PAS by the addition of new membranes, rather than forming from the surfaces of pre-existing organelles or membranes. The steps of autophagosome formation are described in the following sections, with an overview of the processes presented in Figure 1.8.

1.5.5.1 Nucleation

The first step of autophagosome formation is a process known as nucleation, whereby proteins and lipids are recruited in order to prime for synthesis of the phagophore membrane.

Nucleation of the phagophore relies on the generation of PI3P at the PAS and/or phagophore membrane by the protein complex containing a catalytic PI3K subunit. Although there is only one PI3K in yeast, three classes have been characterized in *Drosophila* and mammals, with mutations in Vsp34/VSP34; a type III PI3K (also referred to as PIK3) responsible for PI3P generation, shown to block the formation of autophagosomes[108]. Wortmannin and 3-methyladenine are established inhibitors of autophagy and function by directly targeting Vps34[160]. The core components of the Vps34 complex include Atg6 (mammalian homolog BECLIN-1), a catalytic sub-unit (Vps34), and it's regulatory subunit Vps15 (Vacuolar Protein Sorting 15); which has a serine/threonine domain responsible for phosphorylating Vps34[161] (Fig 1.8). Both Atg6 and Vps34 been shown to have a crucial role for the induction of autophagy in *Drosophila*[108]. Depending on subcellular context the Vps34 complex is able to bind either Atg14 or UVRAG (UV radiation resistance-gene associated protein); referred to as PI3K3C3-C1 and PI3K3C3-C2, respectively[106]. The Atg14-containing complex known to have a role in the formation of autophagosomes in *Drosophila*[106]. This has also been shown in mammalian cells, where it has also been observed that the formation of ATG14-puncta is dependent on the ULK1-FIP200 complex[136]; thus confirming the hierarchical status of the ATG14 in respect to the ULK1 complex. In *Drosophila* the UVRAG-containing complex has a key role endolysosomal degradation but is largely dispensable in the case of autophagy[106]. RUBCN (Run domain Beclin-1 interacting and cysteine-rich containing protein), a negative regulator of autophagy, functions by forming a complex with the VPS34 complex in mammals to suppress autophagosome-lysosome fusion[162]. Recently it has been shown that reductions in Rubicon levels in *Drosophila*, mouse and worm tissue led to extended lifespan, hinting that the autophagy related function of the protein is evolutionally conserved[109].

In mammalian cells, AMPK-mediated phosphorylation functions to activate BECLIN-1 in the setting of glucose starvation, thereby increasing its affinity to bind to VPS34 and ATG14[137]. Furthermore, in energy depleted conditions AMPK functions to phosphorylate VPS34 at residues Thr163 and Ser167, thus inhibiting it's non-autophagic activity and promoting the activity of pro-autophagic complexes[138]. The AMPK-dependant activation of ULK1, which phosphorylates BECLIN-1, VPS34 and ATG14, further promotes the activity of the VPS34

complex[163]. Interestingly, studies in mammalian cells have suggested that VPS34 may also transduce activating nutrient signals to mTOR[164]. However, such modes of regulation are not apparent in *Drosophila* larval fat body*;* with *vps34* shown to be necessary for the induction of autophagy under starvation conditions, but *vps34* null mutants not affecting TOR signalling[108]. This suggests that Vps34 does not act upstream of dTOR in *Drosophila*. However, it is not clear if these differences reflect evolutionary differences, or cell-context specific differences between the studies. It was revealed in the same study, that the recruitment of Vps34 to newly formed autophagosomes, was dependent on the Atg1/dTOR signalling pathway in *Drosophila*[108], presumably where it functions in the localised production of PI3P.

1.5.5.2 The Pre-autophagosomal Complex and Atg9 Cycling

The PI3P found on the phagophore and autophagosome membranes functions to recruit and activate phospholipid effectors[147]. One class of such proteins includes the Metazoan homologs of the yeast WD40 domain, Atg18[165]. A diverse range of Atg18-like proteins are found in eukaryotes; with four known in mammals: WIPI1, WIPI2, WIPI3 and WIPI4[166,167]. Of these, WIPI2 and WIPI4 have been shown to promote autophagosome formation in cells[166]. In *Drosophila*, there are two Atg18 paralogs, referred to as Atg18a and Atg18b, with only the former shown to be required for the formation of autophagosome[116]. The WD40 domain beta-propeller of Atg18a has been found to be the region responsible for its interaction with PI3P on autophagic membranes in *Drosophila*[168] (Fig 1.8), however role of Atg18b in autophagy remains unknown.

In yeast, it is well established that Atg18 forms a complex with Atg2, where acting in parallel to the Atg8-system it functions to recruit Atg9 to the PAS[155]. In *Drosophila,* Atg18a also shows an interaction with Atg2, although more weakly in comparison to its paralog Atg18b[116]. In contrast to yeast, yet consistent with proposed models in mammals and worms, *Drosophila* Atg18 appears to function upstream of Atg8a recruitment during the formation of the phagophore; with Atg8a positive puncta localisation lost in Atg18 mutants[116]. Interestingly, Atg2 was found not to be required for the formation of Atg8a positive puncta formation in the larval fat body[116,169]. Taken together, these observations provide evidence of the respective upstream and downstream activity of Atg18 and Atg2 in *Drosophila*, in relation to Atg8a recruitment and autophagosome formation.

Atg9 is the only known evolutionary conserved transmembrane protein known amongst the *Atg* gene products. It is likely to have a role in the supply of initial vesicles for phagophore nucleation from multiple membrane sources including the ER, endosomes, plasma membrane and Golgi[170], cycling between these sources and the pre-autophogosomal structure (Fig 1.8). Atg9 is widely considered an upstream factor in the Atg protein hierarchy found in higher eukaryotes[116] and has been well established to translocate to autophagic membranes during the induction of autophagy[171]. In mammalian cells, under nutrient depleted conditions AMPK has been shown to directly phosphorylate ATG9 at Ser76, which is interestingly also the site at which ULK1 targets ATG9 in the environment of metabolic stress[172]. These phosphorylation events result in the recruitment of ATG9 (and ATG9 positive vesicles) to LC3-positive autophagosomes, thereby increasing biogenesis, likely through the supply of membrane material. Inversely, under basal conditions phosphorylation of ATG9 is maintained at low levels by AMPK and ULK1[172].

In yeast, the cycling role of Atg9 is regulated by the Atg18-Atg2 complex[155]. In *Drosophila*, Atg9 also interacts with both Atg18a and Atg2 (Fig 1.8), which is likely to be mediated via the WD40 domain beta-propeller of Atg18a[168]. However, reflective of their respective hierarchical position, Atg18 and Atg2 seemingly have different roles in the recruitment of Atg9 in starvation conditions. This is highlighted by protein aggregation positive for Ref(2)P (homolog of mammalian p62; a selective autophagy receptors which mediate interaction with Atg8a and thus select cargo for degradation), found to show an accumulation of Atg9 in *Atg2* mutants, alongside other downstream players Atg7 and Atg8a[3],[116]. However, no accumulation of Atg9 was apparent on Ref(2)P positive aggregates in cells which lack Atg18 or the lipid kinase responsible for PI3P production, Vsp34[116]. Taken together this highlights, that Atg18, independent of Atg2, plays an important role in phagophore nucleation by facilitating the recruitment of Atg9-containing vesicles to Ref(2)P for selective degradation in *Drosophila*.

1.5.5.3 Elongation, expansion and fusion

Subsequent to nucleation, two interrelated ubiquitin-like (Ubl) conjugate systems formed; firstly the Atg5-Atg12 interacts non-covalently with Atg16 to form a multimeric complete, with the formation of this complex acting as an E3 ligase in the reaction between PE and Atg8a[155] (Fig

[3] It must be noted that Atg8b has also been found to localise to autophagic structures[27], however due to its low expression in many tissue types it has not been as explored as Atg8a.

1.8). These play an important role in the elongation and expansion of the forming autophagosome, along with the shuttling action of Atg9 between the PAS and peripheral structures in order to provide supply membrane material[173].

The two Ubl proteins, Atg12 and Atg8a, undergo conjugation in a similar manner as ubiquitin. Atg12 is activated by Atg7, an E1 activating enzyme, and is subsequently transferred to Atg10 (Fig 1.8). This E2-like enzyme functions to catalyse the formation of an Atg12-Atg5 conjugate[112], in which Atg12 is covalently attached to an internal lysine of Atg5[31]. Atg5 contains two ubiquitin related domains which flank a helical region[148]. Unlike ubiquitination, the Atg12-Atg5 conjugate is constitutive, and has yet found to be reversible or not require the action of a specific E3[174]. Atg5-Atg12 then interacts with the coiled-coil protein Atg16; with the newly conjugated Atg12-Atg5-Atg16 multimeric complex forming into a tetramer by self-oligomerisation, thus enabling it to attach to the phagophore[175] (Fig 1.8). Here, the Atg5-Atg12-Atg16 complex functions to enhance the covalent conjugation of Atg8a to the membrane lipid PE, and proceeds to dissociate from the membrane once the autophagosome has formed[13].

The second conjugation system also requires the activity of Atg7 and the E2-like conjugating enzyme Atg3[112]. As previously described in section 1.5.2 , cytosolic Atg8a is modified by the attachment of PE following its cleavage by Atg4[112] (Fig 1.8). This step results in the localization of Atg8a-PE to the isolation membrane, and has been proposed to contribute to elongation of the autophagic membrane[176]. This is thought to partly be as a result of the ability of Atg8 to recruit cargo, thus increasing the density at the site of assembly and influencing membrane expansion and elongation.

Atg8a remains associated with the autophagosome until it is trafficked to the lysosome; where the outer membrane of the autophagosome fuses with the lysosome to form the autolysosome, and Atg4 subsequently releases Atg8a from PE[112]. The mechanisms of the other Atg proteins upon fusion however remain unknown. Once autophagosomes have enclosed autophagy substrates, they can fuse with lysosomes to form autolysosomes. The best known tether in autophagosome-lysosome fusion is the multi-subunit HOPS (Homotypic fusion and vacuole sorting) complex, which is conserved in metazoan organisms[177]. HOPS is essential not for just autophagosome-lysosome fusion, but for almost all lysosomal-fusion events[177] (Fig 1.8). These have been shown to bind to PI3P on the autophagic membrane and facilitate fusion to the lysosome in a process catalysed by SNARE (Soluble N-ethylmaleimide-sensitive factor

Activating Receptor) proteins[177]. Studies in mammalian and *Drosophila* cells have shown that SNAREs Vamp8 and Vamp7 (*Drosophila* only Vamp7), Syntaxin17 (STX17/Syx17 in *Drosophila*) and SNAP-29 (Ubisnap in *Drosophila*) form a SNARE complex that directly mediate autophagosome-lysosome fusion[169,178]. HOPS have also been shown to bind to multiple small GTPases to promote autophagosome-lysosome fusion, of which Rab7 (Ypt7 in yeast), Rab2A (Rab2 in *Drosophila*), and *Drosophila* Arl8 are best characterized so far[177]. Interestingly, autophagosome fusion in *Drosophila* appears to depend on genes which are required for endosomal biogenesis; with mutations in the ESCRT machinery, resulting in an accumulation of LAMP-1-positive structures which are distinct from Atg8-positive structures, thus indicating a failure in autophagosome to lysosome fusion[179]. Furthermore, mutations in an endosomal PI3P 5-kinase, *fab1,* lead to accumulation of autolysosomes in the *Drosophila* fat body which fail to degrade their contents; hinting that it plays an important role in autophagosome maturation[179].

Following lysosomal fusion, the inner autophagosomal membrane (supported by Atg conjugation systems) dissembles, and degradation of the cargo proceeds as the lysosomal lumen becomes acidified by the action of an ATP-dependant proton pump[180]. The resulting small molecules, which have been broken down through the action of hydrolases such as cathepsins[181], are transported back to the cytosol where they work to fuel a number of synthetic energy producing pathways.

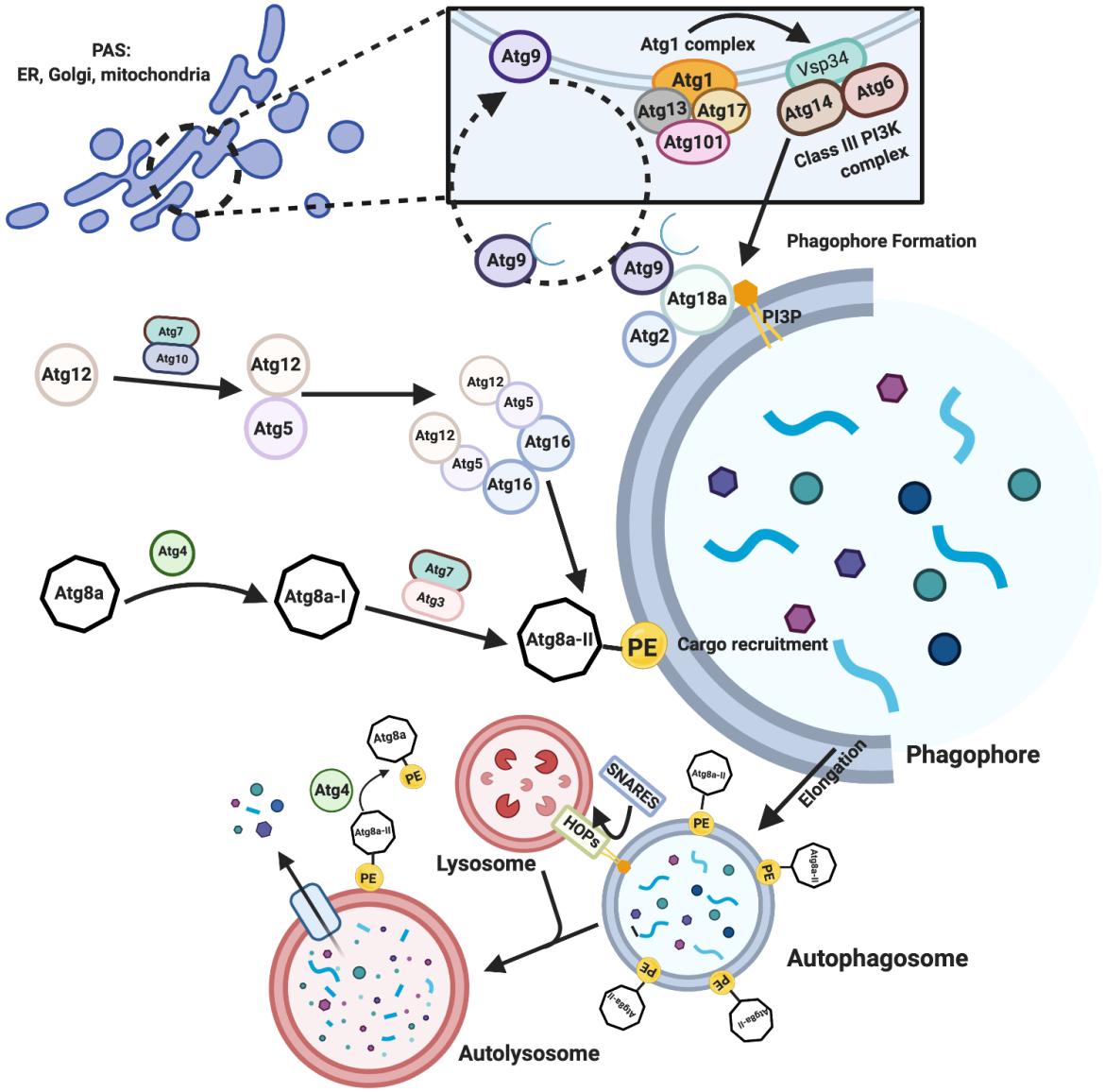

Figure 1.8 Overview of the Core Autophagic Machinery in *Drosophila*.
Starvation induces the activation of the Atg1 complex (Atg1, Atg13, Atg17 and Atg101) at the PAS, which subsequently recruits the class III PI3K (Vsp34) complex (Vsp43, Atg14 and Atg6). Aided by the delivery of membrane material via the cycling of Atg9, the Vsp34 containing complex initiates the construction of the phagophore through the production of PI3P. Here, PI3P is able to associate with the effector protein Atg18 which facilitates the cycling of Atg9. Atg18 is also found to form a complex with Atg2 at this site. The ubiquitin like Atg8 protein is cleaved by the cysteine proteases Atg4 and are subsequently lipidated by the E1-like Atg7 and E2-like Atg3, resulting in the localization of Atg8-PE to the isolation membrane. In parallel to this process, the action o E1-like and E2-like Atg7 and Atg10 aid in the formation of the Atg5-Atg12-Atg16 conjugation at the phagophore membrane, which enhances the covalent conjugation of Atg8 to the membrane lipid PE. Autophagic cargo, which include damaged organelles, aggregated proteins and pathogens are ubiquitinated and are shuttled to the phagophore by selective autophagy receptors. The phagophore membrane begins to elongate and forms the double membraned autophagosome; which is decorated with Atg8 conjugates at its surface. The autophagosome tethers to the lysosome via HOPs, in a reaction catalysed by the SNARE complex: Vamp7-Syx17-Ubisnap. The resulting autolysosome functions to dissemble and degrade the loaded cargo as the lysosomal lumen becomes acidified, with the resulting small molecules transported back into the cytosol.

1.6 Selective Autophagy

Autophagy was initially characterized as a bulk degradation pathway, which served to recycle building blocks, to compensate for the lack of nutrients, in a non-selective manner. However, it is now well established that autophagy is a highly regulated process which, not only acts in response to cellular stress, but also in the contribution to intracellular homeostasis, by selectively degrading cargo material such as; damaged mitochondria[182], excess peroxisomes[183], invading pathogens such as bacteria[184] and viruses[185], ribosomes[186] and protein aggregates[187].

1.6.1 Selective Autophagy Receptors

Atg8-family proteins function as anchor points on the autophagic membrane (Fig. 1.9), here they serve to recruit cargo through the binding of SAR (Selective Autophagy Receptor) proteins. Ubiquitination has long been recognized as a key regulator to determine protein fate by tagging proteins for proteasomal degradation[188]; similarly in some cases here, SARs recognise cargo by interacting with their polyubiquitin chains, thereby, acting as a degradation signal[189]. Examples of pathways in which SARs, such as mammalian p62/Sequestosome 1, NIBR1, OPTN and NDP2, function to target substrates in a ubiquitin dependant manner include aggrephagy[187] (degradation of aberrant protein aggregates and disease-related inclusions), mitophagy[190] (mitochondria), xenophagy[184] (invasive pathogens) and pexophagy[183] (peroxisomes). However, some mammalian SARs within the mitophagy[191], xenophagy[192] and pexophagy[183] pathways have been discovered to function ubiquitin independently. ER-phagy[193] (degradation of the endoplasmic reticulum), nucleophagy[194] (nuclear envelope) and glycophagy [195](glycogen particles) are all also examples of ubiquitin independent pathways.

In the case of Ub dependant selection, the cargo is recognised by a specific ligand-binding domain known as a UBD (Ubiquitin-Binding Domain), as well as a LIR motif, which mediates its interaction with Atg8- family proteins (Fig 1.9). OPTN also functions in a ubiquitin and LIR independent manner, with its C-terminal coiled-coil domain responsible for the binding of protein aggregates and the LIR mutant OPTN reported to have no influence on OPTN localisation to protein aggregates[196]. In mammalian mitophagy, the outer mitochondrial protein NIX (NIP3-like protein X) also functions in a Ub-independent manner by binding to mitochondria directly via a transmembrane domain, anchoring them to the phagophore membrane via a LIR domain which recruits Atg8-family proteins[182] (Fig 1.9).

The first receptor protein identified in mammals is p62/ SQSTM1 (Sequestosome 1). It was discovered in ubiquitylated protein aggregates and was characterised in its ability to selectively target protein aggregates to the autophagosome for degradation by virtue of its interaction with LC3[187]. The human p62 contains several structural and functional motifs including an LIR motif and a C-terminus UBA (Ubiquitin-associated) domain[29], and has since found to be function in xenophagy[184], zymophagy[197], midbody[198] and nucleic acid disposal[199], as well as aggrephagy[187]. The discovery of autophagy receptors such as p62/ SQSTM1 have given an invaluable insight into the way in which selective autophagy functions, highlighting the importance of Atg8-interacting proteins in the process of autophagy. In particular SARs have aided in the important discovery and characterisation of the LIR motif, which will be described in section 1.6.3 in more detail.

Ref(2)P (Refractory to Sigma P), represents the *Drosophila* orthologue to p62/SQSTM1. Like its mammalian counterpart, Ref(2)P harbours a C-terminal UBA domain, which is required for its binging to mono- and poly-Ub, and a putative LIR domain. Several lines of evidence indicated its role as a SAR in *Drosophila*; it has been reported that Ref(2)P forms a major component in protein aggregate in flies which are defective in autophagy[200] and those which have impaired proteasomal function[201]. Kenny (mammalian homolog IKKγ/NEMO) and Blue Cheese (mammalian homolog ALFY) represent the only other selective autophagy receptors characterised in *Drosophila*. The former functions to mediate autophagic degradation of the IκB kinase complex to control innate immune responses[202]. Bluecheese has been characterised as a selective aggregate clearance mediator[203].

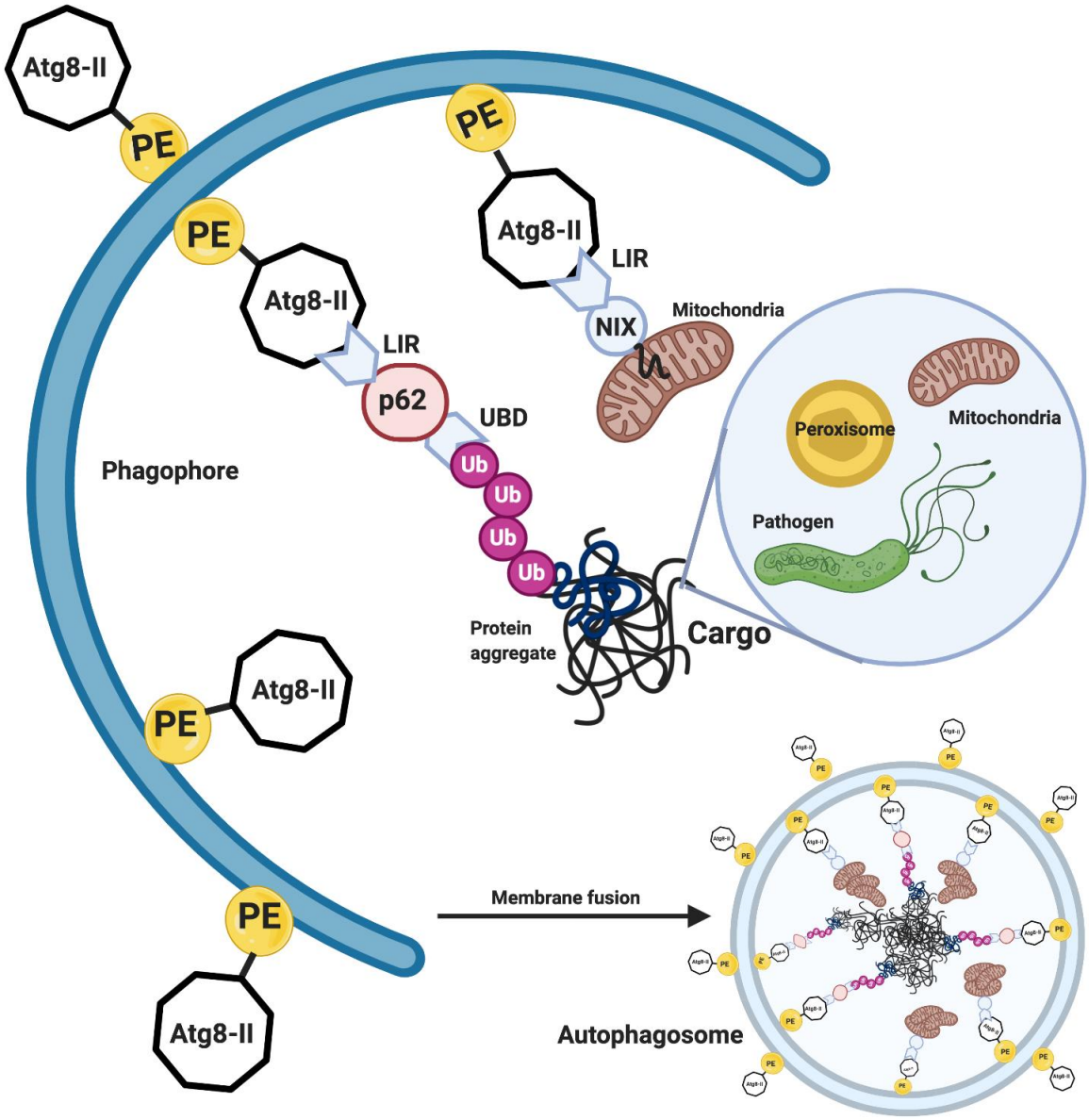

Figure 1.9 Exemplary Mechanisms of Cargo Selection.
Many selective autophagy receptors (such as p62) are dependent on the process of ubiquitination in which the highly conserved 8 kDa Ub peptide is covalently conjugated to the lysine residues of a target protein (both mono- and poly-ubiquitination). This allows these specialised autophagy receptor proteins to bind the cargo via an ubiquitin binding domain (UBD), and anchor it to the phagophore membrane via a LC3-interacting region (LIR); a conserved motif which governs the interaction with Atg8-family proteins. NIX acts as a cargo receptor for the delivery of mitochondria to the phagophore in an ubiquitin independent manner, whereby it directly binds mitochondria via a transmembrane domain. NIX interacts with Atg8-family proteins via a LIR. Atg8-family proteins are tethered to the phagophore membrane via PE conjugation. As a result, the cargo is anchored to the isolation membrane, thus once phagophore extends and fuses, the cargo is enclosed inside the resulting autophagosome, ready for lysosomal fusion and subsequent degradation.

1.6.2 The LIR motif

Various biochemical techniques such as nuclear magnetic resonance and X-ray crystallography, have been exploited on p62 and Atg19, another characterised autophagy receptor[204], in order to characterise the autophagy receptor core consensus motif: [W/F/Y]xx[L/I/V], coined the LIR motif [205] (Fig. 1.10 A[206]). Here, "x" stands for any amino acid, and is often flanked by diverse sequences containing Ser, Thr and/or the negatively charged residues Glu and/or Asp[207]. Importantly, LIR motifs are found to reside in intrinsically disordered regions of proteins, which undergoes disorder-to-order transition and forms a β-strand upon binding LC3[207]. This allows a large number of structurally and functionally diverse proteins to bind to the globular structure of LC3[207]. During interaction two hydrophobic pockets (known as HP1 and HP2) formed by the Ubl fold of LC3, bind the aromatic [W/F/Y] and the aliphatic [L/I/V] residues in the LIR motif [208] (Fig. 1.10 B,C[206]). The now-named LDS (LIR-Docking-Sites) are evolutionary conserved among Atg8-family proteins[209,193,199,20]. It was revealed that a basic groove in the N-terminal of the LDS site (HP1) was formed by Lys46, Arg47 and Lys48 in Atg8; with Lys46 and Lys48 found to be conserved throughout Atg8-family members[210]. In regards to the formation of HP2, this is composed of side chains Tyr49, Val51, Pro52, Leu55, Phe60 and Val63; with Y49 found to be conserved across Atg8-family members[211]. In *Drosophila* Atg8a, the LDS activity depends on two residues: Lys48 and Tyr49, with mutation of these residues shown to prevent it's interaction with LIR harbouring proteins Ref(2)P[212], Kenny[202], and as part of this study, Sequoia (Chapter 3).

It must be noted that the consensus sequence [W/F/Y]xx[L/I/V] can be found in many proteins, even if they don't interact with LC3-family proteins within the cell [213]. For this reason, the sequence has been relaxed and extended to 6 amino acids to integrate most the experimentally verified LIRs; with a LIR motif overlapping a region with the potential to transit from a disordered to an ordered state providing a reliable candidate for a functional binding motif[209]. This new sequence is now defined as the shortest sequence required for the interaction with an LC3-family protein; and was yielded from multiple alignments of LIR sequences from proteins, across species, described to interact in a LIR-dependant manner[209,214,215].

Importantly, the presence of a functional LIR motif spans beyond the role of receptor proteins. For example, members of the ULK1 complex ULK1 and ATG13 both contain LIR motifs, and bind to LC3, however they do not function as cargo receptors[125], thus suggesting that the LIR motif has more than one function in the autophagy paradigm. Given this, a growing number of Atg8 interactors have been named autophagy adaptors. These proteins are not degraded by

autophagy, and fulfil a diverse range of functions ranging from regulation of autophagosome fusion with the lysosome (e.g., PLEKHM1[216]) to autophagosome transport (e.g., FYCO1[217]). Also the formation of the Atg4b-LC3 complex, which functions to process LC3 regulation of PE conjugation and deconjugation is dependent on a LIR interaction[218]. Given this, the presence of the evolutionary conserved LIR has been branded as a hallmark of all LC3-interacting proteins[182,187,209,219–222]. This knowledge is the primary motive of this study and has proved important here in the identification of novel nuclear interactors of Atg8a.

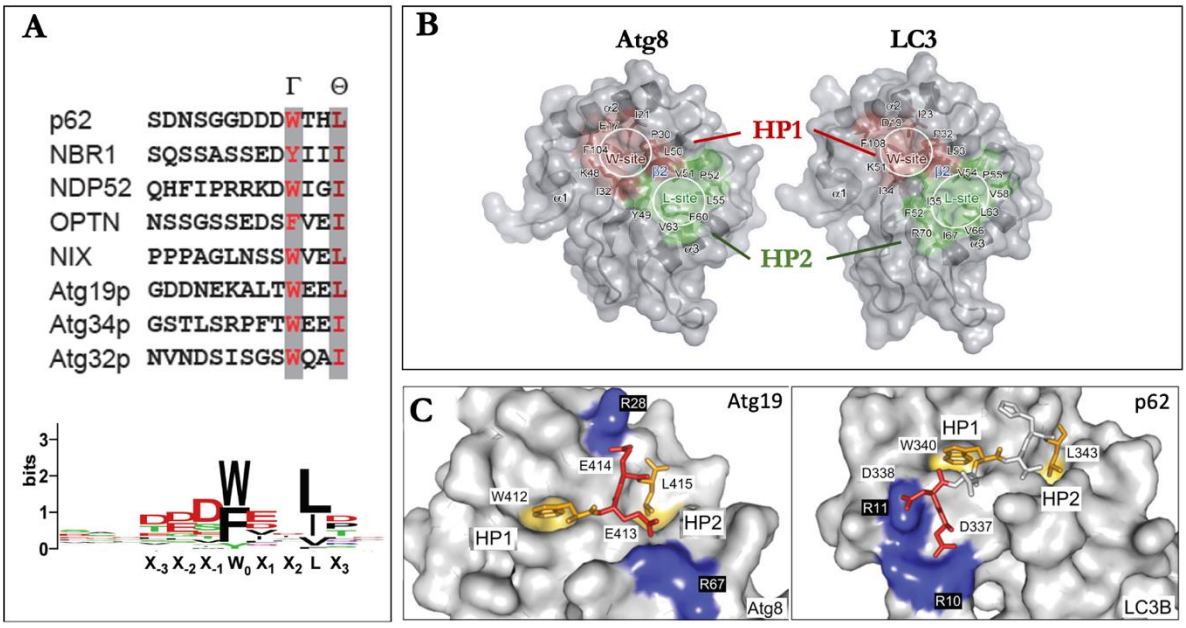

Figure 1.10 Discovery and Characterisation of the LIR-LDS Binding Interface.
(A) Sequence alignment of functional LIRs in autophagy receptors, conducted by Behrends and Fulda (2012)[223]. Alignment of 25 functional LIRs from 21 different proteins that all bind to Atg8-family proteins, conducted by Johansen and Lamark (2011), led to the generation of a consensus sequence logo[29]. (B) LIR binding sites are evolutionary conserved in Atg8-family proteins; the structure of *S. cerevisiae* Atg8 (left) and *Rattus norvegicus* LC3 (right) highlight the position of two hydrophobic pockets in their structure which are responsible for the binding and recognition Trp and Leu in the LIR (WxxL) motif: the sites are also labelled W-site and L-site. (C) Surface representation of yeast Atg8 bound to Atg19 LIR motif (left) and LC3B bound the LIR motif of p62 (right). Hydrophobic pocket 1 and 2 (HP1, HP2) are shown. Figure adapted from Birgisdottir *et al.,* (2013)[207].

1.6.3 The Ubiquitin-interacting motif

Recently, a new class of Atg8 interactors have been described which exploit the UIM (Ubiquitin-Interacting Motif) - like sequences for high affinity binding to an alternative region of Atg8. One of the first studies reporting on this phenomenon came in *Arabidopsis*. Here, the receptor RPN10, which serves to recruit inactive 26S proteasomes, was shown to bind ATG8 via an

unrelated UIM, instead of the canonical LIR[224]. Following from this, multiple assays with candidate UIM containing proteins were conducted alongside unbiased screens, which subsequently identified a large collection of UIM-based ATG8 interactors in plants, yeast, and humans[225]. The amino acid sequence responsible for binding the UIM was also established to be conserved across Atg8-family proteins in a range of species, including *Drosophila* Atg8a (Fig. 1.11, A[226]). This now-named UDS (Ubiquitin-Docking Site), contains a conserved phenylalanine surrounded by hydrophobic residues[225]. Mapping of the UDS region onto the 3-dimensional structure of yeast Atg8 highlighted that it is located near the C-terminal glycine on the surface opposite the LDS region utilised in LIR binding, indicating that LIR and UIM proteins could bind Atg8 simultaneously (Fig 1.11, B)[226]. The UIM-UDS interface has been discovered to function in yeast, mice and humans[225,227,228], but has yet to be explored in *Drosophila*. The discovery of this interface does however enlarge the range of possible autophagy receptors and adaptors and identifies a higher complexity in autophagy cargo selection.

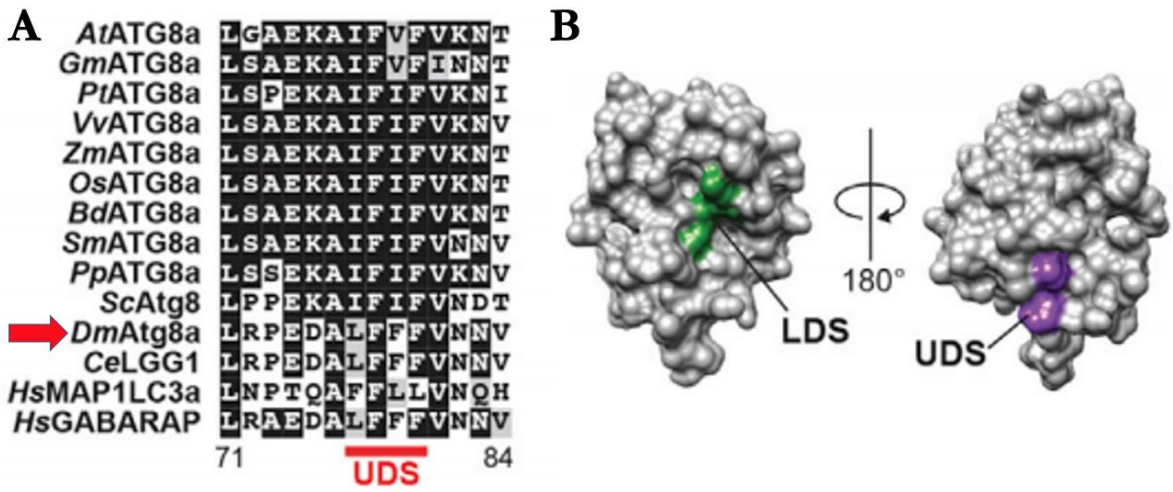

Figure 1.11 The Discovery of the Ubiquitin-Docking Site in Atg8-family Proteins.

(A) Shows the sequence alignment conducted by Marshall *et al., (*2019) in order to characterise the UDS region in plant, fungal, and various animal ATG8 proteins. The core sequence of the UDS is indicated in red, with the presence of *Drosophila* Atg8a indicated by the red arrow. Identical and similar amino acids are shown with black and grey backgrounds, respectively. The numbering corresponds to the *Arabidopsis* ATG8a sequence from which the UIM-dependant interaction was first reported in RPN10[224] (B) A 3-dimensional structure of yeast Atg8 (PDB: 3VXW), highlighting the opposed positions of the LDS (green) and UDS (purple). Figure adapted from Marshall *et al.,* (2019)[226].

1.7 Transcriptional Regulation of Autophagy

In 1999, through the observation that nutritional starvation induced the upregulation of *ATG8*[150], Kirisako *et al.* first reported that autophagy could be induced at a transcriptional level in yeast. The research on transcriptional regulation of autophagy gained momentum in 2011 after a landmark paper that showed that TFEB (Transcription Factor EB) regulates a wide range of autophagy-related genes[229] (Table 1.2).

Under starvation conditions rapid induction of autophagy promotes cellular survival by maintaining adequate cellular energy levels. Accumulating evidence indicates that the autophagic response to stress may proceed in two phases; firstly, a rapid increase in the autophagic flux, which occurs within minutes or hours of exposure to stressful conditions and is entirely mediated by post-translational protein modifications[112,230,231]. This is generally followed by a delayed and sustained autophagic response that relies on the activation of specific transcriptional programs[232].

Table 1.2 Transcriptional Regulation of Autophagy in Response to Stress.
A summary of key transcription factors in the induction and repression of core autophagy genes in mammals.

Transcription Factor	Inducer(s)	Target autophagy related gene(s)	Regulation	Ref.
TFEB	Nutrient deprivation	*BECLIN1*, *WIPI1*, *ATG9B, GABARAP*, *MAP1LC3B, ATG5, RAB7*	Up	[229,233]
FOXO1	Nutrient deprivation, oxidative stress	A*TG5, ATG12, ATG14, BECLIN1, MAP1LC3B, VSP34, PI3K, GABARAP1*	Up	[234–236, 237,238, 239]
FOXO3	Nutrient deprivation, oxidative stress	*ATG4B, ATG12, ATG14, BECLIN1, MAP1LC3B, ULK, VSP34*	Up	[234–236]

p53	Genotoxic stress[4]	*Sestrin1/2, DRAM-1*	Up	[240,241, 242]
	Nutrient deprivation	*Sestrin1/2*	Down	[243]
		ATG2, ATG4, ATG7, ATG10, ULK1	Up	[244]
ZKSCAN	Nutrient deprivation	*ULK1*, *WIPI2, MAP1LC3B, ATG18b, Raptor*	Down	[245]
FOXK1	Nutrient deprivation	*ULK1, ULK2, VPS34, AMBRA1, FIP200, ATG13*	Down	[246]
Rph1/KDM4	Nutrient deprivation (nitrogen starvation in yeast)	*ATG1, ATG7, ATG8, ATG9, ATG14* and *ATG29*	Down	[247]

1.7.1 TFEB and MiT factors: The master autophagy regulators

TFEB is a member of the microphthalmia/transcription factor E MiT/TFE (Microphthalmia/Transcription Factor E) family of transcription factors, which include: MITF, TFE3 and TFEC proteins[248]. They belong to a larger family of bHLH-Zip (Basic Helix-Loop-Helix leucine Zipper) transcription factors, such as MYC; with their HLH-leucine zipper domain being essential for heterodimerization and the activation of transcription[249]. The evolutionary conserved transcription factor MYC drives cellular overgrowth and is required for autophagy in both mammalian and *Drosophila* cells[250,251]. The MiT/TFE proteins harbour the same basic region as bHLH-Zip transcription factors which is required for DNA binding; mediated by the recognition of a common DNA hexanucleotide sequence (CACGTG), known as the E-box[248].

[4] Substances that are genotoxic may bind directly to DNA or act indirectly leading to DNA damage by affecting enzymes involved in DNA replication, thereby causing mutations.

However, the existence of specific nucleotide residues which flank this motif constitute the CLEAR (Coordinated Lysosomal Expression and Regulation) motif (GTCACCTGAC) and are recognised preferentially by MiT/TFE family members[252]. TFEB has been shown to directly bind to CLEAR elements, thereby promoting the entire network of genes that contains the CLEAR regulatory motif in their promotor[252]. These genes have been characterised to belong to numerous lysosomal functional categories including hydrolyses and transmembrane proteins; accordingly, TFEB activation leads to the global enhancement of lysosomal catabolic efficiency[252]. As the completion of autophagic flux requires the degradation of cargo by the lysosome, TFEB has the ability to regulate the upmost step of the autophagic process[229].

The activity of TFEB is tightly controlled by environmental conditions via post-translational modifications, with a number of kinases having been identified to phosphorylate TFEB, including ERK2 (Extracellular signal-Regulated Kinase 2) and AKT[229]. However, mTOR, as part of the mTORC1 complex, represents the main kinase which is responsible for its phosphorylation in full nutrients conditions[253,254]. Under these circumstances, TFEB is sequestered into the cytoplasm as a result of phosphorylation by mTOR, thereby inhibiting it's transcriptional induction of genes[229]. mTOR also functions to inhibit the transcriptional activity of TFEB by modulating the activity of ZKSCAN3 (Zinc finger transcription factors Kruppel-associated box (KRAB) and SCAN domain 3); these in essence represent the transcriptional counterpart of TFEB as they function to repress a number of autophagy genes[245].

Interestingly, Shin *et al.* that transcriptional activation of autophagy genes by TFEB also involve AMPK-dependant changes in histone modifications[255]. Upon nutrient deprivation, the AMP/ATP ratio increases, and AMPK becomes activated. This is turn leads to the suppression of ubiquitin ligase SKP2 (S-phase Kinase-associate Protein 2) via FOXO3, which is turn results in the stabilisation of CARM1 (Coactivator-associated Arginine Methyltransferase 1) (Fig. 1.12). CARM1 functions to interact with TFEB and co-activates TFEB-mediated transcription via histone methylation[255]. AMPK also mediates the nuclear translocation of ACSS2 (Acetyl-CoA Synthetase 2) via phosphorylation, which results in: its interaction with TFEB, the subsequent local production of acetyl-CoA and, an increase in histone H3 acetylation at the promotor region of TFEB target genes[71]. As a result of these events triggered by nutrient starvation, TFEB is observed to translocate into the nucleus where it is able to bind to the promotor of a multitude of *Atg* genes (Fig. 1.12). These function to directly regulate different steps of the autophagy process such as those involved in initiation; *BECLIN1*, *WIPI1*, *ATG9B* and *NRBF2*,

autophagosome membrane elongation; *GABARAP*, *MAP1LC3B* and *ATG5*, and autophagosome trafficking and fusion with lysosome; *UVRAG* and *RAB7*[229,233] (Table 1.2). As a result of its transcriptional abilities, TFEB activation induces a striking increase in autophagic flux[256]. In fact, TFEB has been established as a factor which enables the rapid transcription of ATG proteins which are involved in all steps of the autophagy process, with overexpression sufficient to induce autophagy[229]. TFE2 and MITF have also been identified as regulators of autophagy and biogenesis in mammalian cells in a similar manner to their familial partner TFEB[256,257].

All four members of the MiT/TFE family are conserved in vertebrates, however only a single ortholog, *Mitf*, is found in *Drosophila*[258]. The sole *Drosophila* MIT transcription factor functions in eye development in a similar manner to mammalian MITF[258]. Interestingly, it has been shown to be equally related to both MITF and TFEB in humans, harbouring the basic regions including the HLH-Zip domains, suggesting they bind to DNA in a similar way to their mammalian family members[259]. The regulation of lysosomal biogenesis, autophagy and lipid metabolism by the MiT/TFE family of transcription factors is evolutionarily conserved in different species[259]. In *Drosophila*, *Mitf* downregulation was shown to impair normal cellular response to nutrient deprivation[259]. Also in the absence of *Mitf,* the accumulation of autophagy substrate Ref(2)P is apparent, as well as the presence of enlarged lysosomes which are reminiscent of cellular phenotypes of lysosomal storage disorders[259]. Further to this, several stages of the autophagy process, from the biogenesis of new autophagosomes to fusion with lysosomes for cargo degradation, were shown to be regulated by *Drosophila Mitf*, as well as the regulation of a whole subset of other *Atg* and lysosomal genes[259].

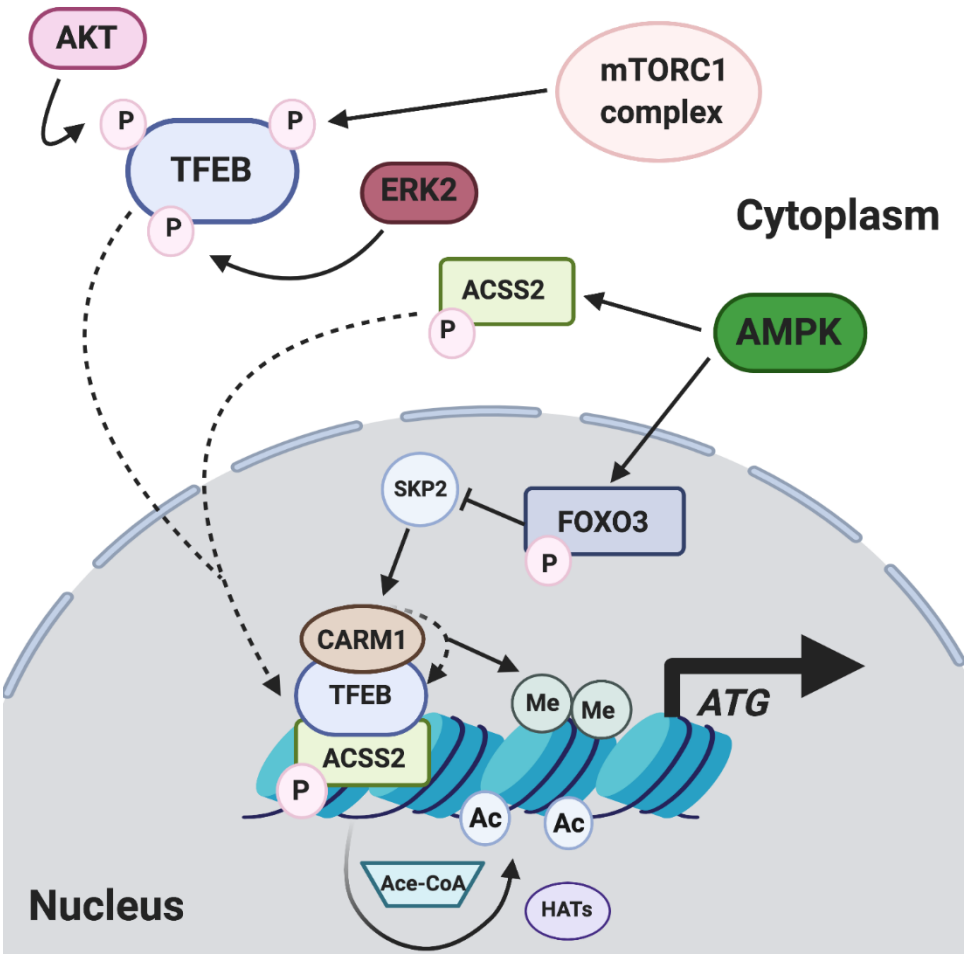

Figure 1.12 Regulation of *Atg* genes by TFEB.
Under nutrient replete conditions, TFEB is phosphorylated by mTORC1, AKT and ERK2, and is sequestered in the cytoplasm. Upon starvation, TFEB is dephosphorylated and subsequently translocates to the nucleus. Simultaneously, AMPK is activated and phosphorylates FOXO3. FOXO3 in turn represses the expression of SKP2, which leads to the stabilisation of CARM1. AMPK also functions to phosphorylate ACSS2, which triggers its nuclear translocation. In the nucleus, both CARM1 and ACSS2 interact with TFEB, and promote the activation of autophagy genes; CARM1 through the increased methylation of histones at the gene promotors, and ACSS2 via the localised increase of acetyl-CoA, which enables the action of histone acetyltransferases (HATs). The regulation of autophagy genes by MiT/TFE family of transcription factors is evolutionarily conserved. Constructed from work presented by Shin *et al.* (2016)[255] and Li *et al.,* (2017)[71].

1.7.2 FoxO: an autophagy inducer in *Drosophila*

The FoxO family of transcription factors were one of the first to be linked to autophagy, and now have an established role in its regulation[235]. The FoxO family fall under the control of multiple signalling pathways such as the InR/PI3K signalling pathway, the oxidative stress mediated JNK pathway, TOR signalling and AMPK pathway[260]. The first report of FoxO regulating autophagy came from work in *Drosophila*; showing that *foxo* larvae mutants had a

significantly reduced response to nutrient deprivation, and that the overexpression of FoxO is sufficient to induce autophagy in the fat body of larvae[261]. This was later confirmed to be functionally conserved in mammals, where the family includes four members: FOXO1, FOXO3, FOXO4 and FOXO6[234]. Like the MiT/TFE family, FOXOs are regulated by phosphorylation events which mediate their shuttling from the cytosol to the nucleus, where they induce the expression of a number of *ATG* genes, including A*TG4, ATG12, BECLIN1, MAP1LC3B* (the gene that encodes cytosolic LC3)*, ULK1, VSP34* and *GABARAP1*[234–236] (Table 1.2). For example, FOXO3a transcription factor activation by AMPK is triggered under starvation conditions, and is shown to induce the expression of the ATG proteins LC3B-II, GABARAP-L1, and BECLIN11 in primary mouse skeletal muscle myotubes[236]. In addition, the nuclear localisation of FOXO1 has been correlated with the transcriptional activation of *ATG5*[237], *ATG14*[238] and production of PI3K[239]. Unlike TFEB however, FOXO1 can also act an autophagy inducer in the cytosol by directly binding to ATG7 to promote autophagosome biogenesis in starvation-induced autophagy, independently of its transcriptional ability[98].

Interestingly, a recent study using *Caenorhabditis elegans,* demonstrated that its FOXO homolog both physically and functionally cooperates with its TFEB homolog, resulting in targeted gene expression in response to cellular stress[262]. However, no such findings have been reported in mammalian or *Drosophila* cells to date.

1.7.3 p53: an autophagy promotor and repressor

A critical component of stress signalling and adaptation is the tumour suppressor p53, which is capable of both positively and negatively regulating a number of *ATG* genes, dependant on its cellular localisation[263]. Under genotoxic stress, p53 was initially described to promote autophagy through the modulation of genes Sestrin 1/2 which are implicated in the regulation of mTOR in mammalian cells[240,241]. Inversely, it has been demonstrated that, under nutrient repleted conditions, endogenous p53 represses autophagy via the inhibition of AMPK and activation of mTOR[243]. These conclusions were supported by observations that NES (Nuclear Export Signal) mutated p53, exclusively resides in the nucleus and is unable to repress autophagy[243]. These findings led to the belief that the anti-autophagic effect of p53 is exclusively linked to its cytoplasmic localization and are therefore independent of its transcriptional function[243]. More recently p53 has been shown to induce the expression of DRAM (Damage-Regulated-Modulator), a lysosomal protein which induces autophagy, although an underlying mechanisms which remain to be elucidated[242]. p53 has been shown to reside on the promotor, and plays an

important role in the regulation, of a number of *ATG* genes, which include *ATG2, ATG4, ATG7, ATG10* and *ULK1*[244] (Table 1.2).

The *Drosophila* homolog of p53 has been shown to function in the regulation of starvation induced autophagy, with mutants lacking *p53* displaying impaired autophagic flux[264]. It has been established that autophagy is differentially regulated by two of the three p53 *Drosophila* isoforms, with the full length p53 isoform (p53B) shown to induce autophagy, whereas p53A, which is analogous to human p53, was shown to have an inhibitory effect[264]. Interestingly, in mammalian cells p53 has been shown to determine both FOXO3a activity[265] and the nuclear localisation of TFEB/TFE3, but these findings have only been shown in the context to DNA damage[266].

1.7.4 Transcriptional repression of autophagy

ATG gene expression is supressed under nutrient replete conditions, with only a few transcription factors having been shown to engage in their repression to date. Of those characterised, ZKSCAN3 has been coined the master repressor of autophagy[245]. Belonging to the zinc finger superfamily which harbour KRAB and SCAN domains[267], here it sits alongside nearly half of all annotated human transcription factors[268]. Members of the zinc finger family have been shown to harbour a C-terminal domain which consists of C2H2 (Kruppel type), which functions to bind to DNA[269]. The N-terminal KRAB domain, has been shown to confer transcriptional repression by recruiting KAP-1, which functions in turn to recruit histone deacetylase and histone methyl transferase machinery which modify chromatin status and influence gene silencing[269]. The SCAN domain, a leucine rich region, governs protein interaction, mediating self-association or selective association with other proteins[267].

In mammalian cells, ZKSCAN3 has been characterised as a repressor of the autophagy-lysosomal pathway. It functions by directly targeting a network of genes which span the sequential stages of autophagy, including the biogenesis, transport and fusion of autophagosomes and lysosomes[270]. ZKSCAN3 was found to be recruited to the promotor region of *ULK1*, *WIPI2* and *MAP1LC3B* in nutrient rich conditions[245]. Knockdown of *ZKSCAN3* upregulates a subset of *ATG* and lysosomal genes, thereby enhancing autophagic flux[245] (Table 1.2). Nutrient deprivation leads to the nuclear export and cytosolic accumulation, along with the de-repression of *ATG* gene expression[245]. It has previously been shown that various kinases function to phosphorylate ZKSCAN3 in order to facilitate its nuclear export, however how its

localisation is governed under starvation conditions and how it functions to repress gene expression remain unknown[271].

1.7.5 Foxk1

FOXK (Forkhead box K) has been shown to transcriptionally repress the early stages of autophagy by binding to the promotor region of gene components of the ULK1 and VSP34 complexes; with *Foxk1* deficiency resulting in an increase in autophagic flux[246] (Table 1.2). FOXK has been shown to function by recruiting the histone deacetylase repressor complex, SIN3a, which facilitates the downregulation of gene expression[246]. Interestingly, the SIN3a histone deacetylase is homologous to the Ume6-Sin3-Rpd3 yeast complex which is shown to negatively regulate autophagy through repression of *ATG8*. Deletion of *Ume6* is shown to result in the accumulation of large autophagosomes, even in full nutrients conditions[272]. As the transcription factor Ume6 is not conserved in mammals[272], it is postulated that the FOXK-Sin3 complex may have evolved from the ancient autophagy regulating pathway in yeast to assume the role of Ume6[246].

In a nutrient replete environment, mTOR functions to phosphorylate both FOXK1 and FOXK2. As a result, the FOXK proteins translocate to the nucleus, where they compete with its familial member FOXO3 for the binding of genomic regulatory sites, where they function to repress *ATG* genes (Table 1.2). When nutrients are re-supplied, AMPK activation leads to the phosphorylation of FOXO3, which is subsequently recruited to the genomic promotor regions to displace FOXK, in order to activate gene transcription[246]. Here, the activation of AMPK also results in the phosphorylation of TSC2 and RAPTOR, thereby rendering mTOR inactive. This induces FOXK to be exported from the nucleus, thus allowing for the maximal activation of *ATG* genes by FOXO3[246].

1.7.6 Hox proteins

Hox proteins are homeodomain (HD)-containing transcription factors which act in the nucleus to regulate the expression of numerous downstream target genes. It was first observed that nuclear accumulation of various Hox proteins, namely Ubx (Ultrabithorax), in the fat body of *Drosophila* larvae, coincided with the repression of developmental autophagy [273]. The repressive action of *Hox* genes was confirmed to be extremely potent over a long period of time, with forced maintenance of *Hox* expression resulting in very few autophagic structures being formed

over an 11-day period[273]. Accordingly, downregulation of *Hox* genes in *Drosophila* larval fat body correlates to the onset of developmental autophagy[273]. A short linear motif called HX (Hexapeptode), which resides upstream of the HD in Hox proteins, is necessary for the nuclear export of Hox proteins, and is tightly regulated in the *Drosophila* fat body in order to control the onset of autophagy[274]. Recent work showed that human HOX proteins also harbour a HX motif which is used to govern its interaction with important co-factors[275].

Hox gene downregulation has also been shown to be required for starvation induced autophagy in third instar stage larvae prior to the onset of developmental autophagy[273]. This indicated that *Hox* downregulation is a general prerequisite for the induction of autophagy, not just in the case of developmental autophagy. This notion was further confirmed through the functional requirement of Hox clearance in the induction of starvation-induced autophagy, mediated by the TOR signalling pathway in *Drosophila*[273]. In regulating both developmental and starvation-induced autophagy, Hox proteins act directly through the regulation of *Atg* genes, with Ubx DNA binding essential and necessary for their repression[273]. Furthermore, the repression of both developmental and starvation induced autophagy by Hox proteins seem to be equally as potent. It is also suggested that the repressive ability of Hox proteins is evolutionary conserved in mice[273].

1.7.7 Rph1/KDM4

In 2016, Bernard *et al.*[247] reported the application of targeted library screening to search for new transcriptional regulators of autophagy. The study utilised a collection of yeast mutants lacking a single DNA-binding protein by analysing the expression of a particular set of *ATG* target genes: *ATG1, ATG7, ATG8, ATG9, ATG14* and *ATG29* (Table 1.2). These were selected as they encode proteins involved in different steps of the autophagy pathway and are shown to be strongly induced in the 'classic' conditions of nitrogen starvation in yeast[276]. Through this method they uncovered that r*ph1*-depletion resulted in a significant upregulation of aforementioned genes, along with the modest induction of *ATG1,* in full nutrient conditions. Interestingly, r*ph1*-depletion had no effect in the transcription of *ATG10*, a gene which displays no change in the response to nitrogen deprivation in yeast, suggesting that Rph1 functions to exclusively repress the expression of *ATG* genes in nutrient-replete conditions[247]. Thus, these findings marked the intriguing potential discovery of transcriptional control specific for starvation-induced autophagy.

Rph1 is a DNA-binding protein which, like ZKSCAN3, belongs to the zinc finger superfamily and contains two C2H2 zinc-finger motifs. This DNA binding domain was found to be critical in its control of autophagy, through the identification of its higher affinity for the promotor regions of *ATG* genes in fed conditions when compared to starved[247]. Rph1 was previously characterised as a Jumonji C histone demethylase catalytic domain containing protein[277], however this region was revealed to act independently of its function in autophagy[247]. In line with its high affinity for *ATG* gene promotor regions correlating to reduced gene expression in fed conditions*;* overexpression of *Rph1* after starvation resulted in a severe block in the *ATG* gene expression, with the reduction in corresponding transcripts correlating with a decrease in autophagy activity.

In r*ph1*-deplete conditions the expression of *ATG* genes is upregulated in nutrient rich conditions but has no effect on mRNA levels after nitrogen starvation. This hinted at a mechanism in which the repressive ability of Rph1 is relieved following an environmental shift from optimum to depleted nutrients. This mechanism was uncovered and attributed to protein kinase Rim15 via its phosphorylation of Rph1[247] (Fig. 1.13). Rim15 had previously been shown to be phosphorylated by TOR and translocate into the nucleus during the induction of starvation inducted autophagy[278]. Interestingly, Rim16 also phosphorylates Ume6, another known transcriptional repressor of autophagy in yeast, leading to an inhibition it it's activity and an upregulation of *ATG8* after nitrogen starvation[272].

Analysis of protein abundance revealed that depletion of *Rph1* alone was sufficient to increase Atg7 protein levels to that higher than seen in 3 hours of nitrogen starvation in WT cells, signifying that Rph1 has a predominant role in the regulation of Atg7[247]. Negative modulation of *ATG7* have been shown to cause defects in autophagy activity in yeast[247] and the same effects in other higher eukaryotes including *Drosophila*[279] having previously been reported. The relative abundance of the other corresponding Atg proteins were found to be higher in *rph1*-depleted cells in comparison to WT cells in full nutrients conditions. However, protein levels were shown to be lower than those seen in starvation conditions, highlighting the role of other pathways contributing to the regulation of the corresponding genes.

The autophagy related functions of Rph1 were confirmed to be evolutionarily conserved in its mammalian homolog KDM4A (lysine (K)-specific Demethylase 4A), whereby a reduction in KDM4 levels was associated with an increased in the expression in a number of *ATG* genes

including *ATG7*, *WIPI1* and *ATG14*, however there was no effect on *MAP1LC3B*[247]. This finding uncovers the potential of other eukaryotic homologs of Rph1/KDM4 to have the same transcriptional control, and thus paves the way for future research to further define the role this intriguing transcription factor has in the role of starvation-induced autophagy.

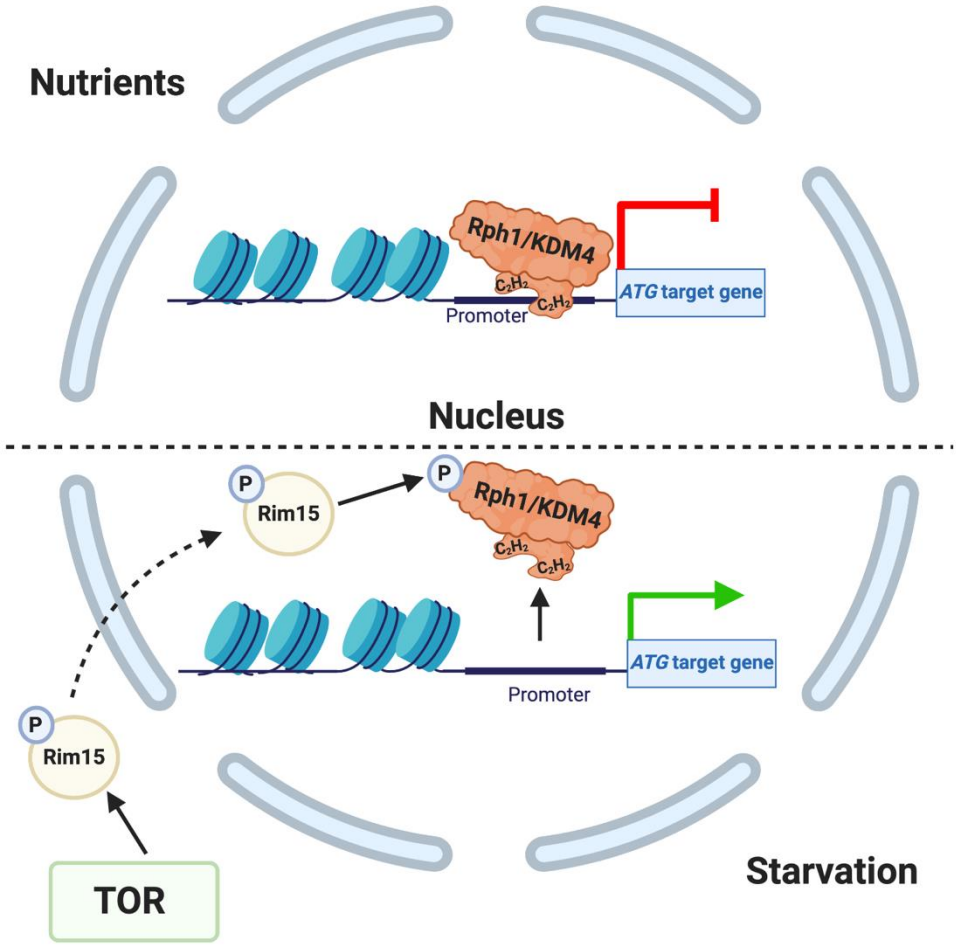

Figure 1.13 Transcriptional Repression of *ATG* genes in Full Nutrient Conditions by Rph1/KDM4.
Rph1, a transcription factor in yeast, resides on the promotor region of *ATG* genes related to the induction of autophagy. These include *ATG1, ATG7, ATG8, ATG9, ATG14* and *ATG29*. Rph1 contains two C_2H_2 zinc-finger motifs, which are responsible for binding the DNA of these target regions. Upon the re-supply of nutrients Rim15, a protein kinase, is phosphorylated by TOR and subsequently translocates into the nucleus. Here it is at least partly responsible for the phosphorylation of Rph1; a modification which results in its repressive abilities to be lifted. This mode of regulation is conserved from yeast to humans with the mammalian homolog KDM4 also functioning as a repressor of autophagy in a similar manner. Constructed from the work presented by Bernard *et al.,* (2016)[247].

1.7.8 Gene regulation by histone modifications

Histone modifications effect the accessibility of transcription factors to chromatin and thus can have an overriding control over how autophagy is transcriptionally regulated. There are a number of histone modifications which have been reported to influence autophagic activity, with a large proportion involving methylation of lysine residues. Tri-methylation of lysine 4 on histone H3 (H3K4me3) is considered a universal chromatin modification, at the transcription start site of active genes in all higher eukaryotes[280]. H3K4me3 has been described as an activating histone modification and assumed to have an instructive role in the transcription of genes, including those which regulate autophagy. For this reason, assessment of this particular epigenetic modification can be seen as a reliable indication of increased transcription. Additionally, tri-methylation of lysine 27 (H3K27me3) histone modifications are associated with active gene repression[281].

Transcriptional regulation of autophagy is also facilitated by factors capable of 'reading' histone modifications such as bromodomain proteins. The epigenetic reader BRD4 (Bromodomain-containing protein 4) has recently been identified as a repressor of a transcriptional mechanism that functions to promote autophagy in mammalian cells[282]. In the presence of nutrients, it functions to repression the induction of autophagy by recruiting the methyl transferase G9a, which deposits a repressive H3K9diMe on the promotors of *ATG* genes[282]. BRD4 knockdown results in the induction of *ATG* gene expression and activates a number of autophagic processes. This is suggestive that BRD4 functions as a repressor of autophagy nutrient rich conditions and that its de-repression contributes to autophagy being sustained in nutrient rich conditions[270].

Lysine acetylation has been studied extensively since it was first described in histones almost 50 years ago[283]. An example of histone acetylation/deacetylation in the control of autophagy is by the HK16 acetyltransferase hMOF (human Males absent On the First). Also known as KAT8 (lysine acetyltransferases 8), it has been described as both a positive regulator of autophagy. During prolonged starvation and subsequent inactivation of mTOR, hMOF degradation coupled with the action of SIRT1-dependant histone deacetylation, has been reported to lead to a decline in HK16 acetylation and the expression of *ATG* genes[284]. More recently however a surprising report emerged that knockdown of *KAT8* appears to induce autophagy in experiments under normal nutritive conditions[285].

1.8 Acetylation of Autophagic Machinery

PTMs (Post-Translational Modifications) are fundamental in the regulation of eukaryotic proteins; with ubiquitination, serine/threonine phosphorylation, lysine acetylation and lysine/arginine methylation, all among the major modifiers. In previous sections, the important roles of phosphorylation, ubiquitination and methylation have been outlined. Here, the focus will be shifted on to exploring the emerging role of acetylation in the regulation of autophagy. Although the acetylation and deacetylation events were first extensively studied in histones, targets for HATs (Histone Acetyltransferases) or HDACs (Histone Deacetylases) often include nuclear non-histones and cytoplasmic proteins[286]. Therefore, the lysine side chains of proteins involved in autophagy control, can be targeted and modified by a number of HATs and HDACs.

1.8.1 Lysine acetyltransferases and deacetylases

Lysine acetylation is defined as the transfer of an acetyl-group of acetyl-CoA to the ε-amino group of an internal lysine residue[283]. This reaction is catalysed by HATs, which are now more commonly referred to as KATs (lysine (K) Acetyltransferases). The reverse reaction governed by HDACs, often referred to as KDACs (lysine (K) Deacetylases)[5]. There are three major families of KATs: KAT2/ GNAT (GCN5-related N-acetyltransferases) family, EP300/p300 (E1A binding Protein of 300KDa) family, and MYST family (Table 1.3). There have also been five classes of deacetylases (HDACs/KDACs) described: I, IIa, IIb, III and IV. The class III family compromises of sirtuins and function by using NAD^+ as a cofactor to deacetylase the reaction, whereas the other classes consist of zinc-dependant enzymes[287]. In regard to autophagy, there is a growing body of evidence that KATs and KDACs play a pivotal role in regulation across multiple levels (Table 1.3), with regulation in most cases specifically seen to be mediated in KAT-KDAC pairs, including EP300-sirtuins and MYST-HDAC3.

[5] Although HDAC is considered more of a 'historical' reference, the sub-class names for deacetylases (Table 1.3) still remain.

Table 1.3 Lysine Acetyltransferases and Deacetylases in the Regulation of Autophagy Machinery. Summary of KATs and KDAC/HDAC involved in the regulation of Atg proteins. Class IIa HDAC4, 5 and 7 have all been linked to the inhibition of autophagy, however the machinery in which they target has not yet be characterised. In all other cases specific targets of regulation via acetylation or deacetylation has been uncovered.

	KATs	**Regulatory role in autophagy**
	EP300-CRECCP family	
CREBBP/KAT3A		Inhibition of Foxo1-mediated transcription[288] Autophagosome maturation[289]
EP300/KAT3B		Inhibition through acetylation of Atg[290–292] proteins and FOXO[293]
	MYST family	
KAT5/TIP60		Induction in mammals through acetylation of ULK1[294] and Atg3 in yeast[295] Autophagosome maturation[296]
	H/KDACs	
	Class I	
HDAC1		Induction of autophagic proteins[297] Inhibition of autophagy[298]
HDAC2		Induction of autophagic proteins[297] Control of autophagosome maturation[289]
HDAC3/RPD3		Inhibition through Atg3 deacetylation in yeast[299]
	Class IIa	
HDAC4, 5, 7		Inhibition[300,301]
	Class IIb	
HDAC6		Induction through cortacin/promotion of autophagosome-lysosome fusion[302]
	ClassIII/Sirtuins	
SIRT1		Induction through deacetylation of ATGs[158,290] and FOXO[234,303,304] Activation of signalling pathways[78,95,305]
SIRT2		Foxo1 deacetylation inhibition[98]
SIRT3		Potential role in mitochondrial induction[306]

1.8.1.1 Striking a balance: EP300-CREBBP and Sirtuins

Nutrient limitation is associated with deacetylation reactions which are orchestrated by a unique family of sirtuin deacetylases. These function in an NAD^+-dependant manner to specifically target non-histone proteins. Sirtuins were first linked to the regulation of life span, with their overexpression in the yeast and *Drosophila* homolog Sir2 shown to extend life expectancy under caloric restrictions in these model organisms[307]. This apparent role in nutrient adaptation led to exploration of the link between sirtuin activity and the induction of autophagy. There are seven sirtuin family members in mammalian cells, however the closest relative to Sir2 is SIRT1[94]. The first autophagy-related observation of sirtuins in mammals showed that mice subjected to starvation overnight increased their expression of SIRT1[308,309]. Since then, a whole body of evidence links the direct role of sirtuin family members to the induction of autophagy in nutrient deplete conditions. Acting in the opposite direction; The CREBBP (the Cyclic-AMP Response Element Binding protein, Binding Protein) and EP300, are two very closely related acetyltransferases which both constitute multi-domain proteins and have the dual capabilities of harbouring a catalytic HAT domain, allowing them directly acetylate proteins. They also harbour a bromodomain that allows them to bind acetylated histones to order to regulate transcription[310]. As ATG proteins can directly be regulated through acetylation/deacetylation, the opposing functions of EP300-CREBBP and sirtuins is a common partnership employed in order to govern autophagic processes.

SIRT1 functions to directly deacetylate and regulate cytosolic targets ATG5, ATG7, LC3 and ATG12 in human (HeLa) and mouse (embryonic fibroblast) cells, which in turn initiates autophagy in response to starvation (Fig. 1.14 B). Consistently *sirt* null mutation$^-$ results in accumulation of damaged organelles and autophagy deficiency[290]. Inverse to the role of SIRT1, the HAT EP300 has been shown to acetylate the aforementioned ATG proteins, with knockdown of EP300 in HeLa cells resulting in the inhibition of acetylation and promotion of autophagy[291]. For example, in mammalian cells EP300 and ATG7 co-localise in the cytoplasm in a nutrient-dependant manner, with their physical interaction resulting in the acetylation of ATG7. In the presence of nutrient-depletion, SIRT1 functions to deacetylate ATG7, which promotes its facilitation of autophagosome formation[290]. Furthermore, the use of resveratrol, a inducer specific to SIRT1 and, spermidine, an acetyl-transferase inhibitor, synergize the induction of autophagy through the direct acetylation of core ATG proteins[311]. The ability of

SIRT1 to directly deacetylate nuclear LC3, thereby dictating its ability to cross the nuclear membrane will be described in detail in section 1.9.

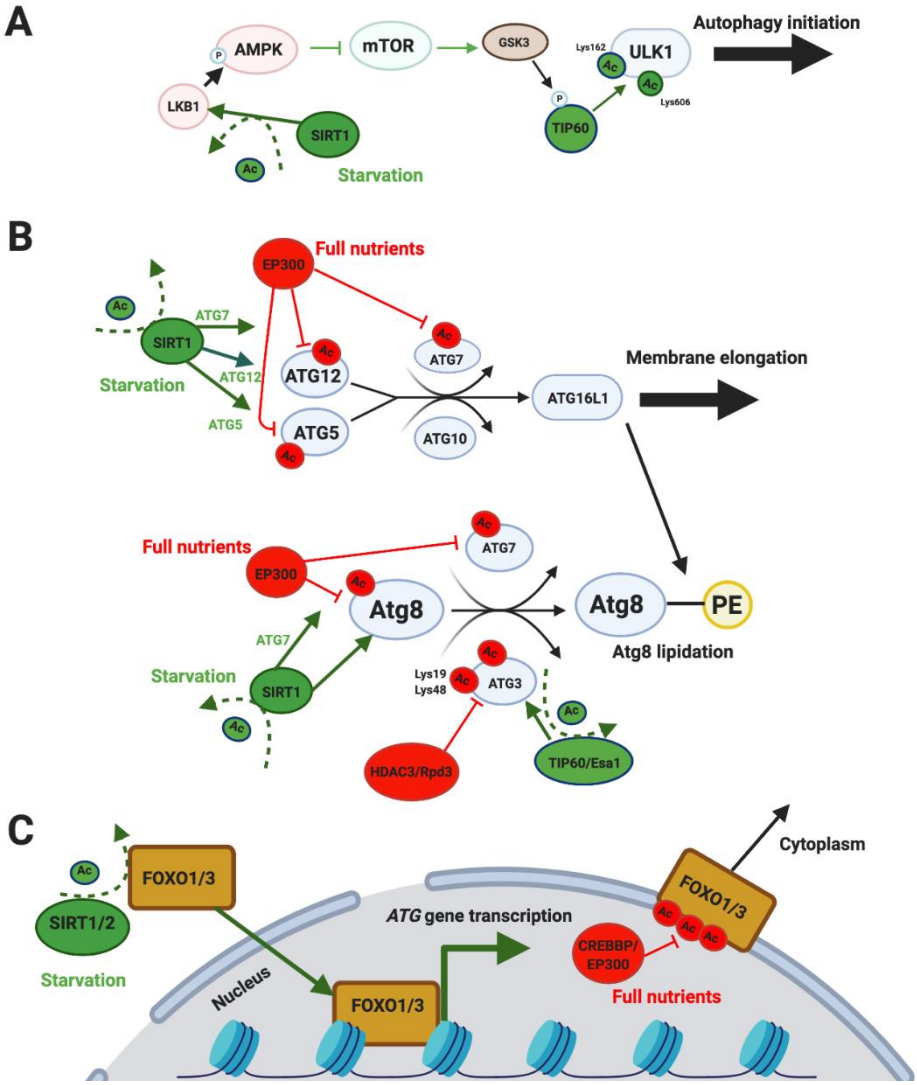

Figure 1.14 The Regulation of Autophagic Machinery via Acetylases and Deacetylases. (A) In a nutrient deplete environment, SIRT1 activates LKB1 via deacetylation. LKB1 subsequently catalyses the activation of AMPK, rendering the autophagy repressor mTOR inactive. In the case of growth factor deprivation, the activation of GSK3 (glycogen synthase kinase-3) occurs, resulting in the phosphorylation of the KAT5 acetyltransferase TIP60. TIP60 acetylates the ULK1 kinase, initiating autophagy. (B-C) The elongation of the autophagosome membrane and Atg8 lipidation is inhibited by the action of EP300 in nutrient rich conditions. EP300 functions to acetylate ATG5, ATG12, ATG7 and ATG8. In starvation conditions, SIRT1 deacetylates these proteins and induces autophagy. In the case of ATG3, acetylation and deacetylation are mediated by HDAC3 and TIP60, respectively, in order to control LC3/Atg8 interaction and lipidation. Observations in yeast show that Rpd3 and Esa1 also regulate Atg3 in a similar manner, with Lys19 and Lys48 representing conserved residues of targeting acetylation/deacetylation. (C) SIRT1 and SIRT2 induce autophagy through the deacetylation of FOXO1 and FOXO3 in the cytoplasm, leading to their nuclear residency and transcriptional activation of ATG genes. In a nutrient replete setting, CREBBP-EP300 acetyltransferases increase FOXO1 and FOXO3 acetylation, which in turn decreases their DNA binding ability and leads to their nuclear export.

Control of autophagy through the acetylation of transcription factors is best illustrated by FOXO family members. SIRT1 is essential for mediating the deacetylation of FOXO3, an essential transcription factor in the control of autophagy induction (Fig. 1.14 C). Following caloric restriction, SIRT1-mediated deacetylation of FOXO3 functions to promote the transcription of *MAP1LC3, PIK3C3/VPS34, GABARAPL1, ATG12, ATG4 and ULK1* in mammalian tissues[234,303]. SIRT1 is also able to control the subcellular localisation of FOXO1, through deacetylation of a specific LXXLL motif which directly impacts its ability to bind to the promotor region of *ATGL;* a lipase which is known to promote autophagy in its control of lipid droplet catabolism[304]. Acetylation of FOXO1 on three lysine regions: K242, K25 and K262, is mediated by the CREBBP acetyltransferase and it functions to impair FOXO1-mediated transcriptional regulation[288]. Away from its transcriptional role FOXO1 is required to translocate from the cytoplasm to the nucleus, an event which too is governed by its acetylation status. In the context of human cancer cells, it has been shown that dissociation from SIRT2 in response to serum deprivation, results in the subsequent nuclear localisation and acetylation of FOXO1, enabling it to bind to ATG7 and promote autophagic processes[98]. In cardiac myocytes, FOXO1 is deacetylated by SIRT1, an event that leads to the activation of the GTPase RAB7 which controls membrane trafficking and results in the maturation of autophagic vesicles[293]. Consistent with this, overexpression of EP300 has also been shown to increase FOXO1 acetylation and inhibit autophagy in these cells[293].

SIRT1 has been suggested to have a role in the control of the stability of mRNAs which encode for lysosomal enzymes[305]. Furthermore, it has been implicated to have a role in maintenance of energy homeostasis through the activation of AMPK. This is achieved via deacetylation of its activator LKB1[95], and by inhibiting mTOR1 signalling by virtue of favouring an interaction with the TSC1/TSC2 complex[78]; both of which constitute key pathways in promoting autophagy (Fig. 1.14 A). Another member of the sirtuin family, SIRT3, has also been suggested to have a role in autophagy induction of mitochondria, with increased levels correlating to an increase in autophagy, however the mechanisms by which it functions remain unknown[306]. Mechanisms of fine tuning to control the dynamic balance between HATs and HDACs is evident; with SIRT2 seen to control the self-acetylation of p300, which in turn may also function to acetylate SIRT2 to inhibit its enzymatic activity[312,313]. Overall, it can be concluded that a balance between the functioning of CREBBP/EP300 and sirtuin family members must be sustained in order for autophagy regulation to be kept in check.

1.8.1.2 MYST family: TIP60 and Esa1

The MYST family of acetyltransferases are defined by a conserved histone acetyltransferase domain harbouring a C_2HC zinc finger and an Ac-CoA domain[314]. The TIP60 acetyltransferase is a member of the MYST family which has been identified in mammalian[315] and *Drosophila*[316] cells. In an nutrient deplete environment in which signalling via the mTOR pathway is repressed by AMPK, the activation of GSK3 (Glycogen Synthase Kinase-3) functions to phosphorylate and activate mammalian TIP60, which in turn functions to acetylate and subsequently acetylate kinase ULK1[294]. These events are integral in the formation of the ULK1 complex in response to nutrient depletion conditions.

In yeast, the ortholog of TIP60, Esa1 has been shown to regulate autophagy through acetylation of Atg3[299] (Fig. 1.14 B). Starvation induces Esa1-mediated acetylation of K19 and K48 of Atg3, which in turn promotes an Atg3-Atg8 interaction and subsequent lipidation of Atg8. The deacetylation of Atg3 is accomplished by a HDAC3 known as Rpd3; with increased K19-K48 acetylation apparent after the deletion of Rpd3, resulting in increased autophagy[299]. It must be noted that Atg3 functions by a different mechanism in yeast in comparison to mammalian cells and other higher eukaryotes.

1.8.1.3 The role of acetylation in autophagosome maturation

Lee *et al.* (2010) reported that acetylation of key macromolecules governs the maturation of autophagosomes[317]. HDAC6 is an important component in the management of protein aggregates and the fusion of autophagosomes and lysosomes in the regulation of basal autophagy[317]. Intriguingly, HDA6 is completely dispensable in the case of starvation-induced autophagy, but at basal level, its deficiency yields autophagosome maturation failure and accumulation of protein aggregates[317]. This suggests that in the context of starvation induced autophagy, p62 is the overriding ubiquitin-binding factor which governs the removal of aggregated proteins through its ability to bind LC3/Atg8. The mechanism by which HDAC6 functions at basal level is suggested to involve the recruitment and deacetylation of a factor named cotactin, which functions to promote autophagosome-lysosome fusion through actin polymerisation machinery[302].

Recently, the GSK3-TIP60 complex was shown to have an integral role in the modulation of autophagosome maturation. A novel autophagy regulator, coined Pacer[296], was found to be phosphorylated by mTORC1 which disrupted its association with the STX17-HOPs complex;

causing abolishment of the Pacer-mediated autophagosome maturation. In nutrient-deprived conditions however, TIP60 functions to acetylate Pacer, resulting in the recruitment of the STFX17-HOPs complex which is required for successful and efficient autophagosome maturation[296]. This gives evidence that mTORC1 and GSK-TIP60 signalling converge in order to regulate the development of autophagosomes.

Direct acetylation of STX17 at its SNARE domain has also been shown to control autophagosome maturation[289]. This modification is mediated by the acetyltransferase CREBBP and the deacetylase HDAC2. As a result of the inactivation of CREBBP, STX17 becomes deacylated during the induction of autophagy by virtue of HDAC2. This thus enables STX17 to interact with SNAP29 and HOPs; promoting the formation of the SNAP29-VAMP8-SNARE complex and subsequent autophagosomal recruitment of HOPs[289]. As previously highlighted, these events in turn lead to the fusion of the autophagosome to the lysosome.

1.9 How are Nuclear Atg8 Proteins Regulated?

Although there is a body of literature which gives evidence that Atg8-family proteins are enriched in the nucleus[156–159,318], the machinery by which they are targeted to the nucleus, and thus the nuclear components in which they interact remain largely uncharacterised.

It has become increasingly clear that association with other proteins/complexes within the nucleus are likely to be the only passport that Atg8-family proteins have out of the nucleus. Proteins are usually found to localise to the nucleus, through virtue of their nuclear localisation region. Intriguingly, LC3 lacks a consensus nucleolar localisation sequence, however it does contain a sequence with some similarity to a NES; a short amino acid sequence of 4 hydrophobic residues, which functions to target a protein for export from the nucleus via a nuclear pore complex. However previous studies have shown that inhibition of the NES in LC3 has no effect on the nucleocytoplasmic distribution of LC3[319]. Interestingly, Kraft *et al.* (2016) showed that mutation of the residues F52 and L53 which regulate the LIR binding with interacting proteins, effected the targeting of LC3 to the nucleus[319]. In principle, LC3 is small enough to passively cross the nuclear envelope even when tagged with GFP[159]. However, it has been shown via quantitative fluorescence microscopy that GFP tagged-LC3 is modestly enriched in the nucleus relative to the cytoplasm, suggesting it is either selectively targeted or retained within this

compartment as part of a complex that is too large to cross the nuclear envelope by passive diffusion[158,320,159].

Several studies in mammalian cells have detected LC3 in the nucleus, and have reported that that cross- nuclear membrane trafficking of LC3 is a regulated event[158,318,]. For example, an IRS-1(Insulin Receptor Substrate 1)-LC3 bound complex was found to repress autophagy, in a process in which nuclear IRS-1 sequestered LC3 inside the nucleus thus preventing its cytosolic translocation and the formation of autophagosomes[156]. Remarkably, the role of the nuclear-derived pool of LC3 was determined to be the major source of autophagosome-targeted LC3 in starved cells. Using photobleaching and photoactivating, enabling either nuclear or cytoplasmic LC3 to be highlighted, it was observed that only the nuclear-derived LC3 is able. to be conjugated to the phagophore membrane following starvation[321].

Following on from the exploration of acetylation events in section 1.8; an intriguing outcome of the workings of SIRT1 was uncovered in regard to how LC3 is sequestered in the nucleus and how it functions to re-locate to the cytoplasm. Deacetylation by SIRT1 is necessary for it to interact with the nuclear component: TP53INP2 (Tumor Protein tp53-Inducible Nuclear Protein 2), also referred to as DOR (Diabetes and Obesity Related gene). The resulting LC3-DOR complex has the ability to translocate into the cytoplasm in response to starvation in mammalian cells[158]. Here it is able to associate with E1-like ATG7, along with other autophagic components, and proceed to undergo PE-conjugation to pre-autophagic membranes[158]. LC3 carries eight lysine residues, among which K8, K49 and K51 are conserved. Huang *et al.* identified that deacetylation by SIRT1 occurred at sites K49 and K51 and were specifically required for it to be exported out of the nucleus[158]. Further to this, an LC3 mutant in which K49 and K51 were replaced by glutamine (mimicking acetylated LC3), were unable to form PE-conjugates, suggesting that deacetylation of K49 and K51 are required for the induction of autophagy[158]. Starvation driven deacetylation of these regions by SIRT1 was recently shown to be essential in enabling the ability of LC3 to form an interaction with the receptor protein p62, whilst acetylation of these regions was confirmed to be governed by p300[292]. Crucially acetylation/deacetylation of LC3 changes its protein structure, thus enabling autophagy related proteins to distinguish between LC3 in autophagic form (deacetylated) and non-autophagic form (acetylated)[292].

1.10 Thesis aims and hypotheses

Uncovering the mechanism in which nuclear Atg8-family proteins are involved in could provide a key insight into how autophagy is regulated from within this powerful cellular compartment. Therefore, the primary motive of the work presented here is to identify and uncover the role of novel nuclear Atg8a-interacting proteins in *Drosophila*, using the presence of a functioning LIR motif as a primary screening tool.

Work in the Nezis lab previously focussed on screening the *Drosophila* proteome for UBD-containing proteins, with the primary purpose to identify new selective autophagy receptors. The rationale behind the screen derives from the functioning of Ref(2)P, which at the time of this work being carried out was the only known autophagy receptor in *Drosophila*. Ref(2)P, along with other characterised autophagy receptors in mammalian cells share two common features: the presence of at least one LIR motif and at least one UBD. The screening revealed a zinc-finger containing protein Sequoia, which has distinct homology to Tramtrack, a DNA binding transcription factor that influences cell fate in both adult and embryonic PNS in *Drosophila*[322]. Using the iLIR tool (Chapter 3), Sequoia was previously revealed to have a predicted LIR motif. It is hypothesised that Sequoia is a nuclear interactor of Atg8a and that this interaction is dependent on a LIR motif. Furthermore, based on the structural presence of a zinc-finger domain in Sequoia, it is predicted that its interaction with Atg8a may function to have a role in the transcriptional regulation of autophagy. The aim of Chapter 3 is to investigate if a LIR dependant interaction between Atg8a and Sequoia is apparent *in vitro*[6] and to explore the potential role of Sequoia in the regulation of autophagy, through the assessment of its impact on the expression of core *Atg* genes.

The aim of the work presented in Chapter 4 is to investigate whether nuclear Atg8a is regulated by its acetylation status and the potential impact this may have on its predicted interaction with Sequoia, and the induction of starvation induced autophagy. In a previously conducted bioinformatics screening of Atg8a-interactors, YL-1 was identified as a candidate protein. YL-1 is interestingly is a component of an acetyltransferase complex shown to control acetylate histones[316,323–326]. Therefore it is hypothesised that YL-1 interacts with Atg8a and regulates its acetylation status. It is also hypothesised that Sir2, the *Drosophila* homolog of SIRT1, has a direct role in mediating deacetylation of Atg8a, as has been shown in a mammalian cell lines[158].

[6] In a test tube, outside of the living organism.

Given the importance of LC3 re-localisation to the cytoplasm in the formation of autophagosomes, it is of interest to establish how the re-location of Atg8a is regulated in *Drosophila*. As previously highlighted, several studies have reported that the trafficking of LC3 in and out of the nucleus is a regulated event in mammalian cells[158,318]. Huang *et al.,* (2015) demonstrated that nuclear LC3 is deacetylated by SIRT1 and is subsequently actively trafficked out of the nucleus into the cytoplasm by virtue of its association with DOR[158]. In Chapter 5 it is aimed to explore the potential of *Drosophila* DOR (dDOR) in having an analogous role to its mammalian counterpart in mediating the cellular relocation of Atg8a. This will be achieved by exploring a candidate LIR interaction between dDOR and Atg8a. One of the main objects is to also generation of a transgenic fly line overexpressing dOR, which will allow for a more in-depth future exploration of dDOR *in vivo*.

Overall, this project will explore the transcriptional regulation of starvation induced autophagy by predicted Atg8a-interacting protein Sequoia, and will aim to propose a potential mechanism of regulation of nuclear Atg8a based on its interactions with YL-1, Sir2 and its acetylation status. It will also lay the foundation for future work to investigate the potential role of dDOR.

CHAPTER 2. MATERIALS AND METHODS

2.1 Fly Stocks

Table 2.1 List of *Drosophila* Stocks for Investigative Use

Short name	Genotype	Description	Source and ID
		Driver Lines	
Cg-GAL4	*w[1118]; P{w[+mC]=Cg-GAL4.A}2*	GAL4 expressed in hemocytes, fat body and lymph gland.	Bloomington Stock Centre (BL) 7011
		FLP-out lines	
FLP-out empty	*y[1] w[1118], PthsFLPu;; ACjCD2jGal4*	Line used for generating mosaic positive and negative clones in one tissue (1st and 3rd chromosome).	Gifted from E. Tailleborg
FLP-out mCherry- Atg8a	*yw, hsflp; UAS- mCherryAtg8a; Ac>CD2>GAL4/SM66*	Line used for generating mosaic positive and negative clones in one tissue (1st, 2nd and 3rd chromosome).	Lab Stock
Hs-FLP:3xmCherry-Atg8a	*hs-Flp; 3xmCherry-Atg8a, UAS-GFP; Act>CD2>Gal4, UAS-Dcr2*	Line used for generating mosaic positive and negative clones in one tissue (1st, 2nd and 3rd chromosome).	Gifted from Gábor Juhász lab, University of Budapest.
FLP-out tandem Atg8a	*yw, hsflp; UAS-GFP-mCherry-Atg8a;Ac>CD2>GAL4/SM66b*	Line used for generating mosaic clones: wild-type cells as unmarked and mutant cells with tandem-Atg8a overexpression. (1st, 2nd and 3rd chromosome).	Lab stock
		Controls used for Gene disruption mutants	
Wild type (WT)	w^{1118}	Wild type (Canton-S) carrying white (w^{1118}) mutation.	Lab stock

***luciferase*-RNAi**	y[1] v[1]; P{y[+t7.7] v[+t1.8]=TRiP.JF01355}attP2	Expresses dsRNA for RNAi of luciferase under UAS control.	BL 31603
GFP nls	*w[1118]; P{w[+mC]=UAS-GFP.nls}8*	Expression of GFP, tagged at its N terminal end with the 15 amino acid SV40 nuclear localisation signal, is governed by UAS regulatory sequences.	BL 4776
UAS overexpression lines			
GFP-Atg8a	*P{ry[+t7.2]=hsFLP}1, y[1] w[1118]; P{w[+mC]=UAS-Atg8a.GFP}3*	GFP tagged Atg8a overexpression under GAL4 regulation (3rd chromosome).	BL 51656
UAS-GFP-Sequoia^{WT}	*w^{1118}; UAS-GFP- Sequoia;+/+*	GFP tagged Sequoia overexpression under GAL4 regulation (3rd chromosome).	Lab stock CG32904
UAS-GFP-Sequoia^{WT}	*w^{1118}; UAS-GFPSequoia ;+/+*	GFP tagged Sequoia overexpression under GAL4 regulation (2nd chromosome).	Lab stock CG32904
UAS-GFP-Sequoia^{LIRm} (Y313A/316A)	*w^{1118}; UAS-GFP- SequoiaLIRm ;+/+*	GFP tagged Sequoia LIR mutant overexpression under GAL4 regulation (3rd chromosome).	Lab stock CG32904
UAS-GFP-Sequoia^{LIRm} (Y313A/316A)	*w^{1118}; +/+; UAS GFP-SequoiaLIRm*	GFP tagged Sequoia LIR mutant overexpression under GAL4 regulation (2nd chromosome).	Lab stock CG32904
UAS-GFP-YL-1 (Lines 1-5)	*w^{1118}; UAS-GFP- YL-1 ;+/+*	GFP tagged YL-1 overexpression under GAL4 regulation (3rd chromosome).	Lab stock CG4621
UAS-Sir2-Myc	*w[1118]; P{w[+mC]=UASp-Sir2.Myc}9c*	Expresses high levels of myc-tagged Sir2 under UAS control.	BL 44216
UAS-3xFLAG-dDOR$_{long}$ (Lines 1-5)	*w^{1118}; UAS-3xFLAG- dDOR$_{long}$;+/+*	Expresses high levels of 3xFLAG tagged dDOR$_{long}$ under UAS control (3rd chromosome).	Lab stock

UAS-3xFLAG-dDOR$_{FENLL}$ (Lines 1-5)	*w^{1118}; UAS-3xFLAG-dDOR$_{FENLL}$;+/+*	Expresses high levels of 3xFLAG tagged dDOR$_{FENLL}$ under UAS control (3rd chromosome).	Lab stock
Mutant Lines			
YL-1SH^{1685}	*w; YL-1[SH1685] FRT40A/CyO*	Transposable element insertion site P{lacW}YL-1^{SH1685} .	BL 29503
Sir2[2A-7-11]	*w[1118]; Sir2[2A-7-11]*	Null mutant lines. A deletion resulting from the precise excision of P{PZ}Sir2^{05327a}, removes sequences from -16 to +859 with respect to the Sir2 transcription start[327].	BL 8838
Atg8a^{KG}	*P{hsFLP} Atg8a [KG07569]*	Atg8a null mutant line.	Gifted from Gábor Juhász, University of Budapest.
Atg9^{B5}	*Atg9^{B5}/CyO*	Homozygous Atg9^{B5} are semi lethal and can be rescued by crossing to DF(2R)ED2487 deficiency.	CG32672 Gifted from Gabor Juhász, Eotvos Lorand University, Budapest[328].
Atg9$^{DF(2R)ED2487}$	*Atg9$^{DF(ED2487)}$/GFP twi CyO*	Hemizygous are semi lethal. Used to create viable Atg9^{B5} mutants. Expresses GFP transgene.	Gifted from Gabor Juhász, Eotvos Lorand University, Budapest[328]
RNA inference inverted repeats lines (RNAi)			
***sir2*-RNAi #2**	*y[1] sc[*] v[1]; P{y[+t7.7] v[+t1.8]=TRiP.HMS00484}attP2*	*Sir2*-RNAi under UAS regulation	BL 32481
***sir2*-RNAi #1**	*y[1] sc[*] v[1]; P{y[+t7.7] v[+t1.8]=TRiP.HMS00484}attP2*	*Sir2*-RNAi under UAS regulation	BL 31636
***sequoia*-RNAi**	*y1 v1; P{TRiP.HMC03316}attP2/TM3, Sb1 Ser1*	*Sequoia*-RNAi under UAS regulation	Vienna Drosophila Resource Centre (VDRC) 50146

***yl-1*- RNAi #2**	*P{KK100166}VIE-260B*	*YL-1*-RNAi under UAS regulation. Balanced by *CyO*, homozygous sterile	VDRC 107951
***yl-1*-RNAi #3**	*y[1] v[1]; P{y[+t7.7] v[+t1.8]=TRiP.JF02229}attP2*	*YL-1*-RNAi under UAS regulation.	BL 31938
Balancer lines			
ICMT	*yw; If/CyO; M(3)76A,kar, ry, Sb(mkrs)/TM6b*	Present on 2nd and 3rd chromosome	Lab stock
HS;mkrs/TM6b	*HS;mkrs/TM6b, Tb, Hu*	Present on 3rd chromosome	Lab stock

2.1.1 The use of balancers

Balancer chromosomes are an essential component of the *Drosophila* genetic toolbox. They keep homozygous lethal or sterile mutations from being lost from a population and prevent multiple alleles on the same chromosome from being separated by meiotic recombination.

All balancers have two essential features - recessive deleterious mutations and inversion breakpoints. A recessive lethal or sterile mutation in one gene can be maintained in a population if it is combined with a recessive lethal or sterile mutation in another gene on the homologous chromosome. This arrangement of mutations is called a 'balanced system' and describes how the term 'balancer' was first coined. It must be noted that a balanced system will only persist if no meiotic recombination occurs between the deleterious mutations to generate chromosomes lacking mutations. This is where the use of inversion breakpoints is essential in preventing the recovery of recombinant chromosomes. This is achieved in two ways; firstly, crossovers do not form in the vicinity of inversion breakpoints, because synapsis is inhibited within these regions. Secondly, single crossovers inside inversions lead to aneuploid gametes that cannot give rise to normal progeny.

Another very useful feature of balancers is that many carry dominant and recessive visible mutations which allow for indications of which members of a progeny harbour a specific mutation through their phenotype. Balancers used for selection in this study include: *CyO,* which is probably the most popular second chromosome balancer and yields the 'curly wing' phenotype in adults, *Tb* 'tubby', which gives rise to progeny with a noticeably short and wide

body, and *Sb* 'stubble', which produces adults with short bristles on their heads and backs. Some balancers also carry transgenes which allow balancers to be followed easily in crosses or to be used in specific experiments, such as insertions that express GFP. *CyO* often carries GFP for example, as it allows for the progeny to be screened during the larval stage before the development of wings.

2.1.2 Working line generation

Transgenic lines UAS-GFP-Sequoia^{WT}, UAS-GFP-Sequoia^{LIRm}, UAS-GFP-YL-1, UAS-3xFLAG-dDOR^{long} and UAS-3xFLAG-dDOR^{FENLL} were generated by BestGene Inc., using P-element insertion (section 2.2.4). Optimal strains for experiments involving UAS-GFP-Sequoia^{WT} and UAS-GFP-Sequoia^{LIRm} lines were established prior to the beginning of this project. For experiments, a line which carried insertion on the 2nd chromosome and one which carried insertion on the 3rd chromosome was used for both UAS-GFP-Sequoia^{WT} and UAS-GFP-Sequoia^{LIRm}. Five lines were received and screened for both UAS-3xFLAG-dDOR^{long} and UAS-3xFLAG-dDOR^{FENLL}. Three lines in total were screened for UAS-GFP-YL-1.

The double balancer line ICMT, was produced by Dr. Anne-Claire Jacomin. Here this line was crossed with UAS-GFP-Sequoia^{WT} and UAS-GFP-Sequoia^{LIRm} to produce the intermediate line; *+/CyO;GFP-Sequoia$^{WT/LIR}$/mkrs*. From here, *CyO* males were collected and crossed with virgin *Tb* and *Sb* females from another lab produced balancer line: HS;mkrs/TM6b. This produced a new stable line: *HS/CyO; GFP-Sequoia$^{WT/LIR}$/TM6b, Tb, Hu*. Larvae which were not expressing the marker *Tb* were selected for experimentation from the F1 progeny.

In order to produce the mosaic Atg8a-expressing line- *yw, hs::FLP; UAS-mCherry-Atg8a; AC>CD2>Gal4*- the 'FLP-out empty' line was previously crossed with the *UAS-mCherry-Atg8a* line from Bloomington. The mCherry-Atg8a line was also crossed with the collagen driver line *Cg-Gal4* in the production of the line which constitutively expresses mCherry-Atg8a in the fat body and in haemocytes: *Cg-Gal4; UAS-mCherry-Atg8a*.

Homozygous Atg9^{B5} and hemizygous Atg9$^{Df(2R)ED2486}$ flies are both semi lethal, and were rescued through the crossing of viable *^{Atg9B5}/CyO* candidates (non-*CyO* males) to *Atg9$^{Df(2R)ED2487}$/CyO twi GFP* deficiency (*CyO* females). Non-CyO flies have a straight wing phenotype and can be easily distinguished from *CyO* "Curly" winged adults. Hemizygous F1 progeny (non-GFP) larvae were collected for experimentation.

2.2 The Genetic Toolbox

2.2.1 Ectopic expression using GAL4/UAS system

The GAL4/UAS (Upstream Activation Sequence) is a system which was originally identified in yeast; where GAL4 is a transcriptional activator and binds the UAS sequence, thus activating the gene downstream of UAS. This system, first described in *Drosophila* by Brand and Perrimon in 1993, now represents one of the most powerful tools for targeted gene expression in this organism[329]. The system works through two components (Fig. 2.1):

1) An enhancer/promoter which is driven by the GAL4 line, termed the 'driver'.
2) A transgene under the control of UAS; this could either be a gene for overexpression or an RNAi construct containing an inverted sequence targeting a specific gene.

Here, we use Cg-GAL4 as a driver line, in which the collagen promotor Cg drives the expression of GAL4 in the haemocytes, fat body and lymph gland (with the tissue of interest here specifically being the fat body). Crossing a GAL4 line with a line in which the gene of interest is attached to UAS allows the gene of interest to be expressed in the F1 progeny[329]. Since both of the aforementioned components are carried in separate fly lines, no expression of the protein will be observed in the parents[330].

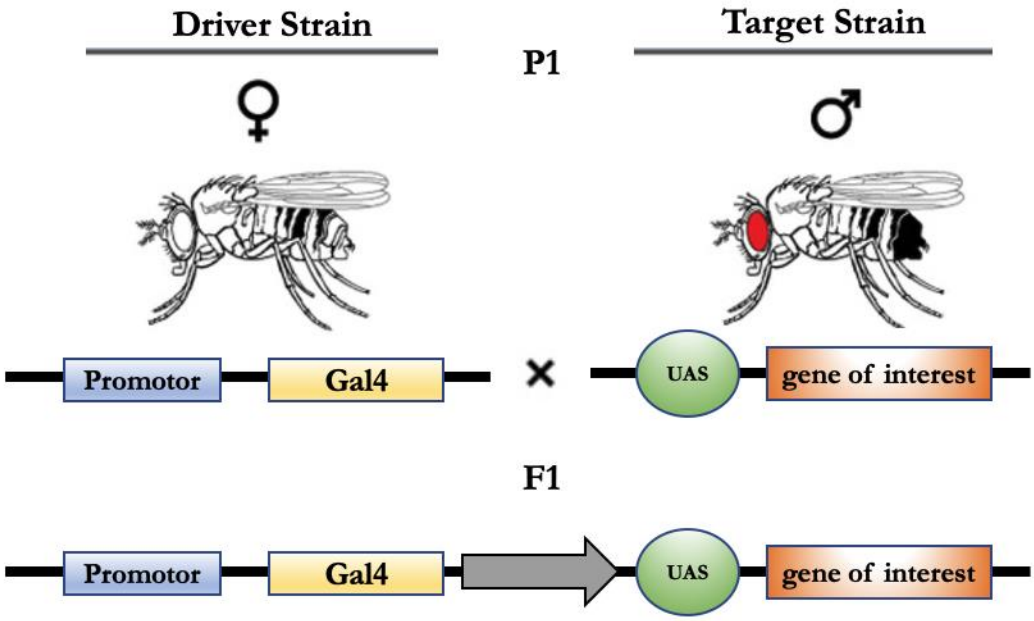

Figure 2.1 Gene Expression using the GAL4/UAS system.
The driver strain carries an insertion which allows for the production of the Gal4 transcription factor, under the control of its promotor. The target strain carries an insertion for the gene of interest with an Upstream Activating System (UAS). When the two strains are crossed the F1 progeny the Gal4 transcription factor will bind to the UAS, thus expressing the gene of interest.

2.2.2 The FLP-out system

The GAL4/UAS system has been combined with the FLP/FRT system to generate the Actin>CD2>GAL4 'flip out system' in order to monitor the expression of a UAS-transgene in clones. The two components of the FLP-out system, which like the GAL4/UAS are taken from yeast, are:

1) Hs-FLP, a heat inducible site-specific recombinase called flipase
2) A FLP-out cassette

The core FLP-out cassette comprises two recognition sites for the flipase, named FRT sites (Flipase Recognition Target). In addition to the FRT sites, the system contains a termination cassette that includes a coding region for a DNA spacer, and a transcriptional termination signal[331]. Here the DNA spacer is CD2 (a cell adhesion molecule from rat) and the constitutive promotor is Ac (Actin). The termination cassette is placed downstream of Ac. Gene expression is controlled by heat-shock induced expression of the Flip recombinase[332]. Flip will recognise the FRT sites in the Ac>CD2>Gal4 cassette. This results in the interruption cassette being 'flipped

out', thus causing CD2 protein expression in the neighbouring control clones, and *Ac* promoting *GAL4* activity in the clone. Subsequently, clones become positively marked with the co-expression of a fluorescent transgene and the UAS-transgene of interest. Here, hsFLP-out mCherry-Atg8a was used to create mitotic clones in the fat body, which express mCherry- Atg8a, with Ac>CD2>GAL4 is on the 3rd chromosome and UAS-mCherry-Atg8a is on the 2nd chromosome. These clones will thus become positively marked via expression of UAS-mCherry-Atg8a, with negative clones remaining unlabelled. The advantages of using the FLP-out system is that it provides the ability to study targeted gene mutations that would otherwise cause lethality if broadly expressed. This system also enables the ability to compare single cells carrying gene mutations to un-manipulated cells in the same environment[333].

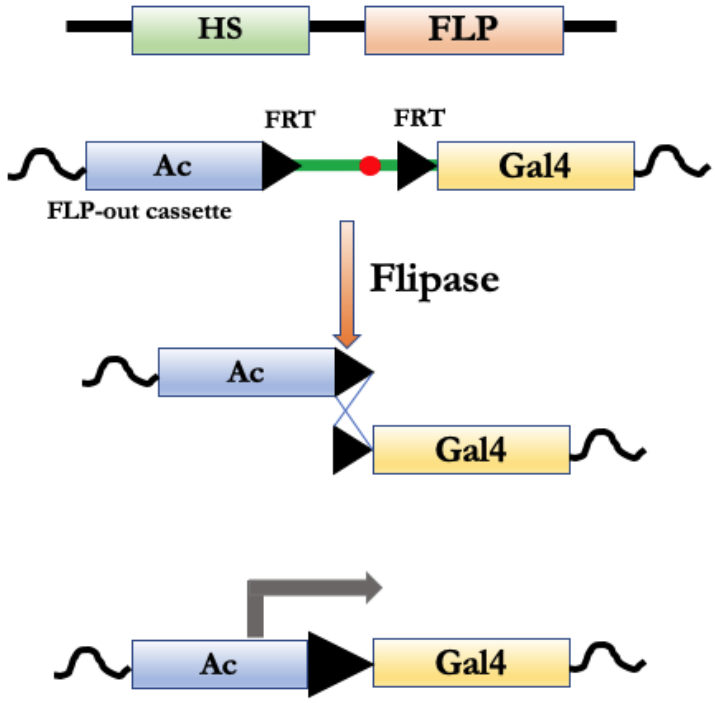

Figure 2.2 Schematic of the FLP-out System.
The system comprises an FLP which is under the control of a heat shock promotor (hs-FLP), and an FLP-out cassette. The cassette is made up of a DNA spacer (green), which encodes a marker, and a transcriptional termination signal (yellow). The FLP-out cassette is flanked by two FRT sites (black arrowheads). The termination cassette is placed downstream of the promotor (Ac) and upstream of the gene of interest (Gal4). Flipase is activated by heat shock, triggering site-specific recombination between the two FRT sites. The DNA spacer is also excised, including the stop codon. This results on the activation of the gene of interest by the promotor.

In all cases, virgin females from the FLP-out mCherry-Atg8a lines were crossed with males from the UAS-transgene line of interest at a 3:1 ratio. In theory to induce the flipase, embryos require to be heat shocked 12-20 hours after egg laying, at 37°C for 15-60 minutes. In many cases the heat shock reporter was found to induce flipase at 25°C [20]. Therefore, the standard heat shock procedure was not essential in order to create clones. However, in some cases heat shock was required in order to increase the frequency of positive clones expressed throughout a sample and was therefore carried out in a subset of experiments.

2.2.3 P-element mediated system

Transgenic flies were created using P-element mediated systems that result in semi-random insertions into the genome. This process involved the insertion of a gene of interest into a plasmid between two P-element ends followed by the microinjection of this construct, along with a transposase, into syncytial blastoderm embryos. Here, the gene of interest was inserted into a construct containing a UAS, allowing implementation of the Gal4/UAS system.

The P-element system is also used to implement alternative reverse genetic approaches; with many of the RNAi lines obtained here generated (by the source Table 2.1) via this method through the targeted silencing of homologous genes through RNAi mediated degradation of cognate messenger RNA[334].

2.2.4 Tandem tagged-Atg8a

An accumulation of Atg8a-positive puncta in the cell can result either from an induction or blockade of the autophagic flux. To make the distinction between these two possibilities, a tandem-tagged Atg8a (GFP-mCherry-Atg8a)[335] can be used. The tandem fusion of GFP and mCherry to Atg8 was first described for use in transfected HeLa and MEF cells[336] and subsequently in *Drosophila* by Nezis and colleagues[337]. Due to the differential pH sensitivity of GFP and mCherry, the GFP-mCherry-Atg8 marker co-labels non-acidified autophagic compartments (phagophore and autophagosome) with both GFP and mCherry signals. Following fusion with acidic late endosomes or lysosomes the GFP fluorescence is subsequently quenched and only the mCherry signal remains intact (Fig. 2.3). Most cells undergoing autophagy will display a combination of both green and red autophagosomes (seen as yellow) as well as red-only autolysosomes. This marker thus provides evidence of both biogenesis of autophagosomes and their successful fusion with a properly acidified lysosomal compartment.

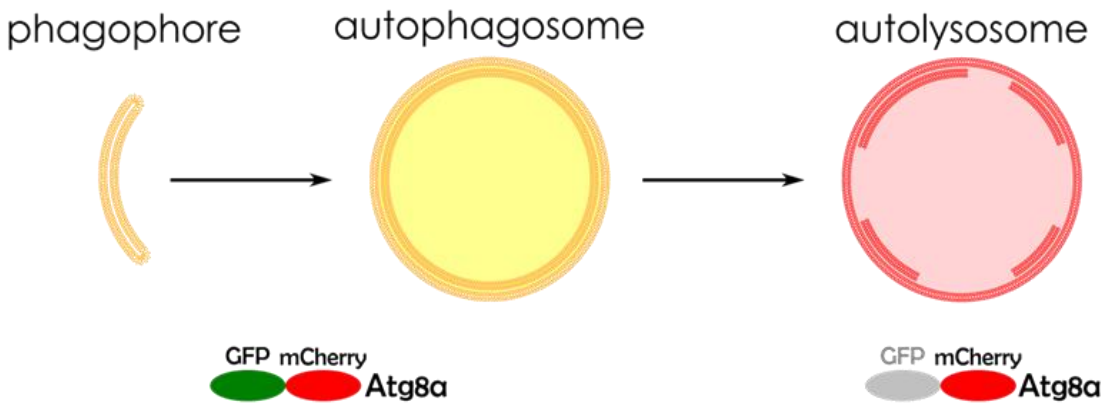

Figure 2.3 Tandem Tagged Atg8a.
The tandem tagged version of Atg8a allows the accumulation of Atg8a puncta between the cell to be distinguished as either the accumulation of autophagosome: since there is structure is non-acidic the GFP and mCherry are both expressed to emit yellow fluorescence. Or autolysosomes: these constitute acidic structures (through the production of acidic lysosomal acid proteases). Resulting in GFP being quenched and only mCherry (Red) being emitted.

2.3 Fly Husbandry

2.3.1 Rearing conditions

Flies used in experiments were kept at 25°C and 70% relative humidity in plastic vials. Genetic crosses were transferred daily. Lab stocks of each fly strain were kept at 18°C and 70% relative humidity and were transferred into new tubes once every two weeks. Extra yeast paste was added into the tubes of weaker strains in order to enhance proliferation.

2.3.2 Fly food recipe

Per litre of water, 42 g inactive dry yeast (Dutscher Ltd. ref. 789126), 60 g yellow cornmeal, 130 g sucrose (Sigma-Aldrich) and 5.5 g agar was added. The mixture was autoclaved at 121°C for 20 minutes. Once cooled, the mixture was supplemented with 6 ml of pure propionic acid and 15 ml of 10% nipagin.

2.3.3 Genetic crosses

Genetic crosses were performed through the addition of males to virgin females at a ratio of 1:3, with the selection of the F_1 progeny for experimentation. Virgins were collected from stocks

maintained at 25°C; here females which have been eclosed within an 8-hour window will reject courtship and thus be suitable for entry into genetic mating scheme. Virgins were identified through the presence of a meconium which is visible through the abdominal cuticle, a pale pigmentation and unexpanded wings. Once collected females were isolated for 2 days in order to confirm their virginity. In order to allow for the identification of the gender and phenotype, adult *Drosophila* flies were anaesthetised on a gas pad using continuous administration of carbon dioxide.

2.3.4 Starvation conditions

For starvation conditions 20% sucrose solution was prepared in distilled water, mixed using a magnetic stirrer and sterile filtered using a 0.2μm syringe filter. The solution was stored at RT (Room Temperature) in a sterile tube.

For harsher starvation conditions, 0.5g of agar was dissolved in 100ml of distilled water; with 3ml of the solution being placed into a sterile tube, which was allowed to cool and set at RT. Tubes were stored at 4°C for up to seven days. Before introduction of the larvae to the tubes, they were placed at room temperature for two hours.

Once larvae reached the second (for 24-hour starvation) or early third (for 4-hour starvation) instar stage, larvae were removed from their tubes and washed in PBS (Phosphate-Buffered Saline) until clean. It must be noted that as larvae take 24 hours to go from L3 to pupae, 24-hour starvation must be done in L2 larvae to avoid the onset of developmental autophagy.

Once washed, larvae were transferred to either a tube with 1ml of 20% sucrose solution or 0.5% agar. Tubes were capped with a cotton plug and placed at 25°C for either 4 or 24 hours.

2.4 Tissue Staining and Confocal Microscopy

2.4.1 Fat Body Dissection

In all cases third instar stage larvae were rinsed in twice PBS and transferred into fresh PBS on a silicon plate. Under a light microscope, larvae were held steadily from one end using sharp tweezers and the posterior extremity was cut open. The intestine, gut and trachea were removed,

and the fat body was isolated. Fat bodies were transferred into a collection basket and immersed in PBS. The time between dissection and fixation was kept to a minimum as to preserve the structure as faithfully as possible compared to the living state. In all cases, 10-15 larvae were used per condition.

2.4.2 Tissue Fixation and Staining

Fat body samples were fixed in 300 µl 4% PFA (Paraformaldehyde) in PBS, for 40 minutes at RT. Permeabilization is performed in 300 µl PBX (PBS+ 0.1% Triton X-100) for 10 minutes, three times. At this point samples which constitutively express a fluorescent (e.g. GFP) tag can undergo nuclei staining or alternatively they can be stored at 4°C overnight. Nuclei staining was carried out in complete darkness through incubation in 300 µl Hoechst 1µg/mL in PBS, at RT for 10 minutes. After this period, samples were transferred into PBS to remove excess Hoechst.

For IF (Immunofluorescence) and the required the use of an antibody; samples were blocked for one hour in PBX+0.1% BSA at room temperature. Incubation with a primary antibody, diluted in PBX+0.1% BSA, was carried out overnight at 4°C. Three washes were carried out for 10 minutes each with PBX+0.1% BSA before incubation with the secondary antibody, diluted in PBX+0.1% BSA, for two hours at RT. Three 10 minute washes were conducted with PBX+0.1% BSA, followed by another three using PBS. Nuclei staining was carried out as described previously.

PBS with 4% formaldehyde, PBX and PBX+ 0.1% BSA were prepared freshly for each new experiment. All fixation, wash and incubation steps were carried out in a 48-well plate.

Table 2.2 List of Immunofluorescence Antibodies.

IF Antibody/Dye	Dilution	Source
Mouse Anti-3xFLAG	1:5000	Sigma F1804
Goat Anti-mouse IgG, CF488	1:500	Sigma SAB4600042
Hoechst 33342	1:1000	New England Biolabs 4082

2.4.3 Tissue Mounting

Mounting slides were loaded with 16 µl of mounting media (2% N-propyl gallate, 20% 5x PBS, and 70% glycerol). Fat body tissues were carefully removed and arranged in the mounting media

in a manner to ensure they were evenly spread and flat. Samples were covered using a coverslip and left for 20 seconds to allow the mounting media to spread to edges. Once stabilised, coverslips were sealed using clear nail varnish. Slides were left to dry lying flat before being stored in complete darkness at 4°C.

Sample slides were visualised using Zeiss LSM 880 confocal laser scanning microscope with 63x objective oil immersion. Images were analysed using Zen Software (Black edition; Version 8.1; Carl Zeiss, Inc.) and Image J software (National Institutes of Health).

2.4.4 Colocalisation Analysis

Images were subjected to colocalisation analysis in order to infer a relationship between a tagged protein of interest (GFP-Sequoia$^{WT/LIRm}$ and 3xFLAG-dDOR$_{Long/FENLL}$) and mCherry-Atg8a. *Coloc2* (a Fiji plug-in) was implemented to perform an intensity correlation over a space method of Pearson's correlation. Using ImageJ, each image was separated into individual fluorescent channels. For nuclear co-localisation analysis involving GFP-Sequoia$^{WT/LIRm}$, the GFP/mCherry nuclear compartments were isolated using the corresponding signal from the Hoechst stained channel. Reversely, for cytoplasmic co-localisation regarding 3xFLAG-dDOR$_{Long/FENLL,}$ the GFP/mCherry nuclear compartment was removed using the same method. The green channel (corresponding to the tagged protein of interest) was further adjusted to decrease noise via the 'Despeckle' tool. The 'Watershed' function was selected in order to create a binary image; with the resulting particles added to the region of interest manager. Particles were overlapped onto the adjusted red channel (mCherry-Atg8a) and the *Coloc2* tool was selected in order to measure Pearson's correlation.

2.4.5 Atg8a puncta counter

In order to quantify the induction of autophagy visualised in different genetic environments, the number of mCherry-Atg8a puncta present in the cytoplasmic region of images was processed. To do this, a previously built ImageJ macro entitled "AtgCOUNTER"[338] was utilised. This functions by creating a binary image in which only cytoplasmic mCherry puncta are present. The channels are firstly split, and a threshold function is applied to the Hoechst stained channel in order to select the nucleus. The corresponding region is subsequently removed from mCherry to avoid any false positive results obtained from nuclear signal. The mCherry channel is processed in order to produce a clean binary image and the number particles are filtered by a set size

threshold; with those remaining being counted and numbered by the 'Analyse Particle' function in ImageJ.

2.5 Molecular Biology

2.5.1 RNA Extraction

RNA extraction was performed using the Ambion® by Life Technologies, Purelink™ RNA Mini Kit. The RNA extraction buffer was supplemented with 10 µl/ml β- mercaptoethanol. A total of 15 full body adult flies or 20 third instar stage larvae were collected in liquid nitrogen. RNA extraction steps carried out using a protocol supplied by Ambion®. RNA concentration was determined using the NanoDrop Spectrometer (Implen, geneflow, NP80). Samples were stored long term at -80°C.

2.5.2 Reverse Transcription

For DNA removal, 1µl of 10x reaction buffer (DNAase I Kit, Thermo Scientific) and 1µl DNAse I was added to 1µg of RNA. Samples were left to incubate for 30 minutes at 37°C. In order to deactivate the enzyme 1µl of 50mM EDTA was added at 65°C for 10 minutes.

2.5.3 cDNA Synthesis

cDNA synthesis was carried with the ThermoScientific RevertAid Kit using 1µg of RNA. Incubation times were as follow: 5 minutes at 25°C, 60 minutes at 42°C and 5 minutes at 70°C. Samples were stored long term at -80°C or carried forward immediately for experimentation.

2.5.4 RT-qPCR

RT-qPCR (Reverse Transcription- quantitative PCR) was performed using the Promega GoTaq qPCR Master Mix (2x), with 1:1000 dilution of the reverse transcription product. Samples were prepared using Table 2.3 below.

Table 2.3 RT-qPCR Experiment Reaction Mixture. Quantities for 1x mixture and scaled up as appropriate.

Reaction Mixture component	Volume
GoTaq (Promega) Master Mix (2x)	12.5 µl
H_2O	6.5 µl
Forward Primer (10 µM)	0.5 µl
Reverse Primer (10 µM)	0.5 µl

Diluted cDNA (5 μ) was added separately to the qPCR plates to give an overall working volume of 25 μl. Amplification was performed on an Agilent Technologies Stratagene Mx3005P qPCR cycler using a SYBR fluorescent tracer and the following thermal profile:

Stage 1: 1x cycle at 95°C for 5 mins

Stage 2: 45x cycles at 95°C for 15 secs/60°C for 40 secs

Stage 3: 1 x cycle at 95°C for 1 min/60°C for 20 secs/95°C for 30 secs

2.5.5 Primer Optimisation

Prior to all qPCR experiments, in order to optimise conditions, the efficiency of all primers was tested using cDNA synthesised from W^{1118} larvae. Primer efficiency was tested on cDNA across a five-fold serial dilution: 1/5, 1/25, 1/125, 1/625, 1/3125. Additionally, a no reverse transcription and an NTC (No Template Control) control were tested. For each *Atg* gene, two sets of primers were designed, with the most efficient set being selected for expression analysis. All primers were diluted to 10 μM. Primers used were designed using the Primer3 software and created by IDT (U.K).

Table 2.4 List of RT-qPCR Primers (5' → 3')

Gene name	Forward sequence	Reverse sequence
	***Atg* genes**	
Mitf	CACCAATTGACTTCGCGTGA	CTACGGTGCCAAGTGACCTA
Mitf II	GCCACAATCACCGAGTTCAA	CTCACGCGAAGTCAATTGGT
Atg4a	CAAACTAAACCAGCCGCAGA	GTTTTGGCCTGTGTTTTCGC
Atg4b	GCCACATCGACATCAACCTC	TTGGGAACTCTCGACGGTAG
Atg4b II	AACCTCCTTGTATCCAGCCC	CAGTCCGAGGTGTAGTTGGA
Atg10	GTCTTTTGGATGTGGAGGCC	GGGCTTTCCGAACTGCTTTA
Atg10 II	CCATCGCCACCAGTTCTTG	ACCTGTGTACAAAGCTGGGT
Atg12	TGCCCCGGATCAGATAATCA	GCGTATCGATTTAGCCCCAC
Atg12 II	GCCCCGGATCAGATAATCAAGA	TGTGCGTATCGATTTAGCCC
Atg16	AGAACCCAAGCCAAGAGTCC	CCTTGAAGTTGTCGCACTCC
Atg101 II	CTCCGATCTCCTGACCGAAA	GCGAGCGTTTCCTTGATGAT
Lamp1	CGGAGCGTTTAAGACACCAG	CACATCCGAAGTTTCCGAGC
Lamp1 II	TGTCGTATCACTGCACTCGT	AACCACATCCGAAGTTTCCG
Atg8b	GTATTCCAGTCCGCCCAGAT	AGTAGAACTGGCCCACTGTC
Tor	ATTCCAACACACACACACCG	AGACAATTCTGGGTGCAAGC

Atg17	GGCAACAGCGAAGAACAGAA	GCTCTGCTTCTTCTCTTGCC
Atg17 II	AGTGGCGTTGAAAGAGAGGA	GGTGTGTTCGTGTTTTGGCT
Atg18a	CTCGATTAGCACTCCCTGGT	TAGCTAACACCTCTGCCTCG
Atg18a II	CTCTGTTGCTGTCCCACTTG	GCTGTTGACTAGTGGTTGGC
Atg18b	CAAGGACAACACGGAGCAAA	AGGATCTTCATGTCGCGGAT
Atg18b II	GGTCTACGCCTGTTCTCGAT	AAAGTGCAGCATCTTGAGGC
Atg1	AGGGCCAGAGAATCACATTTAG	CGTCTTCAGTTGTCCCTTCTT
Atg5 I	ATTAAGCCGGAGCCTTTCTATC	ATCGCCATACGGTTCCATTAG
Atg5 II	GACTGACAAGGTTCGCAAGTA	GTTCCATTAGCCTCCGATTGA
Atg8a	AGGATGCCCTCTTCTTCTTTG	GCTAACTCGCCGTCCATATT
Atg7	GTGGGCTGGGAGCTAAATAAA	CTGACGCACTGGATTAGAGAAC
Atg13 I	ACGCCCGCCTACAAATTATC	GTCGCAACGGCTTCTCTATATC
Atg13 II	ATGGAAGGGCGGTCAATATG	GAGGGCTCAAGCCAAAGTATAG
Atg14 I	GCGTCAGAAACGGAAACATTAC	CTTGACCTTGTCCGGGTATTT
Atg14 II	GGGTCTTCTGGACAGCATAAA	CTTACGACAGAAGTCGCCATAG
	House-keeping genes	
RP49	GCTAAGCTGTCGCACAAATG	CGATCTCGCCGCAGTAAA
	Other genes	
YL-1	TCAGGAGGACGAAGAGGATAAG	CTTGGTGGGACGTGATTTCT
Sequoia	CGCATGGAGAACACCGAATA	CCCTTGACTAGACTTGGATGTG
Sir2 1	TCCGTGCTGTGGGACTATTT	GATCGGGAAAATCATGGGCC
Sir2 2	ACACAGAACATCGACACCCT	CGGAATTCGCTGGGCAAATA
Sir2 3	GGCCCATGATTTTCCCGATC	AGGGTGTCGATGTTCTGTGT
Sir2 4	ACGCAATTCTATCCGCCAAC	TC TCCTCGCCCATTGACTT
Sir2 5	TCAGTGAACACCTTCGACGA	GGTCGTGGATCCCTCTTGAA
Kenny	GGGTTCATACCATCAGGCTAAA	CTGGCCTTCAGCTCGTTAAT
Ref(2)P	CGAAGGCTGCAGAACAAACT	TGGAGTTGGCTGAGTGG
dDOR	GCTGCAGGCGATGTAATTGA	GGAGAAGGAAGACGAGGAGG

Using the MxPro- Mx3005P Comparative Quantitation program (v4. 10 sBuild 389, Schema 85, 2007) the specificity of the PCR product yielded by each primer pair was assessed using the status of the corresponding dissociation curves. A single peak at the thermal dissociation plot was desired as it was indicative of a single amplicon from the PCR reaction. For each primer set, the linear phase of exponential amplification of the PCR reaction was determined. This is based on the formula that resolves the DNA amount according to the Ct (Cycle threshold) value and is generated from the standard curve using the series of diluted cDNA. Here, a shift in linear amplification in correspondence to the dilution factor is indicative of a well-functioning reaction (Fig. 2.4 A, B). All data was generated by MxPro.

A

B

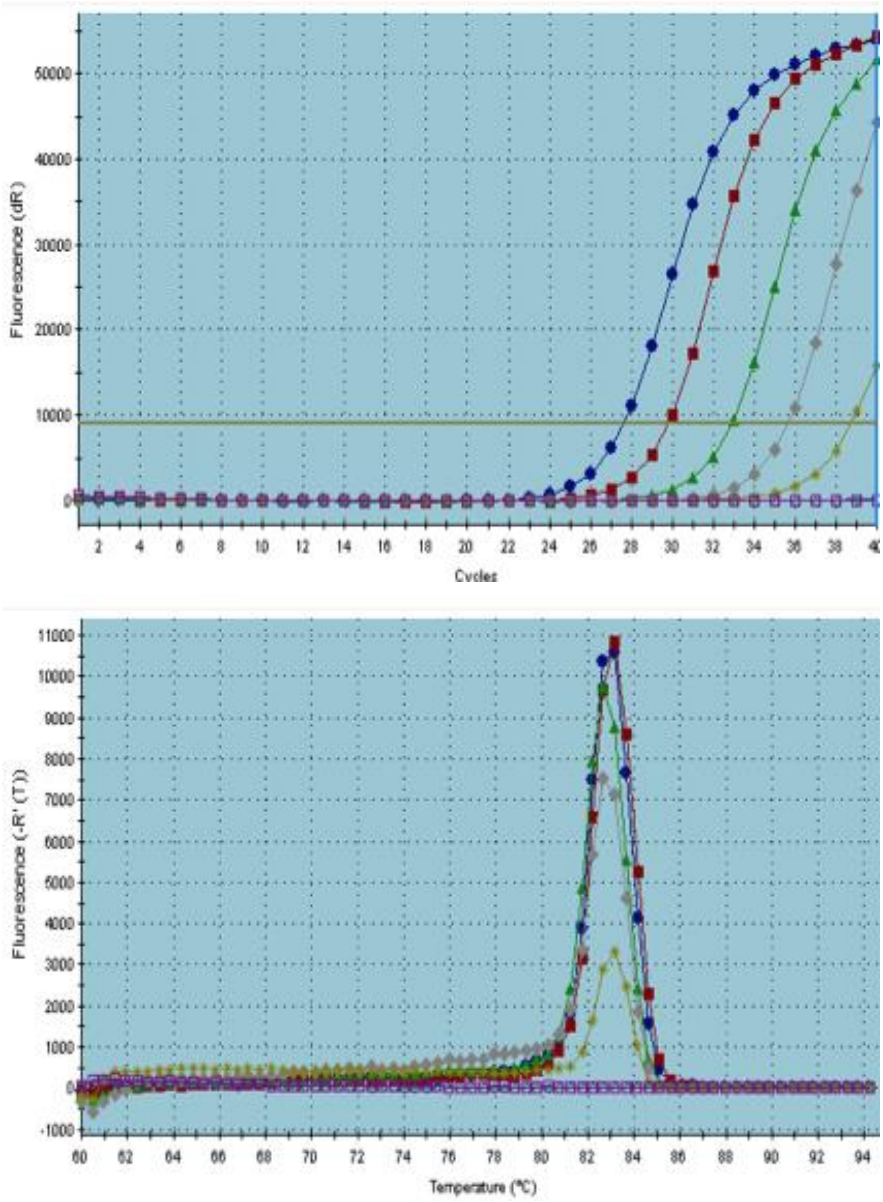

Figure 2.4 Exemplary Output Curve from RT-qPCR Analysis from Primer Optimisation Experiments Conducted with the *Atg5* Primers. A: The first derivative of raw fluorescence plotted against an increase in temperature. The single melt peak at 83°C indicates a single PCR product is being amplified in these samples. **B:** Amplification plots of standards in a dilution series over orders of magnitude: 1/5, 1/25, 1/125, 1/625, 1/3125. As expected, no fluorescence was measured in the NTC and no RT control (overlapping pink). Data generated by MxPro.

2.5.6 qPCR Analysis

Analysis was conducted using the MxPro- Mx3005P Comparative Quantitation program. Relative quantity to a calibrator (W^{1118} *or luciferase*-RNAi) was calculated and relative expression

levels were normalised to the housekeeping gene *rp49,* for all experiments. The reference dye used for all plate analyses was SYBR.

2.6 Plasmid Construction, Cloning and Mutagenesis

2.6.1 Plasmid vectors

The plasmid vectors used for creating the 3xFLAG-dDOR$_{long/FENLL}$ transgenic flies, and for plasmids created for GST (Glutathione S-Transferase)-pulldown assays, are outlined below:

1) **pUASattB**- containing a 5x repeat of the UAS promoter, which controls the expression of the insert gene of interest. The vector was previously recombined with the sequence of an N-terminal appended 3xFLAG tag, and with the fly coding sequence for dTak1-WT by Panos Tsapras, Nezis lab. This was subsequently used as a donor plasmid for the insertion of dDOR$_{long/FENLL}$ in the place of dTAK1. To append the 3xFLAG tag to the DNA of the dDOR $_{long/FENLL}$ insert, cDNAs were made from recombinant donor vectors (pUAST-dDOR$_{long}$ and pUASt-dDOR$_{FENLL}$), which were kindly gifted by Aurielio Teleman[339]. Successful recombinant pUASattB/ 3xFLAG-dDOR$_{long/FENLL}$ clones were prepped, and vectors were sent to BestGene Inc. for embryonic microinjection.
2) **pET28a[+]**-contains the 6xHis-tag sequence, recombined with the fly coding sequence of Sequoia^{WT}, and dDOR^{WT}. pET28a-6xHis-Sequoia had previously been created and validated in the lab. To append the 6xHis tag to the DNA of the dDOR$^{WT/LIR}$ insert, cDNAs were made from recombinant donor vectors pUAST-dDOR$_{long}$. To create the dDOR LIR mutant, an additional mutagenesis step was employed on the successfully recombinant pET28a-6xHis-dDOR^{WT} clone.
3) **pGEX** -contains the GST-tag sequence, either alone, or recombined with the fly coding sequence for Atg8a. Both pGEX-GST and pGEX-GST::Atg8a had both been previously created and validated in our lab.
4) **pDEST15** (contains the GST-tag sequence and a lethal gene, the sequence of which is disrupted upon successful insertion of our gene of interest within that locus). The vector is recombined with the fly coding sequence for Atg8a, or Atg8a^{LDS}. pDEST15-GST::Atg8a, and pDEST15-GST::Atg8a^{LDS} were previously created and validated previously in our lab. Acetylation mimic constructs: pDEST15-GST::Atg8a^{K46Q},

pDEST15-GST::Atg8a^{K48Q} and pDEST15-GST::Atg8a^{K49Q} were received from Terje Johansen lab, University of Tromsø.

All recombined structures were validated for the correct sequence insertion and in-frame orientation via sequencing by GATC Biotech (Konstanz, Germany). Samples were submitted in accordance with guidelines provided.

2.6.2 Polymerase Chain Reaction

PCR reactions were performed using the *Taq* DNA polymerase master mix (Promega, UK; 25 U/ml *Taq* DNA polymerase, *Taq* Reaction buffer, 200µM of each dNTP, 1.5mM MgCl2) with 1µl of each primer and 1-2 ng of plasmid DNA. Primers were designed, using Prime3, to append 5'- and 3'- prime flanking restriction sites to the amplicon in correspondence with the target vector. Primer sets were created by IDT (oligonucleotide sequences are provided in Table 2.5).

Reactions were run in a BIO-RAD T1000 Thermal Cycler, typically for 25 cycles. Annealing temperatures were set at 5°C lower than the lowest primer Tm (melting temperature) with an extension time of 1 min per Kb (length of plasmid).

Standard PCR cycling conditions were:

Stage 1: 1x cycle at 95°C for 1 minutes
Stage 2: 25x cycles at 95°C for 30 secs/-5°C of primer Tm for 30 sec/72 °C for 1 min
Stage 3: 72°C for 5 minutes (+4°C hold)

2.6.2.1 Mutagenesis

To induce amino-acid substitutions at key residues of dDOR^{WT} (DE**W**YI**V** → DE**A**YI**A**), point mutations were created using the QuickChange site-directed mutagenesis kit (Stratgene, 200523) and Pfu Ultra II HS DNA Polymerase (Agilent, 60070). The Sequoia LIR mutant (EE**Y**QV**I** → EE**A**QV**A**) had previously been created in the lab using the same method.

A list of primers that were used during the PCR phase of cloning experiments in the construction of dDOR plasmids, including those used for sequencing, are listed in Table 2.5.

Table 2.5 List of Primers Used in the Construction of dDOR Plasmids

Primer Name	Sequence (5'→3')
Amplification of dDOR from pUAST-dDOR$_{long/FENLL}$	
dDOR DNA amplification Fwd.	TAAGCACATATGATGTTAAGCAGCCTCGCCTCG
dDOR$_l$ DNA amplification Rev	TGCTTAGCTAGCCTAGTAGCAGCACTTGCTGCGTTG
Mutagenesis (pET28a-6xHis-dDOR^{WT})	
dDOR LIR Mutation Fwd.	GACGAGGACGAAGCGTACATTGCGGAGAAGGAAGAC
dDOR LIR Mutation Rev	GTCTTCCTTCTCCACAATGTACCATTCGTCCTCGTC
Insertion of enzyme restriction sites (in pUAST-dDOR$_{long/FENLL}$)	
dDOR *Nde*I site insert Fwd.	TAAGCACATATGATGTTAAGCAGCCTCGCCTCG
dDOR *NheI* site insert Rev	TGCTTAGCTAGCCTAGTAGCACTTGCTGCGTTG
dDOR *Acc65*I site insert Fwd.	CCGGGTACCGGGAATTCATGTTAA
dDOR X*baI* site insert Rev	TGCTCTAGACTAGTAGCACTTGCTGCGTTG
Sequencing primers	
dDOR PCR product 1 Fwd.	CAGCCTCGCCTCGTATCTCTT
dDOR PCR product 1 Rev	GCCAACAACAACGCAGCAAGT
dDOR PCR product 2 Fwd.	GTTCCCTGTACAGTGGGCCC
dDOR PCR product 2 Rev	CAACGCAACTATCTGCAACGCT
T7 Promotor Fwd.	TAATACGACTCACTATAGGG
T7 Promotor Rev	ACCCATTTGCTGTCCACCAG
dDOR insertion Fwd.	GAGACCTCTGAATAGGGAATTGG
dDOR insertion Rev	TAGAGGATCTTTGTGAAGGAACC

2.6.3 DNA Agarose Gel Electrophoresis

Agarose gel electrophoresis was performed in order to analyse DNA products from PCR reactions or restriction enzyme digests. Either 0.7% or 1 % agarose gels (in TAE buffer; 40 mM Tris acetate, 1 mM EDTA, pH 8.3) were used for large or small (<1kb) DNA products, respectively. Addition of SYBR® safe (Invitrogen, UK; 10 µl/100 ml) to the gel allowed the visualisation of the DNA using a blue light transilluminator. Bromophenol blue loading dye (0.25% w/v bromophenol blue, 30 % glycerol v/v in dH2O) was added to the DNA to assist

with the loading. A 1Kb or 100bp DNA ladder (0.5 µl/lane, NEB, UK) was run alongside the DNA products in order to be able to determine the size. Gels were run at 100V for 60 minutes.

2.6.4 DNA Gel Extraction and Purification

DNA fragments yielded for cloning were excised from the agarose gel using a sharp sterile scalpel following visualisation by a blue light transilluminator box. Gel slices were processed according to the QIAquick® Gel Extraction kit (Qiagen, UK) via the manufacturer's instructions (Qiagen, 2019). The DNA concentration was determined using a NanoDrop ND-1000 spectrophotometer (Thermo Scientific, DE, USA).

2.6.5 Restriction Endonuclease Digestion

Plasmids contain several restriction sites that are specifically recognised by restriction enzymes. These enzymes can be used in order to specifically cleave plasmids, allowing for excision and insertion of DNA fragments during sub-cloning. This approach was used to excise $dDOR_{long/FENLL}$ from their donor plasmid (pUAST-dDOR), and to cleave their recipient plasmids: pET28-6XHIS and pUASattb-3xFLAG, to allow for insertion (Fig. 2.5 and 2.6). Digestions were also used to cleave plasmid DNA yielded from transformed candidate clones in order to screen for the presence of newly inserted DNA fragments. In all cases restriction enzymes were accompanied by the addition of CutSmart® Buffer (New England Biolabs). Reactions were incubated for 20 minutes at 37°C followed by a 20 min incubation at 65°C, to inactivate enzyme activity.

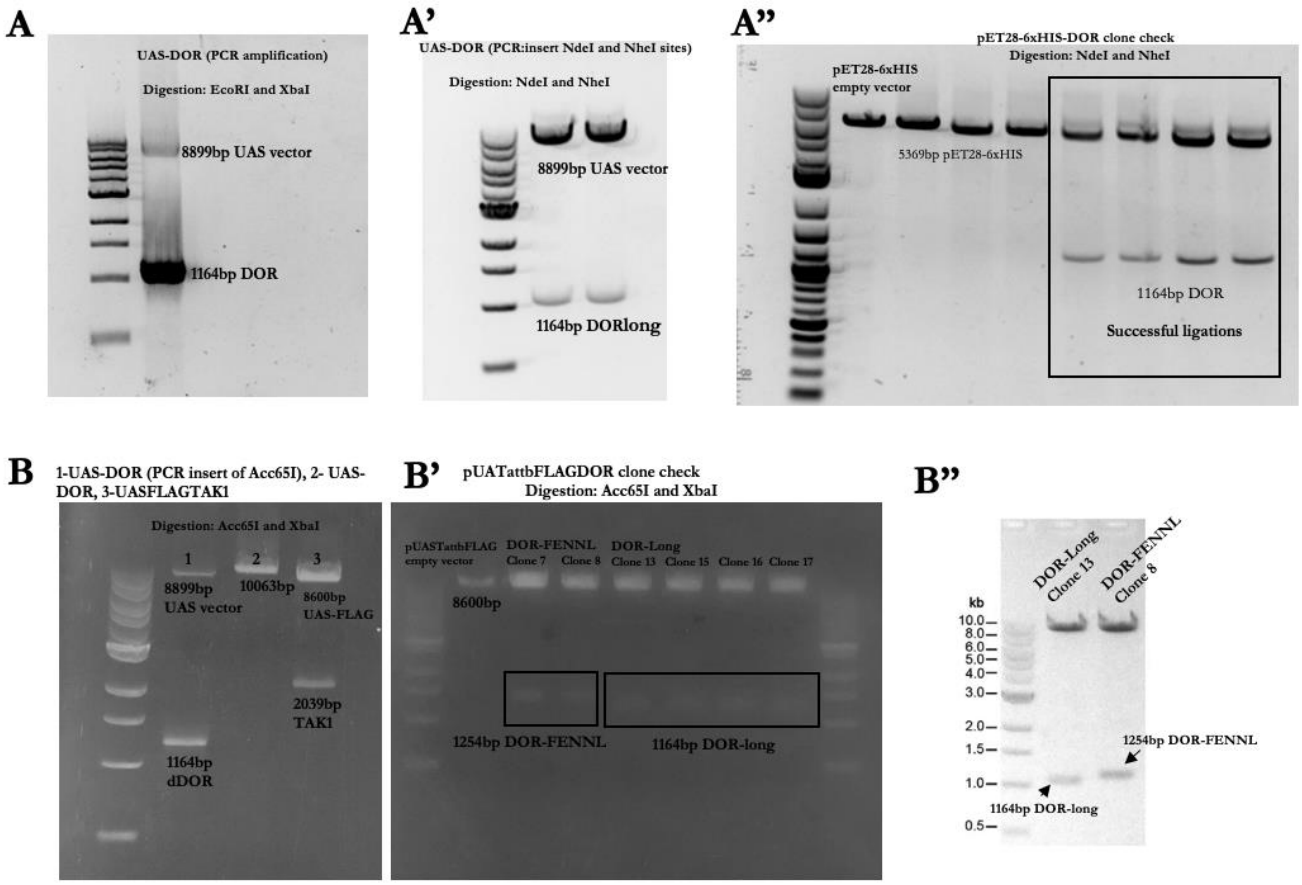

Figure 2.5 Agarose Gel Images to Confirm the Successful Digestion of dDOR Constructs During Cloning. (A) Digestion of pUAST-dDOR plasmid with *Eco*RI and *Xba*I following PCR amplification using primers flanking the expected region of the dDOR insert. The gel image confirms that dDOR is present in the plasmid at the expected length of 1164bp. (A') Digestion of UAS-dDOR following insertion of *Nde*I and *Nhe*I restriction sites via PCR. The gel image confirms that the sites were inserted in that dDOR was successfully excised. Numerous digestions were set up in parallel and the bands corresponding to dDOR (1164bp) were excised in order to be gel purified and ligated. (A") Digestion of candidate clones with *Nde*I and *Nhe*I following ligations of pET28-6x HIS and DOR. The red box indicates the clones which have been successfully ligated and to be sent for sequencing. (B) Digestion of UAS-dDOR: PCR product to insert Acc65I, UAS-dDOR (original plasmid) and UASFLAGattbTAK1 with *Acc65*I and *Xba*I. The DOR insert and UASattbFLAG backbone were subsequently excised, gel purified and ligated. (B') Digestion of candidate UASattbFLAGdDOR clones following ligation. The black box shows the successful insertion of DOR into the UASattbFLAG vector; these were all subsequently sent for sequencing (B") Repeat of digestion with *Acc56I* and *XbaI* of selected clones, these clones were sent for injection.

2.6.6 DNA ligation

Ligation reactions were typically a 3:1 (insert: vector (ng)) ratio, determined using the following formula:

$$\text{Insert mass (ng)} = [3 \times (\text{insert length bp} / \text{vector length bp})] \times \text{vector mass (ng)}.$$

DNA concentration were ascertained using a NanoDrop ND-1000 spectrophotometer (Thermo Scientific, DE, USA). For the ligation reaction 1 µl of T4 DNA ligase (New England Biolabs, UK) was used with 2 µl of T4 buffer (New England Biolabs, UK). All the reactions were incubated at 16°C overnight followed by a 10 min inactivation of the ligase at 65°C.

2.6.7 Bacteria transformation and DNA amplification

During the generation of dDOR transgenic lines and the creation of plasmids used in GST-pull down assays, chemically competent *E. coli* cells (One Shot TOP10®, Invitrogen; U.K) were used in order to amplify plasmid DNA. Transformation was achieved via heat-shock as outlined by the manufacturer, however the quantity of cells used was modified to 50µl as opposed to 100µl. TOP10® SOC media was provided by the manufacturer and used in all cases. For the transformation of ligated plasmids, 1µl of ligation reaction mixture was used as recommended. Post-transformation cells were plated on LB agar plates (20 g/l agar in LB broth) containing either Ampicillin (Amp; 200 µg/ml), Kanamycin (Kan; 200 µg/ml), or both, dependant on the plasmid in question. Plates were incubated overnight at 37°C and individual colonies were harvested in sterile conditions, in LB broth with the addition of appropriate antibodies. Cultures were incubated overnight at 37°C with vigorous shaking. For plasmid purification, 2ml of each culture overnight culture was pelleted via centrifugation.

In the case precious plasmid constructs, glycerol stocks were created from cultures through the addition of 50% v/v sterile glycerol, and stored at -80°C.

2.6.8 Colony cracking

Colony cracking provides a valuable 'check-point' during cloning experiments, as it confirms the presence of a desired insert before proceeding with plasmid purification. The method utilises alkaline conditions to evoke cellular lysis and relies on the identification of positive clones based on electrophoretic mobility variance between supercoiled DNA plasmids, with and without the

presence of an insert. Insert carrying plasmids thus move more slowly through an electrophoresis gel.

To 1ml of 5x colony cracking buffer (25g sucrose, 5ml 5M NaOH, 2.5ml 10% SDS, 40ml ddH_20), 20µl of bromophenol dye was added. From this mixture, 5µl was added to equal volumes of resuspension buffer (50mM Tris-HCL pH 8.0, 10mM EDTA, 100 µg/ml RNaseA), and mixed with 15µl of overnight culture. Mixtures were loaded onto an electrophoresis gel, along with an uncut vector acting as a control. Candidate colonies were considered those which showed a slower electrophoresis mobility in comparison to the control.

2.6.9 Plasmid purification

Use of the QIAprep spin MiniPrep kit (Qiagen, UK) allowed for up to 20µg of plasmid DNA to be purified from *E. coli*. In general plasmids yielded by this method were used during sub-cloning in order to confirm the presence of a desired insert. Pellets produced from overnight culture were processed in accordance to the manufacturer's instructions. Concentrations were determined using a NanoDrop Spectrometer (Implen, geneflow, NP80), with purified plasmids being stored at -20°C.

To provide a greater yield of plasmid DNA, especially in the case of construction for *Drosophila* microinjections, the Qiagen HiSpeed Plasmid MidiPrep kit was used (Qiagen, U.K). This method allowed production of up to 200 µg of purified plasmid DNA. Prior to use of the MidiPrep kits, a 1:1000 inoculation of LB broth, containing 200 µg/ml of appropriate antibiotics, was conducted with overnight culture, and incubated overnight at 37°C. Following incubation, cultures were pelleted and processed in accordance with the Qiagen HiSpeed MidiPrep kit protocol (Qiagen, 2019).

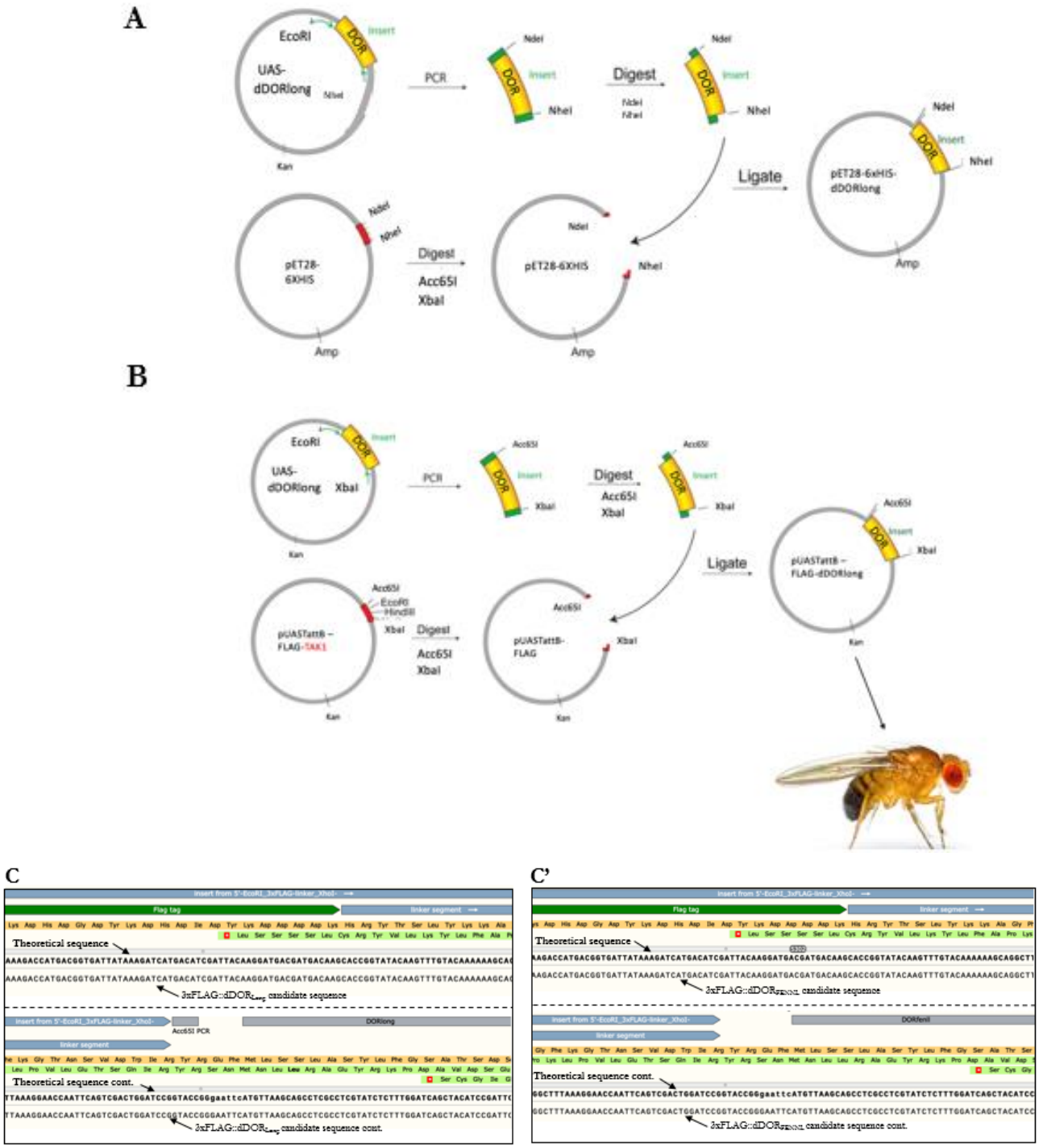

Figure 2.6 Generation of dDOR Plasmids Overview. (A) Schematic overview of workflow carried out to excise dDOR$_{long}$ from the donor plasmid pUAST-dDOR$_{long}$ in order to insert it into vector pET28-6xHIS. The resulting plasmid pET28-6xHIS-dDOR$_{long}$ was used for *in vitro* experiments. (B) Schematic overview of workflow carried out to excise dDOR from the plasmid donor (including the dDOR$_{FENLL}$ variant) in order to insert it into vector pUASTattb-3xFLAG. The resulting pUASattb3xFLAG-dDOR$_{long/FENLL}$ plasmids; to be sent for injection in order to create a new transgenic line. Original pUAST-dDOR plasmids received from Teleman Lab, German Cancer Research Centre, Heidelberg, Germany[340] This was carried out for both long and FENLL isoforms (C) Sequencing results to confirm the successful construction of pUASTattb-3xFLAG-dDOR$_{long}$ and (C') pUASTattb-3xFLAG-dDOR$_{FENLL}$.

2.7 Western Blotting

2.7.1 Protein Extraction and Quantification

All lysates were prepared from seven-day old flies, with 15 whole bodies collected per sample. To each sample 150 µl RIPA lysis buffer (10 mM Tris-Cl (pH 8.0), 1 mM EDTA, 1% Triton X-100, 0.1% sodium deoxycholate, 0.1% SDS, 140 mM NaCl) was added, supplemented with 1x protease inhibitors (Roche cOmplete™, Mini, EDTA-free protease inhibitor cocktail.) Samples were homogenised using a mechanical pestle and mortar and separated via centrifugation. Triton™ X-100 is used as a mild detergent in order to extract only the water-soluble cell fraction.

Protein concentration was determined using a Bradford Assay, against a BSA standard curve with a range of 0-20 µg/ml. BIO-RAD assay dye reagent (reference 5000006) was used as a readout marker and absorbance was measured at 595 nm, on a GENESYS™ 10S Vis spectrophotometer. For each sample, two readings were taken; with 2µl and 4µl of lysate. The intensity of the coloured reaction is a direct function of the protein amount; therefore, the amount (µg) of protein per cuvette was calculated by using the equation generated by the standard curve: (OD 595 – y-intercept)/gradient. An average was calculated across the two sample readings, with the volume needed to obtain 100µg of protein determined. The final sample was made to 75µl with the appropriate addition of lysis buffer.

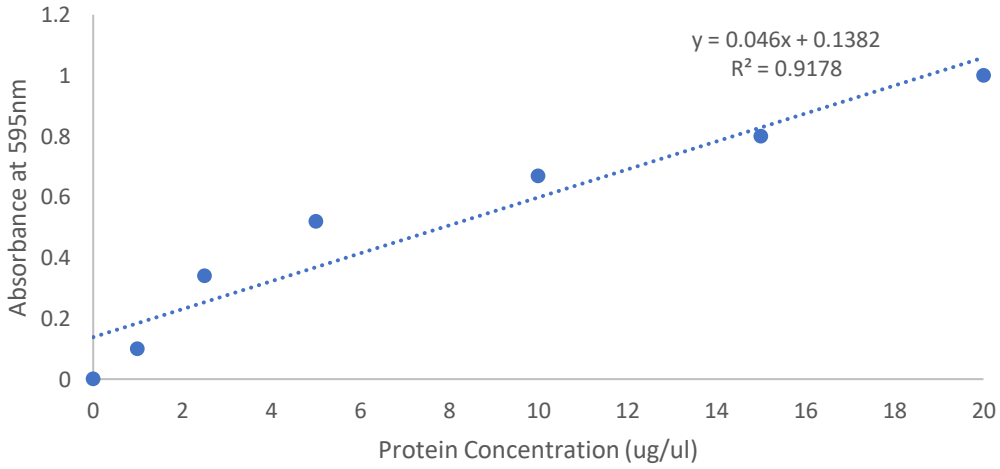

Figure 2.7 Standard Curve for BSA Protein. Absorption of BSA protein standards (0-20 µg/ml) at λ=595nm.

Table 2.6 Determination of Protein Concentration using a BSA Standard Curve.
Absorption (λ=595nm) was measured across samples containing 2µl and 4µl of protein lysate extracted from 7-day old fly body *YL-1*-RNAi flies. Using a BSA standard curve the amount of protein was determined per cuvette, converted to µg/µl and averaged across the two samples. The volume required to obtain 100µg of protein per sample was determined.

***YL-1* RNAi protein lysate**	**OD 595**	**µg/cuvette** (OD 595- y-intercept)/gradient))	**µg/µl**	**100µg** (100/(µg/cuvette)	**lysis buffer** (to 75µl total)
2µl	0.302	3.56	1.8		
4µl	0.825	14.93	3.7		
			2.8	**36.3**	**38.7**

2.7.2 Preparation of Loading Samples

Loading samples were prepared with 25 µl of 4x Laemmli buffer[341]. Laemmli buffer was stored as 6x stock solution: 12g 12% SDS, 60 mL 60% glycerol, 120 mg 0.12% Bromophenol, 37.5 ml Tris-HCL 1M pH 6.8 and H_2O up to 100 mL. The final working concentration of Laemmli buffer was supplemented with 5% ß-mercaptoethanol, prior to addition to lysate; to give an adjusted concentration of 1-5 µg/µl in RIPA lysis buffer+ 1x protease inhibitors. Proteins were denatured by boiling the samples at 80°C for 10 minutes.

2.7.3 SDS-PAGE and Transfer

Self-made 8% Bis-Tris polyacrylamide gels were used for electrophoresis, composed of resolving gel (H20, 1.5M Tris (pH8.5), 30% Acrylamide/0.8% bis-acrylamide, 10% SDS, 10% APS, TEMED) and stacking gel liquid (H20, 0.5M Tris (pH6.8), 30% Acrylamide/0.8% bis-acrylamide, 10% SDS). For stacking gel polymerization, 10% APS and TEMED were added immediately prior to gel casting.

Each gel lane was loaded with 20 µl. Gel separation was performed at 75V for 15-30 minutes and 150V for 60 minutes in 1x running buffer (25mM Tris-HCl (pH8.6), 192 mM glycine, 1% SDS). Separated protein content was transferred onto PVDF membranes, on ice, for 90 minutes at 100V in transfer buffer (25 mM Tris-HCl (pH 8.6), 192 mM glycine, 20% ethanol).

2.7.4 Immunoblotting

Membranes were blocked in 5% powdered milk in TBST (0.1% Tween in TBS), for one hour at RT. All washes were performed three times in TBST for 15 minutes each at RT. Incubation of membrane with primary antibodies (in TBST) were conducted overnight at 4°C. Secondary antibody incubation took place for 45 minutes at RT, in 1% BSA in TBST. Membranes were treated with ECL reagent (ECL, Western Blotting Detection, GE Life Sciences) for 2 minutes, followed by film exposure and development (AGFA automated developer).

2.7.5 Protein band quantification

Image analysis and quantification was performed with Fiji/ImageJ (2.0). Gel films were scanned, generated as high pixel quality Jpeg images, and opened in the ImageJ suite. Images were converted to 8-bit grayscale format and background was subtracted with a rolling ball pixel radius range of 50-200. The rectangular selection tool was used to select each lane across the image; numbering each using the 'Gel' analysis built-in function in ImageJ. Lanes were plotted, generating a histogram in which greyscale intensity is depicted as peaks. Here, the X axis is representative of grey scale pixel values and the Y axis represents the total area selected. Pixel intensity is measured line-by-line across the selected region, thus generating a single value average depicted as a peak in the histogram. Darker protein bands will therefore appear as distinct peaks in the histogram, given they will have a higher greyscale than the background. In order to quantify band intensity, a line was drawn at the base of the peak of interest, where there was a clear distinction of signal against noise; enabling intensity levels to be calculated proportionate to the area under the peak.

Either Tubulin or Ponceau (for GST-pull down assays) staining served as the total protein control. For experiments regarding measurement of a protein fold difference between genotypes, protein intensity levels were normalised to an adjusted Tubulin band intensity value, with fold difference calculated relative to WT normalised values (Table 2.7). For GST-pull down assays, the intensity of the bait band was normalised to an adjusted Ponceau staining intensity value. A second step of normalisation was performed, in which values were adjusted to the WT binding control lane; this was set as the WT bait binding the WT prey, so that a fold difference comparison could be made with the mutant conditions (Table 2.8).

Table 2.7 Western Blot Band Quantification Example: Measuring the Accumulation of Ref(2)P in Atg8a^{KG} versus W^{1118}. Protein (Ref(2)P) band intensity values were normalised by multiplying them by an adjusted Tubulin loading control value (loading W^{1118}/loading $Atg8a^{KG}$). Fold difference was calculated relative to WT by dividing normalised $Atg8a^{KG}$ value by the normalised W^{1118} value.

Genotype	Protein band intensity (Ref(2)P)	Loading control intensity (Tubulin)	Normalization (protein band x (loading W^{1118}/loading $Atg8a^{KG}$))	Fold difference (norm. $Atg8a^{KG}$/norm. W^{1118})
W^{1118} (WT)	1371.062	71387.446	2165.41714	1
$Atg8a^{KG}$(mutant)	21336.144	45199.889	33697.7117	15.5617645

Table 2.8 GST-pulldown Quantification Example: Replicate 1 of Protein Binding Assay to Investigate the Dependency of LIR Motif in dDOR in its Ability to Bind Atg8a. Protein bands were normalized against an adjusted ponceau staining value (WT ponceau/sample ponceau). Binding intensity was calculated as a fold difference relative to the WT by dividing normalized sample values by normalized WT values. WT values here refer to the binding of GST-$Atg8a^{WT}$/$dDOR^{WT}$.

Bait/Prey	Ponceau staining	Protein band	Normalization (protein band x(WT ponceau/sample ponceau)	Fold difference (norm. sample /norm. WT)	%
GST-$Atg8a^{WT}$/$dDOR^{WT}$	11124.501	12053.782	12053.782	1	100
GST-$Atg8a^{WT}$/$dDOR^{LIR}$	12255.794	9817.610	8911.378	0.73930	73.930
GST-$Atg8a^{LDS}$/$dDOR^{WT}$	12456.794	9901.581	8842.576	0.73359	73.359
GST-$Atg8a^{LDS}$/$dDOR^{LIR}$	12355.567	9471.146	8527.473	0.70745	70.745
GST/$dDOR^{WT}$	13768.890	No signal	N/A	N/A	N/A
GST/$dDOR^{LIR}$	15678.098	No signal	N/A	N/A	N/A

2.7.6 Antibodies

Table 2.9 List of Antibodies used in Western Blotting and Immunoprecipitation

Primary Antibody	Dilution/Quantity	Source
Anti-YL-1 24445	1:1000	Custom made
p2E2 (anti-dSir2)	1:50	Developmental Studies Hybridoma Bank
p4A10 (anti-dSir2)	1:1000	Developmental Studies Hybridoma Bank
Anti-Tubulin raised in mouse	1: 40,000	Sigma-Aldrich
Anti-GFP raised in rabbit	1 µl	Ab290 Abcam
Anti-6xHis tag	1:1000	Ab18184 Abcam
Anti-mouse IgG (H+L) HRP in Rabbit	1:5000	0A1653421 Thermo Scientific
Anti-Rabbit IgG (H+L) HRP in Goat Thermo scientific	1:5000	NE171565 Thermo Scientific

Goat anti-Guinea Pig IgG (H+L) Highly Cross-Adsorbed Secondary Antibody, HRP	1:5000	A18775 Thermo scientific/Invitrogen
Anti-dDOR raised in guinea pig	1:1000	Gifted from Teleman Lab, German Cancer Research Centre, Heidelberg, German [340]

2.8 Immunoprecipitation

Larvae (~15 individuals) were collected and proteins were extracted in nuclear lysis buffer (20 mM Tris HCl (pH 7.5), 137 mM NaCl, 1mM $MgCl_2$, 1% Igepal, 10% Glycerol, 1mM Na_3VO_4, 15mM $Na_4P_2O_7$, 5mM Sodium Butyrate) + 1x protease inhibitors, by mechanical pestle and mortar. In experiments concerned with the deacetylation state of the proteins, the lysis buffer was supplemented with 1x deacetylase inhibition cocktail (Santa Cruz Biotechnology, SC-362323). A total of 1 mg/ml of protein was used for immunoprecipitation, with 40 µl of lysate kept as input.

Sepharose protein-G beads were prepared by conducting three washes in nuclear lysis buffer+ 1x protein inhibitors. To account for non-specific binding, incubation of 1 mg of protein with 30 µl of Sepharose protein-G beads was carried out for 30 minutes at 4°C on a rotary shaker. Samples were separated via centrifugation and the pre-cleared supernatant (1µg/1mg) was removed and added to 1µl of anti-GFP primary antibody. Samples were incubated with 40µl of fresh beads at 4°C overnight, to enable the binding of the antibody to the beads and the formation of antigen-antibody complex.

To elute proteins, samples were washed three times in nuclear lysis buffer, and spun down for 30 seconds at max speed after every wash. To the samples 60 µl of 2x Laemmli was added and boiled at 95 °C for five minutes. Eluted proteins were subjected to SDS-PAGE and subsequently western blot analysis to detect the proteins of interest.

2.9 Mass Spectrometry

Protein extracted from GFP-Atg8a larvae was separated by SDS-PAGE. Bands corresponding to the targeted protein (42 KDa) were excised from gels, followed by reduction with 10 mM DTT and alkylation with 55 mM iodoacetamide (both in 50 mM ammonium bicarbinate (NH_4HCO_3)). Samples were washed twice in 50% ethanol in NH_4HCO_3 and dehydrated in 100% ethanol.

Subsequently, in-gel digestion was carried out with sequence grade modified trypsin (2.5ng/µl in 50 mM NH_4HCO_3) and GluC to maximize coverage of the protein. The resulting peptides were extracted from the gel slices using a 5% formic acid/5% acetonitrile solution, vacuum dried and stored at -20°C. Samples were submitted to the WPH Proteomics Facility at The University of Warwick, for LC-MS/MS analysis. High mass accuracy MS/MS scans were used to help resolve ambiguity in the assignment of specific positions of post-translational modifications.

Scaffold (version Scaffold_4.7.2, Proteome Software Inc., Portland, OR) was used to validate MS/MS based peptide and protein identifications. Peptide identifications were accepted if they could be established at greater than 95.0% probability by the Scaffold Local FDR algorithm (Scaffold_4.7.2). Protein identifications were accepted if they could be established at greater than 99.0% probability and contained at least 1 identified peptide. Protein probabilities were assigned by the Protein Prophet algorithm[342].

2.10 Protein-Protein Interaction Assay: GST-Pull Down

This assay was utilized in order to test the direct interaction between two proteins produced separately in bacteria. The 'pull-down' is done on the GST recombinant protein (GST/GST-Atg8a$^{WT/LDS}$) immobilized on the glutathione beads (=bait), in order to measure its interaction with another recombinant protein carrying a 6xHIS tag (=prey).

2.10.1 Protein expression in expression host cells

Transformation of recombinant vectors into Rosetta™ 2(DE3) competent cells (Novagen) was achieved by heat-stock in accordance with the manufacturer's instructions. Transformed cells were streaked on agar plates containing the appropriate antibodies, overnight at 37°C.

Colonies picked from freshly streaked plate of Rosetta™ 2(DE3) competent cells (Novagen) containing the recombinant vector were inoculated overnight (as a pre-culture) in 50 ml of LB medium containing 50 µl of the appropriate antibiotics. A 1:100 dilution of the pre-culture was performed in LB medium and incubated at 37°C until OD_{600} reached 0.6. From this point the cells will use most of their resources for the production of the target protein and will not grow much further, therefore induction of protein expression was achieved by the addition of IPTG 0.5 mM. The main culture was incubated at 20°C for 16 hours.

To optimize the expression conditions, 1 mL of culture is collected just before induction with IPTG, and then at the end of induction. These samples are pelleted, resuspended in 1x Laemmli buffer and probed for protein induction via western blotting.

2.10.2 Lysate preparation

Main cultures were pelleted and resuspended in lysis buffer (10 mM Tris-Cl (pH 8.0), 1 mM EDTA, 1% Triton X-100, 0.1% sodium deoxycholate, 0.1% SDS, 140 mM NaCl), before sonication (EpiShear, Probe Sonicator A5; max 35% amplitude, 10 seconds pulse and 5 seconds off) on ice for 2 x 3-minute pulses or until the lysates appeared clear. The samples were then equilibrated using lysis buffer before being separated by centrifugation, with the supernatant collected for protein purification.

2.10.3 Protein purification

Glutathione Sepharose 4 fast flow (GE health care) beads were sedimented via centrifugation and washed in equal volumes of lysis buffer three times before being resuspended in lysis buffer ready for use. For GST/GST-recombinant proteins (bait) 100 µl of beads per 50 mL bacteria culture was used and incubated for 30-40 minutes at 4°C with gentle agitation. Beads were sedimented and washed with High Salt Wash buffer (25mM Tris pH7.4, 500mM NaCl, 2mM EDTA), followed by lysis buffer.

2.10.4 *In vitro* pull-down

To pre-clear the lysate from the bacteria expressing the prey protein, equal volumes of fresh glutathione beads was added and subsequently sedimented by centrifugation. On the beads previously prepared with the GST/GST-recombinant protein (bait), the pre-cleared prey lysate was added and incubated for 2 hours at 4°C with gentle agitation. The beads were then consecutively sedimented by centrifugation and washed with lysis buffer and Imidazole Wash buffer (25mM Tris pH7.4, 100mM NaCl, 2mM EDTA, 10mM imidazole), before the addition of 2x Laemmli buffer ready for analysis vis SDS-PAGE.

In vitro pull-down assays conducted by our collaborator Dr. Ashish Jain (Johanson lab, University of Tromsø) involved the use of ^{35}S-radiolabeled *in vitro* translated proteins. Here, immobilized GST-alone or GST-tagged fusion protein was incubated with ^{35}S-radiolabeled *in vitro* translated

proteins for 2 hours/overnight at 4°C. The ^{35}S-labeled proteins were generated using TNT T7 Quick Coupled Transcription/Translation System (Promega) in the presence of [^{35}S] methionine (Amersham Biosciences). Bound proteins were eluted through the addition of SDS and subsequently boiled. Eluted proteins were separated by SDS-PAGE and bound proteins were detected by autoradiography.

2.11 Chromatin Immunoprecipitation

A ChIP (Chromatin Immunoprecipitation) assay was conducted in order to verify the binding of Sequoia, GFP-Atg8a and dDOR to the promoter regions of *Atg* genes. Enrichment of specific DNA sequences represent regions on the genome that the protein of interest associates with *in vivo* and can be identified via Real Time-qPCR. Pilot experiments using the anti-Histone H3, were conducted in order to optimize this protocol and assess the reliability of transcriptional detection. This particular antibody detects endogenous levels of total H3 protein and is predicted to react in *Drosophila*, based on 100% sequence homology with reactive species (Cell Signaling, 2020).

2.11.1 Sample preparation and cross-linking

It was determined that 150 larvae per condition was sufficient for experimentation. Upon collection of the third instar stage larvae, forceps were used to pull apart the outer cuticle in order to release the fat body. The tissue samples were rinsed twice in cold PBS + 1x protein inhibitor + 0.5mM PMSF and resuspended in the same solution. Samples were fixed in 37% formaldehyde for 15 minutes at 37°C, before being placed on ice for two minutes and rinsed twice in PBS. Here formaldehyde acts as a reversible protein-DNA cross-linking agent that serves to fix the interaction occurring between the protein and DNA.

2.11.2 Cell lysis and fragmentation of chromatin

In order to prepare the supernatant with protein-DNA conjugation, samples were homogenized through the addition of lysis buffer (50mM Tris-HCL, pH 7.6, 1mM CaCl2, 0.2% Triton X-100. 5mM butyrate, and 1x proteinase inhibitor cocktail) and fresh PMSF stock (final concentration 0.5 mM). Larval tissues were dissociated via a motorized pestle and mortar and stored at room temperature for 10 minutes.

The lysis step yields all nuclear material, which includes unbound nuclear protein, full length chromatin and the cross-linked protein–DNA complexes. In order to analyse protein-binding sequences, the extracted genomic DNA must be sheared into smaller, workable pieces via sonication. To perform sonication, a sonicator microtip (EpiShear, Probe Sonicator A5) was used at power 20; samples were placed on ice and subjected to 10 seconds of sonication, followed by 50 seconds of rest. This was repeated four times. Through this procedure it is expected that the chromatin will have been shredded to length 200-300 bps. This was tested by running the samples on a 0.8% agarose gel and visualized using a UV imager. Once confirmed to be of the correct length, samples were diluted through the addition of 1.8 mL RIPA buffer (10mM Tris-HCL, pH 7.6, 1mM EDTA, 0.1% SDS, 0.1% Na-Deoxycholate, 1% Triton x-100, with protease inhibitors and PMSF, 0.5 mM). From each sample 40 µl was taken as an input control with the addition of 2 µl 5M NaCl and incubated overnight to reverse cross-link. This allows analysis of ChIP DNA generated from this experiment to be determined relative to the no ChIP input.

2.11.3 Immunoprecipitation

The cross-linked DNA fragments associated with the proteins of interest were selectively immuno-precipitated from the cell debris using a protein-specific antibody; to conjugate antibody to the beads; 40 µl of Protein A beads (Sepharose Xtra) were added to 600 µl PBS and placed to rock at 4°C for two minutes. A magnet rack (MagRack6, GE Life Sciences) was applied to the beads and the supernatant was removed. Addition of 100 µl of PBS along with the antibody of interest (See Table 2.10 for quantity/dilution) was added to the beads, followed by a one-hour incubation at RT. Supernatant was removed from the beads by magnet and applied to each of the cross-linked chromatin extracts from the previous step, and left to rotate at 4°C overnight.

The ChIP samples were applied to the magnetic rack and the supernatant was removed. The beads were washed with the following buffers at 4°C, 10 minutes each, in the following order:

1) 2x with 1 mL of RIPA buffer [1.89 mL 'RIPA buffer' + 315 µL 7x protease inhibitors + 20 µL PMSF];

2) 2x with 1 mL of RIPA buffer + 0.3 M NaCl [1.89 mL RIPA buffer + 220 µL 3 M NaCl];

3) 2x with 1 mL of LiCl buffer (0.25 M LiCl, 0.5% NP40, 0.5% NaDOC);

4) 1x with 1 mL of 1x TE + 0.2% Triton X-100;

5) 1x with 1 mL of 1x TE

2.11.4 Crosslink reversal and elution

The cross-link between the DNA and the protein is then reversed through digestion of the protein component with proteinase K. This was achieved by resuspending the beads in 100 µL TE buffer + 3 µL 10% SDS + 5 µL of proteinase K (20 mg/mL) and incubated at 65 °C O/N. The beads were applied to a magnet and the supernatant (containing the DNA sample) was transferred into a new tube. Beads were washed with 100 µL TE + 0.5 M NaCl and the supernatant was combined with that which contained the DNA sample.

In order to extract DNA from the sample 200 µL Phenol: Chloroform: IAA (25:24:1) was added and vortexed. Samples were centrifuged for five minutes at RT. The aqueous layer was transferred into a new tube, and 1 µL of glycogen at 20 mg/mL for every 1 mL of supernatant was added, along with 20 µL of 3M NaOAc and 500 µL 100% EtOH. Samples were mixed well, incubated at 80 °C for 10 minutes and then spun at maximum speed for 20 minutes at 4 °C. The supernatant was removed and washed with 300 µL 70% EtOH. Finally, samples were dried using a spin vacuum, with the remaining pellet resuspended in 50 µL TE buffer. Samples were stored at -20 °C, ready to be used for Real Time- qPCR.

2.12 Analysis of ChIP DNA

As part of the initial pilot experiments, ChIP DNA was diluted as follows in order form standard curve: undiluted, 1/10, 1/100, 1/500, 1/1000, 1/5000. This was to determine the efficiency of the experimental procedure, the specificity of the primer pairs, and to determine the optimal dilution for the samples. During the first round of experiments, anti-Histone H3 and anti-IgG ChIP samples were tested alongside the input control, for expression of the positive control gene *Rpl30*. The ChIP profile generated by these initial experiments were used to verify whether the ChIP experiment had been successful in determining transcriptional binding to genomic regions as *Rpl30* is known to be enriched at histone modifications associated with active gene transcription[343]. Sample mixtures were prepared according to Table 2.10.

Table 2.10 Real-Time qPCR Reaction Mix. Volumes are for 1x and were scaled up accordingly.

Reaction Mixture component	Volume
GoTaq (Promega) Master Mix (2x)	10 µl
Nuclease-free H_2O	3 µl
Forward Primer (10 µM)	1 µl
Reverse Primer (10 µM)	1 µl
DNA (varying dilutions of: input control, or ChIP DNA A blank control was also set up containing H_20)	5 µl

Real Time-qPCR was performed using the following conditions:

Stage 1: 50 °C for 2 min, 1 cycle;

Stage 2: 95 °C for 10 min, 1 cycle;

Stage 3: 95 °C for 15 s, 60 °C for 1 min, 40 cycles;

Stage 4 (dissociation stage): 95 °C for 15 s, 60 °C for 1 min, 95 °C for 15 s

The fluorescent tracer used was SYBR.

As described previously, the MxPro- Mx3005P Comparative Quantitation program was used to analyse qPCR data. A single peak at the thermal dissociation plot indicated a single amplicon from the PCR reaction, confirming the *Rpl30* primer pairs to be specific. The linear phase of exponential amplification of the PCR reaction also corresponded to the standard curve of the series of diluted cDNA (all data generated by MxPro).

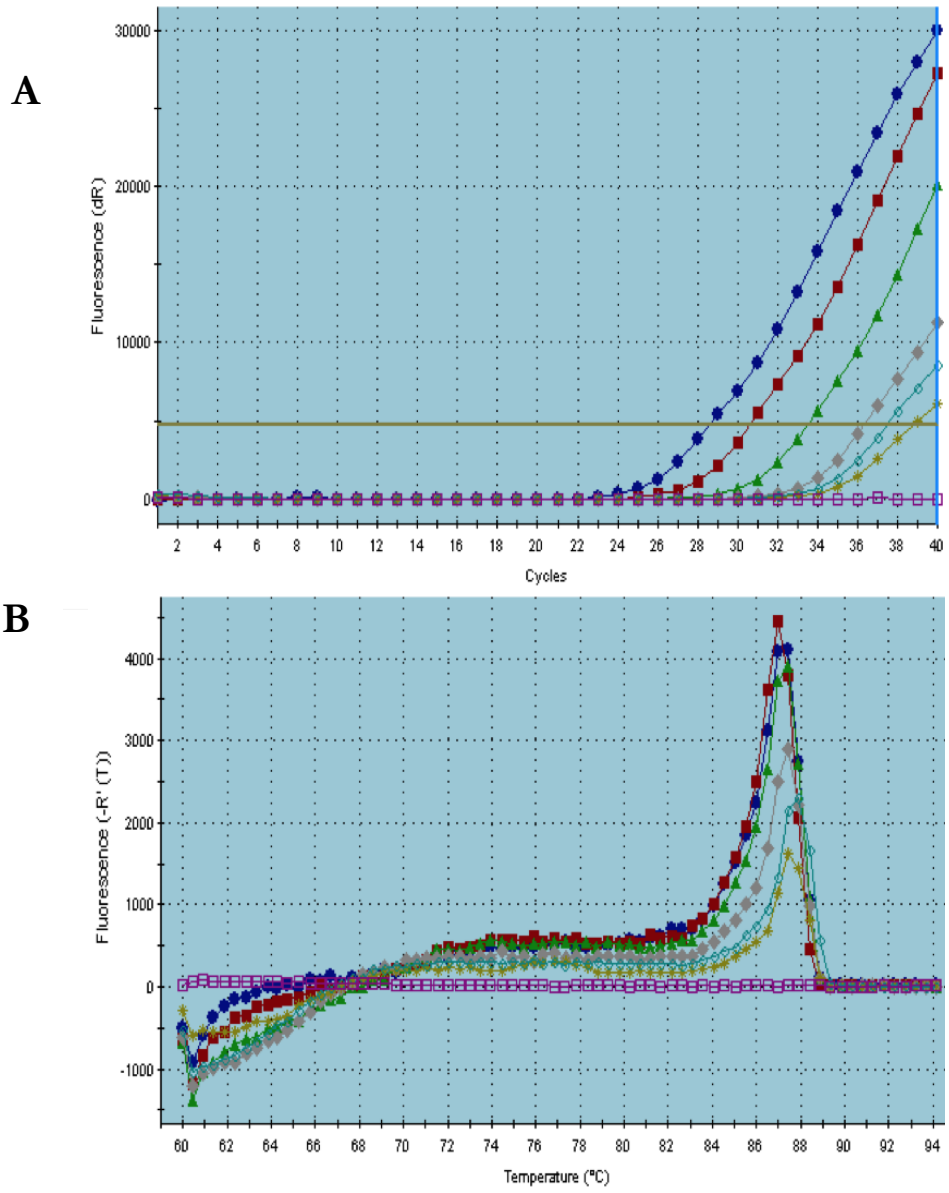

Figure 2.8 Exemplary MxPro Output Data from Real Time qPCR Analysis of H3 histone ChIP DNA, to Analyse the Expression of *Rpl30* exon 1-2. (A) The first derivative of raw fluorescence plotted against an increase in temperature. The single melt peak at 87°C indicates a single PCR product is being amplified in these samples. (B) Amplification plots of standards in a dilution series over orders of magnitude: undiluted, 1/10, 1/100, 1/500, 1/1000, 1/5000. As expected, no fluorescence was measured in the no DNA control (pink).

Based on results shown in Figure. 2.8, it was determined that a dilution factor of 1:1000 was optimal. The EPD (Eukaryotic Promotor Database) was used to design *Atg* gene primers with sequences within the promotor binding region of interest. The efficiency of these primers was tested as previously described (Section 2.5.6), using genomic DNA. Real Time-qPCR was performed on input (chromatin sample obtained before immunoprecipitation) and output (ChIP) DNA with primers complementary to the promotor genomic loci of *Atg* genes: *Atg1*, *Atg5*, *Atg7*, *Atg8a*, *Atg13* and *Atg14*, with *Tubulin* utilised as a non-*Atg* gene control. Normal rabbit IgG was used to control for nonspecific precipitation. The $2^{-\Delta\Delta}$Ct method was used to normalize ChIP DNA to input DNA and express it as a fold change relative to a control sample (immunoprecipitated using normal purified IgG).

To calculate the fold enrichment of the ChIP DNA relative to the input sample, following steps were completed:

1. Ct values of the ChIP and IgG DNA were normalised to the Ct value of the input DNA ($^{\Delta}$Ct) for each primer set by subtracting the Ct value obtained for the input DNA from the Ct value for ChIP and IgG DNA:

$$^{\Delta}\text{Ct} = \text{Ct ChIP/IgG DNA} - (\text{Ct input-Log2 [Input dilution factor]}).$$

2. The percent of input for each ChIP was calculated:

$$\%\text{Input} = 2(-^{\Delta}\text{Ct [normalized ChIP]}).$$

3. The ChIP $^{\Delta}$Ct values were normalized to mock value ($^{\Delta\Delta}$Ct) by subtracting the $^{\Delta}$Ct value obtained for the ChIP from the $^{\Delta}$Ct value for the IgG:

$$(^{\Delta\Delta}\text{Ct} = ^{\Delta}\text{Ct ChIP} - ^{\Delta}\text{Ct IgG}).$$

4. Fold enrichment of the ChIP DNA was calculated over the IgG:

$$\text{Fold enrichment} = 2^{\Delta\Delta} (\text{Ct}).$$

Example calculation for *Rpl30* gene enrichment for H3 ChIP DNA vs IgG DNA:

$$\Delta \text{ (Ct) ChIP: 36.45 (Ct)} - \text{30.73 (Ct input-Log2 [Input dilution factor])} = 5.72$$

$$\Delta \text{ (Ct) IgG: 34.55 (Ct) -30.73 Ct input-Log2 [Input dilution factor]} = 3.52$$

$$\Delta\Delta Ct = 5.72-3.52$$

$$2^{\Delta\Delta} \text{ (Ct)} = 2^{\wedge} (5.72-3.52) = 3.73$$

Table 2.11 ChIP Specific Primer Pairs

Gene name	Forward primer sequence	Reverse primer sequence
	***Atg* genes**	
Atg1	CCCACCACTTCGCTTAGTTG	CACACTTGCAGGATCGATGG
Atg5	TGCCATCTTCGAATGCCAAG	CAGATCATTCGCAGCACCTC
Atg7	GACCTAAGTATGGAAAACTGTACTTATCG	CAAACGTTTGGCTGCAAATTATAAAC
Atg8a	GGTCACACACGGTCAGTCTA	ATATCGATGCGTTGCTGAGC
Atg9	ACCCAGTATTTTGACGTTGGC	GCGGTAGTTGATATGTGGGC
Atg13	GCGAAAGTGTTTATGCAGTCC	TTCACACACACGAGCTTCTG
Atg14	CCAACACTGACGACATCTATTTT	TGCGACATCTGATTCCTCGT
	Control genes	
Rpl30 Exons 1-2	GTGGTATTTTCTCGCATCCCC	CCTGCAGTGCTTTAACCCAA
β-Tubulin	CATGTAGTATGGCCACACTGC	AGCAGTCGAACACAACACAA

Table 2.12 Selected Candidate Gene Promotor Region Sequences for Sequoia Binding.
Promotor region based on EPD database.

Gene symbol	Promotor Region
***Atg* Genes**	
Atg1	ttggcggttcgccacctgcggccacactggccaacccaccacttcgcttAGTTGTGTTTT
Atg5	tgcgatatttcagcgttgccatcttcgaatgccaagtgccatcactattATCAAATAGCA
Atg7	ataagttatcttctcattgtctatcgccatcgAGAGCTTTGTTT
Atg8a	agcgcgtttcgggttggtgtctctgcgcgctcactggtcacacacggtcAGTCTAGCCAC
Atg9	ccttacttattcattacccagtattttgacgttggccaacacttctcttAGGAGAGTCAG
Atg13	cacgcccattatcggactatcgatactatcgcgagtgcTAGCTGACGCT
Atg14	gacatctatttttttcgatatcagcctatcgtttagcaataggtgtcctcATATCGATAGC

Non-*Atg* Control Gene	
β-Tubulin	tggccacactgcggccatcgtataaaagcccgcgctctccaaagcgaatGCACTAATTTT
Rpl30	gtcacaccaacacaaacgtggtacccatttccgcctgttcttcctctttCTTTTGCCATT

Table 2.13 Antibodies Used in ChIP Experiments

Antibody	Dilution/Quantity	Source
Normal Rabbit IgG	1:50/10 µl	Cell Signaling Technologies
Histone H3 #9715	1:50/10 µl	Cell Signaling Technologies
Anti-Sequoia	1:50/2 µl	Gifted from Yuh Nung Jan, University of California.
GFP ChIP grade (290)	1 µl	Abcam
Anti-dDOR raised in guinea pig	1:50/5 µl	Gifted from Teleman Lab, German Cancer Research Centre, Heidelberg, Germany [340].

2.13 Bioinformatics Tools

2.13.1 iLIR web tool

The iLIR web tool (freely available at: http://repeat.biol.ucy.ac.cy/iLIR), was used to identify functional LIR motif patterns, in a given amino acid sequence. Amino acid sequences were sourced from the UniProt database and were input in FASTA format. The concept behind the iLIR tool, and the output data it provides, are described in detail in Chapter 4.

2.13.2 SMART

SMART[344,345] (Simple Modular Architecture Research Tool) was used to screen the *Drosophila* proteome for UBD-containing proteins. In conjugation with the iLIR tool, SMART was used to identify the domain architectures within LIR containing proteins of interest, identified by the initial screening. The database contains domains which are extensively annotated with respect to phyletic distributions, functional class, tertiary structures and functionally important residues. In order to identify homologs of Sequoia, its amino acid FASTA sequence was input into SMART, with all search parameters set to default. Output results led to the identification and

characterisation of its zinc-finger DNA binding domain (Fig. 2.9), and also aided in the identification of Sequoia homologs.

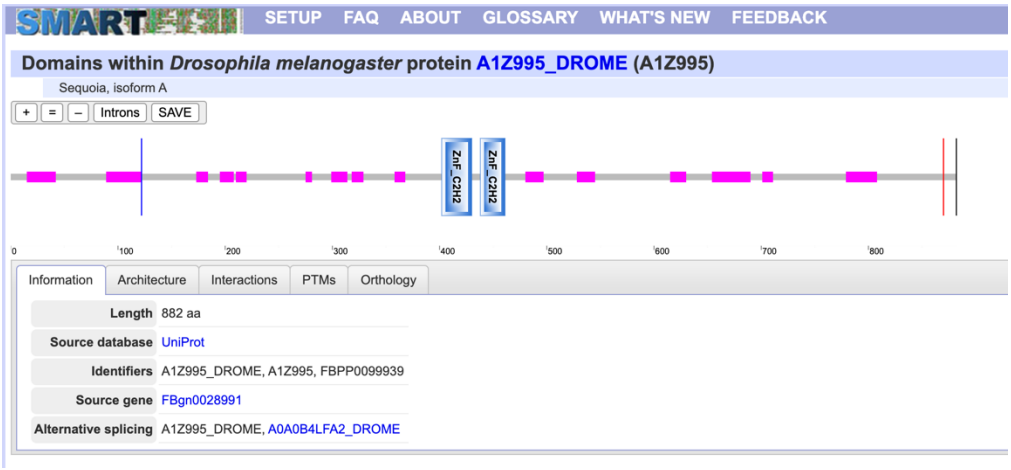

Figure 2.9 SMART Output Screen Following Amino Acid Sequence Submission of Sequoia. The FASTA protein sequence of Sequoia was input into the SMART database, which revealed the presence of two zinc finger domains in its structure. All search parameters were set to default. The tool was used to explore this protein region and search for potential homologs.

2.13.3 COBALT

COBALT was used in the construction of a cladogram linking Sequoia to its homologous partners. The tool functions by performing multiple sequence pair alignments constraints derived from conserved domain database, protein motif databases, and sequence similarity, using RPS-BLAST, BLASTP, and PHI-BLAST [346]. Construction parameters were defined as follows: Maximum difference of sequences= 0.8, Distance= Grishin (protein).

2.13.4 Search for *Drosophila* transcription factor DNA binding regions

Analysis of the DNA binding C_2H_2 domains in Sequoia were conducted using the UniProtJK/Swiss-Prot database, which utilises the Smith-Waterman algorithm[347]. The JASPAR 2018 database was used to search for known *Drosophila* (species ID: 7227) transcription factor DNA binding regions. The 'class' category was filtered to those defined as "C_2H_2 zinc finger factors", with all other search functions set to default. Output data was in a PFM (Position Frequency Matrices) format. JASPAR was also used to align PFMs in order to generate a degree of similarity between inputs. PFMs were converted to PWM (Position Weight Matrix) and ICMs

(Information Content Matrix) format using the 'Biostrings' package in R[348]. The 'Motif Search Tool' function on the EPD was used to scan gene promotor regions using PWMs; p-value cut-off <0.01.

2.13.5 Motif Discovery

MEME (freely available at: http://meme-suite.org/tools/meme) was used in the discovery of novel, un-gapped motifs, for both fixed and re-occurring patterns in the promotor region of experimentally confirmed *Atg* genes[349]. The FASTA formatted *Atg* promotor region sequences were combined into one text file, and input into the classical mode of the tool. The site-specific distribution was set to 'Zero to One Occurrence per Sequence'; this resulted in MEME assuming that each sequence may contain at most one occurrence of each motif. This option functions under the premise that some motifs may be missing from some of the sequences. Here, the motifs found were more accurate than using the "One Occurrence per Sequence" option. GOMo (freely available at: http://meme-suite.org/tools/gomo), a MEME built-in tool, was used to scan output candidate motifs against the promotors of *Drosophila Melanogaster* genes for significant GO (Gene Ontology) terms. GLAM2[350], another in-built MEME tool, was used in order to perform gapped motif discovery using *Atg* promotor regions. The 'Biostrings' package in R[348] was used to further analyse target *Atg* promotors in order to predict DNA binding motifs based on a hidden Markov model; this method is known as TFFM (Transcription Factor Flexible Model)[351]. The functioning of all these tools is described in more detail in Chapter 5.

2.14 Statistical Analysis

All statistical analysis was carried out using Graph Pad, Prism (version 8.4.3 (471)). An unpaired Student's t-test was used to test for statistical significance between two conditions, and a one-way ANOVA was used for multiple comparisons. For correlation analysis Pearson's coefficient was computed between two data sets, using a two-tailed P value and a 95% confidence interval. Values were considered significantly significant when $p < 0.05$, unless stated otherwise. P-values were determined by multiple comparisons using the Holm-Sidak method[352].

CHAPTER 3. SEQUOIA IS A NOVEL TRANSCRIPTION FACTOR WHICH INTERACTS WITH ATG8A IN THE NUCLEUS

3.1 Chapter Introduction: Screening for *Drosophila* LIR motifs in UBD-Containing Proteins

3.1.1 Screening for UBD-containing proteins

Based on the work of Husnjak *et al.,* (2012)[353], the *Drosophila* proteome was screened for UBD-containing proteins using libraries from the SMART database. This screening, conducted by former PhD students in the Nezis lab, was aimed at identifying new selective autophagy receptors. The rationale behind the screen derives from the functioning of Ref(2)P, which at the time of this work being carried out was the only known autophagy receptor in *Drosophila*. Ref(2)P, along with other characterised autophagy receptors in mammalian cells share two common features: the presence of at least one LIR motif and at least one UBD. Although all mammalian UBD family members, of which there are 20, are structurally diverse and have differing modes of interaction; these domains share the ability amongst them to bind covalently to ubiquitin molecules and chains[353].

Following this, the FASTA sequence from the identified UBD-containing proteins were subjected to query via the iLIR tool (section 3.1.2), for identification of at least one putative xLIR located in their anchor regions. The built in SMART parameter of the iLIR tool was also used to reconfirm the presence of the initially identified UBD in the protein under query. Of those *Drosophila* proteins which contained at least one known UBD, a total of 189 individual putative xLIR motifs in anchor regions were found as part of the screening process[354,355].

3.1.2 The iLIR tool.

Kalvari *et al.,* (2014) developed iLIR, a freely available web resource: (http://repeat.biol.ucy.ac.cy/cgi-bin/iLIR/iLIR_cgi), which provides *in silico* tools for assisting the identification of novel LIR containing proteins[215]. The tool allows the analysis of FASTA protein sequences and identification of both the classical and relaxed putative LIR motifs.

The classical LIR motif sequence: [W/F/Y]xx[L/I/V], has been relaxed and extended to six amino acids to integrate experimentally verified LIRs based on in silico analysis[215]. The resulting consensus sequence- referred to an xLIR-constitutes the following: (ADEFGLPRSK)

(DEGMSTV) **(WFY)** (DEILQTV) (ADEFHIKLMOSTV) **(ILV)**. The residues marked in bold at positions three (aromatic) and six (aliphatic) correspond to the most crucial residues for the interaction with Atg8-family proteins[356].

The iLIR software is able to indicate the primary sequence of the motif and its amino acid position. Furthermore, the 'Anchor' result gives a determination of whether the motif is within an intrinsically disordered region[357]. As intrinsically disordered proteins lack stable secondary and tertiary structure, they are able to adopt a fixed three-dimensional structure after binding to other macromolecules; therefore, the presence of a high intrinsically disordered region is associated with a high probability of protein-protein interaction[358]. Based on this logic, the tool recognises that xLIR motif which overlaps a region with the potential to transit from a disordered to an ordered state provides a reliable candidate for a functional binding motif[209,215,359].

Another output, the PSSM (Position Specific Score Matrix) score, is a commonly used representation of motifs or patterns in biological sequences. The matrix is derived from a set of aligned sequences that are thought to be functionally related. Values in the matrix represent a log-odds score for the presence of a residue in the respective position of the alignment. While negative scores are assigned to those rarely observed in the alignment, high positive scores are assigned to the most frequently present residues. The PSSM score can therefore be considered as a measure of confidence, with a score of between 10-13 considered to be the lower boundary cut-off in considering candidate interactors[215,356]. The tool can also designate confirmed and putative domains within the sequence under query using information from the SMART database[344,345]. SMART represents a platform which enables the identification of conserved domains from the entire proteome of an entire organism or a given amino acid sequence[344,345].

A functional instance of the iLIR tool is represented by the iLIR database (http://ilir.uk/model/), created to act as a repository of LIR-containing proteins from a variety of model organisms, obtained through batch analysis of FASTA sequences of the entire proteome of: *Arabidopsis thaliana, Caenorhabditis elegans, Gallus gallus, Homo sapiens, Mus musculus, Rattus norvegicus, Saccharomyces cerevisiae and Danio rerio*[356]. To date there has been no information published on *Drosophila Melanogaster*.

3.1.3 Identification of Sequoia

Of the 189 UBD and xLIR containing proteins, Sequoia was highlighted by the SMART database to also harbour a zinc-finger domain. Since many zinc finger containing proteins constitute transcription factors this was particularly interesting to given its predicted interaction with Atg8a. Located on the 2R chromosome, *sequoia* (CG32904) is a protein coding gene which has two RNA transcripts, represented by two splice variants: isoform A and B (Fig. 3.1 A). Input of both isoforms' protein sequence into the iLIR tool revealed the presence of an xLIR with the sequence EEYQVI at amino acid residue position 311-316; which constitutes an intrinsically disordered region (Fig. 3.1 C-D). Both isoforms have four exons, three of which are coding exons. *seq*-RA has a transcript length of 3,599 bps and a translation length of 882 residues, whereas the transcript length of *seq*-RB is 5,631 bps and its translation length is 878 residues. A functional GO search revealed Sequoia to be involved in biological processes related to development, cellular organisation, stimulus response and gene expression (Fig 3.1 B). It also revealed it to be a cellular component localisation which is exclusively nuclear.

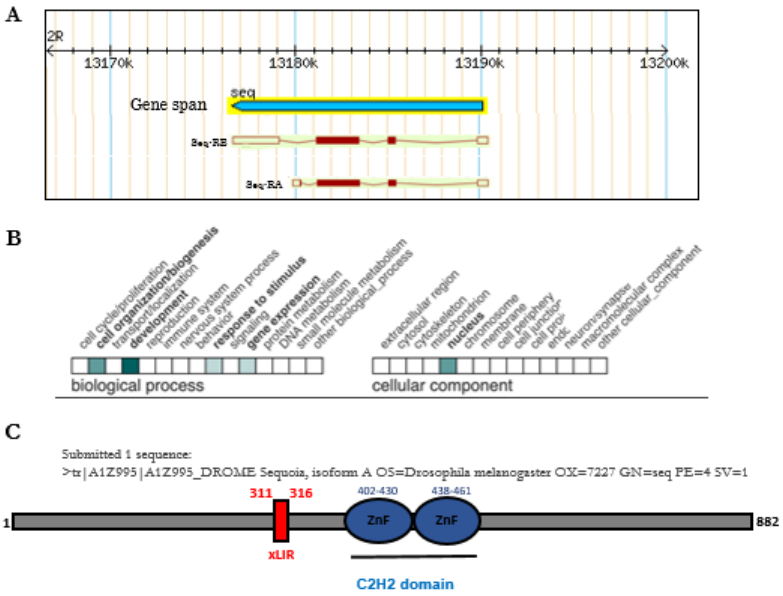

D

MOTIF	START	END	LIR Sequence	PSSM Score	Anchor
xLIR	311	316	EEYQVI	14	Yes
WxxL	167	172	QHYHYI	3	Yes
WxxL	237	242	EEYHVL	11	Yes
WxxL	392	397	ARYEHI	9	No
WxxL	401	406	VAYCLV	1	No
WxxL	728	733	QSYQJL	11	Yes
WxxL	818	823	QQFMEL	6	Yes

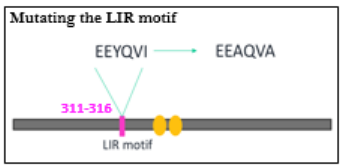

Figure 3.1 Sequoia has a Predicted xLIR Motif.

(A) s*equoia (seq)* is located on the 2R chromosome and has a protein coding gene with two isoforms: *seq*-RA and *seq*-RB. (B) Functional GO summary of Sequoia in *Drosophila Melanogaster* (Fly Base, 2019), here the green shading intensity indicates how strongly the protein is reported to be involved in biological processes and its localization to cellular components. (C) Schematic diagram of Sequoia. Sequoia is a nuclear protein containing two putative zinc fingers (blue), homologous to the DNA binding domain of Tramtrack (D) Submission to the iLIR database revealed a predicted xLIR motif at position 311-316 (red). "Anchor" refers to a prediction of the ANCHOR software overlapping with a given LIR-motif in > 3 residues. 'PSSM score' refers to a position-specific scoring matrix (E) Mutation of the LIR in sequoia was carried out via alanine substitutions of the core aromatic L and hydrophobic Y residues within the predicted LIR motif: Y313A and I316A.

sequoia was first identified in a larval PNS (Peripheral Nervous System) screen[360]. It encodes a nuclear, pan-neuronally expressed transcription factor, with two putative zinc-finger domains which has been reported to show distinct homology to *Drosophila* Ttk (Tramtrack); a DNA binding transcription factor that influences cell fate in both adult and embryonic PNS[322], and adult eye[361]. The encoded pan-neuronally expressed zinc-finger transcription factor Sequoia has proved to have a role in dendrite development[360], axonal targeting of photoreceptor cells[362] and external sensor organs[363]. It has also been shown to be a negative transcriptional regulator of

branchless, a gene which regulates the formation of *Drosophila* tracheal branches[364], as well as having a context dependant role in the regulation of the Notch pathway which mediates the proliferation switch in neuroblasts[365]. Recently, Sequoia has been shown to convert the differentiation role of Notch to a self-renewal role[366].

3.1.4 Chapter aims

- To explore the predicted LIR interaction between Atg8a and Sequoia *in vitro*.
- To identify candidate homologs of Sequoia in mammals and yeast.
- To determine the cellular localisation of Sequoia during the induction of starvation induced autophagy.
- To explore the effects of *sequoia*-depletion on the localisation of mCherr-Atg8a and the accumulation of mCherry-Atg8a puncta.
- To uncover a potential role of Sequoia in the transcriptional regulation of *Atg* genes.
- To use a variety of available bioinformatics tools to identify candidate Sequoia DNA binding motifs.

3.2 Sequoia interacts with Atg8a in a LIR dependant manner

The LDS (LIR docking site) of Atg8a is important in governing interactions with LIR containing proteins. A Lysine-Tyrosine site found within this region has been deemed necessary in governing such interactions[207,211,367]. Such that Atg8a LDS mutants, carrying alanine substitutions at positions Lys-48 and Tyr-49 (K48A, Y49A), are observed to reduce interactions[202]. Alanine substitutions of Tyr-49 alone (Y49A) in the LDS of Atg8-family members have also been observed to be sufficient in reducing its interaction with certain LIR containing proteins[368,369].

To test an interaction between Sequoia and Atg8a, an *in vitro* pull-down assay between 6xHIS-tagged Sequoia^{WT} and GST-tagged Atg8a^{WT} or GST-tagged Atg8a$^{K48A, Y49A}$ was conducted. This revealed an interaction between 6XHIS-Sequoia^{WT} and GST-Atg8a^{WT}, and that the observed interaction is significantly reduced in the presence of the Atg8a LDS mutant (Fig 3.2. A-B). No signal is observed in the GST control condition, indicating that this interaction is Atg8a specific and does not occur by virtue of an interaction with GST.

Sequoia has a predicted LIR motif at position 311-316, with the sequence EEYQVI. Work carried out by a collaborator of the project; Professor Terje Johansen, of The University of Tromsø, set out to determine whether there is a direct interaction between Sequoia and *Drosophila* Atg8a governed by this predicted LIR motif. Given that LIR binding to LC3 is seen to be significantly altered by substitutions within aliphatic and aromatic amino acid residues[370]; a LIR mutant version of Sequoia was created via alanine substitutions of the core aromatic I and aliphatic Y residues within the predicted LIR motif (Y313A and I316A). An *in vitro* pull-down was conducted in which GFP-Sequoia^{WT} and GFP-Sequoia$^{Y313A/I316A\ (LIRm)}$ were translated in the presence of ^{35}S-methionne and tested for binding with recombinant GST-Atg8a^{WT} and GST-Atg8a^{Y49A}. An AR (Autoradiography) analysis revealed the presence of ^{35}S-containing proteins in the GST fraction. Again here, a strong interaction was observed between GFP-Sequoia^{WT} and GST-Atg8a^{WT}. This interaction was significantly decreased in the presence of GFP-Sequoia$^{Y313A/I316A}$. A significant decrease was also observed in the binding of GST-Atg8a^{Y49A} to both GFP-Sequoia^{WT} and GFP-Sequoia$^{Y313A/I316A}$ (Fig 3.2 C-D). No signal is observed in the GST control condition, confirming the specificity of the observed interaction (see Table 2.8 for details on quantification). Taken together these results provide evidence that Sequoia and Atg8a interact *in vitro*, in a LIR dependant manner.

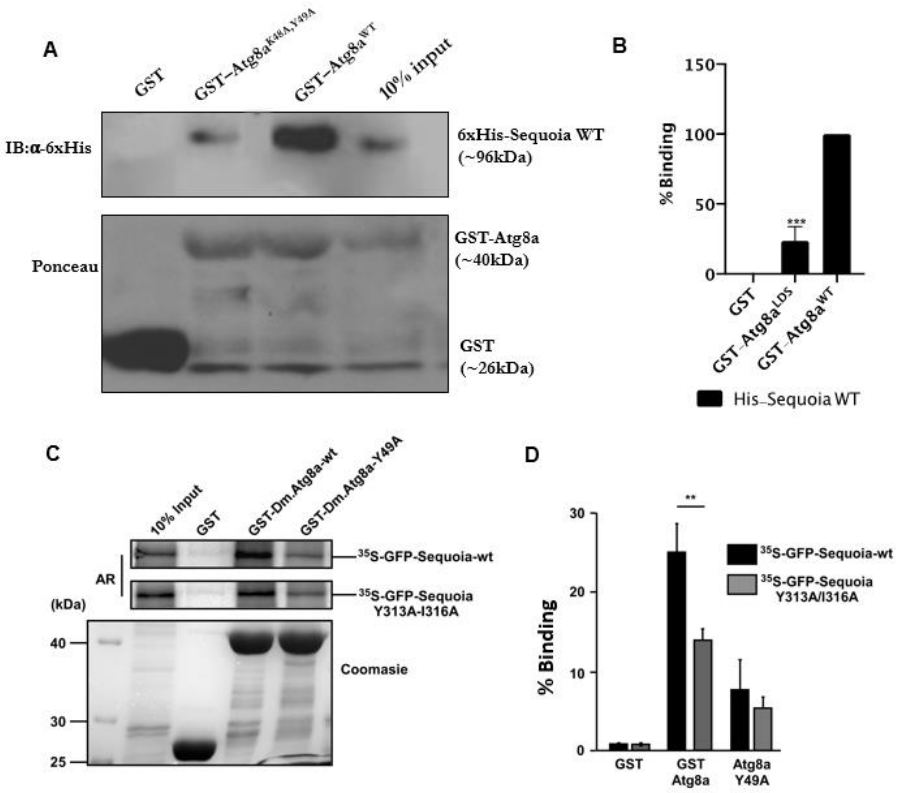

Figure 3.2 Sequoia Binds to Atg8a in a LIR Dependant Manner.

(A) GST- pull-down between GST-tagged Atg8a WT or Atg8a LDS mutant (K48A, Y49A), and 6xHIS tagged Sequoia WT. GST was used as a negative control. Quantification shown in (B), relative to WT binding and normalised against Ponceau staining. Statistical significance was determined using Student's t test; ***$p < 0.005$. (C) GST-pull-down assay between GST-tagged Atg8a-WT or Atg8a-LDS mutant (Y49A), and radiolabelled GFP-Sequoia-WT or GFP-Sequoia-LIR mutant (Y313A/316A). GST was used as negative control. Quantification of the binding is shown in (D), adjusted to 10% input. Statistical significance was determined using Student's t test; **$p < 0.01$. In all cases n=3 independent experiments, error bars denote +SDs. (Experiments relating to C-D were completed by Terje Johansen Lab, University of Tromsø)

3.2.1 Identification of Sequoia homologs

In order to gauge a better understanding of how Sequoia may function *in vivo,* its protein sequence was queried in the search for homologs. Using the 'DIOPT' tool on Flybase, protein sequence similarity was indicated between Sequoia and; Rph1 and Gis1 in yeast, and a JmjN/JmjC domain containing KDM4 in *C.elegans;* which is encoded by the gene *jmjd-2 (jumonji d-2*). Proteins containing these specific Jmj domains are members of the Jumonji family of transcription factors, and are commonly present in numerous eukaryotic proteins containing domains typical of transcription factors, such as zinc fingers[371]. Notably, protein sequence similarity, in reference to Sequoia, was concentrated within the zinc finger domain of these respective proteins, as although Rph1, Gis1 and Jmjd-2/KDM4 all contain JmjN/C regions, Sequoia does not (Fig3.3 A-B).

In yeast, Rph1 and Gis1 constitute paralogs of one another; both of which act as JmjN/JmjC domain-containing histone demethylases and zinc finger transcription factors which function to regulate genes during nutrient limitation. Rph1 has previously been characterised as a master negative regulator of starvation-induced autophagy in yeast[247]. The binding ability of the C2H2Zn domain in Rph1 has been shown to be essential in the control of autophagy, however its JmjC domain is dispensable. The mammalian homolog of Rph1 is KDM4A, and has been observed to regulate autophagy in a similar manner, indicating an evolutionary conserved function[247].

In a search for paralogs of Sequoia it was revealed that Kdm4B showed a high level of sequence similarity, and that *sequoia* and *kdm4b* overlap within the same genomic region on the 2R chromosome (2R: 13,176,553–13,190,086 /2R:13,176,553–13,198,337). Kdm4B, an orthologue of mammalian KDM4, is a histone demethylase that removes methyl groups from histone 3 lysine 9 and 36 and participates in DNA repair and transcription regulation[372]. Sequence analysis revealed that *C.elegan* Jmjd-2/KDM4 is an ortholog of mammalian KDM4C. Interestingly, protein sequence analysis using the SMART tool revealed that Jmjd-2/KDM4 and mammalian KDM4A (homolog of Rph1) both harbour zinc finger domains, however *Drosophila* Kdm4B does not. Kdm4B does contain both a JmjC and N domain, which as previously mentioned is not present in Sequoia. Further analysis revealed Rph1 and Sequoia to both contain a specific C_2H_2Zn domain, whereas mammalian KDM4 and *C.elegan* Jmjd-2/KDM4 harbour a PHD-type domain, which contains two zinc ions[373]. Of particular importance, was the observation that Sequoia showed extremely high levels of sequence similarity within its C_2H_2Zn domain with another of its paralogs; Ttk (Fig. 3.3 A-B). Ttk represents a DNA-binding transcriptional repressor which has been reported to bind to a number of sites in the regulatory region of Ftz (Fushi-tarazu) controlling embryonic development[374] , as well as the repression of inappropriate genes which are incompatible with development of photoreceptor cell fates[375]. Importantly this highlights the transcriptional ability of the C_2H_2Zn domain in *Drosophila*.

COBALT is a multiple sequence alignment tool that finds a collection of pairwise constraints derived from conserved domain databases, protein motif databases, and sequence similarity, using RPS-BLAST, BLASTP, and PHI-BLAST [346]. Using this tool, a phylogenetic tree was created in order to observe the evolutionary relationship between Sequoia and the aforementioned homologous proteins. The constructed cladogram showed all protein sequences

under query observed to diverge from the same ancestral rooted node, with the closest inner species relation of Sequoia to be Ttk (Fig. 3.3 C).

Figure 3.3 support the hypothesis that Rph1 and KDM4 share an evolutionary lineage with Sequoia; presenting evidence that they represent its yeast and mammalian homologs, respectively. Given the conserved C_2H_2Zn region, it was hypothesised that Sequoia may act functionally in a similar fashion to Rph1 in the context of starvation-induced autophagy. Furthermore, work conducted by Professor Terje Johansen showed that KDM4A, interacts with GABARAP and GABARAP-L1 (the closest mammalian homologs to Atg8a), suggesting evolutionary conservation of the interaction (Appendix paper A; Figs. S1 B,C)[376]. However, mutation of the putative LIR motifs of KDM4A did not abrogate its interaction with GABARAP-L1 (Appendix paper A; Fig. S1C).

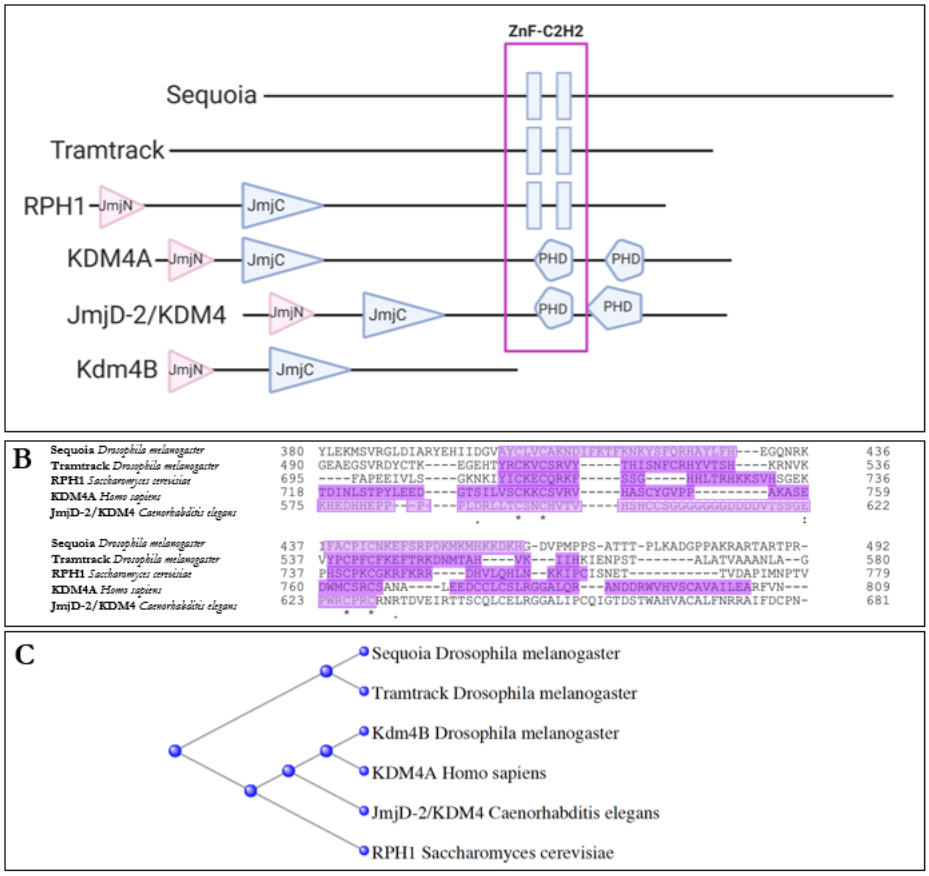

Figure 3.3 Rph1 and KDM4 are the Yeast and Human Homologs of Sequoia.

(A) Graphical representation of functional domains within the structure of Sequoia and its homologs/paralogs: Tramtrack, RPH1, KDM4A, JmjD-2/KDM4 and Kdm4B. Protein architecture was explored using the SMART tool. Protein sequence alignment via COBALT (B) revealed the zinc finger (C_2H_2Zn and PHD-type) domain to be conserved (*= conserved amino acids) throughout queried sequences. This region is highlighted by a pink box in both A and B. (C) Cladogram constructed using COBALT reveals divergence from a common ancestor. Based on this information KDM4A and RPH1 are likely to be the respective human and yeast homologs of Sequoia. Construction parameters: Max difference of sequence= 0.8, Distance= Grishin (protein).

3.2.2 Sequoia is not degraded by basal autophagy

To understand the biological significance of the interaction between Sequoia and Atg8a, western blot analysis was performed by Dr. Anne Jacomin (former Nezis lab member, University of Warwick), in order to compare the accumulation of Sequoia in whole body lysates from WT (w^{1118}), *Atg8a* and *Atg7* mutant flies. There are a number of critical autophagy genes, including *Atg8a* and *Atg7,* which are characterised by the loss of gene function resulting in the inactivation of the pathway. The $Atg8a^{KG}$, $Atg7^{D14}$ and $Atg7^{D77}$ mutant lines were obtained from Dr. Gábor Juhász (Eötvös Loránd University). In the case of $Atg8a^{KG}$, expression is blocked by the insertion a P-element at codon 28 of the *Atg8a* ORF (Open Reading Frame), thus rendering the line

incapable of initiating autophagy. *In vivo* experiments using this line have previously shown to cause a significant decrease in starvation-induced autophagy[111]. The transcription and translation start sites and the majority of the *Atg7* coding region was removed in order to generate $Atg7^{D14}$. In the case of $Atg7^{D77}$, exons 5 and 6 and most of exon 4 of *Atg7* have been removed[279].

A Sequoia antibody which was previously generated via injection of a GST-Sequoia fusion (amino acids 185-703) construct, as an antigen in rabbit[360], was used to probe for protein accumulation. Immunodetection was also conducted using an antibody against Ref(2)P; a known autophagy substrate, acting here as a direct comparison for accumulation. No difference in Sequoia accumulation was observed between w^{1118}, *Atg8a* and *Atg7* mutants suggesting that Sequoias is not degraded by basal autophagy, and that it's interaction with Atg8a does not contribute to its degradation (Fig. 3.4).

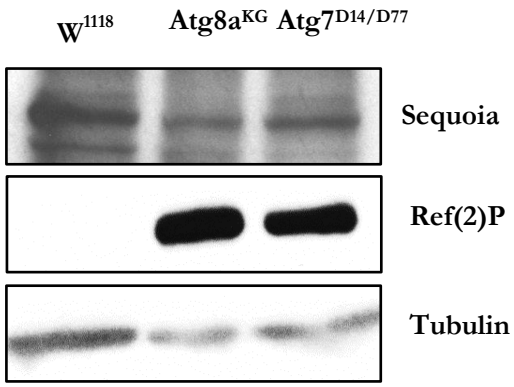

Figure 3.4 Sequoia is Not Degraded by Basal Autophagy. Whole body lysates from wild-type (WT) and Atg8a and Atg7 mutant flies were subjected to SDS-PAGE and immunoblotting for Sequoia and Ref(2)P. Tubulin was used as loading control. Genotypes: *w^{1118}, P{hsFLP} Atg8a [KG07569], $Atg7^{D14}$/$Atg7^{D77}$*. Experiment conducted by Dr. Anne Jacomin, formerly of University of Warwick.

3.3 The Cellular Localisation of Sequoia in Autophagy

Owing to the well described genetics of *Drosophila*, it is possible to control the ectopic expression of several proteins at the same time, in order to study their behaviour in relation to one another. UAS-GFP-$Sequoia^{WT}$ (WT) and UAS-GFP-$Sequoia^{LIRm}$ (LIR mutant) were previously created via cloning of the gene CDS of GFP-$Sequoia^{WT}$ and GFP-$Sequoia^{LIRm}$ into the *Drosophila* pGW vector, downstream of the UAS. The resulting transgenic lines were created by P-element mediated transformation of the aforementioned constructs.

Using the binary GAL4/UAS system the expression of constructs can be controlled both spatially and temporally. A GAL4 driver line which carries an insertion for the 'flpout' system

represents a genetic tool which allows for mosaic ectopic expression, where the extent of the mosaic is controlled by the amount of heat-shock applied to the F1 progeny of the genetic cross at embryo stage. Recombination of the *UAS-mCherry-Atg8a* with the *flpout*;*GAL4* driver has allowed the creation of a stable line which constitutively expresses mCherry-Atg8a in clonal cells[202]. This allows one to investigate the expression or silencing of a protein under the control of the UAS in an environment in which the process of autophagy can easily be observed.

3.3.1 Sequoia localises to the nucleus in fed and starved conditions

In order to elicit the function of Sequoia in the induction of autophagy, its cellular localisation was investigated. This was achieved through the use of the previously established stable transgenic line which is capable of overexpressing Sequoia^{WT} with an N-terminal GFP attached to it, in conjunction with the recombined mCherry-Atg8a line. It must be noted that endogenous *sequoia* is still expressed in these lines. Expression of GFP would therefore allow for an indication of the localisation of overexpressed Sequoia to be observed *in vivo,* with an impact on autophagy induction expected to be shown through the accumulation of mCherry-Atg8a puncta in the cytoplasm[111].

Males from the GFP-Sequoia^{WT} transgenic line were crossed with virgin females from the recombined mCherry-Atg8a line. The embryos of the genetic crosses were subjected to one-hour heat-shock, 24 hours after laying. This was previously established as the optimum duration for sufficient clonal expression. Third instar stage larvae were either collected directly from full nutrient conditions or subjected to four-hour starvation in 20% sucrose in order to induce autophagy. Fat body tissue was subsequently isolated, processed by IF and directly observed by confocal microscopy.

It was observed that Sequoia was overexpressed exclusively in the nucleus of clones in both fed and starved conditions. This gave an early indication that its predicted interaction with Atg8a is nuclear and therefore it is unlikely to have a role in physically mediating its translocation across the nuclear membrane (Fig. 3.5 A-B). As expected in the starved condition, an accumulation of mCherry-Atg8a puncta is observed in the cytoplasm. Without starvation, mCherry-Atg8a was diffusely expressed in the cytoplasm, however a large proportion was retained within the nucleus.

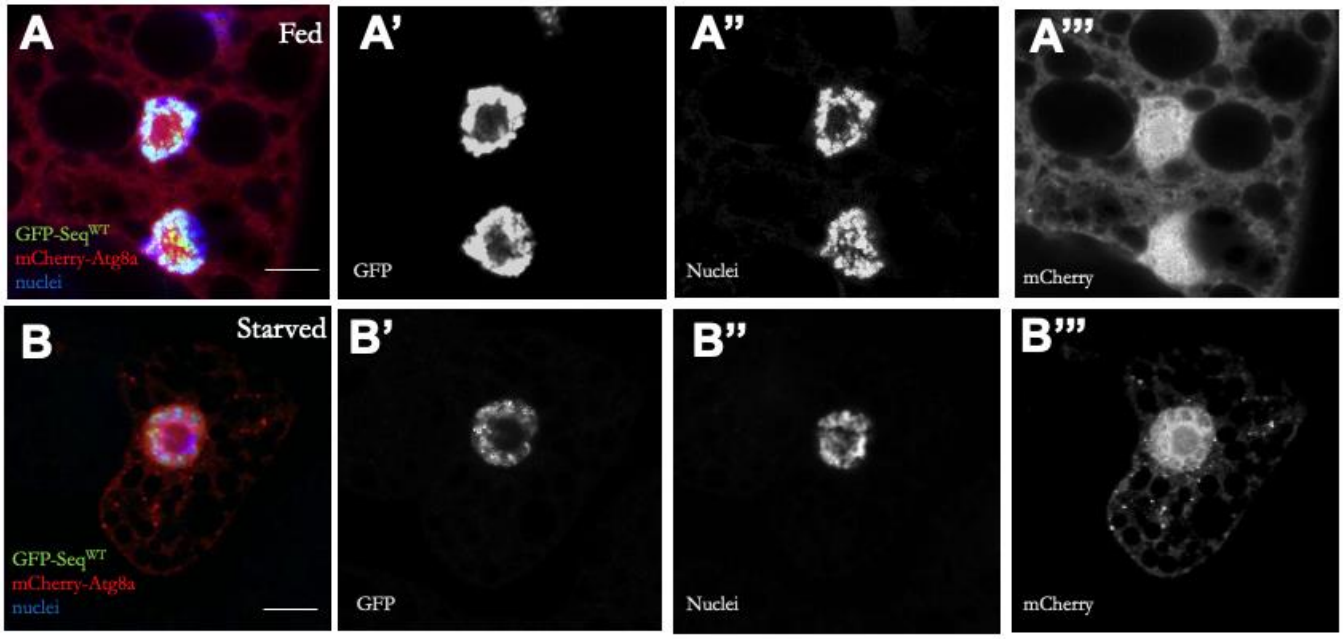

Figure 3.5 GFP-Sequoia Localises to the Nucleus in Fed and Starved Conditions.

(A–B) Confocal sections of larval fat bodies clonally expressing the autophagy marker mCherry-Atg8a (red) in combination with GFP-Sequoia WT (green). Larvae were well fed (A) or starved for 4 h (B). Fixed fat bodies were stained for nuclei (blue) using Hoechst. Scale bar: 10 µm. Grey panels depict split channels. Genotype: *yw hs-Flp;Ac > CD2 > GAL4/UAS-GFP-Sequoia-WT;UAS-mCherry-Atg8a/+*.

3.3.2 Overexpression of Sequoia^{LIRm} results in mCherry-Atg8a accumulation in the cytoplasm

In order to investigate the localisation of Sequoia^{LIRm}, and the effects it has on the induction of autophagy; males from the GFP-Sequoia^{LIRm} transgenic line were crossed with virgin females from the recombined mCherry-Atg8a line, and processed as previously described, exclusively in full nutrient conditions. This experiment was conducted alongside GFP-Sequoia^{WT} and GFP nls (nuclear localisation signal). The latter constitutes a control condition in which expression of GFP, tagged at its N terminal end with the 15 amino acid SV40 nuclear localization signal, is governed by UAS regulatory sequences, resulting in nuclear expression of the GFP protein[377].

The relative expression levels of *sequoia* were compared in third instar stage larvae of GFP-Sequoia^{WT} and GFP-Sequoia^{LIRm}, via RT-qPCR. There was no significant difference in expression between the two constructs (Fig 3.6 D). Confocal images of positive clones were collected and analysed using a previously developed Fuji/ImageJ[378] tool referred to as 'AtgCOUNTER'[338]. This

is a semi-automated macro which permits measurement of specific mCherry-Atg8a dots while excluding background pixels and potential nuclear mCherry-Atg8a from the analysis.

Interestingly, the overexpression of GFP-Sequoia^{LIRm} resulted in a significant increase of mCherry-Atg8a puncta (Fig 3.6 A,E) in the cytoplasm, which resembles the induction of autophagy by starvation. A significant difference was calculated when compared to both GFP-Sequoia^{WT} and GFP nls (Fig. 3.6 E). The overexpression of GFP-Sequoia^{WT} (Fig. 3.6 B) showed no significant difference in the accumulation of puncta when compared to GFP nls (Fig 3.6 C) conditions. As previously observed in GFP-Sequoia^{WT}, GFP-Sequoia^{LIRm} localised exclusively to the nucleus in all positive clones.

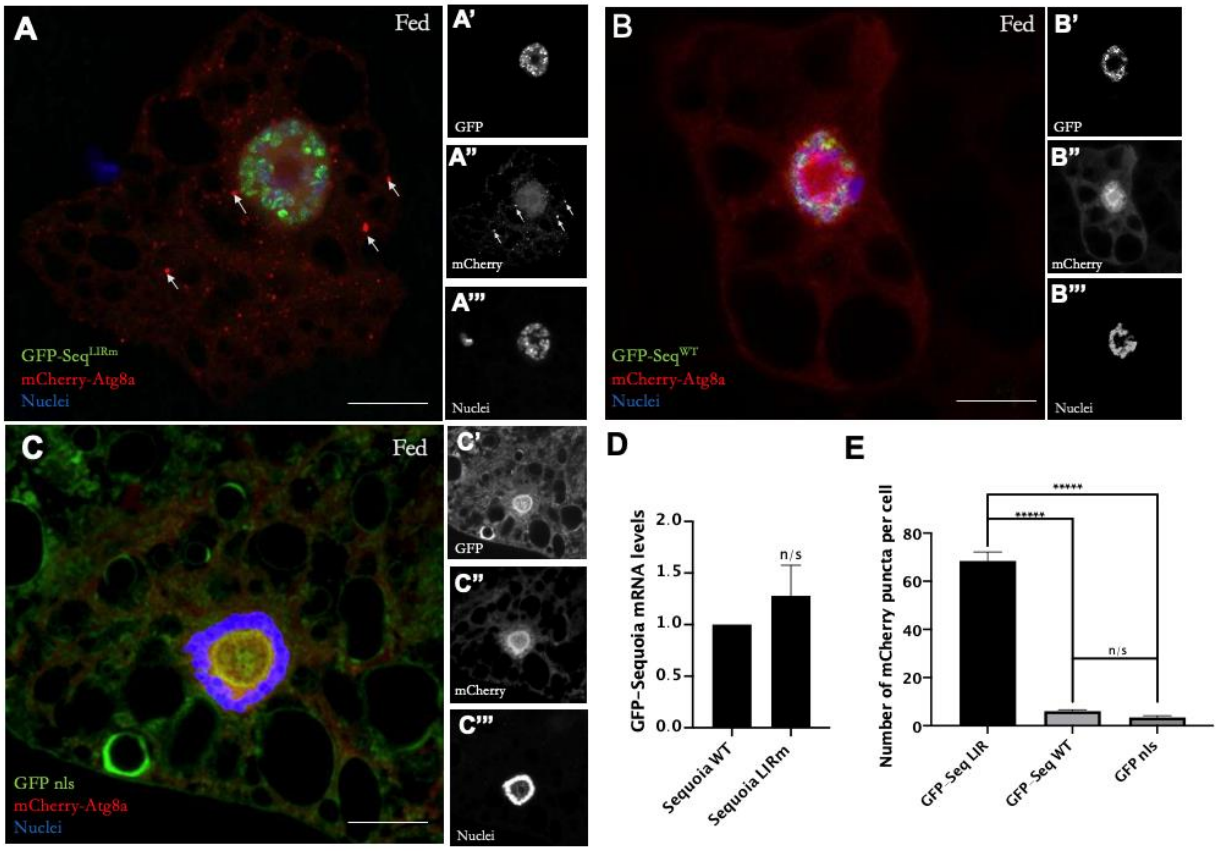

Figure 3.6 Overexpression of Sequoia LIR Mutant Results in the Accumulation of mCherry-Atg8a Puncta in Fed Conditions.(A–C) Confocal sections of larval fat bodies clonally expressing the autophagy marker mCherry-Atg8a (red) in combination with GFP-Sequoia-WT (A), GFP-Sequoia-LIRm (B), or GFP-nls (C) (green). Larvae were well fed in all conditions. Fixed fat bodies were stained for nuclei (blue). Scale bar: 10 µm. (D) mRNA expression of GFP-Sequoia in Sequoia LIR mutant, relative to Sequoia WT. Statistical significance was queried via Student's t-test; n/s= not significant, p> 0.05. n= independent experiments. (E) Quantification of the number of mCherry-Atg8a dots per cell. Bars denote means ± SDs. Statistical significance was determined using 1-way ANOVA; *****p < 0.00005. (50 clones were included per genotype). Genotypes: (A) *yw hs-Flp;Ac > CD2 > GAL4/UAS-GFP-Sequoia-WT;UAS-mCherry-Atg8a/+*. (B) *yw hs-Flp;Ac > CD2 > GAL4/UAS-GFP-Sequoia-LIRm;UAS-mCherry-Atg8a/+*. (C) *yw hs-Flp;Ac > CD2 > GAL4/+;UAS-mCherry-Atg8a/UAS-GFPnls*.

3.3.3 Sequoia and Atg8a co-localise in the nucleus under fed conditions

After establishing a direct protein interaction between Atg8a and Sequoia *in vitro*, it was sought to investigate this *in vivo*. As previously described GFP-Sequoia^{WT} and GFP-Sequoia^{LIRm} transgenic lines were crossed with virgin females from the recombined mCherry-Atg8a line in order to co-express the proteins in larvae. Fat bodies were isolated, processed and visualised as before.

In the measurement of co-localisation, Mander's overlap coefficient is known to be the most commonly used method. However, as Mander's coefficient is reliant on the strength of an overlapping signal in the area of interest, it is highly susceptible to background noise. When working in the setting of singular cell layers, such as in cell culture, this can be easily corrected and maintained whilst performing observations with a microscope, mainly due to the limited variation in the architecture of the tissue sample. In the case of *Drosophila* fat body tissue however, the tissue will inevitably vary in thickness and orientation across the sample, as well the case of natural variations in protein expression across clones; this environment thus requires the confocal laser output and the photo-multiplier settings to change accordingly to the ever changing landscape and thus background noise is far more prominent. Given the number of limitations faced when observing whole tissues, Pearson's coefficient was favoured[379,380].

Calculation of Pearson's correlation coefficient indicated a significantly higher co-localisation between GFP-Sequoia^{WT} (Fig. 3.7 I) and mCherry-Atg8a in the nucleus, in comparison to GFP-Sequoia^{LIRm} (Fig 3.7 II, III, and VI). Interestingly, in the case of the LIR mutant, a small proportion of clones were observed to retain more mCherry-Atg8a in the nuclear compartment than others, which empirically seemed to coincide with those in which mCherry puncta in the cytoplasm were less abundant; however the correlation coefficient, depicted by the channel overlays (Fig 3.7, III), were consistent in showing a significantly lower co-localisation between GFP-Sequoia^{LIRm} and mCherry-Atg8a. The majority of the GFP-Sequoia^{LIRm} clones were observed to have very little mCherry-Atg8a expression in the nuclear compartment (Fig 3.7, II).

It must be emphasised that co-localisation is not evidence of a physical interaction; more so it is representative of the co-occurrence of two components through their spatial overlap; this is determined through a correlation, in which the two probes not only overlap with one another but also co-distribute in proportion to one another within a structure. Given an *in vitro* interaction has already been observed however, this strengthens the possibility that an *in vivo* interaction may occur between the two proteins. As an *in vivo* interaction was not explored

directly during this project it would be beneficial for future work to explore this using a technique such as FRET (Fluorescence Resonance Energy Transfer). This is a fluorescence microscopy-based biophysical approaches could be used to directly observe whether there is an interaction between Atg8a and Sequoia in the nucleus of living cells. For example, Kraft et al., (2016) reported on interactions between LC3 and SQSTM1 can be readily detected using a FRET microscopy[159]. FRET is a process by which exited-state energy is transferred directly from one fluorophore (the "donor") to other nearby molecules (the "acceptors") through electromagnetic dipole interactions[381]. Quantification of FRET signals in microscopic images can provide measurements of spatial relationship between the fluorophores labelling proteins inside the living cell. Kraft et al., (2016) measure FRET between Cerulean- and Venus-tagged versions of LC3 and SQSTM1 through acceptor photobleaching; a well-characterized method to quantify energy transfer by fluorescence microscopy[319].

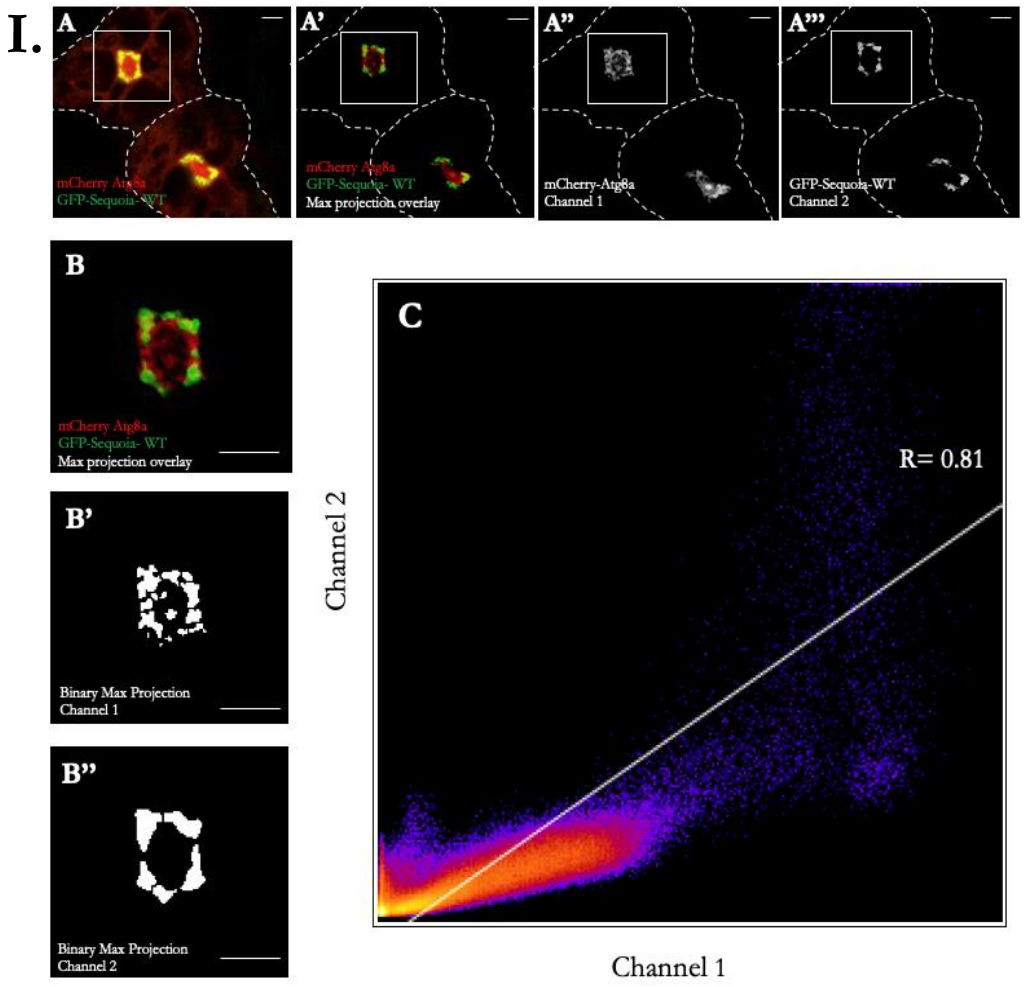

II.

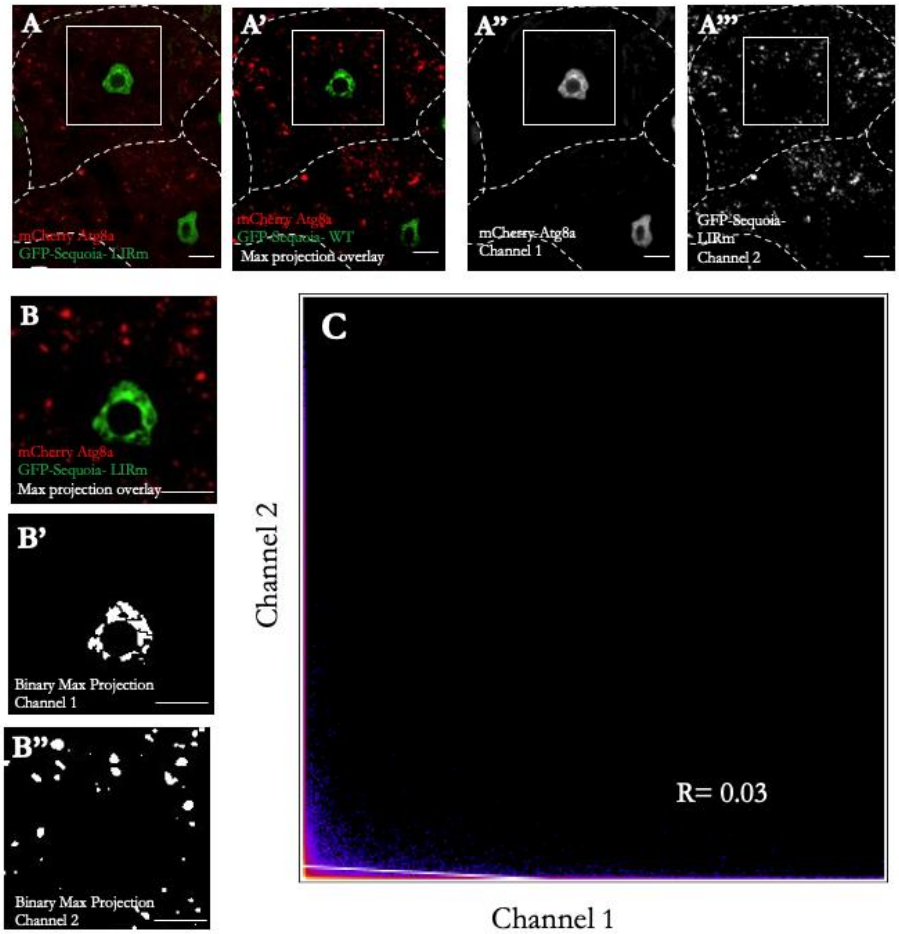
A
mCherry Atg8a
GFP-Sequoia- LIRm
A'
mCherry Atg8a
GFP-Sequoia- WT
Max projection overlay
A''
mCherry-Atg8a
Channel 1
A'''
GFP-Sequoia-
LIRm
Channel 2
B
mCherry Atg8a
GFP-Sequoia- LIRm
Max projection overlay
B'
Binary Max Projection
Channel 1
B''
Binary Max Projection
Channel 2
C
Channel 2
R= 0.03
Channel 1

III.

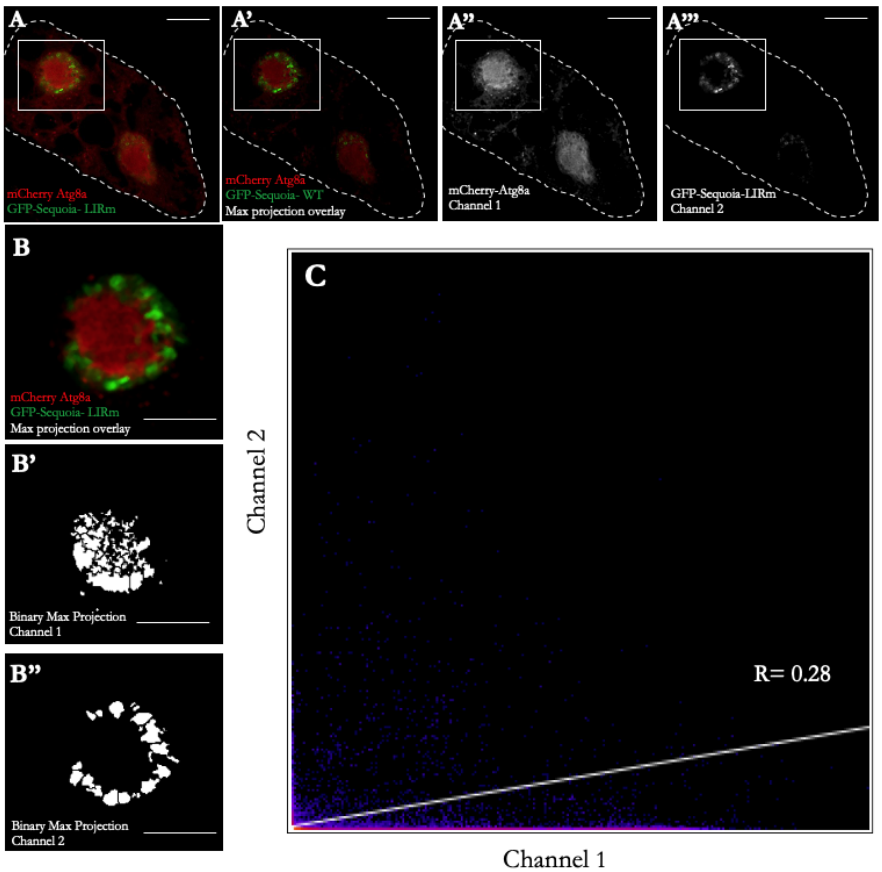
A
mCherry Atg8a
GFP-Sequoia- LIRm
A'
mCherry Atg8a
GFP-Sequoia- WT
Max projection overlay
A''
mCherry-Atg8a
Channel 1
A'''
GFP-Sequoia-LIRm
Channel 2
B
mCherry Atg8a
GFP-Sequoia- LIRm
Max projection overlay
B'
Binary Max Projection
Channel 1
B''
Binary Max Projection
Channel 2
C
Channel 2
R= 0.28
Channel 1

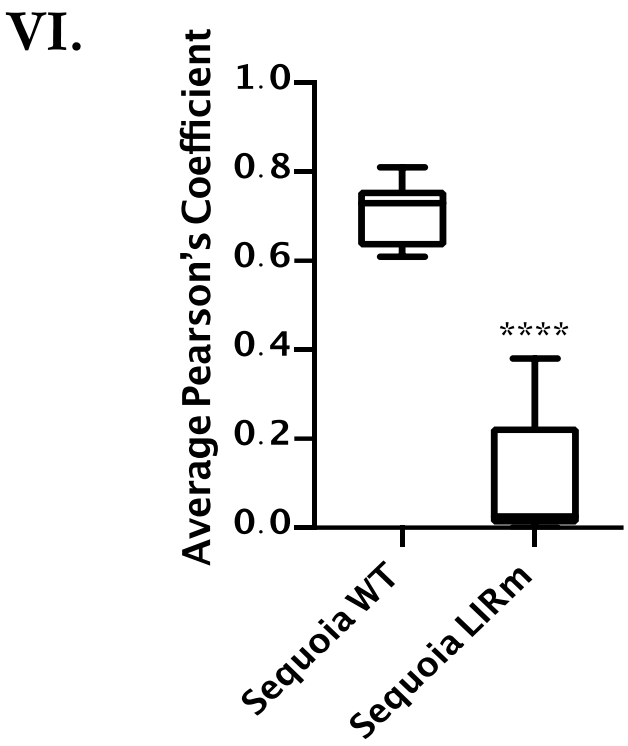

Figure 3.7. Wild Type Sequoia Co-localises with Atg8a in the Nucleus Under Fed Conditions.

Confocal sections of fat body from fed pre-wandering third-instar larvae, clonally expressing mCherry-Atg8a and either (I) GFP-Sequoia WT or (II and III) GFP-Sequoia LIRm. In all cases: (A-A') mCherry and GFP channel overlay, where max projection only considers intensity points above a set threshold. (A"-A"') Greyscale panels depict the max projection points of split channels where mCherry=Channel 1 and GFP=Channel 2. (B) Representative of the zoomed area shown in A-A"'; this region constitutes the nucleus, and where the co-localisation analysis was conducted in the clone. (B'-B") Binary max projection of each channel: where particles within the nucleus are separated for analysis. (C) Channel 1(mCherry) vs Channel 2 (GFP) intensity plot conducted over the space of the nuclear region, with R signifying Pearson's correlation coefficient. Scale: 10μm. (VI) Average Pearson's correlation coefficient for mCherry-Atg8a and GFP-Sequoia across wild type and mutant genotypes. Colocalisation analysis was conducted using the Coloc2 tool in ImageJ/Fuji. Box plot denotes ± SD and average. Two-tailed Student's t-test showed ****$p<0.00005$. Genotype: *yw hs-Flp;Ac > CD2 > GAL4/UAS-GFP-Sequoia-WT;UAS-mCherry-Atg8a/+*. *yw hs-Flp;Ac > CD2 > GAL4/UAS-GFP-Sequoia-LIRm;UAS-mCherry-Atg8a/+*.

3.3.4 Depletion of *sequoia* results in the induction of autophagy in fed conditions

In order to further examine the role of Sequoia in autophagy, a *Drosophila* line allowing for the RNAi mediated silencing of *sequoia* was obtained from VDRC. Expression of *sequoia* was confirmed to be significantly reduced when the *sequoia*-RNAi line was expressed, in comparison to a *luciferase*-RNAi control (Fig 3.8, D).

An accumulation of Atg8a-positive puncta in the cell can result either from an induction or a blockade of the autophagic flux[337]. To make the distinction between these two possibilities, a tandem-tagged Atg8a (UAS-GFP-mCherry-Atg8a) was utilised[337]. The double tagged Atg8a emits yellow (green merged with red) fluorescence in non-acidic structures such as autophagosomes. The structure will only emit a red fluorescence during a formation of an autolysosome due to acidic conditions causing GFP to become quenched. Therefore, an accumulation of red puncta in the cytoplasm will be indicative of the induction of autophagic flux. As previously described for the mCherry-Atg8a line, recombination of the *UAS-GFP-mCherry-Atg8a* with the *flpout*; *GAL4* driver allowed for the creation of a stable line with constitutively expresses GFP-mCherry-Atg8a in clonal cells.

sequoia-RNAi and *luciferase*-RNAi males were crossed with the GFP-mCherry-Atg8a line, and the number of yellow and red puncta were quantified in fed conditions. The control condition, *luciferase*-RNAi, was also investigated in starvation conditions. In all conditions significantly more mCherry red puncta were observed in comparison to mCherry-GFP yellow puncta. In fed conditions, cells expressing *sequoia*-RNAi, showed an increased accumulation of red puncta that lack GFP fluorescence compared to the control, suggesting an induction of autophagic flux (Fig 3.8 A, C, E). The number of mCherry puncta in control starved conditions and *sequoia*-RNAi fed conditions were comparable, implying that *sequoia*-depletion results in the induction of autophagy, thus mimicking starved conditions (Fig 3.8 B, C, E).

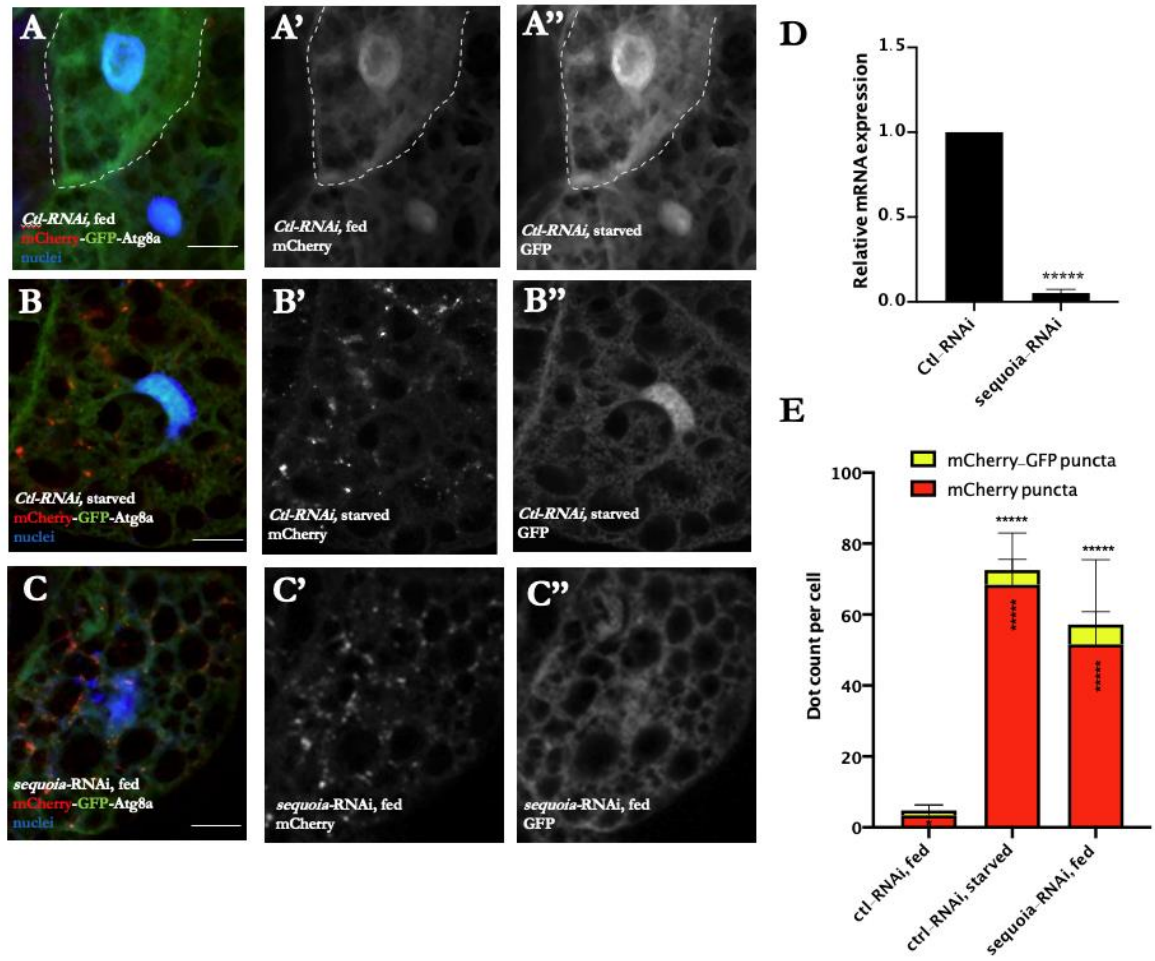

Figure 3.8. Depletion of *sequoia* Results in the Accumulation of Autolysosome in Fed Conditions.

(A-C) Confocal sections of larval fat bodies clonally expressing the autophagy flux marker GFP-mCherry-Atg8a (red and green) in combination with a control-RNAi in fed (A) or starved (4h, 20% sucrose) (B) or *sequoia*-RNAi in fed larvae (C). Sequoia depletion induces accumulation of autolysosomes. Fixed fat bodies where stained for nuclei (blue). Scale bar: 10 μm. (D) mRNA expression of *sequoia* in *sequoia-RNAi* relative to control-RNAi. Statistical significance was determined using a Student's t-test; *****$p < 0.0001$. n= 3(E) Quantification of the yellow (autophagosome) and red only (autolysosomes) puncta per cell. Statistical significance was determined using one-way ANOVA test; *****$p < 0.0001$. (50 clones were used per genotype, per condition) Genotypes: (A and B) *yw hs-Flp;Ac > CD2 > GAL4/+;UAS-mCherry-GFP-Atg8a/UAS-luc-RNAi.* (C) *yw hs-Flp;Ac > CD2 > GAL4/+;UAS-mCherry-GFP-Atg8a/UAS-sequoia-RNAi.* (D)*ctl: Cg-GAL4/+;UAS-luc-RNAi/+, seq-RNAi: Cg-GAL4/+; UAS-sequoia-RNAi/+.*

As an extension of this work, *sequoia*-RNAi lines were crossed with another hs-FLP line: *hs-Flp; 3xmCherry-Atg8a, UAS-GFP; Act>CD2>Gal4, UAS-Dcr2*[382,383]. This line results in GFP positive clones being created in cells corresponding to those in which express *sequoia*-RNAi, alongside 'negative cells' which have been unmanipulated. The marker 3xmCherry-Atg8a is expressed throughout the fat body in all cells, labelling both autophagosomes and autolysosomes; allowing

for the side by side comparison of 'positive' and 'negative' cells within the same tissue, thus ensuring exposure to confounding variables is the same for both. Given this was a newly obtained line, this work was conducted in order to explore its potential as an autophagy marker in conjunction with *sequoia*-RNAi as well as to verify findings outlined above. mCherry-Atg8a puncta were quantified using the previously described 'AtgCONTER' tool, with the number of dots per cell considered in order to account for the variation in positive versus negative clones observed across samples. GFP positive clones (those expressing *sequoia*-RNAi) were found to be present in ~80% of the tissue sampled.

Consistent with previous observations under fed conditions, a significantly higher accumulation of red 3xmCherry-Atg8a puncta were present in 'positive' cells expressing *sequoia*-RNAi, in comparison to neighboring 'negative' control cells, in which *sequoia* had not been depleted (Fig 3.9). This further strengthens the notion that *sequoia*-depletion results in the induction of autophagy and hints at a repressive role of Sequoia in fed conditions. Interestingly this also gives an insight into the autonomous nature of individual cells throughout a tissue in the induction of autophagy, with 'negative' cells observed to accumulate significantly less 3xmCherry-Atg8a puncta despite the activity of their "positive" neighbours.

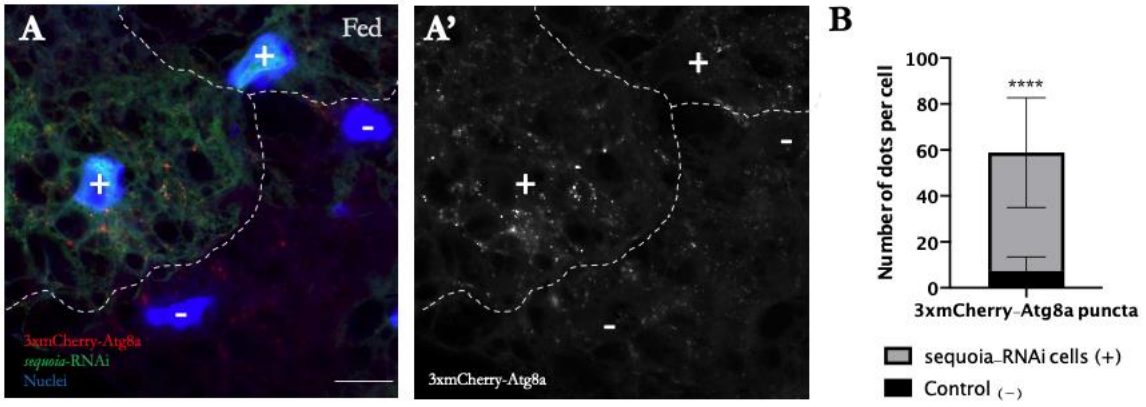

Figure 3.9. *sequoia*-depleted positive cells show mCherry-Atg8a accumulation.

(A) Confocal sections of larval fat bodies clonally expressing the autophagy marker 3xmCherry-Atg8a (red) in combination with *sequoia*-RNAi in fed larvae. Sequoia depletion induces accumulation of autophagosomes and autolysosomes. Fixed fat bodies where stained for nuclei (blue). Scale bar: 10 μm. (B) Quantification of and red puncta in positive cells (green; GFP expression) and negative cells (no GFP expression). Statistical significance was determined using 1-way ANOVA test; ****$p < 0.0005$. (Clones were obtained across 15 samples) Genotype: (A) *hs-Flp; 3xmCherry-Atg8a, UAS-GFP; Act>CD2>Gal4, UAS-Dcr /UAS-sequoia-RNAi.*

3.4 Sequoia is a Negative Transcriptional Regulator of Autophagy

As sequence analysis revealed the presence of a C_2H_2 zinc finger domain within Sequoia, the next phase of investigation was aimed at determining whether it had a transcriptional role in the induction of autophagy. Given the observations that *sequoia*-depletion in larval fat body resulted in the accumulation of autolysosomes, and on published reports that Rph1 and KDM4, the putative yeast and human homologs of Sequoia, act as a transcriptional repressor of autophagy under fed conditions[247]; it was hypothesised that Sequoia may play a similar role.

3.4.1 Sequoia silencing results in the upregulation of autophagy genes

Firstly, the expression of numerous *Atg* genes upon *sequoia*-depletion was investigated. The gene set: *Atg1, Atg4a, Atg4b, Atg5, Atg7, Atg8a, Atg9, and Atg10. Atg13, Atg14, Atg18a and Atg101*, was selected as they encode proteins across all stages of autophagy, from initiation to autolysosome fusion. Furthermore, these genes have also been shown to be upregulated by several folds in response to nutrient limitation in the *Drosophila* larvae fat body[27,384]. Therefore, querying which of these are affected by *sequoia*-depletion may be indicative of the specific influence Sequoia has in the induction of autophagy. In addition to these *Lamp1, Mitf* and *Tor,* were also included; *Lamp1* encodes a protein which is widely distributed amongst autophagic organelles, specifically targeting lysosomal and is known to be upregulated in response to cellular stress[385]. *Mitf,* encodes a transcription factor which constitutes the *Drosophila* homolog of mammalian TFEB; coined a master up-regulator of autophagy, with *Mitf* also having been shown to govern autophagic responses to nutrient deprivation in *Drosophila*[259]. And finally, *Tor* which encodes TOR, a known repressor of starvation induced autophagy, and therefore known to be downregulated in its induction[90].

Sequoia-RNAi and *luciferase*-RNAi were crossed with the driver line Cg-Gal4, with RNA extracted from fed third instar stage larvae of the F1 progeny. Remarkably, RT- qPCR analysis revealed that the expression of all *Atg* genes were significantly increased in a *sequoia*-depleted setting, with the exception of *Tor*, which concordantly, was inversely downregulated amidst an up-regulated trend which is indicative of an induction of autophagy (Fig. 3.10). This up-regulated *Atg* expression pattern is characteristic to that reported upon the induction of autophagy in the *Drosophila* fat body[384].

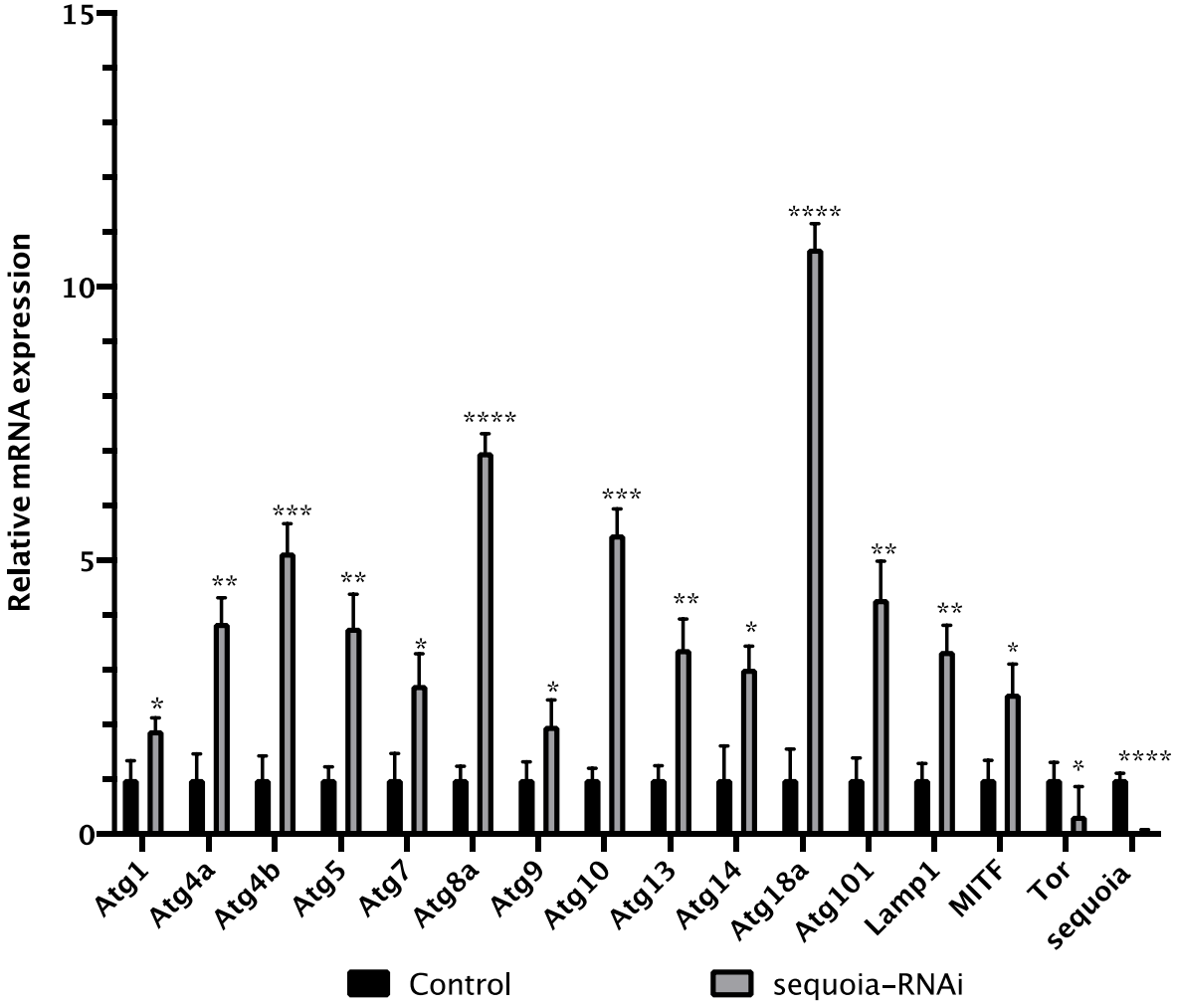

Figure 3.10. Sequoia Negatively Regulates Autophagy Genes.

Analysis of the mRNA levels of autophagy-associated genes in control (*luciferase*-RNAi) and Sequoia depleted (*sequoia*-RNAi) fat bodies in fed conditions, using real-time qPCR. Expression levels are shown relative to the control and normalised to the expression of *rp49* (housekeeping gene) over 3 biological replicates. Statistical significance was determined using a Student's t-test; *$p < 0.05$ and ****$p < 0.0005$. Genotype: ctl: *Cg-GAL4/+;UAS-luc-RNAi/+, seq-RNAi: Cg-GAL4/+;UAS-sequoia-RNAi/+*.

3.4.2 *Sequoia*-depletion results in the downregulation of *ref(2)p* and *kenny*

Interestingly, continued investigation in the same experimental setting (*sequoia*-RNAi) revealed the relative expression of genes encoding the autophagy receptors, Ref(2)P and Kenny, to both show significant downregulation compared to the control (Fig. 3.11 A). Both protein products are autophagy substrates and thus are degraded in conjunction with cargo, however why their mRNA expression is reduced when *sequoia* is knocked down is intriguingly unclear. Remarkably, expression levels of *kenny* were observed to be very strongly downregulated. However, accumulation and degradation of Kenny has been shown to be a post-translational event with mRNA levels for *kenny* reported to be similar between wild-type and autophagy mutant flies[202]. The transcriptional regulation of *kenny* however has not previously been explored in a setting in which autophagy is significantly elevated in relation to basal conditions. Interestingly, comparison of the lengths of larvae used for mRNA analysis, clearly indicated that the expression of *sequoia*-RNAi results in a significantly smaller body size when compared to the control (Fig. 3.11 B-C). This may be indicative of a hyper-activation of autophagy in the fat body cells of *sequoia*-depleted larvae, resulting in a hampered accumulation of body mass due to cellular breakdown. This observation points towards the idea that these particular cells may have to cap their autophagic capacity by limiting the transcription of other autophagic components, such as Kenny and Ref(2)P, in order to remain viable.

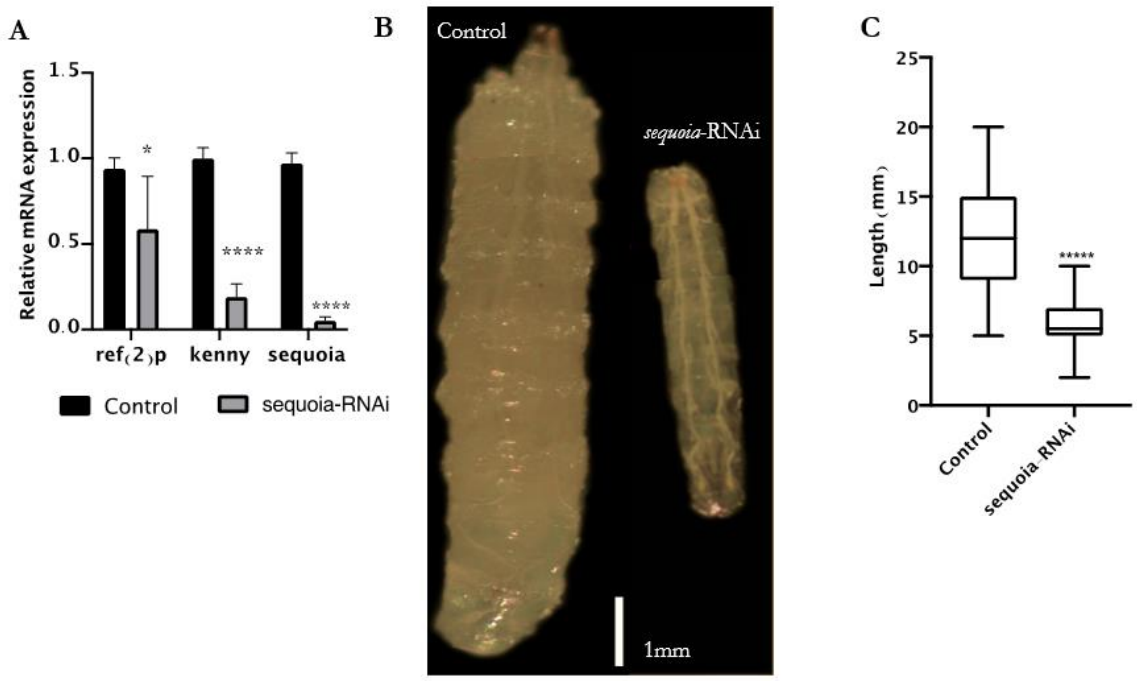

Figure 3.11. Depletion of *sequoia* Results in Smaller Larvae Size and Downregulation of *ref(2)P* and *kenny*.

(A)Analysis of the mRNA levels of *ref(2)P* and *kenny* in control (*luciferase*-RNAi) and Sequoia depleted (*sequoia*-RNAi) fat bodies in fed conditions, using real-time qPCR. Expression levels are shown relative to the control and normalised to the expression of *rp49* (housekeeping gene) across 3 biological replicates. (C) Control (*luciferase*-RNAi) and *sequoia*-RNAi well fed third instar stage larvae were collected and measured (length ways). Scale= 1mm. Lengths across all larvae is shown in (B), with 150 larvae per condition. Statistical significance was determined using a Student's t-test; *****$p < 0.00005$. Statistical significance was determined using a Student's t-test; *$p < 0.05$ and ****$p < 0.0005$. Genotypes: ctl: *Cg-GAL4/+;UAS-luc-RNAi/+, seq-RNAi: Cg-GAL4/+;UAS-sequoia-RNAi/+*.

3.4.3 Sequoia is enriched on the promotor region of *Atg* genes

In order to investigate whether Sequoia is enriched at the promotor region of the previously investigated *Atg* genes, and thereby control their expression directly, a ChIP assay was conducted. As there are no published protocols for this assay in *Drosophila* larvae fat body, multiple rounds of pilot experiments using anti-Histone H3, were conducted in order to determine and optimise experimental conditions. H3 histone modifications are associated with active gene repression[281]. The ribosomal protein L30 coding region (*Rpl30* exon 1-2) is representative of euchromatin; a lightly packed form of chromatin which is reflective of transcriptional activity, and is therefore used as an indication of H3 histone modifications associated with transcriptional regulation[343]. The detection of enrichment of H3 at *Rpl30* exon 1-2 here is indicative of the reliability of the experimental procedure in detecting transcriptional activity (Fig 3.12 A). Pilot experiments also allowed for determination of how much tissue would be required for experimentation; with 150 whole body larvae per condition deemed sufficient.

From fed conditions, WT larvae were collected, dissected and subjected to IP using normal rabbit IgG; a control for nonspecific precipitation and anti-Sequoia; for precipitation of endogenous Sequoia. Enrichment of specific DNA sequences represent regions on the genome that the protein of interest associates with *in vivo* and can be identified via Real Time-qPCR. Suitable ChIP specific *Atg* gene primers were designed via selection of exon sequences within the transcription factor promotor binding region of interest. Promotor regions were identified and selected using the EDP (2019). Real Time-qPCR was performed on input (no ChIP) and output (ChIP) DNA, for direct comparison, with primers complementary to the promotor genomic loci of the following set of *Atg* genes: *Atg1, Atg5, Atg7, Atg8a, Atg13 and Atg14*. Since primer design and optimisation were relatively time consuming, only a subset of *Atg* genes were selected for this study. The rationale behind the selection of these genes lies behind their homology to those which exhibited a strong induction in yeast cells following nitrogen starvation, and were upregulated in *rph1*-depleted yeast cells; *Atg1*, *Atg7, Atg8, Atg9, Atg14, Atg29 and Atg32*[247]. Also, these had previously been shown to been upregulated in the *Drosophila* fat body following starvation[27,384].

Sequoia was observed to be significantly enriched at the promotor of all *Atg* genes queried when compared to the control (Fig. 3.12 A). No convincing levels of correlation between relative gene expression and promotor enrichment was observed, in that a larger decrease in relative expression of an *Atg* gene does not seem to correlate to a higher level of fold enrichment at its

promotor (Fig. 3.12 B). Taken together, these observations strongly suggest that Sequoia functions as a transcriptional repressor of *Atg* genes. Further verification of the activation of autophagy in *sequoia*-depleted cells was shown by the accumulation of Atg1 in *sequoia*-depleted larvae (conducted by Dr. Stavroula Petridi, Nezis lab; Appendix paper A; Fig. S2 A-D)[376]. Further validation of these results could have been obtained by conducting the outlined ChIP experiment in parallel with *sequoia*-depleted larvae.

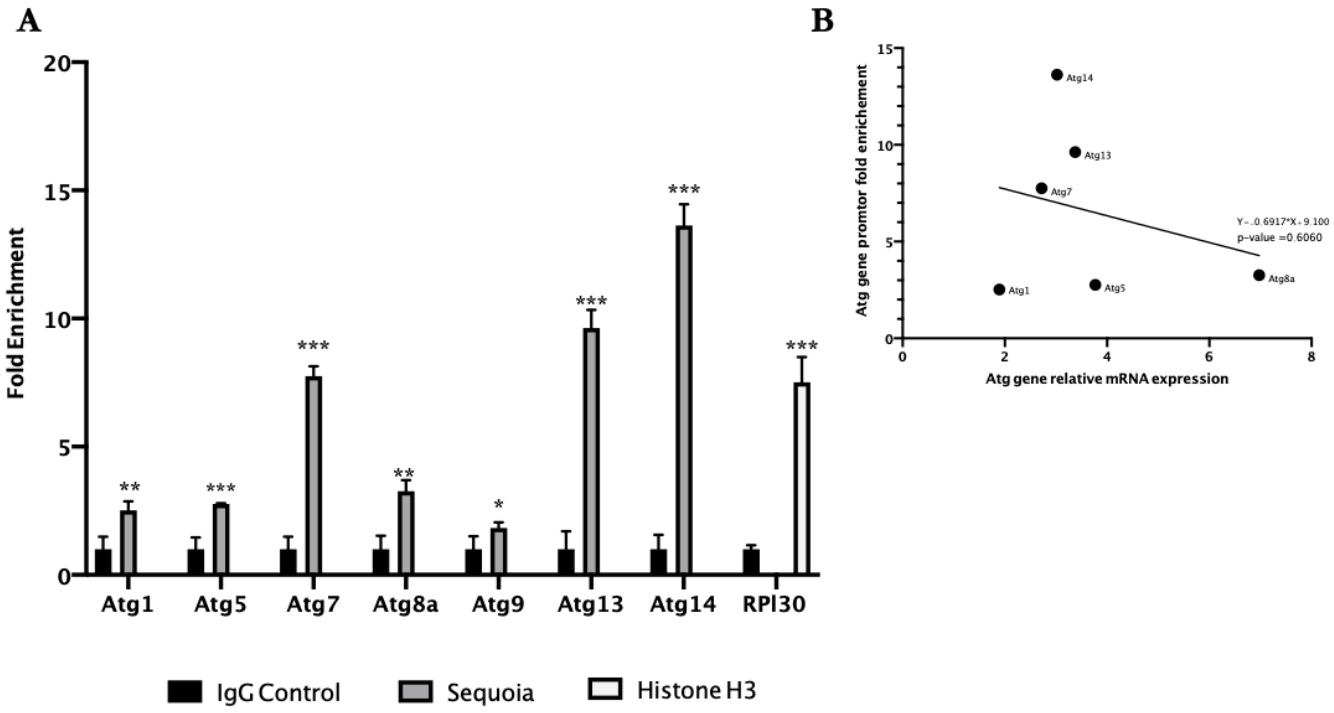

Figure 3.12 Sequoia is Enriched on the Promotor Region of *Atg* Genes.

(A) Analyses of Sequoia binding to the promoter of autophagy genes in fed conditions, as detected by ChIP (chromatin immunoprecipitation) using a Sequoia antibody. ChIP DNA values were normalized to input DNA using the $2^{-\Delta\Delta}$ (Ct) method. Fold enrichment values are shown relative to the immunoglobulin G (IgG) control. Histone H3 enrichment to *Rpl30* (exon 1-2) was used as a positive control. All data shown as means ± SDs, n = 3 independent experiments. Statistical significance was determined using Student's t test; *$p < 0.05$ and ***$p < 0.005$. (B) Correlation analysis (Pearson's) between promotor enrichment and mRNA expression of *Atg* genes. No correlation observed. P= 0.60. Genotype A: *Cg-GAL4/+;W^{1118}*.

3.5 Investigating the Role of the LIR in Sequoia's Ability to Repress Autophagy

Previous *in vivo* observations indicated that loss of a functioning LIR motif in Sequoia results in the accumulation of Atg8a positive puncta in the cytoplasm (Fig. 3.6), suggesting the induction of autophagy. With knockdown of *sequoia* confirmed to result in an upregulation of *Atg* genes (Fig 3.10), the transcriptional effects of an overexpression of Sequoia^{LIRm} was investigated.

3.5.1 Sequoia LIR mutant induces an upregulation of autophagy genes in fed conditions

As previously described, GFP-Sequoia^{WT} and GFP-Sequoia^{LIRm} transgenic lines were crossed with the mCherry-Atg8a line, with embryos from the genetic crosses subjected to one-hour heat-shock, 24 hours after laying. Prior to any experimentation the expression of GFP-Sequoia was confirmed in F1 progeny via immunoblotting with anti-GFP (Fig 3.13 B). RT-qPCR revealed that overexpression of the GFP-Sequoia^{LIRm} in fed conditions resulted in a significant increase in the induction of *Atg* genes in comparison to GFP-Sequoia^{WT}, when calibrated against the expression pattern of a WT control (Fig. 3.13 A). Results in the GFP-Sequoia^{LIRm} also show a significant reduction in *Tor* expression, consistent with the pattern seen in the *sequoia*-depleted larvae, further suggesting the induction of autophagy.

As expected, the mRNA levels of *sequoia* detected in GFP-Sequoia^{WT} and GFP-Sequoia^{LIRm} were higher than those in the WT, however overexpression of Sequoia^{WT} had no significant effect on the induction of autophagy genes in comparison to the WT control. This suggests that endogenous levels of Sequoia are sufficient in maintaining a repressive cap on the expression of these genes, and that its overexpression has no effect on their down regulation. This in fact highlights even more so the exceptional effect in which overexpression of LIR mutant has on the regulation of *Atg* genes.

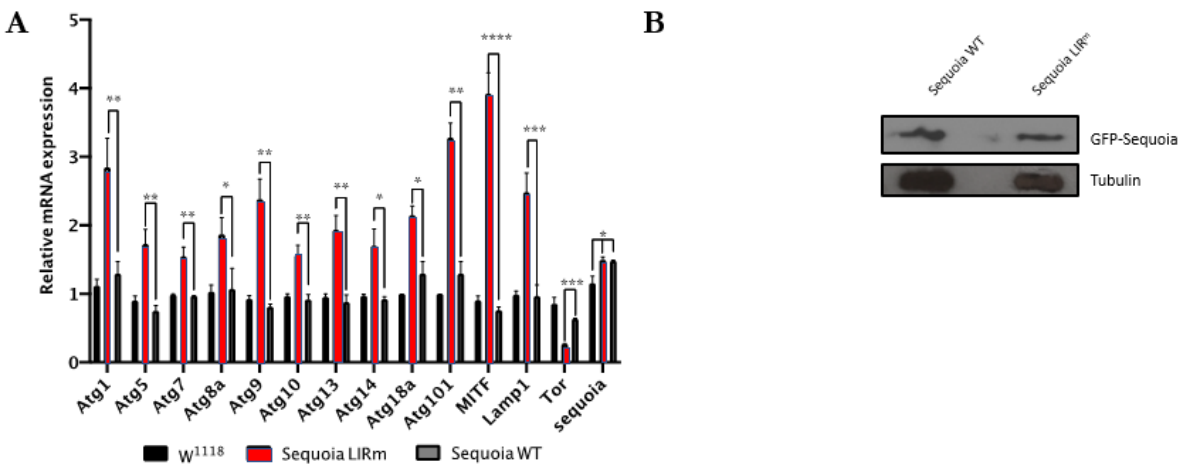

Figure 3.13 Overexpression of Sequoia LIR Mutant Results in the Upregulation of *Atg* Genes.

(A) Analysis of the mRNA level of autophagy-associated genes in W^{1118}, Sequoia LIR mutant, and Sequoia WT fat bodies in fed conditions, using real-time qPCR. Expression levels were relative to W^{1118} and normalised to *rp49*, with statistical significance determined between relative levels shown for Sequoia WT versus Sequoia LIR mutant. All data shown as means ± SDs, n = 3 independent experiments. Statistical significance was determined using Student's t test; *$p < 0.05$ and ***$p < 0.005$. (B) Expression of GFP-Sequoia protein in Sequoia WT and Sequoia LIR mutant following heat shock. Tubulin was used as a loading control. Genotypes: W^{1118}: *Cg-GAL4/+;W1118,* Sequoia WT*: hs::Gal4/UAS-GFP-Sequoia-WT,* Sequoia LIRm: *hs::Gal4/UAS-GFP-Sequoia-LIRm*

3.5.2 Sequoia LIR mutant is less enriched at *Atg* promotor regions

After establishing the effects of GFP-Sequoia^{LIRm} overexpression on the expression of *Atg* genes, its enrichment levels at corresponding gene promotor regions were investigated. To do this, a ChIP assay was carried out on the F1 progeny of the same genetic crosses as used for mRNA analysis and were processed as previously described. Here anti-GFP was used to target GFP-Sequoia^{WT} and GFP-Sequoia^{LIRm}, along with the addition of *tubulin* as a non-*Atg* gene control. In line with results obtained for a previous ChIP assay conducted in a WT setting using anti-Sequoia, GFP-Sequoia^{WT} was seen to be enriched at the promotor of all *Atg* genes queried. Consistent with the upregulation of genes observed in the presence of GFP-Sequoia^{LIRm}, the assay detected significantly less enrichment of the mutant on the promotor region of *Atg* genes (Fig. 3.14 A). The only exception to this was seen in the case of *Atg7*, in which there was no significant difference observed in enrichment levels. In fact, the LIR mutant did not demonstrate enrichment at the promotor of *Atg1, Atg8a, Atg13* and *Atg14* when compared to the IgG control. No difference in enrichment was observed in the case of the control gene *tubulin*, strengthening the suggestion that the differences in enrichment are reflective of autophagy specific genes. Further validation of these results could have been obtained by conducting the outlined ChIP experimental in parallel with GFPnls larvae. Pearson's correlation analysis revealed that there was no significant relationship between relative gene expression and promotor enrichment in the LIR mutant (Fig. 3.14 B).

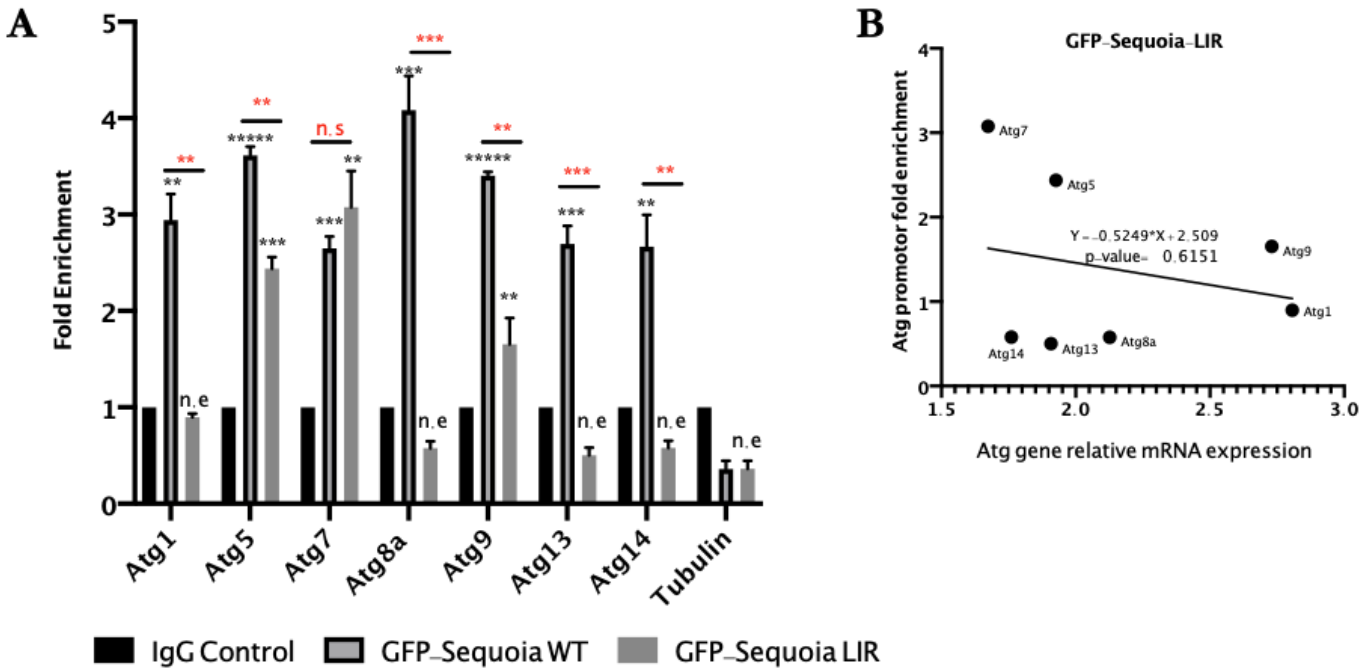

Figure 3.14 Sequoia LIR Mutant is Less Enriched at the Promotor Region of *Atg* Genes.

(A) Analyses of GFP-Sequoia binding to the promoter of autophagy genes in fed conditions, as detected by ChIP (chromatin immunoprecipitation) using a GFP antibody. ChIP DNA values were normalized to input DNA using the $2^{-\Delta\Delta}$ (Ct) method. Fold enrichment values are shown relative to the immunoglobulin G (IgG) control. Tubulin was used as a non-autophagy-related gene control. All data shown as means ± SDs, n = 3 independent experiments. Statistical significance was determined using Student's t test; *p < 0.05 and *****p < 0.00005. n.s= not significant, n.e= not enriched (Red indicated difference between GFP-Sequoia WT and -LIR. (B) Correlation analysis (Pearson's) between GFP-Sequoia LIR mutant promotor enrichment and mRNA expression of *Atg* genes. No significant correlation observed. P= 0.6151. Genotypes: Sequoia WT*: hs::Gal4/UAS-GFP-Sequoia-WT,* Sequoia LIRm: *hs::Gal4/UAS-GFP-Sequoia-LIRm.*

3.6 Identification of Candidate Sequoia DNA Binding Motifs

As Sequoia is a novel transcription factor in the context of autophagy, there is no pre-existing information in regard to its DNA binding motifs. Here, three bioinformatics approaches are utilised in order to predict these regions, based on information available for other similar transcription factors, and through use of *de novo* discovery tools which utilise the sequences of the experimentally confirmed enriched regions.

3.6.1 Predictive analysis based on paralogs of Sequoia

High homology in DNA-binding domains are suggestive that they could bind similar motifs[247]. Therefore, specific analysis of the DNA binding C2H2 domains in Sequoia were conducted in order to identify which transcription factors were convincingly similar, and thus could be used for predictive analysis. The translated protein sequences of both domains (referred to from herein as C_2H_2A and C_2H_2B) were queried by protein sequence similarity analysis against the UniProtJK/Swiss-Prot database, using the Smith-Waterman algorithm[347]. Importantly, the Smith-Waterman algorithm allows identification of maximally homologous sub-sequences among sets of long sequences. This functions through the use of a local sequence alignment which determine regions of similarity between strings of nucleic acids sequences of all possible lengths, thus optimising the measure of similarity. Based on score and percentage identity, C2H2A showed the highest level of similarity to the C2H2 region in Ttk isoform A. C2H2B showed high levels of similarity to both Ttk isoform A and to another *Drosophila* zinc finger transcription factor Btd (Buttonhead) (Fig. 3.15). These were the only two *Drosophila* proteins which were indicated by the search and both showed convincing levels of sequence similarity (Ttk/ C2H2A: 88.9% and Btd/ C2H2B: 85.7%). Given these proteins are both members of the C2H2 zinc finger family of proteins, and that they have high levels of amino acid similarity to Sequoia across their DNA binding domains, it was postulated that the DNA motif recognised and bound by these regions may be similar.

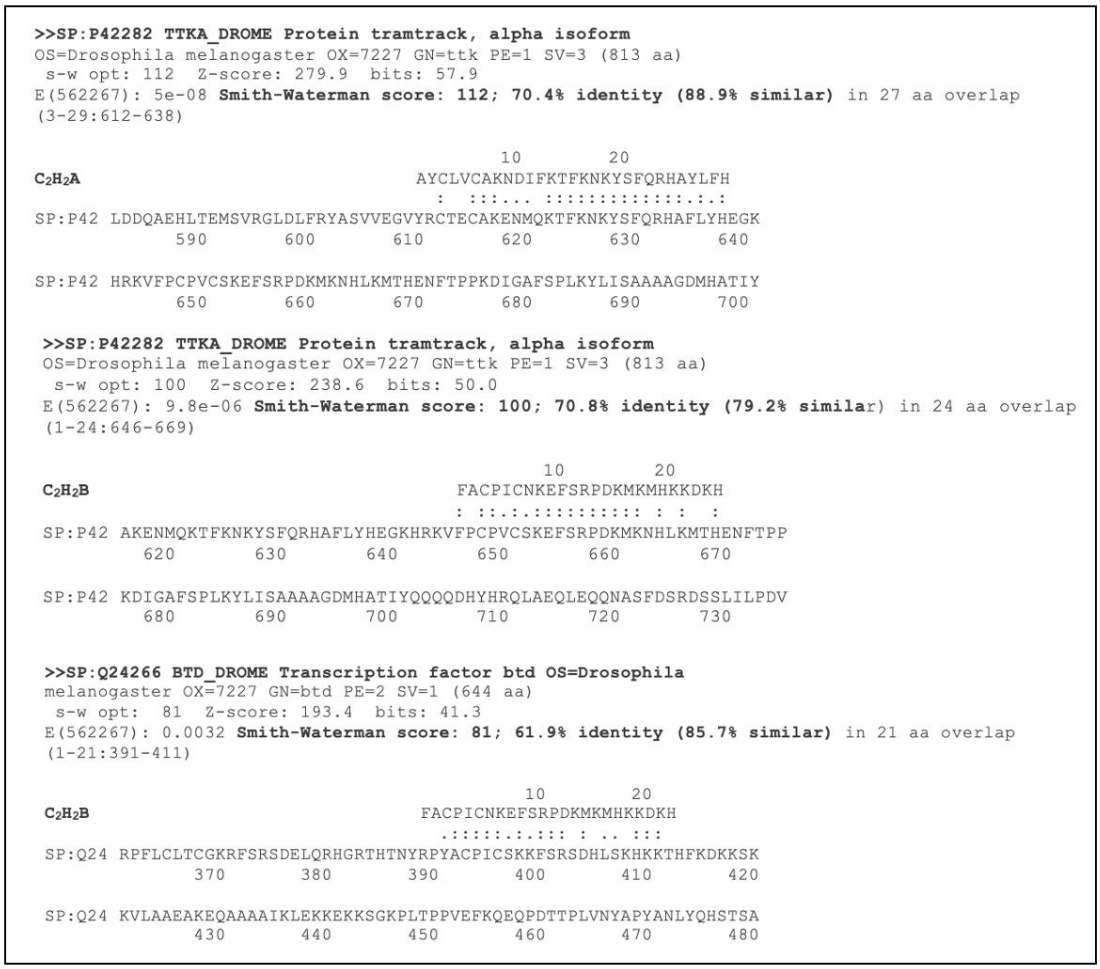

Figure 3.15 Sequence Similarity of Zinc-Finger Binding Domains of Sequoia and its Paralogs.
The translated protein sequences of both C2H2 domains in Sequoia (C_2H_2A and C_2H_2B) were queried by protein sequence similarity analysis against the UniProtJK/Swiss-Prot database, using the Smith-Waterman algorithm. This revealed similarity of C2H2A (Smith-Waterman Score- 112, 70.4% identity) and C2H2B (100, 70. 8% identity) to a C2H2 region in Tramtrack and C2H2B to a C2H2 region in Buttonhead (81, 61.9% identity).

JASPAR is a collection of transcription factor DNA-binding preferences, modelled as matrices. These can be converted into a PSSM and used for scanning genomic sequences. It represents the only database with this scope where the data can be used with no restrictions. To characterise the binding preference of a transcription factor, the aligned sequences bound by the transcription factor are aggregated into a PFM, which are stored and easily accessible in the JASPAR database. PFMs can be used to derive two matrices: PWM, which are most commonly used kind of PSSM and ICM. The former allows you to scan a query nucleotide sequence with a pattern that is represented in a single or multiple PWMs, and the latter allows production of a

visual representation of the nucleotide sequence, based on the probability of getting each nucleotide in a certain position.

A search of the JASPAR 2018 database revealed that the collection includes PFMs for 158 known *Drosophila* (species ID: 7227) transcription factor DNA binding regions. To further narrow the search, the 'class' category was filtered to those defined as 'C_2H_2 zinc finger factors.' This revealed the presence of 27 transcriptional binding domains, including that of Ttk isoform A (Matrix ID: MA0460.1) and Btd (MA0443.1). The PFM-converted PWMs of the two transcription factors were subsequently used to search for putative binding sites in the promotor region of *Atg* genes; this is achieved by 'scanning' the string of nucleotides (corresponding to the promotor) with the pattern represented in the PWMs, and assigning a score of based on sequence similarity. It must be noted here that the usage of PWMs needs as a prerequisite, the knowledge of the statistical significance of a 'hit' according to its score. This is done by defining the P-value of a score, which is the probability that the background model can achieve a score larger than or equal to the observed value. Here, empirical p-values for match scores were calculated through the use of TFM-Pvalue[386]; an algorithm capable of finding exact P-values efficiently for any score, even for matrices with non-integer coefficient values. This number of 'hits' with the best score-converted P-values (cut-off < 0.01) is shown in Table 3.1 for each the *Atg* genes on which Sequoia showed enrichment experimentally. The promotor of the *Atg* genes which showed upregulation in *sequoia*-depleted cells, but had not been included in the ChIP assay, were also queried. Of these, *Atg4a/b*, *Atg18a*, *Mitf* and *Tor* were all indicated to contain the binding motif. The exact positions relative to the transcription start site are indicated in the brackets. All of the experimentally confirmed enriched promotor regions showed binding to a sequential pattern indicated in at least one of the two matrices. *Rpl30* was used as a control for active transcription, with binding regions across both matrices confirmed. Conversion of PWMs to ICMs generated a visual representation of the matrices, where each position gives the information content obtained for each nucleotide (Fig. 3.16). Thus, the larger the letter of a corresponding nucleotide, the larger the information content and the higher the probability of getting that nucleotide at the position indicated.

Table 3.1 Transcription Factor DNA Binding Regions in *Atg* Genes.

Number of nucleotide sequence matches found in the promotor region of *Atg* genes when searched with the binding region matrix of *Drosophila* transcription factors Ttk (MA0460.1) and Btd (MA0443.1). Matrices were sourced from the JASPAR 2018 insect database, and *Atg* promotor regions were scanned using the "Motif Search Tool" function on the Eukaryotic Promotor database (EPD. A p-value cut-off was set at <0.01. The position of the binding site(s) within the promotor is shown in brackets. Bold genes represent those which Sequoia have confirmed to bind to experimentally. Rpl30 was used as a control of active transcription.

Candidate Binding motif (matrix ID)		
Gene Name	MA0460.1	MA0443.1
Atg1	0	1 (45)
Atg4a/b	3 (14,32,58)	0
Atg5	2 (62, 93)	1 (19)
Atg7	0	1 (139)
Atg8a	0	1(41)
Atg9	2 (33,64)	1 (4)
Atg13	0	1(100)
Atg14	1(12)	0
Atg18a	3 (36, 63, 88)	1(8)
Mitf	2 (73,84)	0
Tor	1(58)	0
Rpl30	1(59)	2 (49,29)

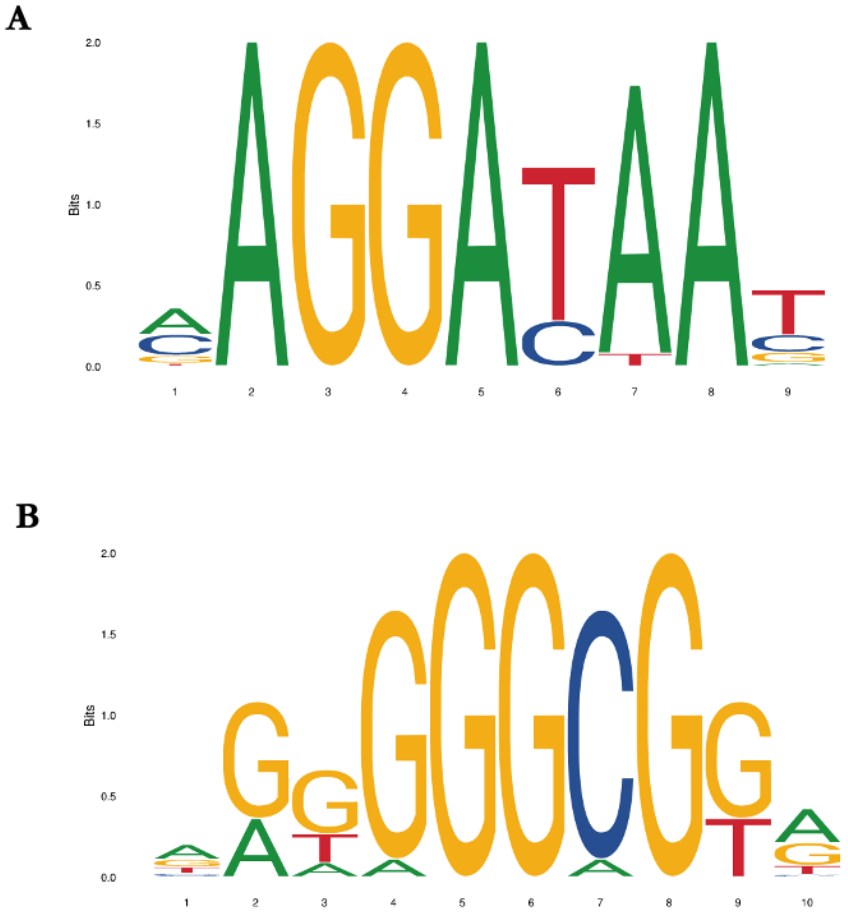

Figure 3.16 Visual Representation of *Drosophila* Transcription Factor DNA Binding Matrices.
Visual representation of nucleotide bases presence in the binding region matrices of Ttk: MA0460.1 (A) and Btd: MA0443.1 (B): Each position gives the information content obtained for each nucleotide. The larger the letter of a corresponding nucleotide, the larger the information content and the higher the probability of getting that nucleotide at the position indicated.

3.6.2 *De novo* motif discovery

MEME is a tool which allows for discovery of novel, un-gapped motifs, for both fixed and re-occurring patterns[349]. The motifs are represented as position-dependent letter-probability matrices, which describe the probability of each possible letter at each position in the pattern. Each motif generated by MEME does not contain gaps, therefore patterns with variable-length gaps are split into two or more separate motifs. MEME usually finds the most statistically significant (low E-value) motifs first. The E-value of a motif is based on its log likelihood ratio, width, sites, the background letter frequencies, and the size of the set of training sequences given

to predict the motif. It functions to give an estimate of the expected number of motifs with the given log likelihood ratio (or higher), and with the same width and site count, that one would find in a similarly sized set of random sequences.

In order to generate candidate binding motifs for Sequoia, the nucleic acid sequence of the bound *Atg* genes promotor regions were queried via the MEME tool. Two candidate motifs were generated, illustrated in Figure 3.17 A-B (referred to hereafter as Motif 1 and 2), along with their location on either the 5' (+) or 3' (-) strand. The position *p*-value is assigned to each individual motif located in each sequence. It is defined as the probability that a random sequence (with the same length and conforming to the background) would have a match to the motif under test with a score greater or equal to the largest found in the sequence under test. The combined match *p*-value (shown in Fig. 3.17 A) denotes the probability that a random sequence (with the same length and conforming to the background) would have position *p*-values such that the product is smaller or equal to the value calculated for the sequence under test. Here, all generated *p*-values show a very convincing level of confidence ($p<0.0001$). The E-value assigned to each motifs is defined as the expected number of sequences in a random database of the same size that would match the motifs as well as the sequence does (this is equal to the combined p-value of the sequence times the number of sequences in the database). Therefore, the motif E-value is a fairly conservative estimate of how likely it is that the motif is not just a statistical artefact; based on Motif 1 shows the highest level of confidence (E=0.02) (Fig. 3.17 B).

Additional analyses were carried out on the discovered motifs in order to better characterise them and assess their credentials as candidate DNA binding motifs recognised by Sequoia. GOMo is a tool that scans all promoters using an input nucleotide motif to determine if any motif is significantly associated with genes linked to one or more GO[349]. The significant GO terms associated with the candidate motifs searched against the promotors (-1000, +200bp relative to the TSS (Transcription Start Site)) of *Drosophila* genes are shown in Figure 3.17 C. The terms identified for Motif 1 are particularly interesting as they hint at a specific binding site which matches the known functions of Sequoia, including BP (Biological Process) terms for imaginal disc morphogenesis and neuron projection morphogenesis. In addition to this another BP term indicates a role in negative transcription. Interestingly, both the nucleosome and the nucleus CC (Cellular Compartment) associated terms were identified in relation to Motif 2, along with the MF (Molecular Function) term DNA binding. The MF zinc-ion binding was also associated to Motif 2 (outside of the top 5 enrichment terms); which gives an indication that

perhaps this region mediates an interaction with the C_2H_2 region Sequoia. However, it has been reported such regions aren't strictly necessary in order to form an interaction with C_2H_2 regions, as many zinc-finger family members function independently of such sites[387].

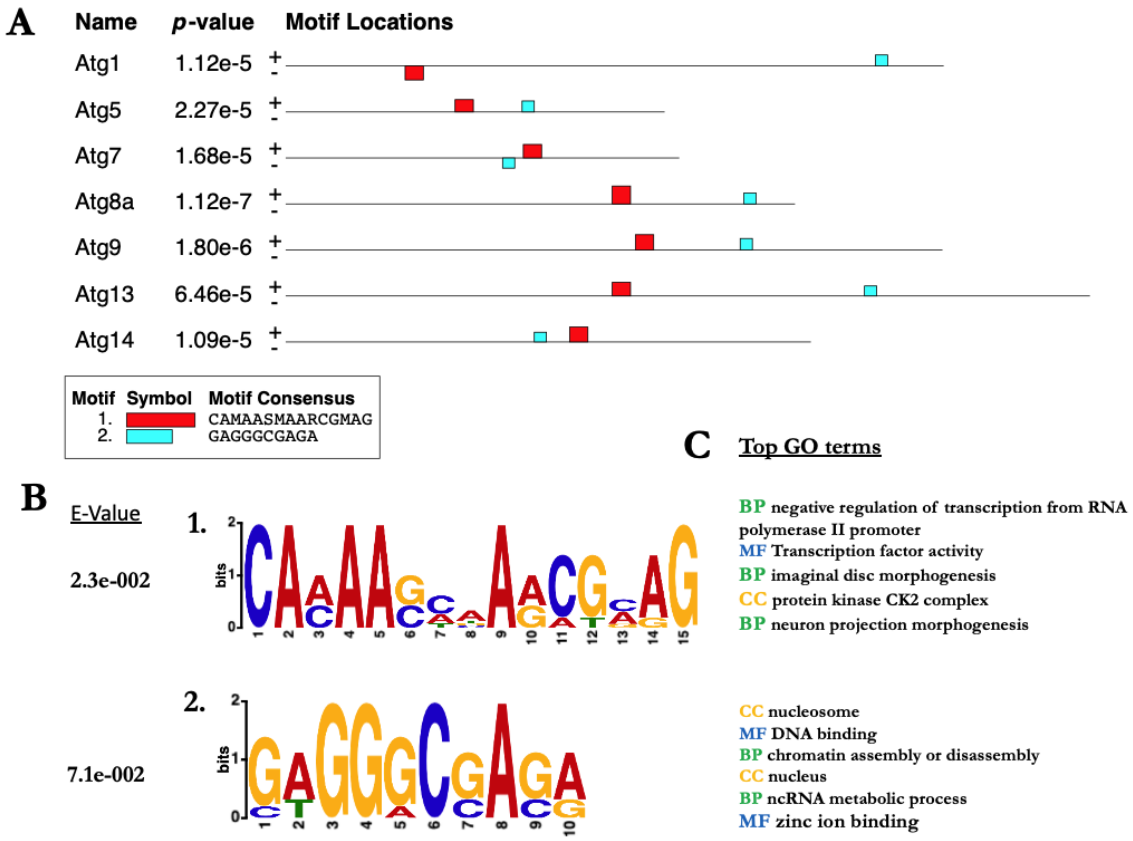

Figure 3.17 *De novo* Motif Discovery for Sequoia DNA Binding Region.

MEME was used to conduct sequence analysis of experimentally confirmed promotor regions, in order to predict an un-gapped candidate binding motif for Sequoia. (A) Two candidate motifs were generated (1 and 2) with the p-value and location (+/- strand) shown. For all p<0.0001. (B) A visual representation of the nucleotides contained with the motifs matrices are shown, with the corresponding E-Value. (C) Top five Gene Ontology hits determined by GOMo. Significant GO terms are associated to the candidate motifs 1 and 2 searched against the promotors (-1000, +200bp relative to the TSS) of *Drosophila* genes.

Interestingly comparative analysis of Motif 2 revealed high levels of matrix similarity to MA0443.1 (Btd), (p-value= 5.16e-03) when compared against the JASPER insect database, however given Motif 1 produced an E value > 0.05, it cannot be considered a reliable candidate motif. Interestingly, Motif 1 showed the highest level of similarity to another *Drosophila* zinc-

finger family transcription factor called br(var.3) (p-value= 6.36e-03, Matrix ID: MA0012.1). No similarity was found to the binding motif of Ttk however.

Some bio-sequence motifs exhibit mutations, insertions and deletions, however the MEME tool cannot discover such motifs, because it is strictly used for un-gapped discovery. To overcome this limitation, the GLAM2[350] software was used to verify motif discovery. This tool reports a score for each motif that it discovers, with higher scores indicating stronger motifs. GLAM2's formula for assigning scores to alignments is a generalization of the formula used by previous Gibbs samplers for alignments without indels[350,388,389]. Discovering gapped motifs is intrinsically more difficult than discovering un-gapped motifs, because there are vastly more possible gapped motifs than un-gapped motifs; therefore, it is recommended to perform both gapped and un-gapped analysis in conjugation to complement one another. Another further strength of using GLAM2 is its ability to perform replicates in an attempt to discover the strongest possible motif 10 times, displaying the results in order of score. Thus, the top few results being similar, is indicative of successful replication. Submission of target *Atg* promotor region sequences into the GLAM2 tool revealed the discovery of the gapped motif shown in Figure 3.18. Of the 10 replicates carried out by the algorithm, 8 revealed to be identical with a score of 76.0942. Of particular interest GO term search revealed MF and BP terms associated with the gapped motif to be indicative of a possible role in transcriptional activity and DNA-dependant regulation of transcription.

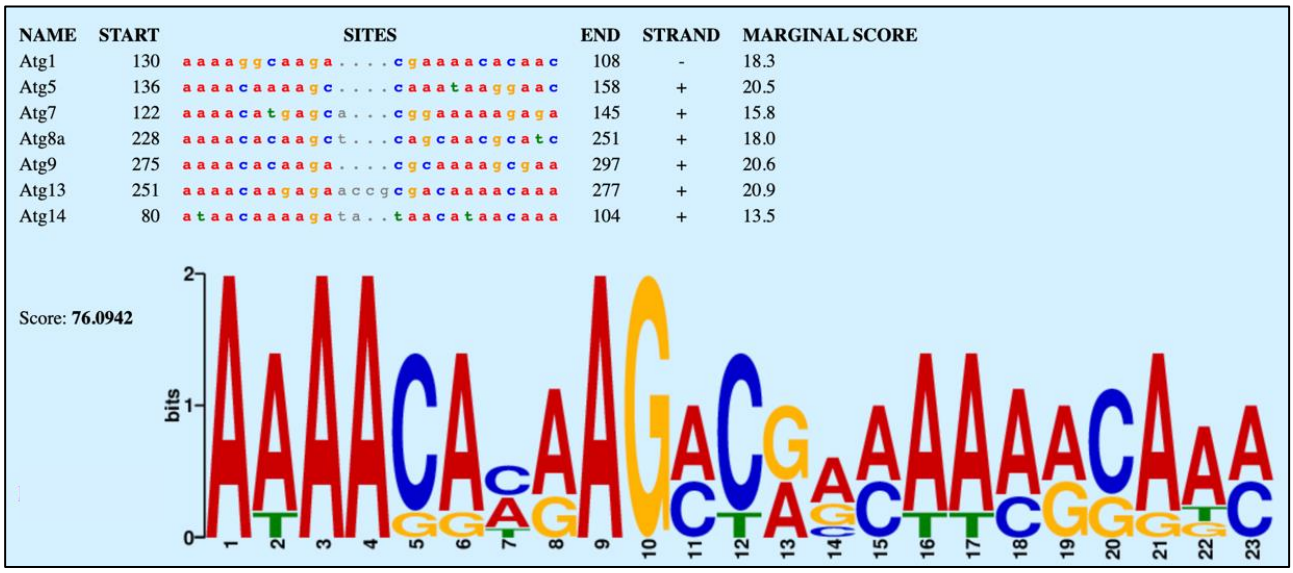

Figure 3.18 *De novo* Motif Discovery Using an Un-gapped Method.

GLAM2 was used to conduct sequence analysis of experimentally confirmed promotor regions, in order to predict a gapped candidate binding motif for Sequoia. The output motif consists of aligned columns (coloured letters) and insertions (grey letters). The aligned columns may include deletions (grey dots). GLAM2 does not try to align inserted (grey) letters with one another: it assumes their identity is unimportant. "Marginal scores" are assigned to each site, with higher scores indicating better matches to the motif. The output motif shown was generated after 10 rounds of alignment, with the motif shown here generated in 8 of 10 replicates, with a score of 76.0942.

3.6.3 The use of a Transcription Factor Flexible Model

All of the previous methods utilised in this analysis have been based on PWMs. Such models however make strong assumptions that each nucleotide pair participates independently in the corresponding DNA-transcription factor interaction. To account for this, a TFFM has been established based on hidden Markov models[351]. The graphical representation of a TFFM takes into account nucleotide interdependence and variable motif length. Here, results from TFFM *Atg* target promotor analysis are shown in Figure 3.19, where opacity of the nucleotide base is proportional to the probability of possible row to be used by the method. The method also generates an IC (Information Content), which quantifies the sensitivity of transcription factor binding affinity to the binding site sequence from the consensus sequence, whilst taking into consideration the probability of a site occurring in a random stretch of DNA[390]. For Eukaryotes, an average of 12.1 is considered a reliable IC value[391]. Here, the motif has an IC score of 12.33 and can therefore be considered a reliable candidate binding motif for Sequoia.

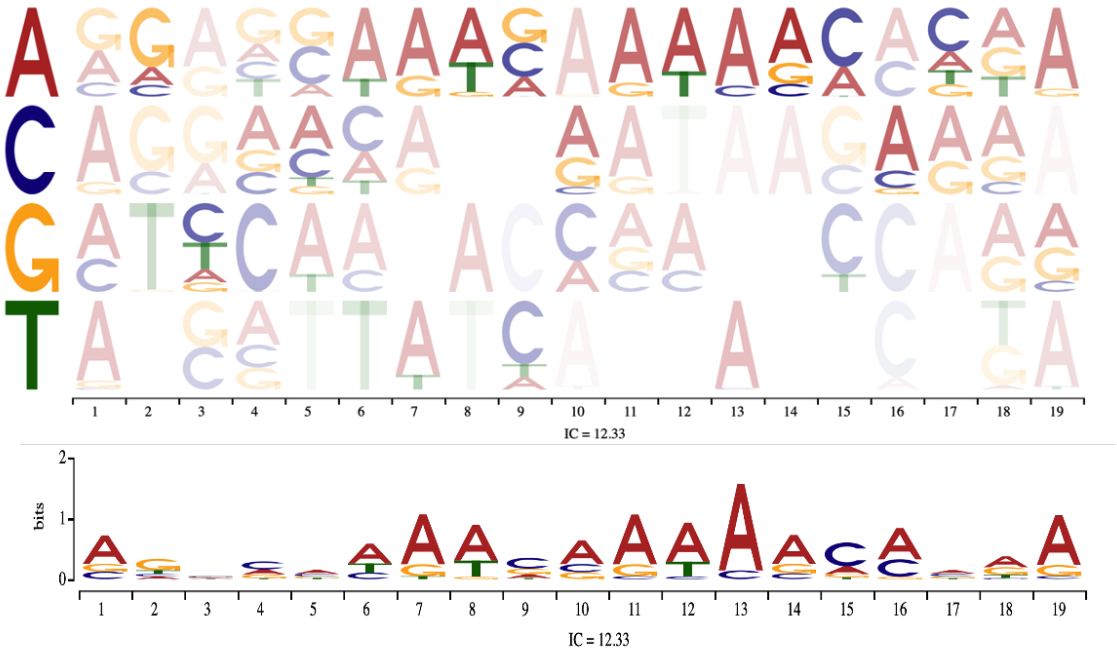

Figure 3.19 Using a Transcriptional Factor Flexible Model to Predict a Sequoia DNA Binding Consensus.

The opacity of the nucleotide base is proportional to the probability of possible row to be used by the TTFM. Nucleotide probabilities at position p for each possible nucleotide at position p – 1 are represented. The intersection between a column corresponding to position p and row corresponding to nucleotide n gives the probabilities of getting each nucleotide at position p if n has been seen at position p -1. A summary of the motif is shown in the lower image. The Information content (IC) score = 12.33 (Average for eukaryotes =12.1).

3.6.4 The search for a Sequoia binding motif

In this section a number of available bioinformatics tools were utilised in order to predict a consensus DNA motif in *Atg* genes bound by Sequoia. Firstly, the method of utilising the binding sites of characterised paralogs, Btd and Ttk, based on their similarity in DNA binding domains, was utilised. Given the availability of *de novo* bioinformatics tools, which allow for far more tailored modes of motif discovery, this method can be deemed insufficient. Although, *de novo* un-gapped motif discovery did reveal a high degree of similarity between a novel motif (Motif 1 Fig. 3.17 B) and that of Btd (Fig. 3.16 B), the generated E value (0.07) for Motif 1 did not reflect a high degree of confidence.

It must be emphasised that a limitation of this analysis was the availability of only 7 target sequences to train the algorithm for discovery. However, high confidence levels in the motif generated by un-gapped de novo discovery (Fig. 3.18) and the TFFM method (Fig. 3.19) are indicative that the consensus motif of Sequoia is likely to be contained within these predictive sequences. Future work with Sequoia and its activity as an autophagy related transcription factor would provide far more stringent analysis of this region; allowing for a much more concise motif to be established. This is an exciting prospect which could be guided by generating Sequoia binding mutants (based bioinformatics predicted binding sites) and testing the ability of these mutants to regulate the expression of the *Atg* genes investigated in this study. It must be noted that RPH1 has multiple binding consensus sites, which have been identified in the promotors of *Atg* genes[247], therefore it is also likely that multiple regions to which Sequoia binds preferentially exist.

3.7 End of chapter conclusions

In collaboration with Professor Terje Johansen, we have shown here that Sequoia has a previously undescribed xLIR motif, which is essential in mediating its interaction with Atg8a. We show that mutation within the aromatic [W/F/Y] and the aliphatic [L/I/V] residues of the Sequoia LIR motif (Y313A, I316A) reduce its interaction with Atg8a; to a degree which is reciprocated by mutations in the previously characterised Atg8a LDS mutant (K48A, Y49A). Given that LIR binding to mammalian LC3 is seen to be significantly altered by substitutions within the aliphatic and aromatic amino acid residues of the motif[370], findings here further exemplify the nature of the LIR motif by confirming that these residues are integral to the binding functionalities of the motif across species.

Upon first discovery of Sequoia, the structural presence of a C2H2 zinc finger DNA binding domain pointed to its potential role in transcriptional regulation. This was confirmed when it was observed to bind to the promoter regions of *Atg* genes in fed conditions, thereby reducing their transcription (Fig. 3.12). This was exemplified by an observed induction in the expression of *Atg* genes in *sequoia*-depleted larvae (Fig. 3.10), along with the accumulation of mCherry-Atg8a puncta in the cytoplasm, under fed conditions (Fig. 3.8 and 3.9). This remarkably revealed the potential of Sequoia in modulating the expression of genes involved across all stages of the autophagy induction cascade, including: *Atg1, Atg4a, Atg4b, Atg5, Atg7, Atg8a, Atg9, Atg10. Atg13, Atg14, Atg18a and Atg101*. Results here draw comparisons with the transcriptional ability

of Rph1 and KDM4 in yeast and mammals[247], respectively, suggesting an evolutionarily conserved role for the zinc-finger containing transcription factors in autophagy.

CHAPTER 4. THE ROLE OF ACETYLATION AND NUCLEAR ATG8A IN THE INDUCTION OF AUTOPHAGY

4.1 An Introduction to YL-1 and Sir2

With a transcriptional role of Sequoia outlined in the previous chapter, work here sets out to establish the potential role of two other Atg8a-interactors, which may play a role in mediating the regulating the acetylation status of Atg8a. The sections below outline how these Atg8a-interactors where identified and why they are of interest to study.

4.1.1 YL-1

Accumulating evidence exists that links the induction of autophagy to the acetylation status of regulatory proteins, with a number of regulatory roles have been reported in the event of acetylation (Table 1.3). For example, mammalian KAT5/TIP60, the catalytic subunit of the NuA4 complex, has been observed to directly acetylate and stimulate the protein kinase ULK1, thereby linking protein acetylation to the induction of autophagy in nutrient deplete conditions[294]. Furthermore, the yeast ortholog of Tip60, Esa1, has been shown to promote autophagy through the acetylation of Atg3 at regions K19 and K48, thereby allowing Atg3 to interact with Atg8, and to catalyse its lipidation[299]. In order to explore the potential regulation of nuclear Atg8a by acetylation, the Nezis lab conducted a bioinformatics screening using PAIL (Predictive of Acetylation on Internal Lysines). This identified YL-1 (CG4621) as a candidate protein which could regulate the acetylation of Atg8a. The iLIR tool predicted YL-1 to have a LIR-motif at position 246-251. It must be noted that this screen was conducted independently of the UBD driven screen, which was responsible for identifying Sequoia.

YL-1 belongs to the multi-subunit chromatin-remodelling complexes called SWR1 in yeast and the related SRCAP and NuA4/Tip60 complexes in mammals; all of which shown to control histone acetylation[316,323–326]. The NuA4/Tip60 histone acetyltransferase complex functions to acetylate four conserved internal lysine regions of histone H4 N-terminal tail and acetylate histone H2A[392]. Higher eukaryotes express YL1, a highly conserved Swc2 homolog, which also has specific H2A.Z-binding properties. In *Drosophila*, the crystal structure of the histone binding

domain in YL-1 shows a whip-like architecture which allows it to wrap over H2A.Z -H2B[326]. *Drosophila* Tip60 has been identified to have acetyltransferase activity, whereas the YL-1 subunit has a regulatory role[316]. Given as its residency in the acetyltransferase complex, it was predicted that an interaction between YL-1 and Atg8a may function to regulate the acetylation status of Atg8a.

Following on from this, work conducted the lab of Terje Johansen showed that *in vitro* translated YL-1 (^{35}S-Myc-YL1) bound very strongly to the N-terminal half (amino acid residues 1-71) of recombinant GST-Atg8a (Appendix paper A, Fig. 4 A-B)[376]. Interestingly, mutation of either the LDS of Atg8a, or the predictive putative LIR motifs of YL-1 did not abrogate significantly the *in vitro* interaction between Atg8a and YL-1, suggesting that this interaction is likely to be LIR-motif independent. Although it cannot be ruled out that there is an unidentified LIR motif which may be involved in this interaction.

4.1.2 Sir2

During nutrient deprivation deacetylation reactions are orchestrated by a unique family of sirtuins. Sirtuins have been shown to play a role in lipid metabolism and insulin resistance[393–395]. They were first linked to the regulation of life span, with their overexpression in the *Drosophila* homolog, Sir2, shown to extend life expectancy under caloric restrictions[307]. This apparent role in nutrient adaptation led to exploration of the link between sirtuin activity and the induction of autophagy. The mammalian homolog, SIRT1, has been reported to directly deacetylate autophagy machinery components in response to starvation[290]. Further to this, it has been reported that deacetylation of LC3 by SIRT1 occurs at sites K49 and K51, and is required for it to be exported out of the nucleus during the induction of autophagy[158].

Based on previous literature, the potential of Sir2 to govern Atg8a was explored. An interaction between the two proteins was investigated via GST- pulldown by Dr. Anne-Claire Jacomin, Nezis lab. Sir2 shown to directly interact with Atg8a. Furthermore, preferential binding was observed in starvation conditions, and to deacetylated Atg8a (Appendix paper A: Fig.4 H-K)[376]. These results suggested that Sir2 may function to deacetylate Atg8a in starvation conditions.

4.1.3 Chapter Aims

- To investigate the acetylation status of Atg8a in fed and starved conditions
- To interpret structural modelling of LC3 LIR binding to predict how acetylation could modulate the binding of Atg8a-Sequoia in fed and starved conditions.
- To determine the localisation of YL-1 and Sir2 in the context of starvation induced autophagy (in fed and starved conditions).
- To assess the impact on Atg8a acetylation status when YL-1 is silenced via RNAi, and Sir2 is overexpressed.
- To assess the roles of YL-1 and Sir2 in regulating the acetylation status of Atg8a in the induction of starvation induced autophagy.
- To explore the role of nuclear Atg8a in the transcriptional regulation of autophagy.

4.2 Atg8a is Acetylated in Nutrient Rich Conditions

Firstly, the acetylation status of Atg8a in nutrient rich versus starvation conditions was investigated. In mammalian cells LC3 is acetylated and deacetylated at regions with constitute the proteins hydrophobic pockets (K49 and K51)[158]. Given this, it was predicted that residues within the hydrophobic pocket of the *Drosophila* homolog Atg8a (peptide IGDLD**KKK**): K46, K47 and K48 were strong candidate residues for acetylation in nutrient rich conditions and subsequent deacetylation in starvation conditions.

Using mass spectrometry, acetylation sites within the Atg8a protein were explored in larvae expressing GFP-Atg8a, in fed and starved conditions. Firstly, in order to confirm the cellular residency of Atg8a in each setting, *CgGAL4; UAS-GFP-Atg8a* larvae were assessed using immunofluorescent staining in order to visualise the expression of GFP-Atg8a in the larval fat body. Images showed a pattern consistent with the previously used autophagy marker mCherry-Atg8a; with GFP-Atg8a nuclear in fed conditions (Fig. 4.1 A), and the presence of bright GFP-Atg8a positive puncta in the cytoplasm indicative of the formation of autophagic structures in starvation conditions (Fig. 4.1 B).

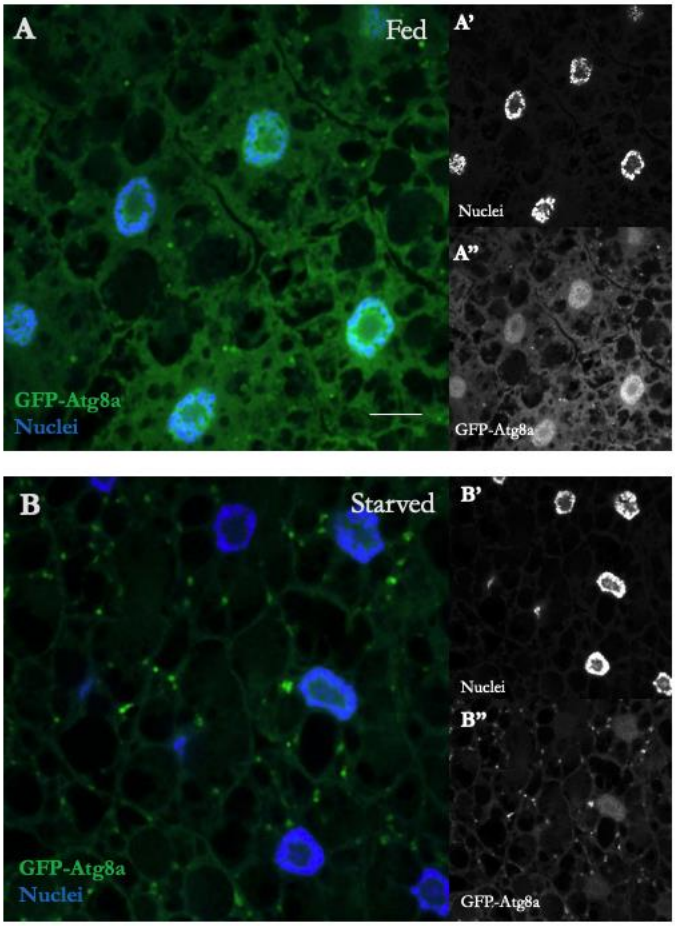

Figure 4.1 The Cellular Localization of GFP-Atg8a in the Induction of Autophagy.

(A-B) Confocal sections of third instar stage larval fat bodies clonally expressing the autophagy marker GFP-Atg8a (green) in fed (A) or starved conditions (4h, 20% sucrose) (B). Fixed fat bodies where stained for nuclei with Hoechst (blue). Scale bar: 10 μm. Genotype: *CgGAL4; UAS-GFP-Atg8a.*

LC-MS/MS was used to identify Atg8a (peptide IGDLDKKK) in fed and starved larvae. Following protein extraction from third instar stage larvae, IP of GFP-Atg8a was performed. This was proceeded by peptide extraction via SDS-PAGE, with in-gel digestion carried out using sequence grade modified trypsin. This could be used to investigate acetylation of Atg8a in fed and starved conditions as trypsin is a protease which does not cleave at an acetylated lysines. Tryptic peptides were specified with two missed cleavages and a mixed modification of carbamidoethylation on Cysteine residues, variable oxidation on Methionine (which can arise during sample preparation), and acetylation on Lysine residues (+42.010 Da). The spectra shown in Figure 4.2 represent a pattern of distribution of ionized peptides by mass-to-charge ratio (m/z) within fed (479.8 m/z) and starved (458.78 m/z) samples. The difference in mass between

peptide fragments sharing either a common N- or C-terminus essentially corresponds to the residue mass of a single additional amino acid between the fragments. Here, the difference cannot be accounted for by the residue mass of lysine alone but rather by the mass of lysine plus a nominal mass shift of 42.010 Da. Therefore the possibility of an acetylated rather than unmodified lysine being present in the peptide fragment from nutrient rich conditions is likely. The lysine referred to in Figure 4.2 is at position 46 (K46).

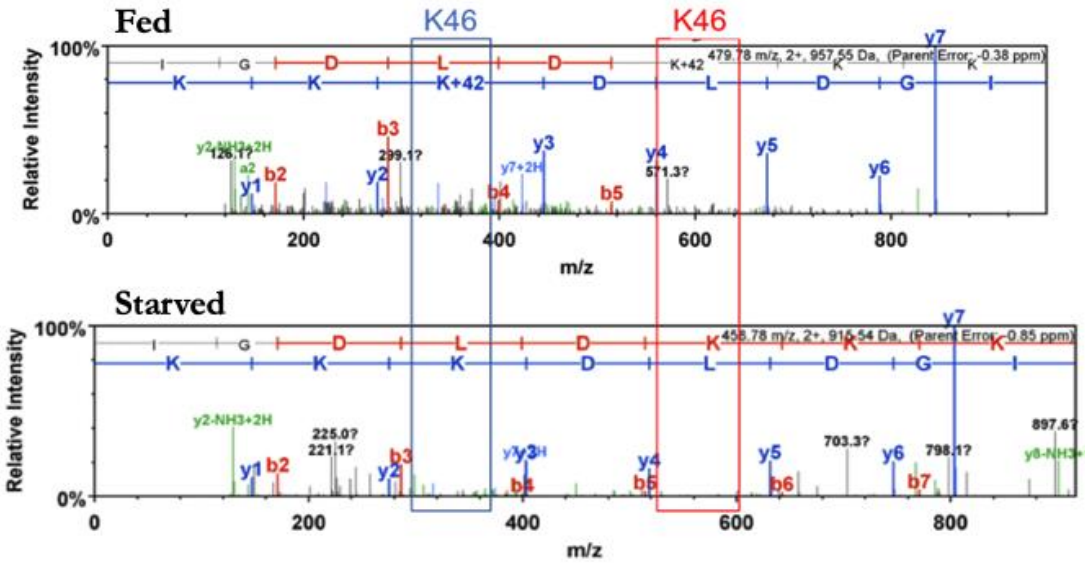

Figure 4.2 Atg8a is Acetylated at K46 in Fed Conditions.

Protein was extracted from third instar stage GFP-Atg8a larvae; immunoprecipitation was performed using anti-GFP, followed by peptide extraction via SDS-PAGE. LC-MS/MS was conducting revealing the presence of the peptide IGDLDKKK (Atg8a) in fed (top panel) and starved conditions (bottom panel). A mass-to-charge ratio value of 479.89 m/z is recorded in fed conditions, with the mass shift of +42 at position K46, consistent with an acetyl moiety (42.010 Da). Peptide identifications were accepted if they could be established at greater than 95.0% probability by the Scaffold Local FDR algorithm.

4.3 The Role of Acetylation in the Interaction Between Atg8a and Sequoia

Work conducted by the Johansen lab proceeded to explore whether the interaction between Atg8a and Sequoia is regulated by the acetylation status of Atg8a. To test this, the binding of WT and acetylation mimic forms of Atg8a to Sequoia was investigated via GST-pulldown. Acetylation mimic mutants constitute versions of Atg8a in which the lysine at residue K46, K48 and K49 have been replaced with glutamine, thereby mimicking the acetylated variant of Atg8a

(K46Q. K48Q and K49Q). Importantly, these mimic of LC3 have been confirmed to have similar nuclear and cytoplasmic distribution to their wild-type cpunterparts[158]. However, they are unable to form cytoplasmic puncta upon cellular starvation, thus hinting that deacetylation of these regions is an essential requirement for LC3 accumulation on autophagic membranes. Interestingly, the GST-pulldown conducted by the Johansen lab revealed that K46Q and K47Q have no significant effect on binding to Sequoia, but that K48Q acetylation mimic significantly reduces binding to Sequoia.

In order to validate the effects of the acetylation mimics, it would have been interesting to test the interaction of Sequoia to an Atg8a mutant in which a neutral residue had been mutated, and also to an Atg8a triple mutant at positions K46-K47-K46.

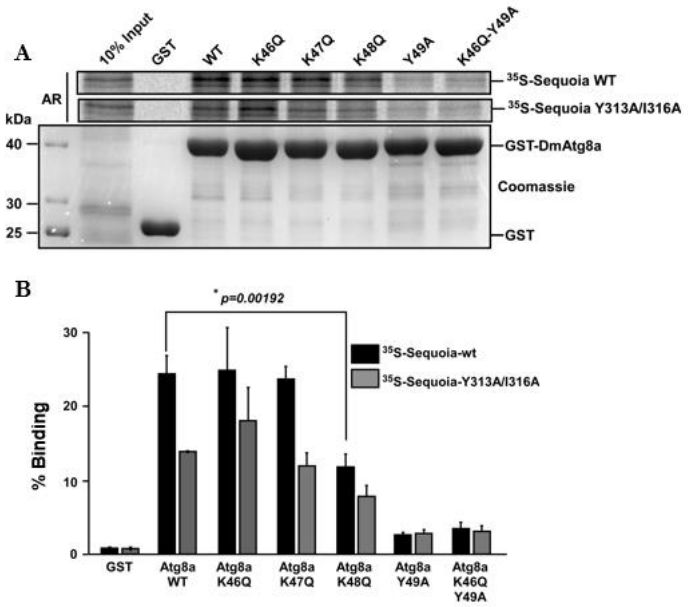

Figure 4.3 Acetylation Mimic Atg8a K48Q Exhibits Reduced Binding to Sequoia *in vitro.*

GST-pull-down assay between GST-tagged Atg8a-WT; the acetylation mutants K46Q, K47Q, and K48Q; the LDS mutant (Y49A); and radiolabelled ^{35}S-labeled Sequoia-WT or 35S-labeled Sequoia-LIR mutant. (M) Quantifications of the binding of radiolabelled Sequoia-WT or LIR mutant (Y313A/I316A) to GST-ATG8a-WT or the respective mutants represented as percentage binding relative to 10% of the input. The bars represent the mean values with +SD from 3 independent experiments. The statistical significance of the Sequoia binding with Atg8a-WT compared to its mutation K48Q was determined with Student's t test; p = 0.00192. All other values were shown to be statistically insignificant. Work conducted by Dr. Ashish Jain (Johansen lab, University of Tromsø).

Despite these observations, it was not possible to detect the acetylation at K48 with mass spectrometry. It is speculated that *Drosophila* Atg8a is also acetylated at K48 and that this was not possible to detect experimentally due to the possible highly sensitive nature of larvae tissue. Given this, it is speculated that acetylation of this region may be lost following sample preparation and analysis via mass spectrometry. In attempts to try and detect acetylation at region K48, the protocol was adapted through the implementation of deacetylation inhibitors to both the fly food and experimental buffers. This aimed to prevent any loss of acetylation which may occur during the sample preparation stage, however despite multiple rounds of experimentation, with a range of inhibitor concentrations, no acetylation of this region was detected.

4.3.1 A structural model for Atg8a binding Sequoia

To further examine the effect of K48 acetylation on binding to Sequoia, a homology model of the LIR peptide of Sequoia binding to *Drosophila* Atg8a was created, in collaboration with Prof. Alex Cameron, University of Warwick. The model was derived from the structure of GABARAP- L1 ATG4B LIR complex (PDB: 5LXI) (Fig. 4.4). Using homology mapping the electrostatic surface associated with the acetylated protein were calculated with a methionine as a mimic of the acetylated K48.

During LIR governed interactions, the two hydrophobic pockets, formed by the Ubl fold of LC3/Atg8, bind to the aromatic [W/F/Y] and the hydrophobic [L/I/V] residues in the LIR motif [208]. Based on the model, the residues Y313 and I316 of the LIR peptide of Sequoia are likely to bind HP1 and HP2 of Atg8a, respectively. The negatively charged glutamates (E) will likely interact with the positively charged K residues of the 44-LDKKKYLVP-52 motif (shown as a green backbone under the surface (Fig 4.4)). It is well reported that acetylation of K residues is a process that leads to neutralization of the position's positive electrostatic charge[396]. Since the interaction is largely ionic in nature, this modification may well weaken the interaction in question and alter the conformation of complex. Here, upon acetylation of Atg8a, the K48 residue is likely to become bulkier as a result of the acetyl group modification (as seen by the structural protrusion (Fig. 4.4)), resulting in the loss of its positive charge. It is predicted that as a result of this, the potential salt-bridge interaction between K48 and E309 will be disrupted by acetylation, thus weakening the interaction between Atg8a and Sequoia. However, it is unlikely that acetylation would not prevent binding due to steric hindrance. These data suggest that starvation reduces acetylation of Atg8a and therefore enhances its binding to Sequoia. To

confirm this experimentally, the binding of Atg8a and Sequoia could be tested in both fed and starvation conditions.

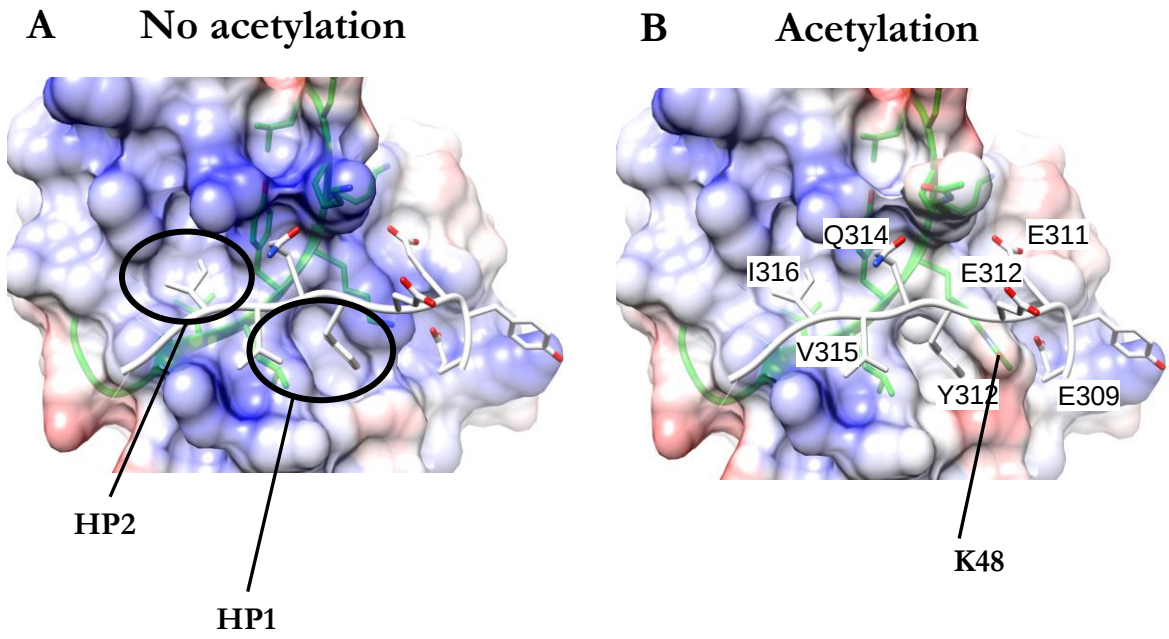

Figure 4.4 Homology Model of Atg8a Binding Sequoia.

Homology model of a peptide of Sequoia binding to *Drosophila* Atg8a LIR complex in starved (A) and fed (B) conditions. Atg8a is represented by a semi-transparent surface coloured according to electrostatic charge; where blue is positive, white is neutral and red is negative. HP1 and HP2 represent hydrophobic pockets. The grey peptide back-bone structure is representative of the Sequoia LIR peptide. Essentially all residues in the structure were mutated to the correct sequence, with the structures and electrostatic surfaces were displayed in PyMol. Modelling conducted by Prof. Alex Cameron, University of Warwick.

4.4 Investigating the Role of YL-1 and Sir2 on the Acetylation Status of Atg8a and the Induction of Autophagy

4.4.1 GFP-YL-1 expressed in *Drosophila*

Following the confirmation of an interaction between YL-1 and Atg8a (Appendix paper A, Fig. 4 A-B)[376], five transgenic lines expressing *UAS-GFP-YL-1* were previously generated by random P-element insertion, in order to observe the localisation of YL-1 *in vivo*. The following

experiments were conducted in order to assess the localisation of YL-1 in the context of starvation induced autophagy.

4.4.1.1 Transgenic line screening

All five lines were screened in order to select which displayed the best expression of GFP-YL-1. To do this, males from the transgenic lines were crossed with virgin females, carrying an insertion for the heat-induced 'flpout' system (FLP-out empty). As the ectopic overexpression of GFP-YL-1 was unknown in regard to how it may affect fly physiology or viability, the mosaic expression system was used in order to express the transgene in only a small proportion of cells in the organism. To ensure this, no heat-shock was applied in order to limit the activity of the flipase, the promoter of this system, which resulted in around 10% of cells expressing GFP-YL-1.

Of the five lines, lines 1, 2 and 3 showed strong expression of GFP-YL-1 in the nucleus under fed conditions (Fig. 4.5 A, B, C). Line 4 and 5 initially did not express the construct at all, so the embryos of these genetic crosses were subjected to 30 minutes heat-shock at 37°C in order to optimise the activity of flipase. Following this, line 4 displayed nuclear expression of GFP-YL-1, however staining was observed to be diffused, with the presence of noisy GFP background signal seen across clones (Fig. 4.5 D). Line 5 failed to express the construct following the application of heat-shock (Fig. 4.5 E). All five lines were kept at 18°C during the screening process, with general health and proliferation deemed good. It must be noted that based on previous reports that YL-1 resides in the nucleus[326], the effect of the GFP tag on YL-1 was not tested. However, this should be investigated in the future.

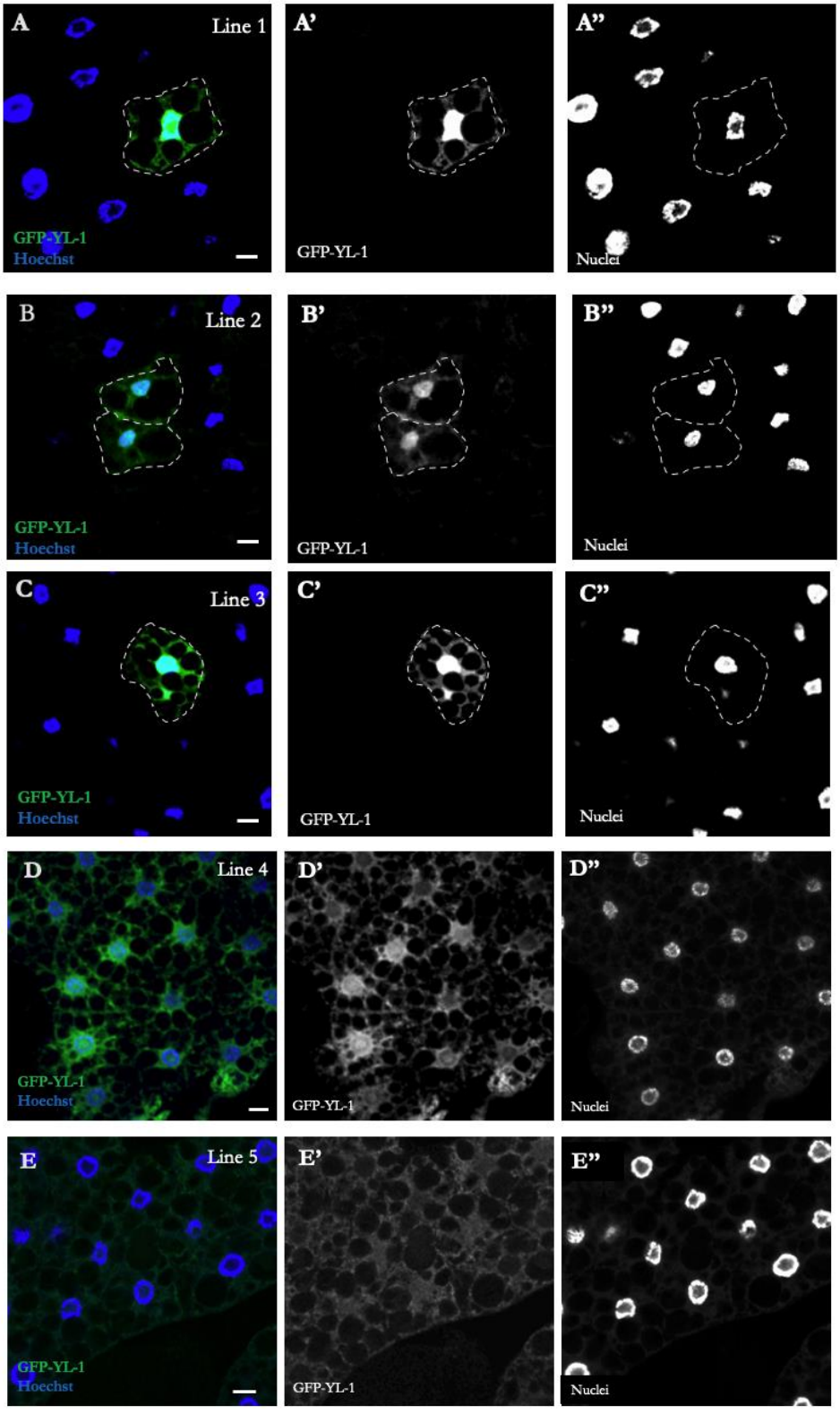

Figure 4.5 Expression Screening of GFP-YL-1 Across Five Transgenic Lines.

(A-C) Confocal section of *UAS-GFP-YL-1* expression in larvae (no heat shock administered) in fed conditions, for lines 1 (A), 2 (B) and 3 (C). (D-C) Genetic crosses subjected to heat-shock to promote GFP-YL-1 expression. Line 4 (D) shows moderate expression, line 5 (E) fails to express construct. Scale= 10um, nuclei stained with Hoechst. Genotype: *y w hs-Flp ;Ac>CD2>GAL4 / UAS-GFP-YL-1.*

4.4.1.2 Investigating the localisation of YL-1 in the induction of autophagy

In order to investigate the localisation of GFP-YL-1 in the context of autophagy, line 1 was crossed with the recombinant mCherry-Atg8a line; thus, allowing expression of both GFP-YL-1 and mCherry-Atg8a. Line 1 was selected as it was identified to show strong expression of GFP-YL-1 in the screening process, and overall this line showed particularly good healthy and was very easy to propagate. Given it's reported association with histones[326], YL-1 was predicted to localise exclusively to the nucleus. This was confirmed, with GFP-YL-1 observed to be expressed in the nuclear compartment in both fed and staved conditions (Fig. 4.6). The expression pattern of mCherry-Atg8a was consistent with that seen in previous investigations, with the accumulation of Atg8a positive puncta clearly shown in starvation conditions.

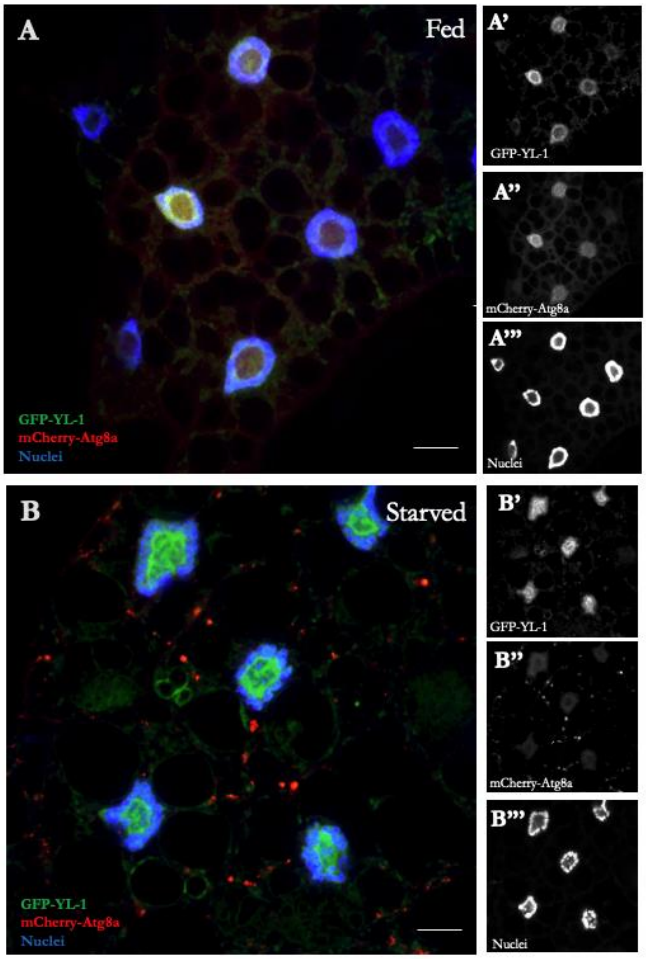

Figure 4.6 GFP-YL-1 Localises exclusively to the Nucleus in Fed and Starved Conditions.
Confocal section of *UAS-GFP-YL-1* (line 1) expression (green) in larvae fat body in fed conditions (A) and starved, 4h, 20% sucrose (B)with autophagy maker mCherry-Atg8a (red). Nuclei stained with Hoechst (blue). Scale= 10um Genotype: *yw hs-Flp;Ac > CD2 > GAL4/UAS-GFP-YL-1;UAS-mCherry-Atg8a/+*.

4.4.2 Testing the efficacy of YL-1 and Sir2 lines

In order to investigate the role of YL-1 and Sir2 in *Drosophila,* a number of lines were obtained: *yl-1*-RNAi (lines 2 and 3), mutant YL-1^{SH1685}, *sir2*-RNAi (lines 1 and 2) and mutant $Sir2^{2A-7-11}$.

The YL-1^{SH1685} mutant, obtained from BDSC, was created by insertional mutagenesis using the P-element construct P{lacW}. The relative expression of *yl-1* was investigated in the YL-1^{SH1685} mutant alongside both *yl-1*-RNAi lines. For RNAi lines, males were collected and crossed with Cg-GAL4 virgin females. Three sets of primers were designed in order to flank different genomic regions within the target *yl-1*, with all three lines observed to have a significantly reduced expression in comparison to the WT control (Fig. 4.7).

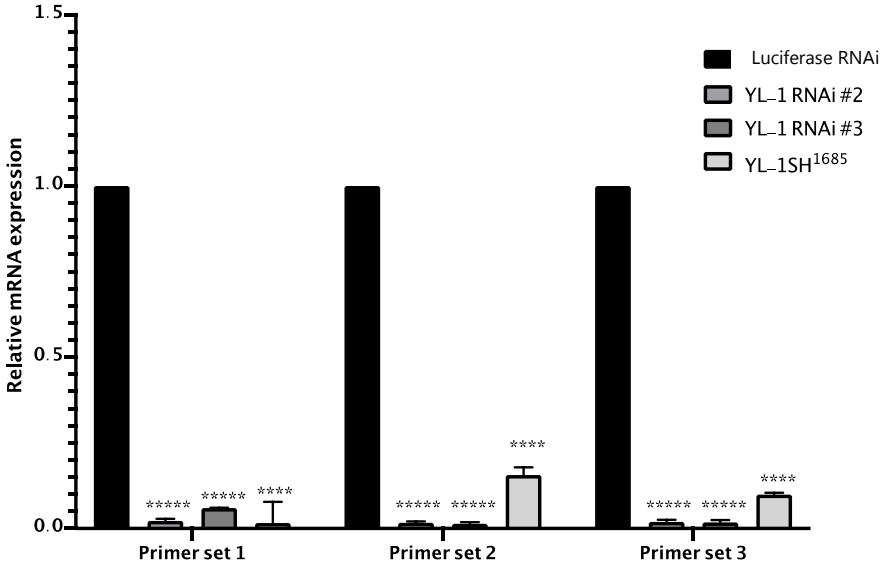

Figure 4.7 Efficient *yl-1* Knock-Down in Mutant and RNAi Lines.

mRNA expression analysis of *yl-1* gene in larvae of *YL-1^{SH1685}* and two *UAS-YL-1-RNAi* lines. Expression levels are relative to wild-type (W^{1118}) and normalised to *rp49*. N= 3 biological replicates and statistical significance was determined using a Student's t-test; ****p> 0.00005-*****p<0.000005. Genotypes: control: *Cg-GAL4/+; UAS-luc-RNAi/+*. YL-1 RNAi: *Cg-GAL4/+; UAS-yl-1-RNAi/+*. *w;* YL-1^{SH1685}: *YL-1[SH1685] FRT40A/CyO.*

Next the efficiency of a custom-made antibodies against YL-1 were trailed. The trial aimed to probe protein expression levels in the YL-1^{SH1685}. The reasoning behind selecting to solely investigate this genotype was because the antibody had unknown results in immunodetection, therefore it was deemed more efficient to limit the initial investigation and optimisation to one genotype which did not require any genetic crosses.

From the mutant line, 7-day old flies collected from the F1 progeny and subjected to protein extraction. Probing with anti-YL-1 produced a band at 41KDa (indicative of the MW of YL-1) which is clearly seen in the WT (Fig. 4.8 A) and observed to be significantly reduced in the mutant line (Fig 4.8 A, B). Initial rounds of use with this antibody too yielded unspecific bands as depicted in Fig. 4.8 A. Given the repeated use of new antibody in order to optimise conditions and achieve consistent replicates, the quality of the probes was observed to reduce in quality with each subsequent use. Therefore, it was decided not to conduct protein expression analysis in the *yl-1-RNAi* lines, especially given that the results from gene expression analysis was very convincing (Fig. 4.7). Ideally, protein lysates from GFP-Yl-1 overexpressed lines would also have been probed as an alternative control to WT.

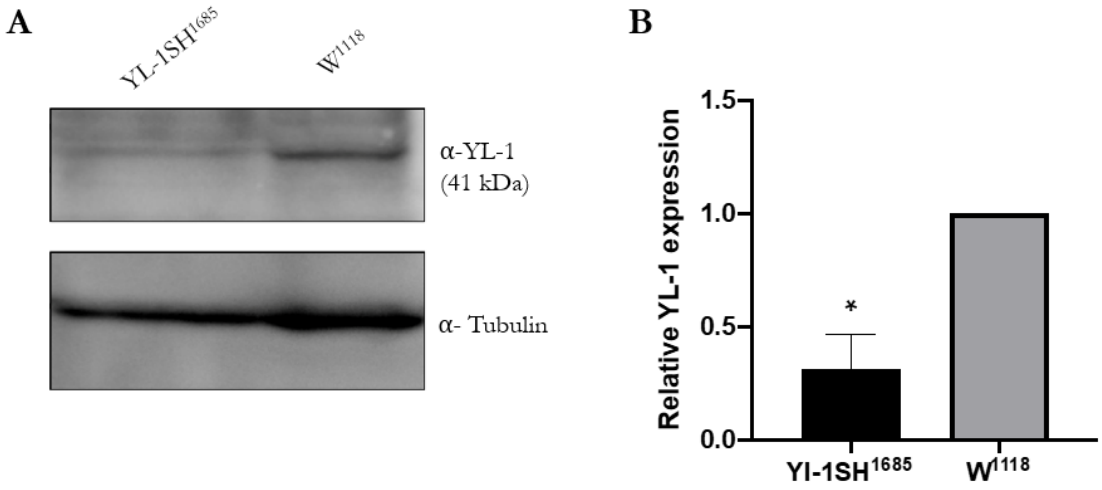

Figure 4.8 Expression of YL-1 protein reduced in Mutant Line.

Immunodetection of YL-1 protein in 7-day old YL-1SH^{1685} mutant flies, using a custom made anti-YL-1 antibody (A) Example blot to the band corresponding to YL-1 at 41kDa is evident in WT and less abundant in YL-1SH^{1685}. Protein expression quantified in (B), normalised to Tubulin and relative to W^{1118}. N=3 independent biological replicates, error bars + SD. Statistical significance determined by a Student's t-test; *p<0.05. Genotypes: *W^{1118}. w; YL-1[SH1685] FRT40A/CyO.*

For Sir2 lines, two primer sets were designed in order to target different areas of the *sir2* genomic region; this would allow an accurate representation of how efficient the lines were in silencing the gene, when queried by RT-qPCR. Of the two RNAi lines, results for line 1 were most convincing, with a significant reduction in *sir2* relative expression observed in both genomic loci (Fig. 4.9 A). The mutant $Sir2^{2A-7-11}$, obtained from the BDSC, was generated by targeted knockout which precisely removes the coding sequence of $Sir2^{327}$. The relative mRNA expression for the mutant line showed significant downregulation of *sir2* (Fig. 4.9 A).

To build upon these observations, a verified anti-dSir2 antibody[393] was used to probe the protein expression levels of *sir2*-RNAi line 1 and $Sir2^{2A-7-11}$. The predicted molecular weight of Sir2 is 92kDa, however it has also been observed at 110kDa[393]. Consistently, the correct band observed here for controls WT and *luciferase-RNAi* were between 100-110kDa. For both $Sir2^{2A-7-11}$ and *sir2*-RNAi line 1, the band corresponding to this region was significantly reduced in comparison to their respective controls (Fig. 4.8 B).

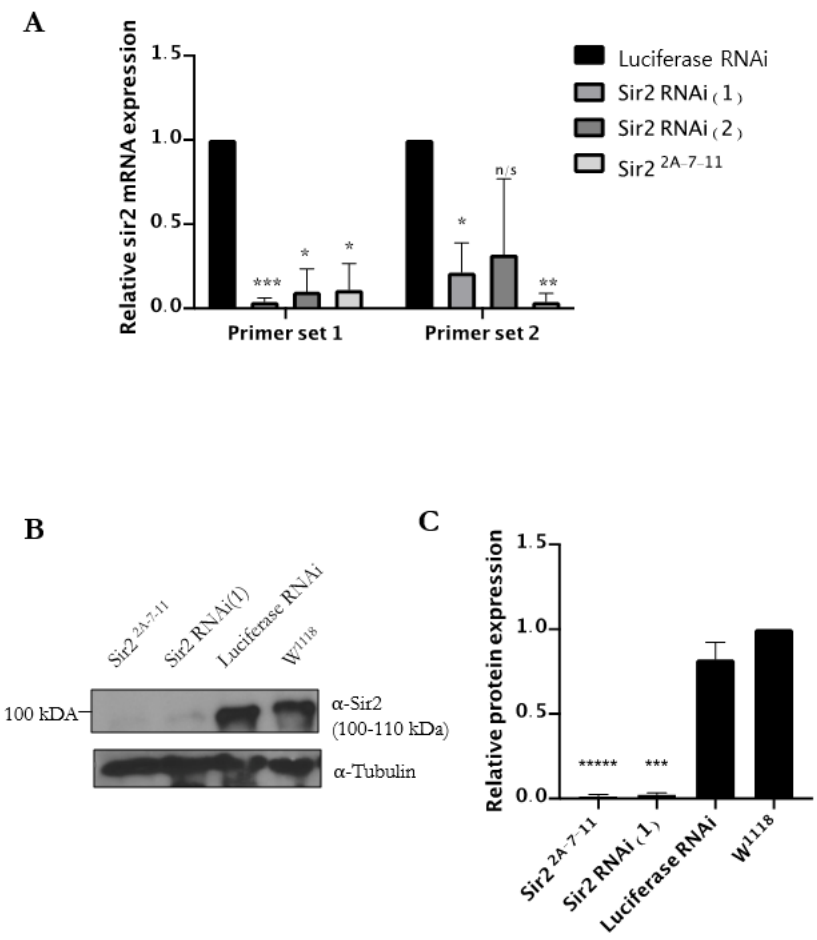

Figure 4.9 Testing the Efficacy of *sir2* Knockdown in Mutant and RNAi Lines.

(A) mRNA expression analysis of *sir2* gene in larvae of $Sir2^{2A\text{-}7\text{-}11}$ and two *UAS-sir2-RNAi* lines, across 5 primer sets. Expression levels are relative to wild-type (W^{1118}) and normalised to *rp49*. (B) Sir2 protein expression in $Sir2^{2A\text{-}7\text{-}11}$ and *UAS-sir2-RNAi* line 1, quantification shown in (C) relative to respective controls and normalised to Tubulin loading. In all cases n= 3 biological replicates and statistical significance was determined using a Student's t-test; *p>0.05-*****p<0.000005. Genotypes: *W1118*. *Cg-GAL4/+; UAS-sir2-RNAi/+*. $Sir2^{2A\text{-}7\text{-}11}$*/+*. *Cg-GAL4/+; UAS-luc-RNAi/+*.

4.4.2.1 Sir2-Myc remains nuclear in fed and starved conditions

Another line, UAS-Sir2-Myc, was obtained from BDSC, which allows a high level of *sir2* to be expressed under the control of the UAS. Importantly it has been reported that the Myc tag does not interfere with Sir2 histone deacetylase activity[397]. The relative expression of *sir2* in this line was determined against a WT, revealing a significant upregulation of *sir2* across all four genomic loci queried (Fig. 4.10).

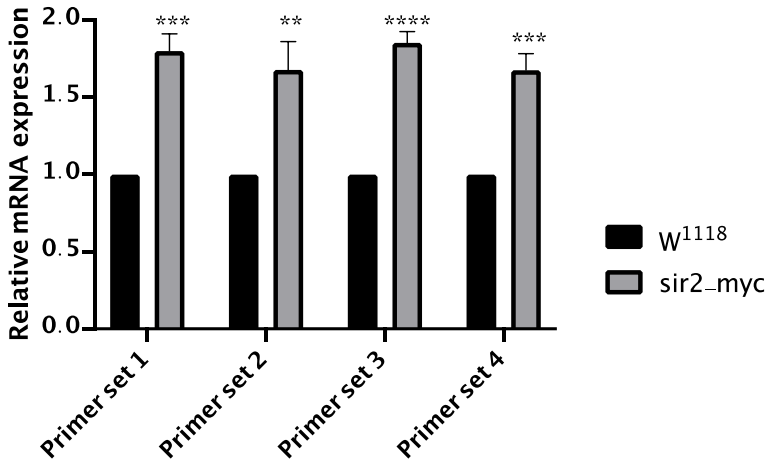

Figure 4.10 Overexpression of *sir2* in UAS-Sir2-Myc Line.

mRNA expression analysis of *sir2* gene in larvae of *sir2*-myc, across 4 primer sets. Expression levels are relative to WT (*W1118*) and normalised to *rp49,* across three independent experiments. Statistical significance was determined using a Student's t-test; ****p>0.00005- **p>0.005. Genotypes: *W1118*. *Cg-GAL4/+; UAS-sir2-myc/+*.

In order to evaluate the expression of Sir2 *in vivo* and to identify its cellular localisation, UAS-Sir2-Myc males were crossed with Cg-Gal4 virgin females and IF staining was carried out using anti-Sir2 on fed and starved, third instar stage larvae dissected fat bodies. This revealed Sir2 to reside in the nucleus in both conditions (Fig. 4.11 A, B).

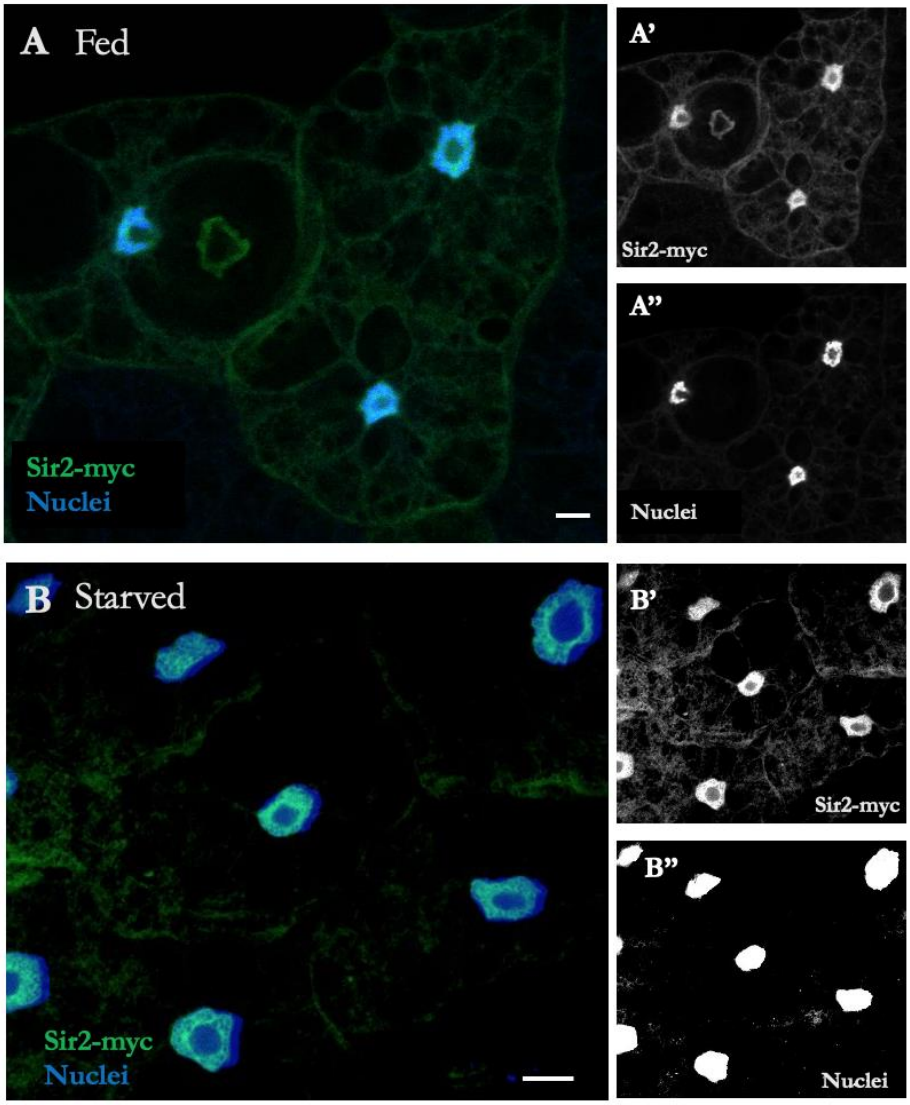

Figure 4.11 Sir2 Resides in the Nuclear Compartment in Both Fed and Starved Conditions.
Confocal section of *UAS-sir2-myc* expression (green channel) in larvae in fed conditions (A) and starved, 4h, 20% sucrose (B). Nuclei stained with Hoechst (blue). Scale= 50 um. Genotype: *Cg-GAL4/+; UAS-sir2-myc/+*.

4.4.3 YL-1 and Sir2 regulate the acetylation status of Atg8a *in vitro*

Following on from findings which revealed that Atg8a is acetylated in fed conditions and deacetylated in starved conditions; the role of YL-1 and Sir2 in governing this modification was investigated. Genetic environments in which loss of acetylation/deacetylation was promoted across both fed and starved conditions were created. This allowed for the effects of YL-1 and

Sir2 to be assessed on both the acetylation status of Atg8a, and the induction of autophagy. In order to detect Atg8a in these settings, flies constitutively expressing GFP-Atg8a in their fat bodies were crossed with control *luciferase*-RNAi, *yl-1*-RNAi (line 2) and Sir2-Myc lines. As an additional control Cg-GAL4 was crossed with UAS-GFP. In the GFP-Atg8a line, cleavage of GFP from Atg8a results from the formation of an acidic environment which suggests the induction of autophagy; therefore, the effects of starved conditions, *yl-1* knock-down and *sir2* overexpression could be assessed by observing the presence of free GFP.

Third instar stage larvae of the F1 progeny were collected, with protein extracted from full body larvae in fed conditions or following 4-hour starvation in 20% sucrose. The acetylation of GFP-Atg8a was determined by IP with anti-GFP followed by western blotting using an antibody which recognises acetyl-lysine residues. Figure 4.12 A shows two independent replicates for each condition loaded side by side. In the control condition (*luciferase*-RNAi) a strong band is indicative of acetylation of Atg8a in fed conditions, with a reduction in the corresponding region detected in starvation conditions (Fig. 4.12 B). Free GFP was observed in starvation conditions, indicating an induction of autophagy, and was absent in fed conditions. Interestingly, in an *yl-1* depleted setting, acetyl lysine staining was seen to be significantly reduced in fed conditions (Fig. 4.12 B), however this did not result in the cleavage of GFP from Atg8a. Free GFP was however observed in starvation conditions at similar levels to that seen in the control. In the case of *sir2* overexpression, acetylation was observed to be reduced significantly in both fed and starved conditions, in comparison to the control (Fig. 4.12 B). The overexpression of *sir2* resulted in the cleavage of GFP from Atg8a in starvation conditions at similar levels compared to the control. In fed conditions, no free GFP was detected. These results taken together suggest that Yl-1 and Sir2 may have a role in regulating the acetylation status of Atg8a, however whether or not they directly impact the induction of autophagy is inconclusive from these results alone as GFP cleavage is not specific enough to prove the induction of autophagy.

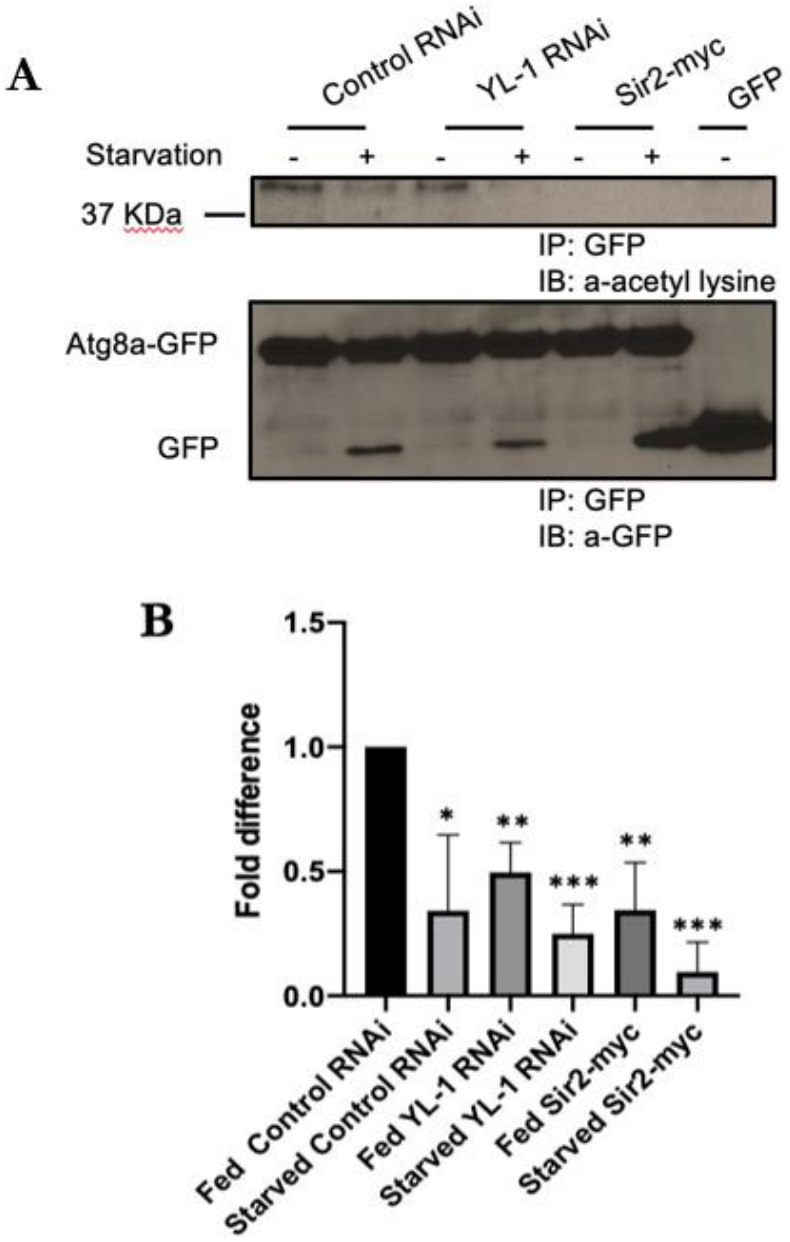

Figure 4.12 YL-1 and Sir-2 regulate the acetylation status of Atg8a.

(A) Larvae constitutively expressing GFP-Atg8a in their fat bodies were crossed with the control *luciferase-RNAi*, *yl-1-RNAi*, and *sir2-myc* lines and their F1 third instar stage larval progeny were collected. Protein acetylation was determined by IP with a GFP antibody followed by western blotting for an antibody recognizing acetyl-lysine residues. IP was performed with 1 mg protein lysate from full larvae both in fed and starved (4 h in 20% sucrose) conditions. (B) Quantification of the quantity of Atg8a protein normalized to GFP. Bar chart shows means +SDs. Statistical significance was determined using 2-tailed Student's t test; *$p < 0.05$, **$p < 0.01$, and ***$p < 0.001$. Quantification presented in (B) include biological replicates produced by Dr. Stavroula Petridi, Nezis lab, University of Warwick. N=4 independent biological replicates. Genotypes: Control RNAi: *Cg-GAL4 UAS-GFP-Atg8a/+;UAS-luc-RNAi/+,* YL-1-RNAi: *Cg-GAL4 UAS-GFP-Atg8a/+;UAS-YL-1-RNAi/+*, *Sir2-myc:Cg-GAL4 UAS-GFP-Atg8a/+;UAS-Sir2-myc/+,* GFP: *Cg-GAL4/+;UAS-GFP/+*.

4.4.4 Sir2 knockdown results in less acidic structure accumulation in starvation conditions

As results of the *in vitro* acetylation study did not reveal any impact of *sir2* overexpression in induction of autophagy, the implications of *sir2* knockdown were explored *in vivo*. LysoTracker is an acidotropic dye that stains cellular acidic compartments, which can indicate the presence of lysosomes and autolysosomes. It can therefore be used to detect autophagy-associated lysosomal activity in *Drosophila* fat body tissue. A low level of LysoTracker staining can be observed under well fed conditions and is increased following autophagic stimuli such as starvation. Here, third instar stage larvae were collected and processed in either full fed conditions or were subjected to 4 hours starvation in 20% sucrose. Fat bodies from WT and $Sir2^{2A\text{-}7\text{-}1}$ were dissected and stained with LysoTracker red dye. In fed conditions, there is no staining of acidic compartments in either WT or Sir2 mutant fat bodies (Fig. 4.13 A, B). In starvation conditions, WT showed an accumulation of autolysosomes in the form of bright red puncta (Fig. 14 A'). However, in $Sir2^{2A\text{-}7\text{-}1}$, there is no observed accumulation of autolysosome puncta in starvation conditions (Fig. 4.13 B'). An ideal control for the use of lysotracker staining would be the inclusion of chloroquine, a commonly used agent to block the induction of autophagy. This would have allowed a better evaluation of whether the accumulation of acidic structures were potentially reflective of lysosomes. These results in combination with those which showed $Sir2^{2A\text{-}7\text{-}1}$ to have decrease in endogenous Atg8a positive puncta in the cytoplasm (Appendix paper A; Fig. S3 F)[376] and a decrease in Atg8a lipidation (Appendix paper A; Fig. S4 A)[376] in starvation conditions, suggest that Sir2 is required for the activation of autophagy during starvation.

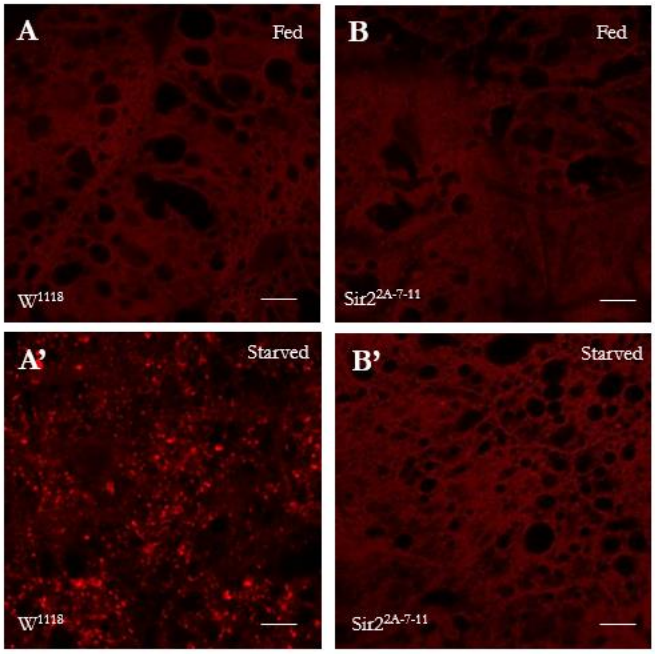

Figure 4.13 Sir2 Mutant Fails to Accumulate Acidic Structures in Response to Starvation.

Confocal sections of fat bodies from *W1118* (A), *Sir2 2A-7-11* (B) Larvae stained with LysoTracker Red in fed (upper panels) and 4 h of starvation (lower panels). Scale bar: 10 μm.

4.4.5 Depletion of *yl-1* results in the formation of autophagic structures *in vivo*

In order to investigate if knockdown of *yl-1* has an effect on the induction of autophagy *in vivo, yl-1*-RNAi was expressed alongside the autophagy reporter 3xmCherry-Atg8a. To do this, *yl-1*-RNAi flies were crossed with the driver line: *hs-Flp; 3xmCherry-Atg8a, UAS-GFP; Act>CD2>Gal4, UAS-Dcr2*[382,383]. This cross allowed for GFP positive clones being created in cells corresponding to those in which express *UAS-yl-1-RNAi*, alongside 'negative cells' which have been unmanipulated. The marker 3xmCherry-Atg8a is expressed throughout the fat body and labels autophagic structures. This experiment was conducted alongside a *luciferase*-RNAi control in fed conditions.

It was observed that the expression of *yl-1*-RNAi in fed larval fat bodies resulted in the accumulation of 3xmCherry-Atg8a puncta in the cytoplasm (Fig. 4.14 A). Neighbouring 'negative' clones were observed to have less accumulation of Atg8a positive structures. Furthermore, no Atg8a-positive puncta were observed in the *luciferase*-RNAi control (Fig. 14 B). This data is in contrary to that presented in Figure 4.12 where no free GFP was observed in *yl-1* RNAi, thus suggesting that loss of *yl-1* in fed conditions results in the formation of Atg8a

positive puncta. Although YL-1 was previously shown to regulate the acetylation status of Atg8a (Fig. 4.12) it cannot be determined conclusively that loss of *yl-1* induces autophagy due to loss of Atg8a acetylation, as YL-1 could possibly have multiple functions which impact the formation of Atg8a-positive puncta. These results, in the context of autophagy induction, were supported by findings by colleagues conducted in the same *yl-1*-RNAi which show a moderate increase in Atg8a lipidation (Appendix paper A; Fig. S2 A)[376].

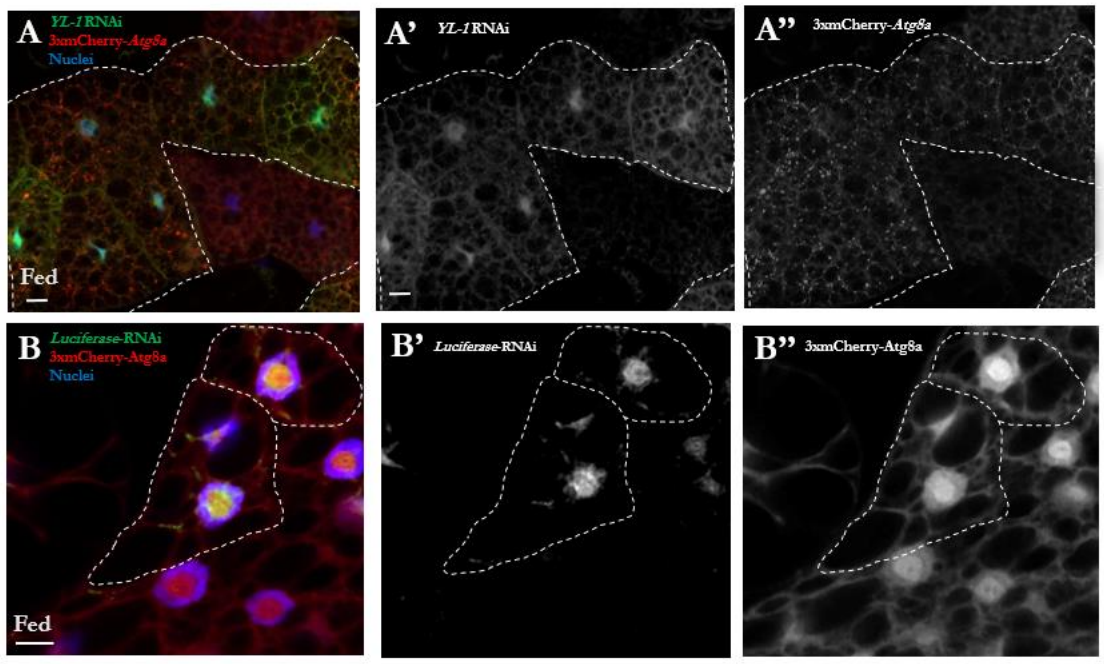

Figure 4.14 *In vivo* Knockdown of *yl-1* Results in the Accumulation of mCherry-Atg8a Puncta in Fed Conditions.
Confocal sections of larval fat bodies clonally expressing UAS-*yl-1-RNAi* (A') and UAS-*luciferase-RNAi* (B') in fed condition in combination with the autophagy marker 3xmCherry-Atg8a (A", B", red). YL-1 depletion results in the formation of autophagic structure in UAS-YL-1-RNAi positive clones, which are absent in negative neighbouring clones. There is no accumulation of 3xmCherry puncta in fed conditions in UAS-luciferase positive clones). Fixed fat bodies where stained for nuclei (blue) with Hoechst. Scale bar: 10 µm. Genotypes: (A) *hs-Flp; 3xmCherry-Atg8a, UAS-GFP; Act>CD2>Gal4, UAS-Dcr /UAS-yl-1-RNAi.* (B) *hs-Flp; 3xmCherry-Atg8a, UAS-GFP; Act>CD2>Gal4, UAS-Dcr /UAS-luciferase-1-RNAi.*

4.5 Investigating the Impact of Atg8a on the Regulation of *Atg* genes

The first part of this chapter set out to explore two Atg8a-interactors and their potential role in regulating the acetylation status of nuclear Atg8a. With structural modelling of Atg8a-bound Sequoia (Fig. 4.4) revealing the potential of acetylation of Atg8a to modulate its interaction with Sequoia, it was of interest to understand the transcriptional impact in which Atg8a has on the expression of *Atg* genes, given the transcriptional regulatory role of Sequoia outlined in Chapter 3.

There are a number of critical autophagy genes, including *Atg8a,* which are characterised by the loss of gene function resulting in the inactivation of the pathway. An *Atg8a* mutant line was obtained from Gábor Juhász, in which expression is blocked by the insertion a P-element at codon 28 of the *Atg8a* ORF, thus rendering the line incapable of initiating autophagy. *In vivo* experiments using this line have previously shown it to cause a significant decrease in starvation-induced autophagy[111]. Here this line was utilised in order to investigate the effects of Atg8a null mutants ($Atg8a^{KG}$) on the expression of *Atg* expression.

4.5.1 Atg8a mutants show reduced levels of *Atg* gene expression in starvation conditions

In full nutrient conditions, $Atg8a^{KG}$ larvae were subjected to RT-qPCR analysis in order to measure the relative expression of *Atg1, Atg4a, Atg4b, Atg5, Atg7, Atg8a, Atg9, Atg10, Atg13, Atg14, Atg18a, Atg101, Lamp1, Mitf* and *Tor*. This was the same gene set investigated in Chapter 3 and shown to be upregulated (with the exception of *Tor*, which was downregulated) following *sequoia* silencing (Fig. 3.10). As expected, a significant knockdown of *Atg8a* was observed in $Atg8a^{KG}$ (Fig. 4.15 A). Interestingly, during fed conditions the knockdown of *Atg8a* had no significant effect on *Atg* gene expression in comparison to a WT control (Fig 4.15 A). This suggested that during full nutrient conditions, the repression of *Atg* genes may be independent of the presence of Atg8a. In order to explore its effects in the induction of autophagy, *Atg* expression levels were investigated in starvation conditions (Fig. 4.14 B). Interestingly, here it was observed that loss of *Atg8a* significantly reduced the expression of *Atg* genes, hinting that nuclear Atg8a may have a role in the transcriptional regulation of genes in starvation conditions. The expression of *Tor* was also observed to be significantly increased in this setting, further highlighting the effects of *Atg8a* loss on the transcriptional control of autophagy.

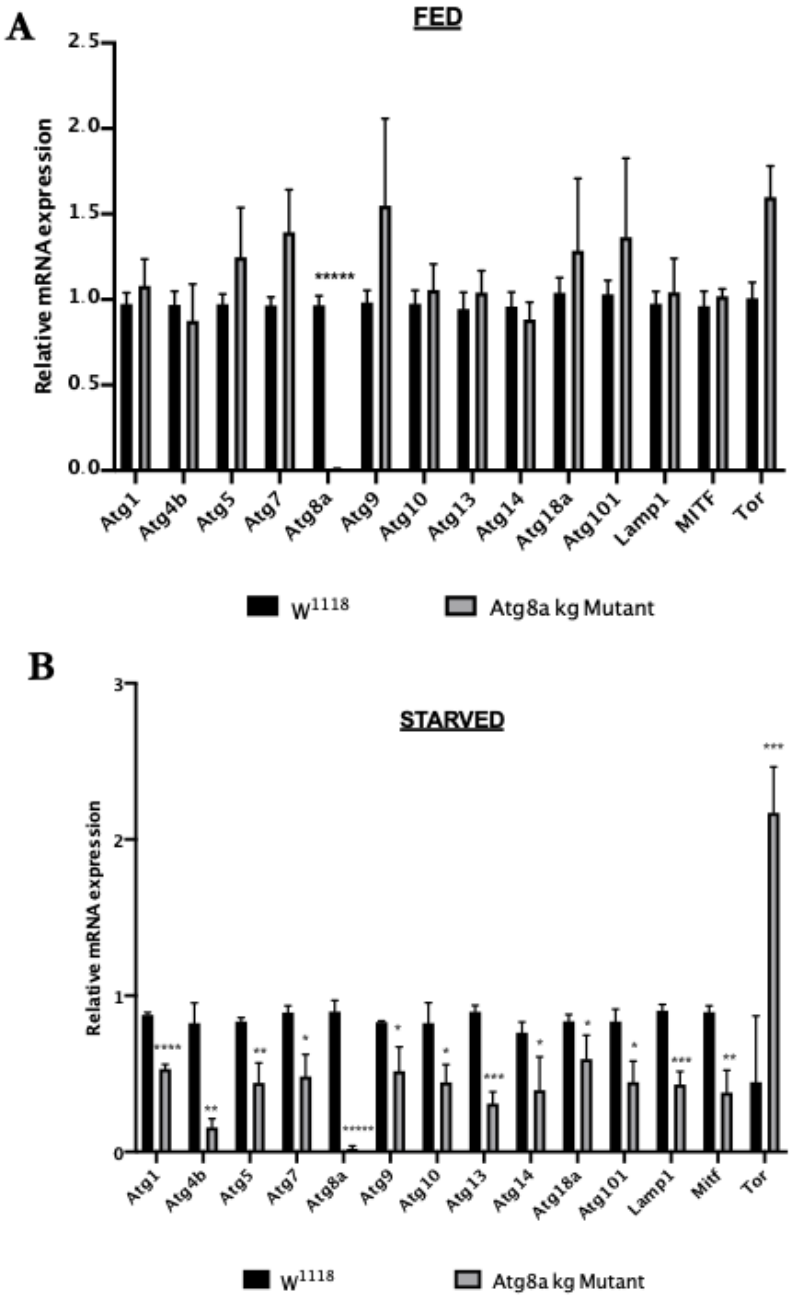

Figure 4.15 Knockdown of *Atg8a* Reduces the Expression of *Atg* genes During Starvation.

Analysis of the mRNA levels of autophagy-associated genes in Atg8a^{KG} mutant fat bodies in fed (A) and starved, 4h (B) conditions, using real-time qPCR. Expression levels are shown relative to the control (W^{1118}) and normalised to the expression of *rp49* (housekeeping gene) over 3 biological replicates. Statistical significance was determined using a Student's t-test; *****p<0.000005- *p<0.05. Genotypes: *W^{1118},* hs::FLP,*atg8a*KG07569.

4.5.2 Atg9 null mutants show no effect on the regulation of *Atg* genes

In order to validate the results presented in Figure 4.15, the regulation of *Atg* genes in Atg9 mutants was explored. Since Atg9 is considered to act in parallel to Atg8a, and functions as part of another Atg complex, a direct comparison between could be used to evaluate the specific impact of loss of *Atg8a* on *Atg* gene expression levels under starvation conditions. Furthermore, Atg9 is expressed exclusively in the cytoplasm, therefore the impact of the nuclear residency of Atg8a can be inferred.

Atg9 has been shown to be necessary for the efficient functioning of both Atg1, Atg4a, Atg4b, Atg5, Atg7, Atg8a, Atg9, Atg10. Atg13, Atg14, Atg18a and Atg101 starvation induced and basal autophagy[328]. Previously RNAi knockdown of *Atg9* revealed the crucial role of Atg9 in the induction of autophagy in the cytoplasm[398,399], and more recently *Atg9* null mutants have been shown to inhibit the formation of autolysosome and autophagic structures in starvation conditions, whilst the accumulation of autophagy substrate p62 was observed in fed conditions[328]. Amongst the *Atg* gene products, Atg9 is the only known conserved transmembrane protein, and like in its mammalian counterpart, it is likely to function in *Drosophila* cells by supplying initial vesicles for phagophore nucleation from multiple membrane sources including the ER, endosomes, plasma membrane and Golgi[170].

Atg9 mutant lines were kindly received from Gábor Juhász; these were generated using CRISPR/Cas9 in order to create the $Atg9^{B5}$ allele[328]. This mutation functions through the removal of the protein coding sequence which lies in the right arm of the second chromosome. In order to create Atg9 mutants, viable $Atg9^{B5}$ flies were crossed to Df(2R)ED2487 deficiency, with hemizygous larvae selected for experiments. As described for $Atg8a^{KG}$ mutants, expression levels of *Atg* genes were investigated in fed and starved conditions in hemizygous $Atg9^{B5}$ larvae. RT-qPCR analysis revealed the successful knockout of *Atg9*. Remarkably, when compared to a WT control, no significant change was observed in both fed and starved conditions (Fig. 4.16 A, B). Taken collectively with observations that $Atg8a^{KG}$ show a significant reduction in *Atg* gene expression in starvation conditions, these results suggest that nuclear Atg8a may have a role in regulating the expression of *Atg* genes in a nutrient deplete setting.

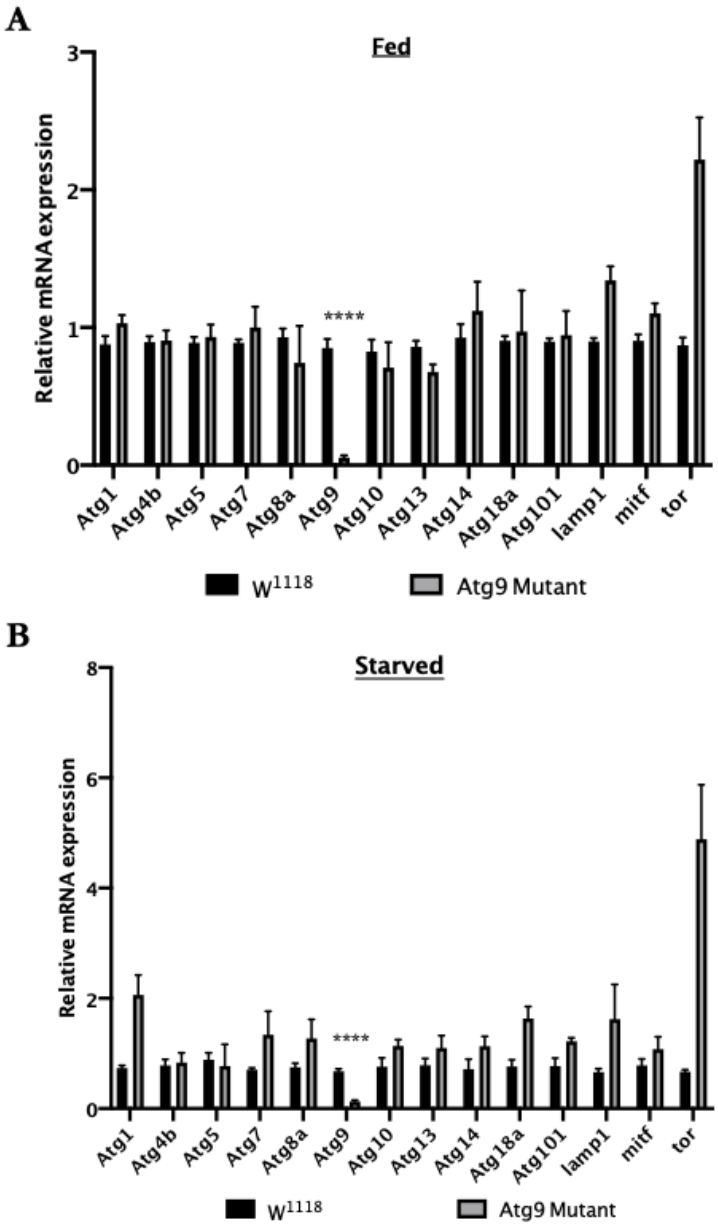

Figure 4.16 Knockdown of *Atg9* has no Effect on the Expression of *Atg* genes.

Analysis of the mRNA levels of autophagy-associated genes in *Atg9* mutant fat bodies in fed (A) and starved, 4h (B) conditions, using real-time qPCR. Expression levels are shown relative to the control (W^{1118}) and normalised to the expression of *rp49* (housekeeping gene) over 3 biological replicates. Statistical significance was determined using a Student's t-test; ****$p<0.00005$ (for *Atg9*), all other genes $p>0.05$. Genotypes: W^{1118}, $Atg9^{B5}/Atg9^{Df(ED2487)}$.

4.6 Investigating the Association of Atg8a to *Atg* Promotor Regions

Observations that *Atg* gene expression remains unaffected in the absence of *Atg8a* during full nutrient conditions, is suggestive that Sequoia's ability to repress the expression of a number of core *Atg* genes (Fig. 3.10, 3.12) may be independent of its interaction with Atg8a. In order to elucidate the mechanism by which the interaction between Atg8a and Sequoia regulates the expression of *Atg* genes, it is crucial to assess under which conditions each of the proteins is associated to gene promotor regions.

4.6.1 Atg8a shows enrichment at the promotor region of *Atg* genes in fed conditions

Given the interaction previously established to occur between nuclear Atg8a and Sequoia, and Sequoia's enrichment at the promotor region of *Atg* genes, it is expected that by virtue Atg8a is localised or associated to these regions during fed conditions. It is well reported that via ChIP is sensitive enough to detect the factors which are associated to a promotor via an interaction with a transcription factor bound to this region[400]. In order to investigate the association of Atg8a with gene promotors, GFP-Atg8a was expressed in the larval fat body using the driver line Cg-GAL4; with 150 fed larvae subjected to ChIP using anti-GFP, and normal rabbit IgG, used as a control for nonspecific precipitation. The genomic regions which were investigated here were those in which Sequoia had previously shown to be enriched at; *Atg1, Atg5, Atg7, Atg8a, Atg13 and Atg14,* with *Tubulin* used as a non-*Atg* control. Results revealed Atg8a to be significantly enriched at all regions queried (Fig. 4.17).

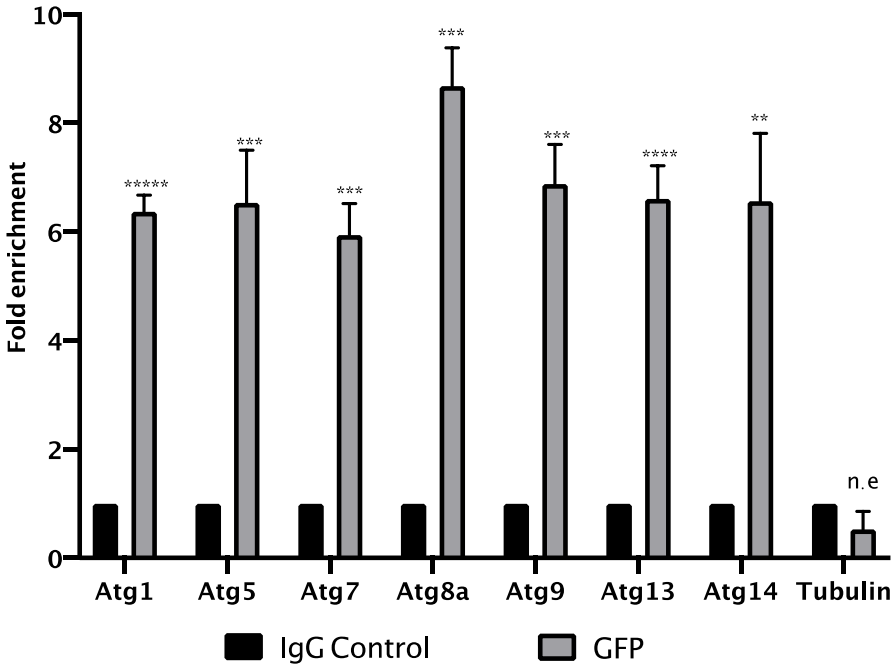

Figure 4.17 Atg8a is Associated with the Promotor Region of *Atg* genes in Full Nutrient Conditions.
Analyses of GFP-Atg8a binding to the promoter of autophagy genes in fed conditions, as detected by ChIP (chromatin immunoprecipitation) using a GFP antibody. ChIP DNA values were normalized to input DNA using the $2^{-\Delta\Delta}$ (Ct) method. Fold enrichment values are shown relative to the immunoglobulin G (IgG) control. Tubulin was used as a non-autophagy control locus, which was showed no enriched (n.e). All data shown as means ± SDs, n = 3 independent experiments. Statistical significance was determined using Student's t test; *$p < 0.05$ - *****$p < 0.000005$. Genotype A: *Cg-GAL4/+; UAS-GFP-Atg8a.*

4.6.2 The enrichment of Sequoia WT and LIR mutant in a *Atg8a*-deplete setting

In order to directly asses the effects of *Atg8a* knock-down on the residency of Sequoia on *Atg* promotor regions, inducible heat-shock Sequoia WT and LIR mutant stable lines were generated in order to cross these genotypes with $Atg8a^{KG}$ mutants. To do this, males from the previously described GFP-$Sequoia^{WT}$ and GFP-$Sequoia^{LIRm}$ lines were crossed with various balancer introducing lines in order to generate stable lines in which the F1 progeny would be viable, fertile, and genetically stable. Once established and deemed healthy, F1 adult flies from these newly created lines were selected against certain balancer phenotypes and were subsequently crossed with the $Atg8a^{KG}$ flies. The F1 progeny of these crosses were subjected to to one-hour heat-shock, 24 hours after laying in order to induce expression of *sequoia.* Overexpression of

sequoia and knockdown of *Atg8a* was confirmed in both lines via mRNA expression analysis (Fig. 4.18). The progeny derived from the GFP-Sequoia^{LIRm} produced an abundance of larvae, allowing for experimentation to be conducted in both fed and starved conditions. However, as offspring derived from GFP-Sequoia^{WT} was in poorer health and not able to lay well, it was decided to only investigate this line in fed conditions. It is unclear why the GFP-Sequoia^{WT} line was in poor health, but this may be due to the genotype.

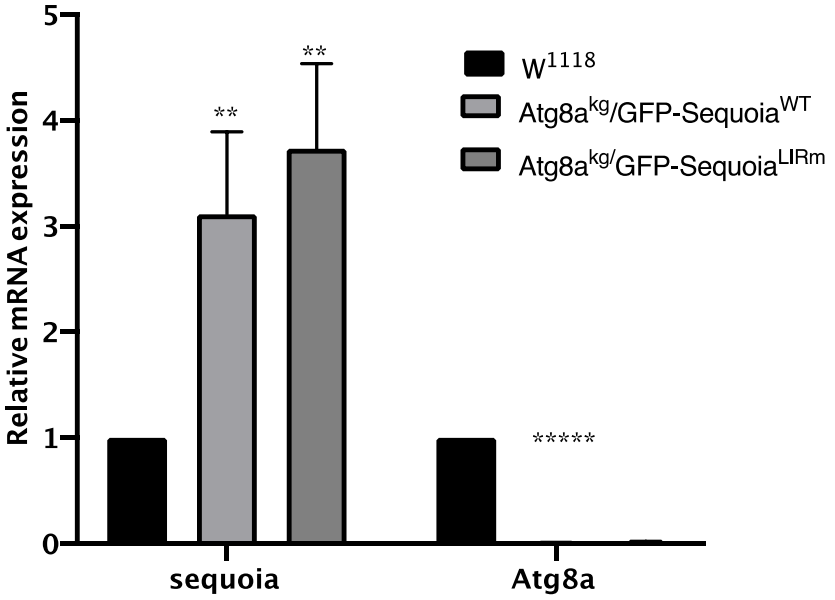

Figure 4.18 Expression of Target Genes in Atg8a^{KG}/GFP-Sequoia lines.

Analysis of the mRNA level of *sequoia* and *Atg8a* genes in W^{1118}, Sequoia WT/Atg8a^{KG} and Sequoia LIR mutant/Atg8a^{KG} fat bodies in fed conditions, using real-time qPCR. Expression levels were relative to W^{1118} and normalised to *rp49*, with statistical significance determined in comparison to W^{1118}. All data shown as means ± SDs, n = 3 independent experiments. Statistical significance was determined using Student's t test; **p < 0.005 and *****p < 0.000005. Genotypes: *W^{1118}, atg8aKG07569/Y; hs::GALA;UAS-GFP-Sequoia^{WT}/+*, *atg8aKG07569/Y; hs::GALA;UAS-GFP-Sequoia^{LIRm}/+*

4.6.2.1 Wild type Sequoia is enriched on *Atg* genes promotor in the absence of Atg8a

A ChIP experiment was conducted using the F1 progeny of the Atg8a^{kg} /GFP-Sequoia^{WT} line, with larvae processed as previously described using anti-GFP and normal rabbit IgG. This allowed for the enrichment of GFP-Sequoia^{WT} to be determined in an *Atg8a* depleted setting. Here, Sequoia was observed to be significantly enriched on the promotor region of all *Atg* genes queried; *Atg1, Atg5, Atg7, Atg9, Atg13* and *Atg14* (Fig. 4.19). No level of significant enrichment

was recorded for the *Tubulin* control. This supports previous findings which indicate that depletion of *Atg8a* does not result in an increase of expression of *Atg* genes (Fig. 4.15 A). Results here also mirror those obtained for GFP-Sequoia^{WT} observed in an *Atg8a* unmanipulated setting. These results further support the suggestion that *Atg8a* is not required for Sequoia to remain on promotor regions and thereby repress the expression of *Atg* genes in fed conditions.

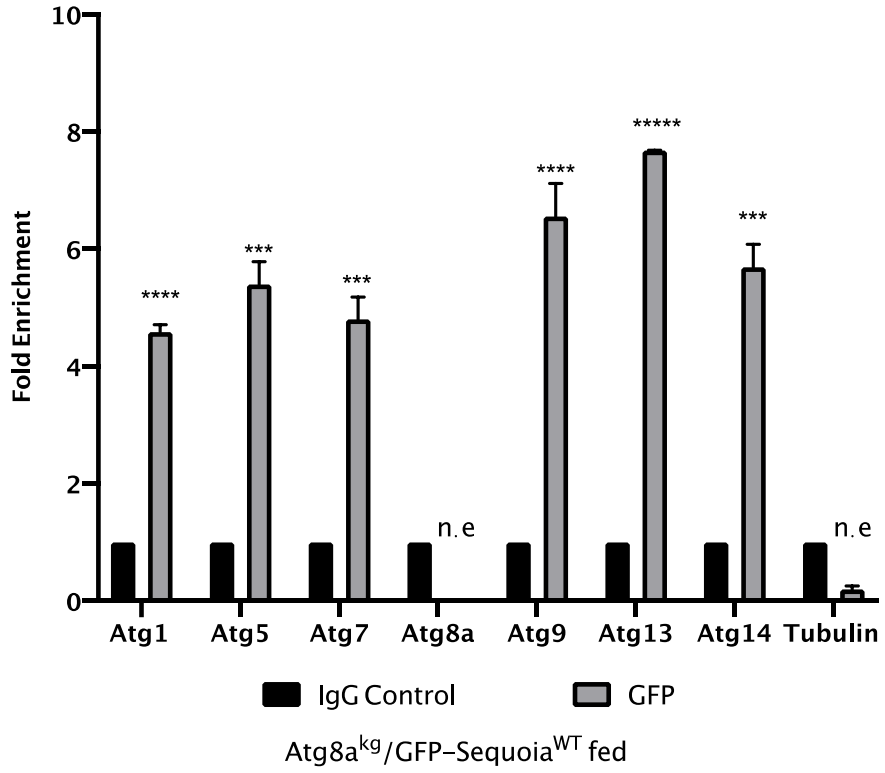

Figure 4.19 Sequoia Remains Enriched at the Promotor Region of *Atg* genes in the Absence of *Atg8a.*
Analyses of GFP-Sequoia binding to the promoter of autophagy genes in *Atg8a^{KG}*/GFP-Sequoia WT larvae, under fed conditions, as detected by ChIP (chromatin immunoprecipitation) using a GFP antibody. ChIP DNA values were normalized to input DNA using the 2-ΔΔ (Ct) method. Fold enrichment values are shown relative to the immunoglobulin G (IgG) control. Tubulin was used as a non-autophagy-related gene control. All data shown as means ± SDs, n = 3 independent experiments. Statistical significance was determined using Student's t test; ***p < 0.0005 and *****p < 0.00005. n.e= not Genotypes: *atg8aKG07569/Y; hs::GAL4;UAS-GFP-Sequoia^{WT}/+*.

4.6.2.2 Sequoia^{LIRm} shows enrichment on *Atg* promotors in the absence of *Atg8a*

ChIP was conducted in Atg8a^{kg} /GFP-Sequoia^{LIRm} larvae, in both fed and starved conditions. Remarkably when compared to the IgG control, enrichment of GFP-Sequoia^{LIRm} at *Atg* promotors revealed significant enrichment across all genes in both conditions, with significant difference in enrichment levels determined between the two conditions (Fig. 4.20). Previous investigation via ChIP revealed GFP-Sequoia^{LIRm}, in an *Atg8a* WT background, not to be enriched across all these regions (Fig. 3.14). This suggests that in the absence of Atg8a (represented here by the Atg8a^{kg}), Sequoia is unable to be maintained at the promotor of Atg genes. This suggests that it may be the translocation of Atg8a into the cytoplasm (and subsequent presence in the cytoplasm), rather than its interaction with Sequoia which subsequently impacts the residency of Sequoia on the promotor region of *Atg* genes. This possibility is strengthened here by the observation that the LIR mutant is also significantly enriched on the promotor region of *Atg* genes in starvation conditions in an Atg8a^{kg} background (Fig. 4.20). This also suggests that *Atg8a* may play a role relieving the repression imposed by Sequoia at the promotor in the induction of starvation induced autophagy. This is supported by findings in Fig. 4.15 B, which suggest that knockdown of *Atg8a* reduces the expression of *Atg* genes during starvation. Unfortunately, due to the poor health and reproductive activity of the GFP-Sequoia$^{WT/LIRm}$ stable lines, and the length of time in which is required to establish their viability, mRNA express analysis of *Atg* genes these lines could not be conducted. It must be noted that these conclusions are all speculative and that further experimentation would be needed to characterise the regulatory role in which the interaction between Atg8a and Sequoia has on the expression of *Atg* genes.

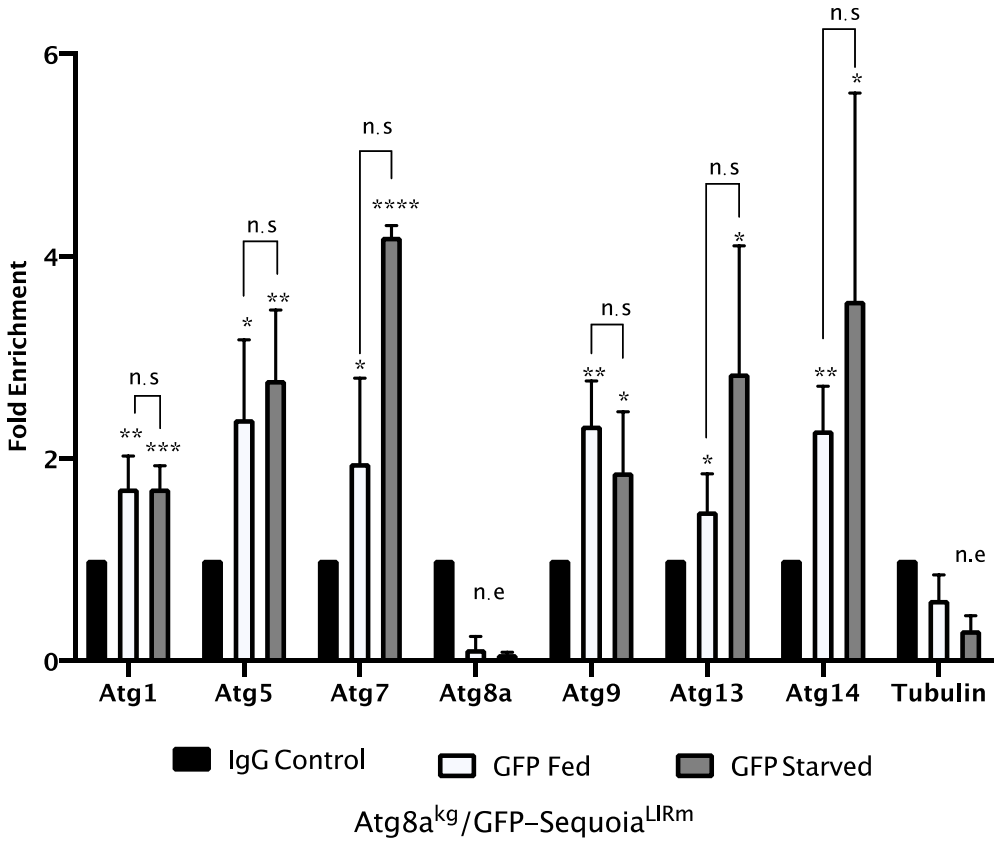

Figure 4.20 Atg8a Knockdown results in the *Atg* Promotor Enrichment of Sequoia LIR mutant in both Fed and Starved Conditions.
Analyses of GFP-Sequoia LIR mutant binding to the promoter of autophagy genes in GFP-Sequoia WT/ *Atg8a*^{KG} larvae, under fed (white) and 4h starved (grey) conditions, as detected by ChIP (chromatin immunoprecipitation) using a GFP antibody. ChIP DNA values were normalized to input DNA using the 2-ΔΔ (Ct) method. Fold enrichment values are shown relative to the immunoglobulin G (IgG) control, with * directly above the error bars representative of statistical difference versus the control. Tubulin was used as a non-autophagy-related gene control. All data shown as means ± SDs, n = 3 independent experiments. Statistical significance was determined using Student's t test; *p < 0.05- ****p < 0.0005. n.e= not enriched. N.s= not significant= p> 0.05, with values above the adjoining bars denote statistical outcome of comparison between fed and starved enrichment values. The * above individual bars represent statistical significance compared to the IgG control, and the overarching bars represent a comparison between GFP fed and starved. Genotypes: *atg8aKG07569/Y; hs::GAL4;UAS-GFP-Sequoia*^{LIRm}/+.

4.7 End of chapter conclusions

Here, we report a novel role for *Drosophila* YL-1, a component of a nuclear acetyltransferase complex and relation to mammalian NuA4-KAT5/Tip60, in the regulation of acetylation of non-histone proteins and the regulation of autophagy induction. We also confirm the

evolutionary conserved role of sirtuins in the induction of autophagy, with *Drosophila* Sir2 shown to mediate deacetylation of Atg proteins in response to starvation conditions[158,401].

Work previously conducted by colleagues showed that the interaction between Atg8a and histone-interacting YL-1 is direct and does not depend on a functional LIR motif[376]. Depletion of YL-1 by using an RNAi line, is shown here to result in a reduced level of acetylated Atg8a in both fed and starved conditions (Fig 4.11), whilst acetylation of Atg8a at position K48 is shown to modulate the binding of Atg8a to Sequoia (Fig 4.3).

Acetylation of Atg8a by YL-1 is shown to be counter-balanced by the deacetylase Sir2, the *Drosophila* homolog of the mammalian SIRT1. Prior to work conducted here, it was established by colleagues that Sir2 preferentially interacts with Atg8a in starved conditions[376]. The observed lack of accumulation of acidic structures in *Drosophila* larvae fat body cells upon starvation in Sir2 mutants (Fig. 4.13) is supported by reports in starvation conditions showing $Sir2^{2A-7-1}$ to have a decrease in endogenous Atg8a-positive puncta in the cytoplasm (Appendix paper A; Fig. S3 F)[376] and a decrease in Atg8a lipidation (Appendix paper A; Fig. S4 A)[376]. Results here show that Sir2 overexpression leads to decreased acetylation of Atg8a both in fed and starved conditions (Fig. 4.11). Taken together, these observations suggest that the binding of Sir2 to Atg8a may contribute to Atg8a deacetylation and export to the cytoplasm.

Following findings which revealed the potential of acetylation events regulating the binding between Sequoia and Atg8a, the final part of the chapter explored the potential role of nuclear Atg8a in the regulation of *Atg* genes. Here, it was revealed that during fed conditions the absence of *Atg8a* was seen to have no effect on the regulation of *Atg* genes (Fig 4.15 A), with Sequoia remaining enriched at their promotors (Fig. 4.19). Interestingly, the absence of *Atg8a* was observed to have a significant negative impact on the expression of the same set of *Atg* genes during starvation (Fig. 4.15 B); however, a lack of Atg9 demonstrated no impact on their expression (Fig 4.16 A, B). This highlights the transcriptional importance of the nuclear LIR-dependant interaction between Atg8a and Sequoia in the expression of autophagy genes in starvation conditions. This is further emphasized in the observed association of Atg8a with the promoter region of *Atg* genes (Fig 4.17), which is suggested to be by virtue of its interaction with Sequoia. Taken together, it is suggested under nutrient stress conditions, Atg8a in its deacetylated form plays an integral role in lifting Sequoia off the promotor of *Atg* genes.

CHAPTER 5. UNCOVERING THE POTENTIAL OF dDOR IN THE INDUCTION OF AUTOPHAGY

5.1 An introduction to dDOR

The interaction between Atg8a and Sequoia has been well described in Chapters 3 and 4. However, given the observation that Atg8a translocates into the cytoplasm under starvation conditions; the question is raised of how this re-location is governed in *Drosophila*. With Sequoia observed to be strictly nuclear under both settings, it is postulated that an interaction with another factor may be responsible in facilitating the re-location of Atg8a during the induction of autophagy. Understanding the nucleus-to-cytoplasm translocation of Atg8a is crucial since it's a mechanism upon which the formation of autophagosomes is dependent on during the induction of autophagy.

In mammalian cells, several studies have reported that the trafficking of LC3 in and out of the nucleus is a regulated event[158,318]. Huang *et al.,* (2015) demonstrated that nuclear LC3 is deacetylated by SIRT1 and is subsequently actively trafficked out of the nucleus into the cytoplasm by virtue of its association with DOR[158]. DOR is a nuclear protein enriched in cells with high metabolic levels, is was primarily identified as an activator of the thyroid hormone receptor[402]- reflective in the name DOR, which is derived from the **D**iabetes- and **O**besity-**R**egulated gene. The DOR human homolog, TP53INP2, shuttles between the nucleus and the cytoplasm, depending on cellular stress conditions and re-localizes to the autophagosomes upon autophagy activation[403]. It has also been characterised to have a LIR motif and directly binds with LC3/GABARAP family proteins via this region[403]. TP53INP2 also has a known UIM, but it is reported to be dispensable in its interaction with LC3/GABARAP[227] Overexpression of TP53INP2 is shown to promote basal autophagy, and *TP53INP2* knockdown inhibits the induction of starvation induced autophagy[158,339,404]. Given that the redistribution of LC3 by DOR is dependent on its deacetylation by SIRT1; our findings that the action of Sir2 on Atg8a is necessary for the induction of starvation induced autophagy in *Drosophila* draws attention to the possibility that the function of DOR may be conserved in *Drosophila*. High-throughput two hybrid screening has identified the *Drosophila* homologue of DOR, dDOR (CG11347) to interact with both Atg8 homologs: Atg8a and Atg8b[405]. Thus, suggesting that the interaction between DOR and Atg8 is conserved from mammals to *Drosophila*.

The dDOR locus is predicted to encode six different transcripts, giving rise to three different polypeptides (Fig. 5.1 A)[406]. The -RA, -RB, -RD, and -RE isoforms all encode a protein referred to as $dDOR_{long}$, which has a length of 387 amino acids. The use of an alternative splice donor yields another product with an extended third exon, resulting in 30 amino acids containing the sequence FENLL being inserted into the middle of the $dDOR_{long}$ protein (Fig 5.1 A, B). This particular motif is similar to the LXXLL motif found in nuclear receptor proteins. This isoform is thus referred to as $dDOR_{FENLL}$[407]. The -RC isoform encodes a shorter protein with a length of 273 amino acids, referred to as $dDOR_{short}$. The -RF isoform encodes an even shorter protein which is similar to $dDOR_{short}$ but lacks 44 amino acids at the N terminus (Fig. 5.1 A)[407]. *dor* is found to be highly expressed in the larval fat body, where it is required for developmentally regulated autophagy[339]. dDOR is also a known coactivator of the ecdysone receptor which is required during metamorphosis, and is required for maximal EcR transcriptional activity[407].

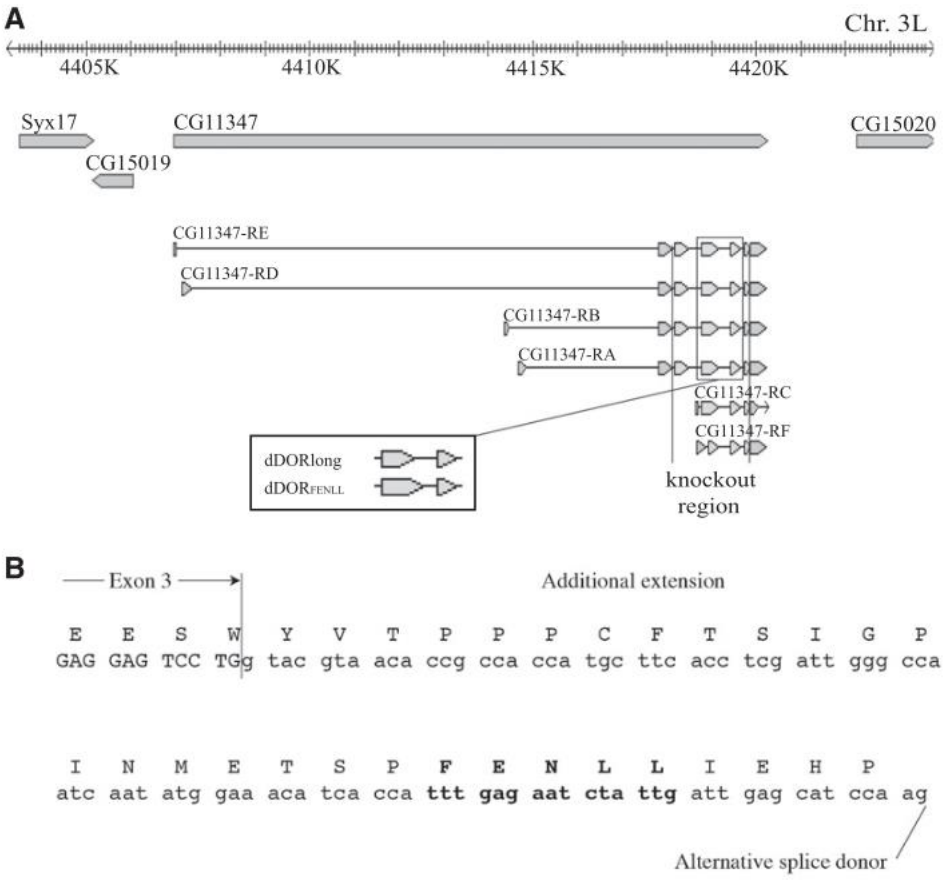

Figure 5.1 dDOR Gene Structure and Splice Isoforms. (A) The dDOR (CG11347) genomic region codes for six splice variants, plus an additional splice variant which has been referred to as $dDOR_{FENLL}$, which contains an extended third exon. (B) Additional nucleotide and amino acid sequence present in the splice variant $dDOR_{FENLL}$. Figure reproduced from Francis *et al.* (2010)[407].

The abundance of all three isoforms have been established *in vivo*, with DOR_{long} representing the most abundant, followed by the DOR_{FENLL} and then DOR_{short}, which is expressed at the lowest levels[407]. This pattern of expression is true across all stages of development in full body animals, and also in the fat body of third instar stage larvae. The FENLL isoform predominates expression in the fat body of early pupae however[407].

5.1.2 Chapter Aims

- Based on findings from a yeast two-hybrid screen and the iLIR tool, a LIR mutated dDOR plasmid will be generated.
- To investigate the top candidate LIR (as indicated by the iLIR tool) in the interaction between Atg8a and dDOR.
- To explore the binding of deactylated Atg8a (starvation conditions) to dDOR.
- To investigate the role of dDOR in the transcriptional regulation of *Atg* genes.
- To assess the potential of the future investigation of $dDOR_{FENNL}$, and the UIM in the interaction between dDOR and Atg8a.
- To generate a transgenic line overexpressing $dDOR_{long}$, and another overexpressing $dDOR_{FENLL}$. This will allow for future experimentation to be conducted on their potentially individual roles in starvation induced autophagy, *in vivo*.

5.2 Generating a dDOR LIR mutant

5.2.1 A Yeast Two-hybrid screen predicts dDOR to interact with Atg8a

In order to predict Atg8a protein interactors, a yeast two-hybrid screen was conducted by Hybrigenic Services. This assay has been established in genetically modified yeast strains and is based on the reconstruction of a transcription factor, when two proteins interact[408]. Here, two fusions 'hybrids' are constructed between the protein of interest and either the DNA binding domain or the activation domain of the transcription factor[408]. Upon the interaction of two proteins, a functional transcription factor is reconstituted upstream of the reporter resulting in a transcription of a reporter gene and the development of a specific phenotype. A yeast two-hybrid screen can also allow a target protein, in this case Atg8a, to be used as a 'bait' to screen libraries of protein fragments of an entire organism; with successful results previously obtained in *Drosophila*[409]. The identity of the interacting partners is obtained through sequencing of the corresponding plasmids, selected from yeast colonies harbouring the desirable phenotype. Here, a screening in both *Drosophila* third instar stage larvae and heads from adult flies revealed dDOR-

RE, to interact with Atg8a (Fig. 5.2A). The SID (Selected Interacting Domain) of dDOR was identified to reside between amino acid residues 107-162 and was shown to coincide with the interaction domain of mammalian TP53INP2. It must be noted that the yeast two-hybrid screen was performed after the previously described screening processes (In Chapters 3 and 4) which identified Sequoia and YL-1, however Sequoia, YL-1 and Sir2 were all identified as part of this screen.

Interestingly, input of the dDOR -RE protein sequence into the iLIR tool revealed a candidate LIR motif within the SID: 116-121 (Fig. 5.2 B). This was not representative of an xLIR motif, but rather the classical consensus sequence WxxL, however the tool did reveal this region to be similar to the LIR motif in TP53INP2. These data led on to the investigation of a potential LIR-dependant interaction between Atg8a and dDOR, which will be described in the following sections.

A

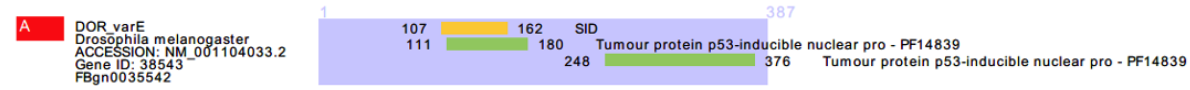

B

Submitted 1 sequence
>NP_001097503.1 diabetes and obesity regulated, isoform E [Drosophila melanogaster]

Motif	Start	End	LIR Sequence	PSSM score	Similar LIRs	Anchor
WxxL	**116**	**121**	**DEWYIV**	**18 (1.6e-02)**	**T53I1 HUMAN 29-34**	**Yes**
WxxL	257	262	SVYHSI	5(1.0e+00)		Yes
WxxL	270	275	DSFVNL	12(1.1 e-01)	OTPN HUMAN 176-181	Yes

Figure 5.2 dDOR has a Predicted LIR motif at Position 116-121.

(A) Results from a yeast-2-hybrid screening conducted by Hybrigenic Services indicate that dDOR variant E is an Atg8a interacting protein, with the selected interacting domain (SID) indicated to be between amino acid positions 107-162. (B) Submission of the dDOR varE (-RE) (Uniprot Q9VZC7_DROME) protein sequence to the iLIR tool revealed a classical consensus (WxxL) LIR motif to be present at position 116-121 (DEWYIV). iLIR server (http://ilir.warwick.ac.uk/): xLIR relaxed LIR motif; WxxL: conventional LIR motif; PSSM: position-specific scoring matrix. Anchor indicates the presence of a disordered region.

5.2.2 Generation of a 6xHIS tagged dDOR plasmid

In order to investigate the interaction between Atg8a and dDOR, plasmids containing each isoform version of dDOR were requested and received from Aurielio Teleman, University of Heidelberg[407]. Since the -RE isoform encodes the $dDOR_{long}$, it was of interest to isolate and excise the DNA of this region, and insert into a plasmid which was of functional use in determining an interaction with Atg8a. Plasmids contain several restriction sites that are specifically recognised by restriction enzymes; these can be used in order to specifically cleave plasmids, allowing for excision and insertion of DNA fragments during sub-cloning. This approach was used to excise $dDOR_{long}$ from the donor plasmid, UAS-$dDOR_{long}$, and cleave it into a recipient plasmid: pET28a (+). This specific plasmid was selected as the presence of the 6xHIS tag allows for the simple detection of dDOR in an interaction assay.

5.2.3 Generation of a dDOR LIR mutant

$dDOR_{long}$ has a candidate LIR motif at position 116-121 with the sequence DEWYIV (Fig. 5.2 B). In order to decipher whether an interaction between Atg8a and $dDOR_{long}$ is apparent, and if this interaction is dependent on this particular LIR, alanine substitutions of the aromatic and hydrophobic residues (W118A and V121A) of dDOR were conducted in order to yield a LIR mutant ($dDOR^{LIRm}$) (Fig. 5.3 A-C).

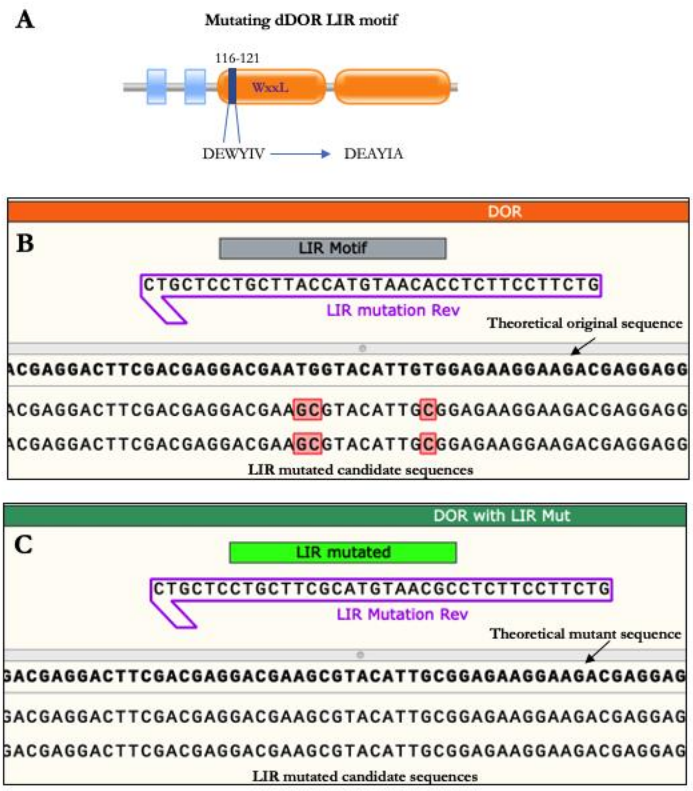

Figure 5.3 Generation of a dDOR LIR mutant

Mutation of the predicted LIR motif in dDOR via alanine substitutions of the aromatic and hydrophobic residues: W118A and V121A. (B-C) Sequencing (conducted by GATC (Biotech (Konstanz, Germany) confirmed successful mutation of the LIR motif through alignment, with the dDOR unmanipulated sequence (B), and with a theoretical LIR mutant sequence (C). All alignments were conducted via SnapGene.

5.3 Investigating the Interaction Between Atg8a and dDOR

5.3.1 dDOR does not bind Atg8a with its DEWYIV LIR domain

Following expression in 'Rosetta2' cells (Fig. 5.4 A, B), an *in vitro* pull-down assay was conducted between 6xHIS-dDOR^{WT} or 6xHIS-dDOR^{LIRm} and GST-Atg8a^{WT} or GST-Atg8a$^{K48A, Y49A}$ (LDS mutant). This confirmed an interaction between 6xHIS-dDOR^{WT} and GST-Atg8a^{WT} (Fig. 5.4 C, D). Surprisingly however, the observed interaction was not significantly reduced in the presence of the Atg8a LDS mutant or the dDOR LIR mutant (Fig. 5.4 C, D). Given that the results of the yeast two-hybrid screening indicated that the region responsible for interaction lies between residues 107-162 of dDOR; this suggests that this sequence may harbour another motif which is responsible for its interaction with Atg8a, or that another motif is required.

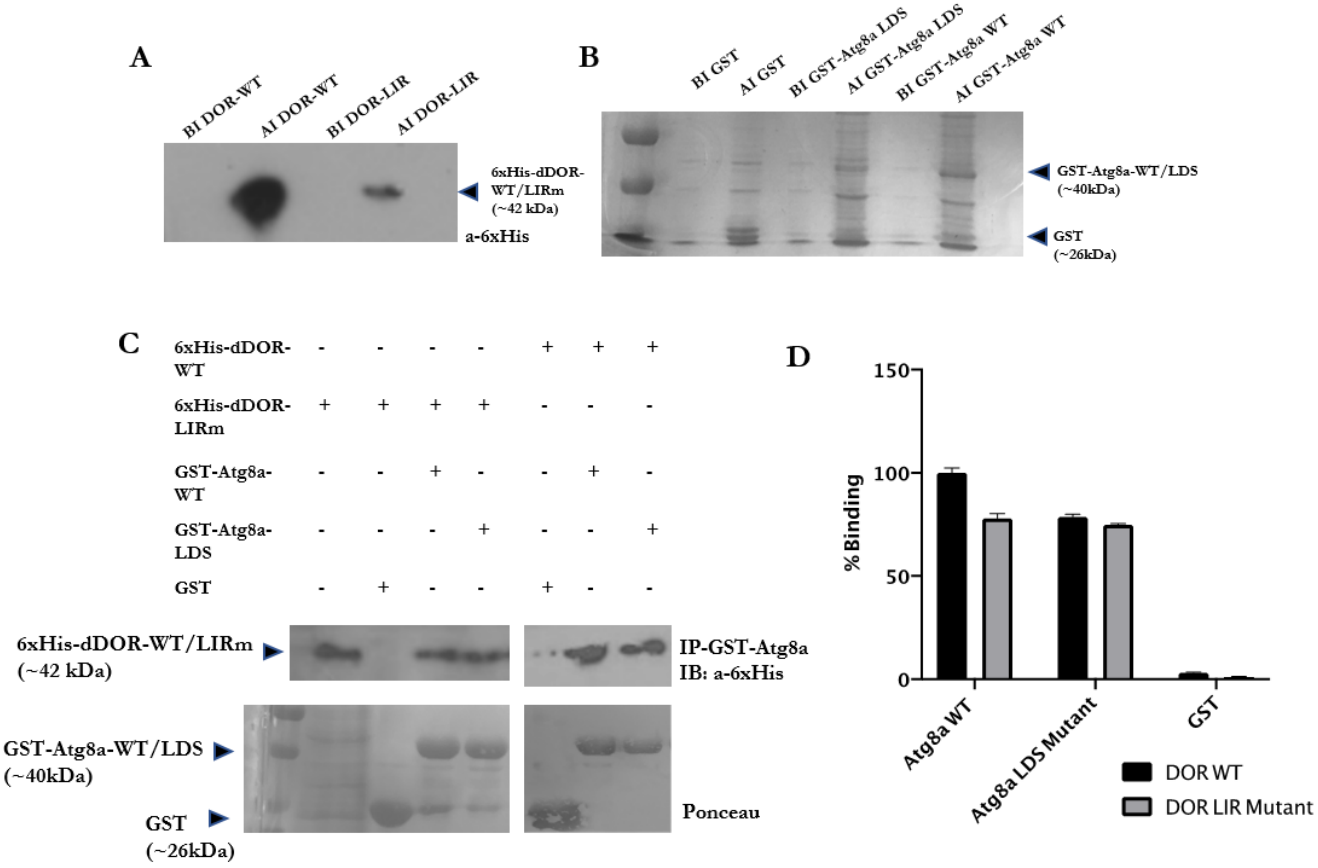

Figure 5.4 dDOR Does Not Interact with Atg8a with its DEWYIV LIR domain

(A-B) Confirmation of protein, dDOR (A) and GST/GST-Atg8a (B), expression in 'Rosetta2; bacterial cells following induction. BI shows total lysate 'before induction' of protein and AI shows 'after induction' of protein (C) GST- pull-down between GST-tagged Atg8a or Atg8a-LDS mutant, and 6xHis tagged dDOR WT and -LIR mutant. GST was used as a negative control. Quantification shown in (D), relative to WT binding and normalised against Ponceau staining. Statistical significance was determined using Student's t test; $p > 0.05$ was indicated in all cases.

5.3.2 The role of the UIM in dDOR binding Atg8a

The UIM-UDS interface was recently uncovered as a new interface required for Atg8a-interacting partners[228] (section 1.6.3). As previously mentioned TP53INP2 has a known UIM, but it is reported to be dispensable in its interaction with LC3/GABARAP[227]. However, given findings indicating that the selected LIR motif of dDOR has an insignificant role in mediating an interaction with Atg8a, our attention turned to the possibility that the presence of a UIM motif could play a role. In order to investigate this, the previously created pET28-6xHIS-dDOR

plasmid was sent to the lab of Terje Johansen, where it was used to construct a Myc-tagged version of dDOR; which was subsequently translated in the presence of ^{35}S-methionne. Based on the structural presence of the UDS in GABARAP, where the UDS lies on its opposite side relative to its LDS[410], a Atg8a UDS mutant was generated by the Johansen lab, via alanine substitutions at residues 76, 77 and 78. The presence of these two well-separated binding surfaces in Atg8-family proteins enables them to simultaneously binding LIR-containing protein to the LDS and a UIM-containing protein to the UDS[410]. Given this, a double-LDS-UDS mutant was also generated (Atg8a $^{Y49A-L76-77-78A}$).

Recombinant GST-Atg8a^{WT} and -Atg8a^{Y49A}, -Atg8a $^{L76-77-78A}$ and -Atg8a $^{Y49A-L76-77-78A}$ were tested for binding with ^{35}S-Myc-dDOR$_{long}$ by Terje Johansen's lab. AR analysis revealed the presence of ^{35}S-containing proteins in the GST fraction. Firstly, this data confirmed an interaction between Atg8a^{WT} and dDOR^{WT}, and showed that mutation of LDS site in Atg8a has only a moderate effect on binding (Fig. 5.5 A, B). Interestingly, it was observed that mutation of UDS site in Atg8a greatly reduces it's binding to dDOR (Fig. 5.5 A, B), highlighting its potential as a binding region. However these results are very preliminary, and will need to be repeated in any future investigation.

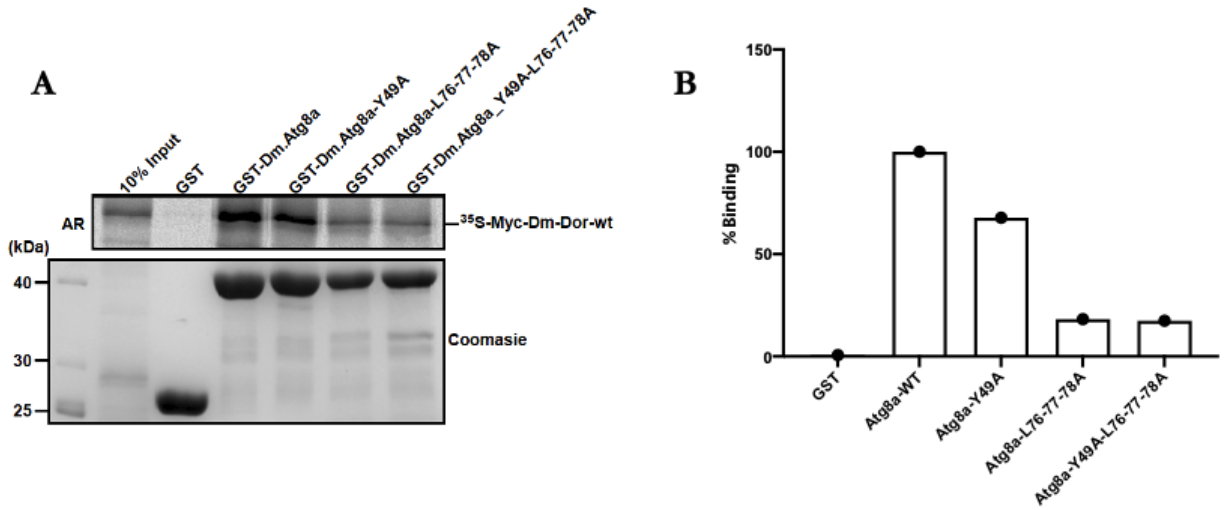

Figure 5.5 Mutation of Ubiquitin Docking Site May Compromise Binding Between Atg8a and dDOR.

GST-pull-down assay between GST-tagged Atg8a-WT, Atg8a-LDS mutant (Y49A), Atg8a-UDS mutant (L76-77-78A) or Atg8a-LDS-UDS mutant (Y49A-L76-77-78A), and ^{35}S-Myc-dDOR$_{long}$. GST was used as negative control. Quantification of the binding is shown in (D), n=1. Experiments presented here were conducted by Johansen Lab, University of Tromsø.

5.3.3 Uncovering a candidate UIM motif in dDOR

Recently it has been reported that TP53INP2, the mammalian homolog of DOR, mediates autophagic degradation of ubiquitinated proteins through its UIM[227]. The UIM sequence of mammalian TP53INP2 is shown in Figure 5.6 A. Interestingly a BLAST search of the TP53INP2 sequence against the *Drosophila* genome revealed that the dDOR- RG[7] to be the only statistically similar sequence result (Fig. 5.6 B). dDOR-RG encodes the $dDOR_{FENLL}$ polypeptide (Fig 5.1 A). All previous work presented here (Figs. 5.4 and 5.5) investigates $dDOR_{long}$ (encoded for by –RE- (Fig. 5.1 A)). Therefore, in order to investigate a potential UIM region in $dDOR_{long}$ its protein sequence was aligned to that of TP53INP2. The area in which the two sequences align in relation to the known UIM of TP53INP2 were not shown to be conserved at the key residues defined by the classical consensus sequence (Fig. 5.6 A, C). Furthermore, the alignment of the TP53INP2 UIM region did not fall within the region of dDOR- RE which was indicated by the yeast-two-hybrid to potential interact with Atg8a (position 107-162 (Fig. 5.2 A)).

Another approach taken to identify a candidate UIM region in dDOR-RE, involved manually scanning the sequence at position 107-162 for potential residues which align with the UIM classical consensus sequence[411]. This revealed a potential region which shows partial similarity to the UIM consensus (Fig. 5.6 D). This region would have to be investigated experimentally in order to decipher if mutation of critical residues disrupt its ability to interact with Atg8a, however this will not be explored any further here.

[7] The NCBINIH search tool refers to dDOR-RE and –RG as 'isoform E' and 'isoform G', respectively, in the output results shown in figure 5.6.

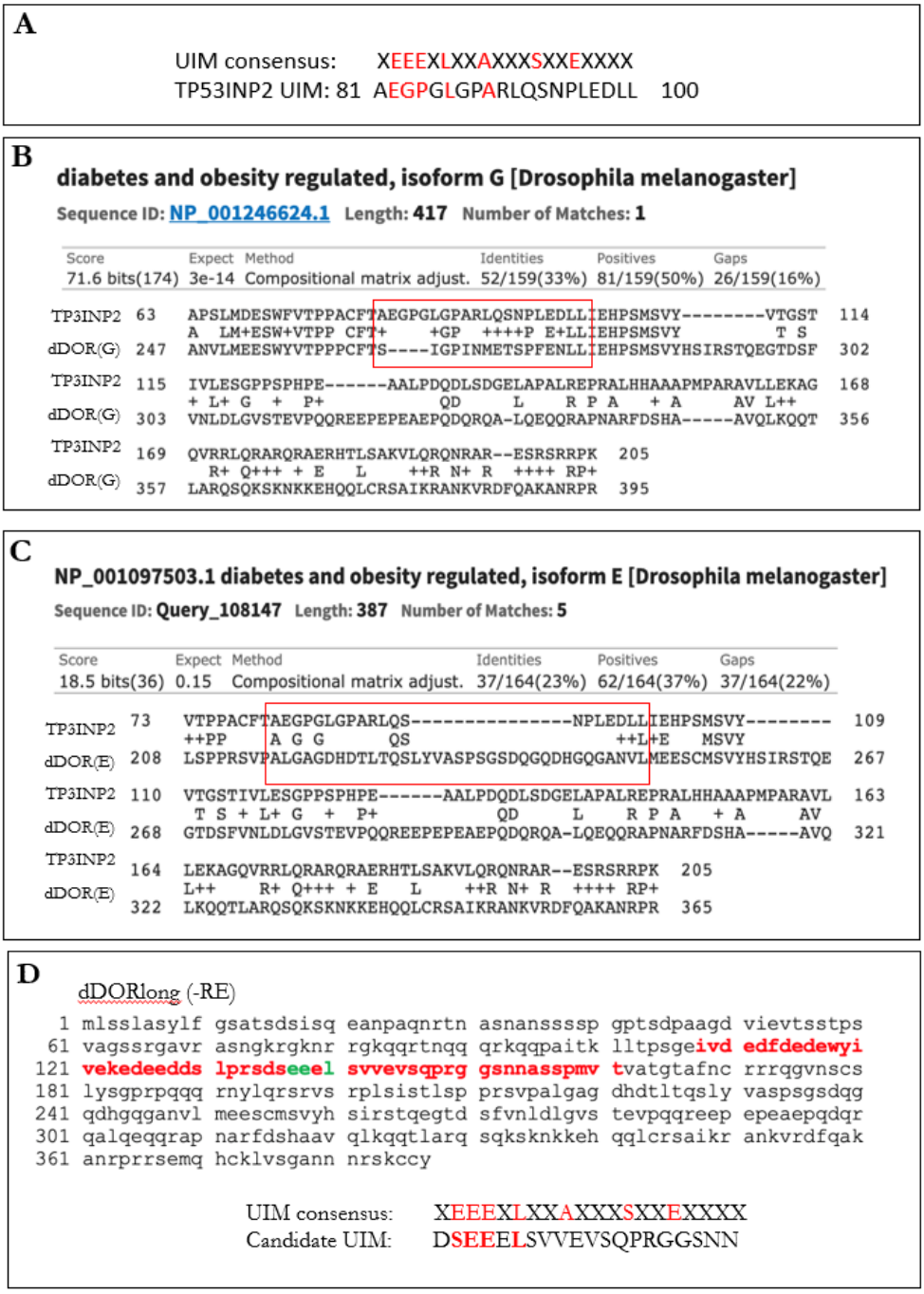

Figure 5.6 Bioinformatics Screening to Predict UIM in dDOR$_{long}$

(A) The classical consensus UIM sequence and the TP53INP2 UIM^{411}. (B) A BLAST (NCBI.NIH) search using the protein sequence of TP53INP2 (query) revealed that the only sequence with significant similarity to it was the dDOR isoform G/-RG (subject). The red box highlights the UIM region in TP53INP2, and where it aligns to dDOR isoform G (-RG). A repeat of the residue in between the alignments indicates that they are identical and the presence of a "+" indicates they are conserved or semi-conserved. (C) Sequence alignment of TP53INP2 (query) and dDOR isoform E/-RE (subject). (D) Sequence Isolation the region of dDOR$_{long}$ (-RE) sequence which was predicted to interact with Atg8a by the Yeast-2-Hybrid (107-162; shown in red), and identification of potential region which is similar to residues shown in the UIM consensus sequence. SEEEL: residues in green are seen to be similar. Full UIM consensus sequence and dDOR E candidate sequence is also shown in panel (D).

5.3.3.1 Investigation of $dDOR_{FENLL}$

A higher level of sequence similarity was observed between dDOR-RG (which encodes $dDOR_{FENLL}$) and mammalian TP53INP2 in the area representative of its UIM (Fig 5.6 B). Interestingly, the domain surrounding the FENLL sequence in DOR_{FENLL} has been shown to have 75% identity and 85% homology to TP53INP2, aligning with its transactivation domain (LEDLL)[407]. The sequences of dDOR-RG and -RE were aligned, confirming that this region is not present in the $dDOR_{long}$ sequence (Fig. 5.7 A). This indicates at the possibility that the FENLL containing sequence region may harbour its own UIM, and thus opens up the possibility that it may have a similar autophagy-related function in *Drosophila* as in its mammalian counterpart. With previous studies reporting $dDOR_{FENLL}$ to bind Atg8a[407], submission of its protein sequence to the iLIR database revealed that it has a candidate motif at position 274-279 (Fig. 5.7 B), which interestingly corresponds to the region of the FENLL sequence. However, given the lower boundary for a LIR PSSM score to be considered is 13[215], a PSSM score of 7 for this region poses a low likelihood of mediating an interaction with the LDS of Atg8a. This further strengthens the possibility that this region may be responsible for binding the UDS in Atg8a. However it cannot be ruled out that this LIR region, or another, may be involved in binding Atg8a.

Given its potential, it was decided that future *in vivo* investigation of dDOR would include both $dDOR_{long}$ and $dDOR_{FENLL}$. The candidate motif which governs the interaction between $dDOR_{FENLL}$ and Atg8a will not be investigated any further. However, future experiments should aim to investigate the interaction between Atg8a and both $dDOR_{long}$ and $dDOR_{FENLL}$. The first step in any future investigation should involve the generation of a number of candidate LIR and UIM mutants for both $dDOR_{long}$ and $dDOR_{FENLL}$ in order to test their interaction with Atg8a, and determine which region/s are responsible for regulating this interaction. It is hypothesised that $dDOR_{long}$ and $dDOR_{FENLL}$ may binding Atg8a through different motifs and therefore may have different roles in the regulation of starvation induced autophagy.

A

Score	Expect	Method	Identities	Positives	Gaps
770 bits(1988)	0.0	Compositional matrix adjust.	386/417(93%)	386/417(92%)	30/417(7%)

```
dDOR(G)   1    MLSSLASYLFGSATSDSISQEANPAQNRTNASNANSSSSPGPTSDPAAGDVIEVTSSTPS  60
                MLSSLASYLFGSATSDSISQEANPAQNRTNASNANSSSSPGPTSDPAAGDVIEVTSSTPS
dDOR(E)   1    MLSSLASYLFGSATSDSISQEANPAQNRTNASNANSSSSPGPTSDPAAGDVIEVTSSTPS  60

dDOR(G)   61   VAGSSRGAVRASNGKRGKNRRGKQQRTNQQQRKQQPAITKLLTPSGEIVDEDFDEDEWYI  120
                VAGSSRGAVRASNGKRGKNRRGKQQRTNQQQRKQQPAITKLLTPSGEIVDEDFDEDEWYI
dDOR(E)   61   VAGSSRGAVRASNGKRGKNRRGKQQRTNQQQRKQQPAITKLLTPSGEIVDEDFDEDEWYI  120

dDOR(G)   121  VEKEDEEDDSLPRSDSEEELSVVEVSQPRGGSNNASSPMVTVATGTAFNCRRRQGVNSCS  180
                VEKEDEEDDSLPRSDSEEELSVVEVSQPRGGSNNASSPMVTVATGTAFNCRRRQGVNSCS
dDOR(E)   121  VEKEDEEDDSLPRSDSEEELSVVEVSQPRGGSNNASSPMVTVATGTAFNCRRRQGVNSCS  180

dDOR(G)   181  LYSGPRPQQQRNYLQRSRVSRPLSISTLSPPRSVPALGAGDHDTLTQSLYVASPSGSDQG  240
                LYSGPRPQQQRNYLQRSRVSRPLSISTLSPPRSVPALGAGDHDTLTQSLYVASPSGSDQG
dDOR(E)   181  LYSGPRPQQQRNYLQRSRVSRPLSISTLSPPRSVPALGAGDHDTLTQSLYVASPSGSDQG  240

dDOR(G)   241  QDHGQGANVLMEESWYVTPPPCFTSIGPINMETSPFENLLIEHPSMSVYHSIRSTQEGTD  300
                QDHGQGANVLMEES                          MSVYHSIRSTQEGTD
dDOR(E)   241  QDHGQGANVLMEESC----------------------------MSVYHSIRSTQEGTD  270

dDOR(G)   301  SFVNLDLGVSTEVPQQREEPEPEAEPQDQRQALQEQQRAPNARFDSHAAVQLKQQTLARQ  360
                SFVNLDLGVSTEVPQQREEPEPEAEPQDQRQALQEQQRAPNARFDSHAAVQLKQQTLARQ
dDOR(E)   271  SFVNLDLGVSTEVPQQREEPEPEAEPQDQRQALQEQQRAPNARFDSHAAVQLKQQTLARQ  330

dDOR(G)   361  SQKSKNKKEHQQLCRSAIKRANKVRDFQAKANRPRRSEMQHCKLVSGANNNRSKCCY  417
                SQKSKNKKEHQQLCRSAIKRANKVRDFQAKANRPRRSEMQHCKLVSGANNNRSKCCY
dDOR(E)   331  SQKSKNKKEHQQLCRSAIKRANKVRDFQAKANRPRRSEMQHCKLVSGANNNRSKCCY  387
```

B

Motif	Start	End	LIR Sequence	PSSM score	Similar LIRs	Anchor
WxxL	116	121	DEWYIV	18 (1.6e-02)	T53I1 HUMAN 29-34	Yes
WxxL	261	266	PCFTSI	5(1.0e+00)		Yes
WxxL	**274**	**279**	**SPFENL**	**7(5.3-01)**		**Yes**
WxxL	287	292	SVYHSI	5(1.0+00)		Yes
WxxL	300	305	DSFVNL	12(1.1 e-01)	OTPN HUMAN 176-181	Yes

Figure 5.7 Sequence Analysis of dDOR$_{FENLL}$ Isoform.

(A) Alignment of dDOR$_{long}$ (subject) and dDOR$_{FENLL}$ (query; Uniprot Q9VZC7_DROME) isoforms using BLAST (NCBI.NIH). The residues 255-285 containing the FENLL sequence (red box) are not present in dDOR$_{long}$ (B) Results reproduced from the iLIR server (http://ilir.warwick.ac.uk/) following input of the protein sequence of dDOR-RG which encodes dDOR$_{FENLL}$. A conventional LIR is present at position 274-279, which falls within the FENLL region, however a low PSSM score of 7 indicates this region is unlikely to constitute a functional LIR motif. xLIR relaxed LIR motif; WxxL: conventional LIR motif; PSSM: position-specific scoring matrix. Anchor indicates the presence of an intrinsically disordered region.

5.4 dDOR in Autophagy

As an interaction between Atg8a and dDOR is considered likely (Fig. 5.4), its potential role in starvation induced autophagy was explored.

5.4.1 dDOR accumulates in autophagy deficient mutants

Whole body lysates were prepared from 7-day old WT and Atg8a^{KG} flies, starved for 4 hours in 20% sucrose. Proteins were separated by SDS-PAGE and wet-transferred onto nitrocellulose membranes, to be probed with an anti-dDOR antibody which was kindly received from Aurielio Teleman[407]. The dDOR band was predicted to be at 52 kDa. The membranes were then stripped

and re-probed using an anti-Ref(2)P antibody; a known substrate of autophagy, which was used for comparison. As expected, Ref(2)P was seen to accumulate in autophagy mutant flies with around a fifteen-fold increase observed. Similarly, an observed twelve-fold increase in the amount of dDOR was recorded in autophagy mutants compared to the WT flies (Fig. 5.78 A, B). This increase is statistically significant by some margin and gives evidence that dDOR degradation may be a general autophagy phenomenon, rather than being specific to its interaction with Atg8a. This observation provides evidence that upon the induction of autophagy, dDOR is either present in the cytosolic region and functions localises to the autophagosome where it is degraded, or that protein production is transcriptionally downregulated.

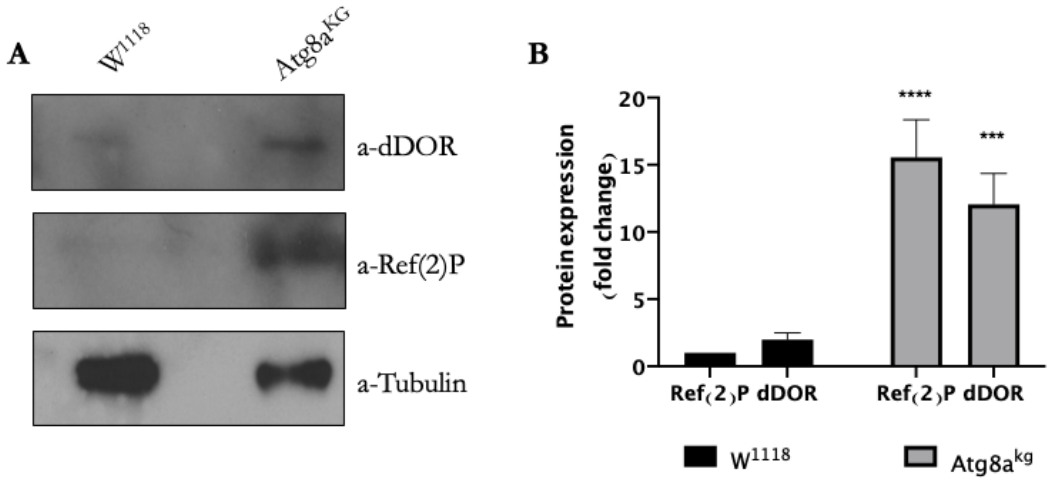

Figure 5.8 dDOR Protein Accumulates in Autophagy Mutant.

(A) Whole body lysates from starved WT (W^{1118}) and $Atg8a^{KG}$ mutant flies were subjected to SDS-PAGE and immunodetection using antibodies against dDOR and Ref(2)P. Tubulin was used as loading control. (D) Ref(2)P and dDOR protein expression quantification in W^{1118} versus Atg8a mutant flies. Bars denote ± SD, n= 3 independent experiments. Fold change relative to levels of Ref(2)P in WT, and normalised against Tubulin. ***p <0.0005- ****p<0.0005.

5.4.2 $Atg8a^{K46Q}$ shows a reduction in binding to dDOR

To explore whether the interaction between dDOR and Atg8a is regulated by the acetylation status of Atg8a in fed conditions (when Atg8a is acetylated) and in starved conditions (when Atg8a is deacetylated); the binding of $Atg8a^{WT}$ and Atg8a acetylation mimics (K46Q and K48Q),

to dDOR was examined. Despite mass-spectrometry revealing that region K46 of Atg8a is acetylated in fed conditions (Fig. 4.2), it was also previously found that acetylation mimic K46Q had little effect on its ability to bind to Sequoia (Fig. 4.3). Here however, acetylation at K46 was observed to have a moderate effect on binding to dDOR (Fig. 5.9 B, C), whereas the K48, which had previously showed a significant reduction in its binding to Sequoia (Fig. 4.3), had no effect in its ability to bind dDOR (Fig. 5.9 B, C). Future experimentation should be aimed towards investigating if Atg8a acetylation of regions K46 and K48 independently regulate the interaction with Sequoia and dDOR in fed conditions, respectively. How acetylation of K46 impacts the structural conformation of the interaction between Atg8a and dDOR would need to be investigated further.

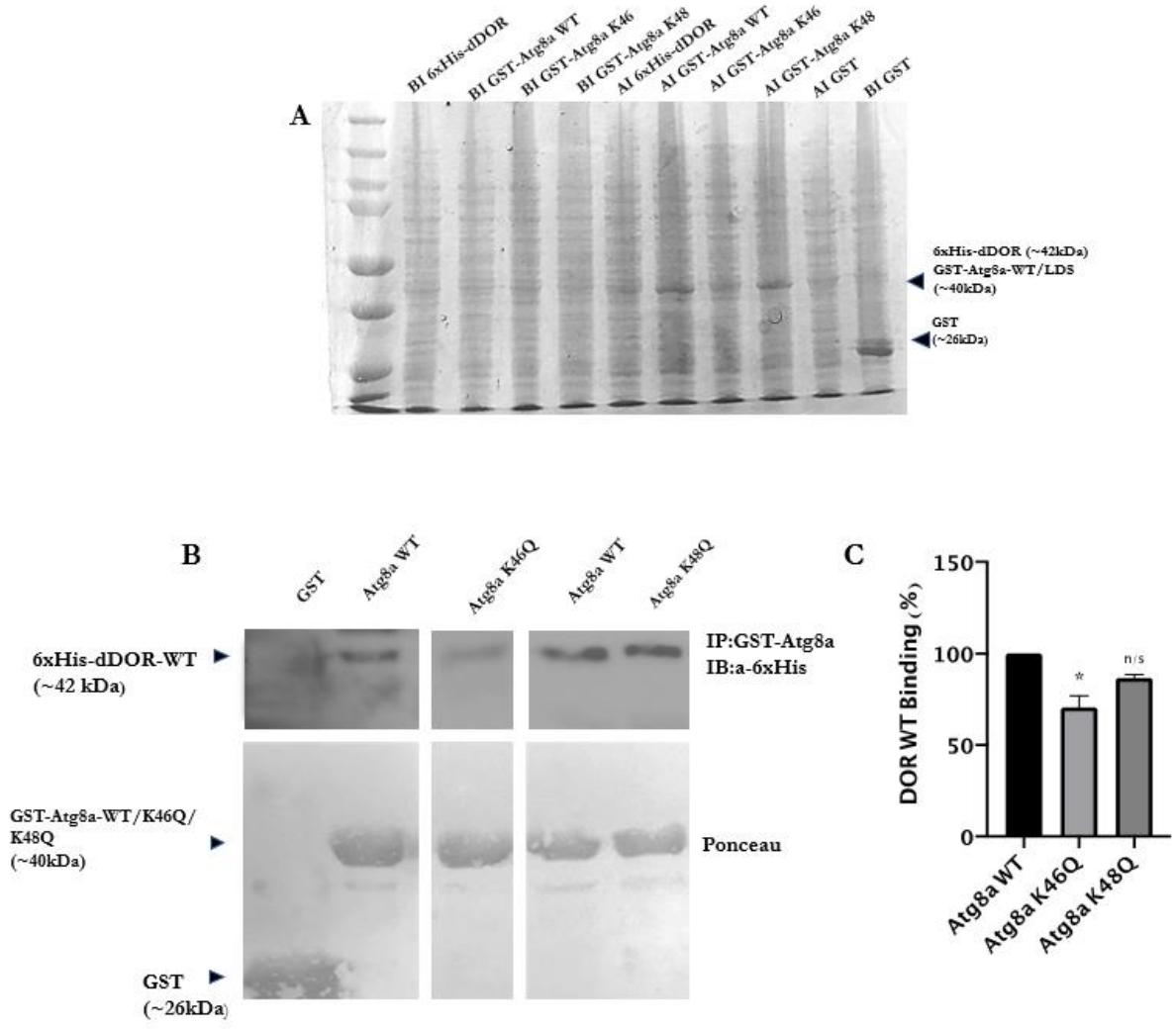

Figure 5.9 Investigating the Effects of Atg8a Acetylation on dDOR Binding.

(A)Confirmation of protein expression in Rosetta2 bacterial cells following induction. BI= before protein induction, AI= after protein induction. (B) GST- pull-down between GST-Atg8a -WT, -K46Q and -K48Q with 6xHis tagged dDOR WT. GST was used as a negative control. Quantification shown in (C), relative to WT binding and normalised against Ponceau staining. Bars denote ± SD. Statistical significance was determined using Student's t test; *$p < 0.05$. n.s= not significant ($p>0.05$).

5.4.3 Does deacetylated Atg8a bind dDOR and Sequoia equally?

It is hypothesised that dDOR and Sequoia bind Atg8a through two independent motifs and that both bind more strongly to deacetylated Atg8a. In order to explore this mechanism further, the strength of Atg8a binding to Sequoia was compared to that of dDOR. A GST-pulldown assay was conducted between GST-Atg8a^{WT} with 6xHis-Sequoia^{WT} and 6xHis-dDOR^{WT}. Through the

use of anti-6xHis, no significant difference was observed in the binding of the two proteins with GST-Atg8a (Fig. 5.10). However this particular assay is not conclusive enough to determine if dDOR competes with Sequoia in binding Atg8a. In order to investigate this mechanism more robustly, a competitive binding assay could be employed. This would allow for the binding affinity of dDOR and Sequoia for Atg8a to be assessed. Typically this assay measures the binding a labelled ligand (i.e. 6xHis-Sequoia) in the absence and presence of an unlabelled ligand (i.e. $dDOR^{WT}$) and calculates the concentration that displaces 50% of the labelled molecule from the binding site.

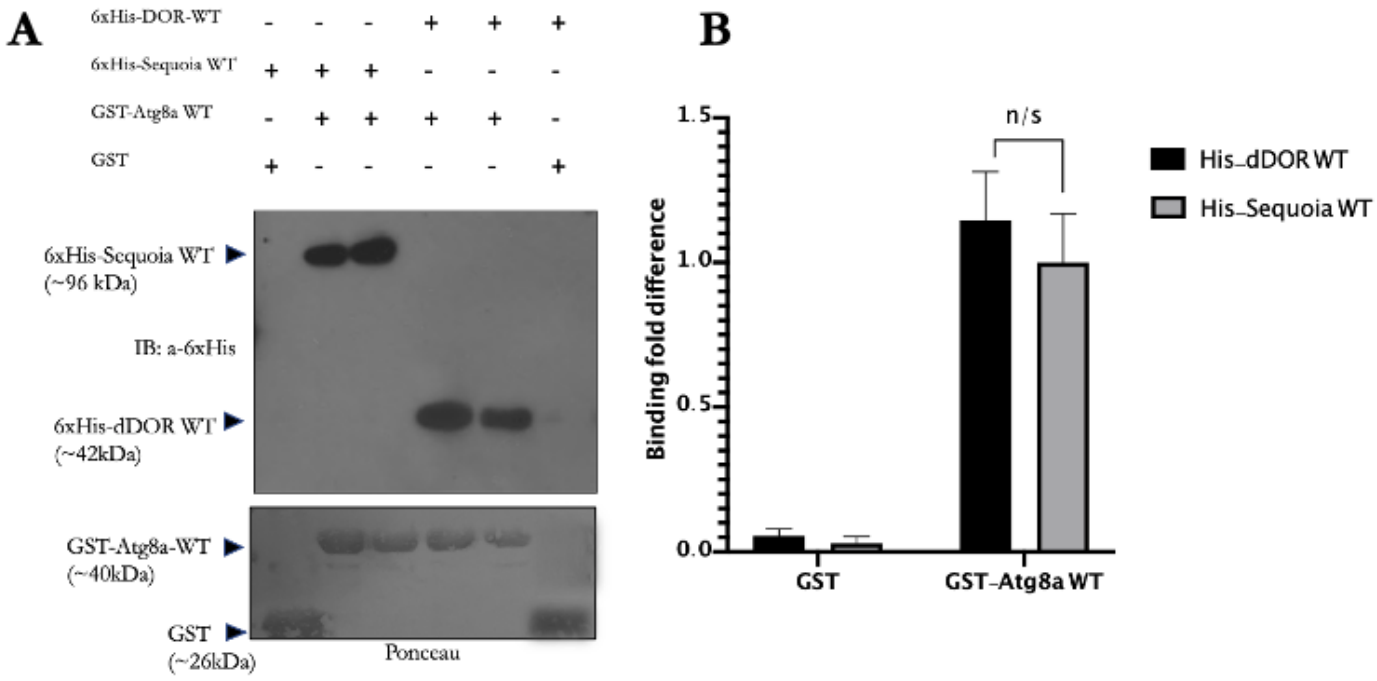

Figure 5.10 Atg8a Binds to dDOR and Sequoia Equally *in vitro*.

(A) GST- pull-down between GST-tagged Atg8a with 6xHis tagged -dDOR WT and -Sequoia WT. GST was used as a negative control. Two independent biological replicates are shown here side by side. Quantification shown in (B), fold difference calculated relative to Atg8a-Sequoia binding and normalised against Ponceau staining. Bars denote ± SD. Statistical significance was determined using Student's t test; $p > 0.05$ was indicated between conditions.

5.4.4 Assessing the transcriptional impact of dDOR in fed conditions

It was of interest to assess whether dDOR, like Atg8a was associated to the promotor region of *Atg* genes, either by virtue of an interaction with Sequoia (as shown in the case of Atg8a) or by direct binding. This would also allow an assessment of the role of dDOR under basal conditions from a transcriptional perspective. In terms of its impact on transcription in *Drosophila*; in context of metamorphosis, $dDOR_{FENLL}$ has been shown to bind and activate the EcR (Ecdysone Receptor) and is needed for maximal transcriptional activity of the EcR[407], however no transcriptional role has been reported in relation to the $dDOR_{long}$ isoform.

In order to explore if dDOR is associated to the promotor regions of *Atg* genes in fed conditions, a ChIP assay was conducted using the previously described anti-dDOR. A similar investigation has been described in mammalian cells using a specific anti-DOR antibody in order to measure enrichment at the promotor region of thyroid hormone receptor genes[402]. Previously established ChIP conditions were used, with 150 WT larvae collected, dissected and subjected to ChIP using anti-dDOR and normal rabbit IgG as a control for nonspecific precipitation. Real Time-qPCR was performed on input (no ChIP) and output (ChIP) DNA, for direct comparison, with previously optimised primers complementary to the promotor genomic loci of the following set of *Atg* genes: *Atg1, Atg5, Atg7, Atg8a, Atg13 and Atg14*. Additionally, *Tubulin* was included as a non-*Atg* gene control. Analysis of fold enrichment levels relative to input DNA revealed dDOR to be significantly enriched the promotor of *Atg8a* in comparison to the IgG control (Fig. 5.11 A). No significant enrichment was measured at any other loci.

In order to uncover further the transcriptional influence of dDOR of in fed conditions, relative mRNA expression analysis was carried out on a *dDor*-RNAi line, obtained from VDRC. This line had previously been reported to result in a significant reduction in autophagosomes and autolysosomes in wandering third-instar stage larvae during the onset of developmental autophagy[339]. *dDor*-RNAi flies were crossed with Cg-GAL4 virgin females in order to express the RNAi construct in the fat body, with *luciferase*-RNAi was used as a control. RNA was extracted from pre-wandering third-instar stage larvae of the F1 progeny in fed conditions. Here, a significant knock-down of *dor* was established (Fig. 5.11 B). Interestingly, the relative mRNA expression of *Atg8a* was seen to be higher in the *dDor*-RNAi in comparison to the *luciferase*-RNAi control (Fig. 5.11 C). This hints at the possible role of dDOR in maintaining lowered levels of *Atg8a* under fed conditions. Although, expression levels were quite variable over the three experiments, as reflected by the sizeable error bars, a convincing degree of significance was

calculated. Given that knock-down of *dor* did not have any effect on the regulation on any other *Atg* gene investigated, it is suggested that the role of dDOR may be tightly linked to the expression of *Atg8a* in fed conditions.

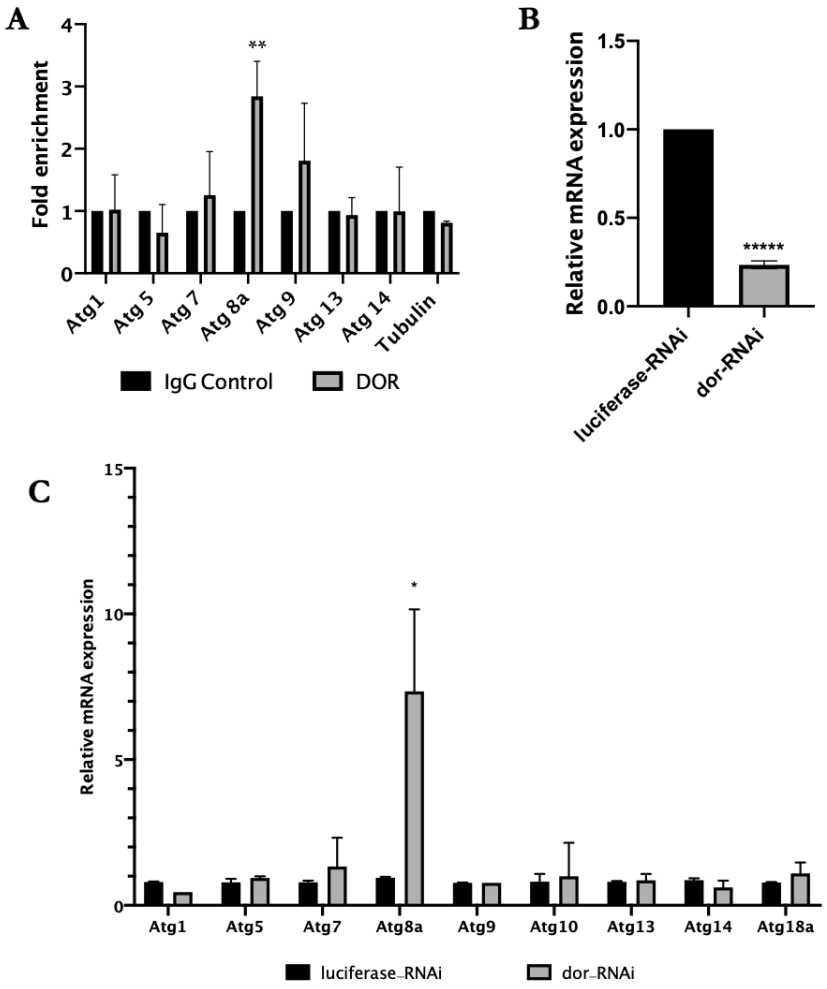

Figure 5.11 dDOR Regulates the Expression of *Atg8a* in Fed Conditions.

(A) ChIP assay to query enrichment of dDOR at promotor of Atg genes using anti-dDOR. IgG was used as a negative control, and *Tubulin* as a non-*Atg* gene control. (B) Analysis of the mRNA levels of and *dor* in control (luciferase-RNAi) and dDOR depleted (*dDor-RNAi*) fat bodies in fed conditions, using real-time qPCR. Expression levels are shown relative to the control and normalised to the expression of *rp49* (housekeeping gene). (C) mRNA expression analysis of *Atg* genes in control (luciferase-RNAi) and dDOR depleted (*dDor-RNAi*) fat bodies in fed conditions. In all cases, n= 2 independent experiments, bars denote ± SD, statistical significance was determined using a Student's t-test; **p < 0.05 and ****p < 0.0005. Genotype: *Cg-GAL4/+; UAS-luc-RNAi/+*. *Cg-GAL4/+; UAS-dor-RNAi/+*.

5.5 Investigating dDOR *in vivo*

5.5.1 Generating FLAG-tagged dDOR transgenic lines

Having verified the interaction between dDOR and Atg8a, work proceeded to investigate whether this association is maintained *in vivo*. For this purpose, transgenic flies overexpressing either the long or FENLL isoforms of dDOR, with a 3xFLAG-tag appended at the N-terminus were generated. To do this, long and FENLL isoforms were cloned into recipient plasmid UAS-3xFLAG-dTak1 was kindly gifted by Panos Tsapras (Nezis lab, University of Warwick). The insertion of the P-element in the *Drosophila* genome is random and thus produces different expression levels depending on where it is inserted[412]. A total of 5 lines for UAS-3xFLAG-$dDOR_{long}$ and 5 lines for UAS-3xFLAG-$dDOR_{FENLL}$ (all on the 3rd chromosome) were received from BestGene Inc. All lines appeared to be healthy with the exception of $dDOR_{long}$ line 5, which seemed to struggle with mobility and had a very short lifespan.

5.5.2 Investigating the localisation of dDOR in the induction of autophagy

Males from the dDOR transgenic lines were crossed with virgin females, carrying an insertion for the recombinant mCherry-Atg8a system[202]. As the effects of ectopic overexpression of $dDOR_{long}$ and $dDOR_{FENLL}$ on fly physiology and viability was unknown, no heat-shock was applied in order to limit the activity of the system promotor flipase. The resulting F1 progeny of these crosses will contain double recombinant clones in every tissue, that express 3xFLAG-$dDOR_{long}$ or $dDOR_{FENLL}$ and mCherry-Atg8a. The induction of autophagy can easily be monitored here as autophagosomes formed in these clones are clearly visible due to the mCherry-tag on Atg8a, which coupled to the use of anti-FLAG, allows the assessment of the localization of $dDOR_{long}$ and $dDOR_{FENLL}$ in fed and starved conditions.

Of the ten genetic crosses (five lines from each construct: $dDOR_{long}$ and $dDOR_{FENLL}$), six were observed to lay well. Third instar stage larvae from successful crosses were either collected directly from full nutrient conditions or subjected to four-hour starvation in 20% sucrose in order to induce autophagy. Fat body tissues were subsequently isolated, processed by IF using anti-FLAG and directly observed by confocal microscopy.

5.5.2.1 dDOR predominantly localises to the nucleus in fed conditions

In fed conditions 3xFLAG-dDOR$_{long}$ was found to localise predominantly in the nucleus, as had been reported in mammalian cell lines[339]. All three lines showed a similar visual pattern, with strong nuclear localisation of dDOR, and the presence of some sporadic structures in the cytosolic compartment (Fig. 5.12 A-C). It was considered that some of the signal observed in the cytosol may be a product of diffused staining, however since the appearance of distinctive puncta (Fig 5.12 A'-C', yellow arrows) is apparent, and given that staining was not observed in neighbouring non-recombinant cells, it is likely to be specific for dDOR. Furthermore, ImageJ was used 'clean' the images to remove the presence of 'noise', with the cytoplasmic speckles significant enough to remain following this procedure. In the case of dDOR$_{FENLL}$, localisation was also predominantly seen in the nucleus under fed conditions Fig. 5.12 D-F), however the number of distinctive structures within the cytosol were less apparent in comparison to dDOR$_{long}$ (Fig. 5.12 D'-F'). These observations are however not strong enough to draw any conclusions in the differences between the expression of dDOR$_{long}$ and dDOR$_{FENLL}$ *in vivo*.

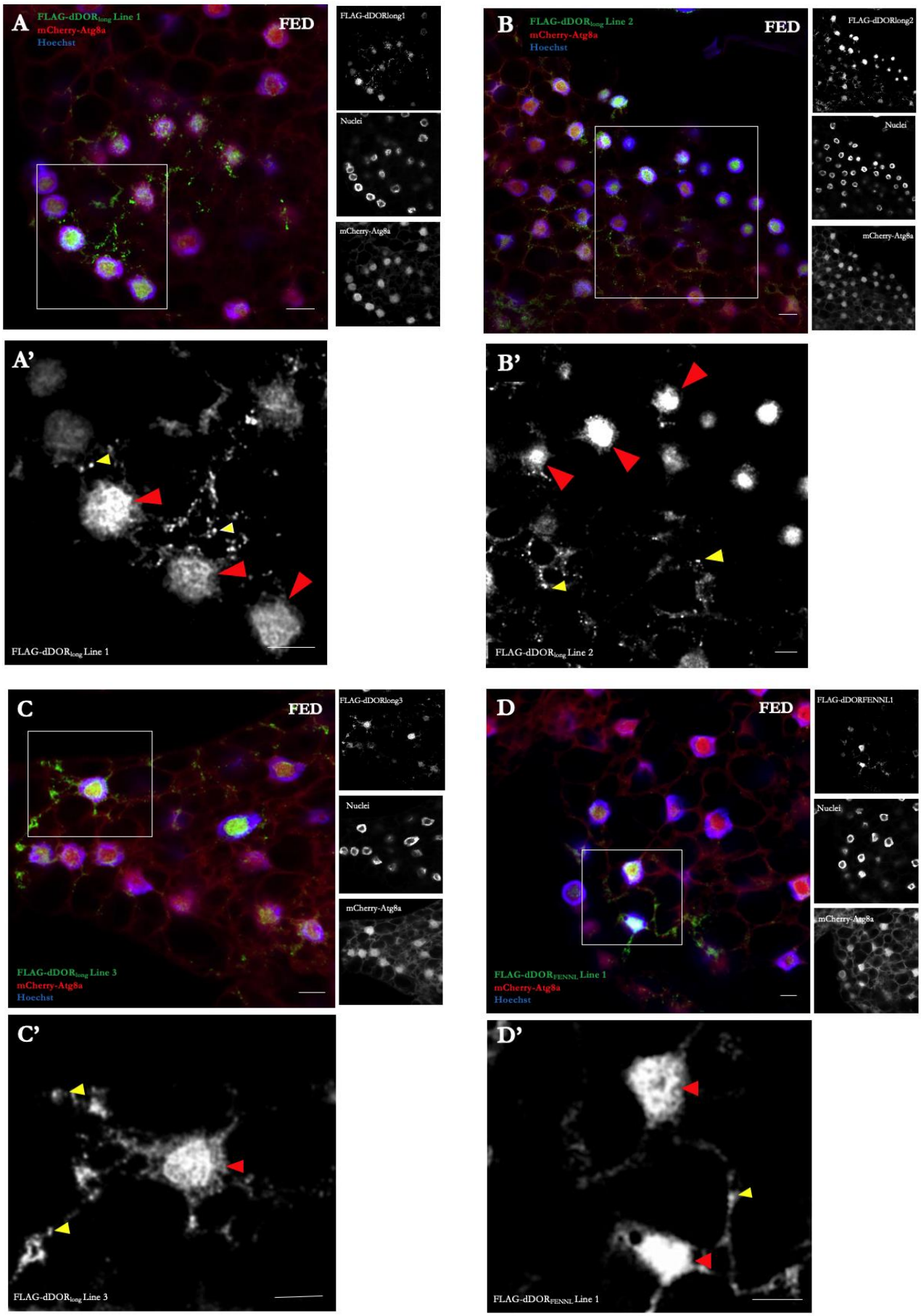
A
FLAG-dDORlong Line 1
mCherry-Atg8a
Hoechst
FED
FLAG-dDORlong1
Nuclei
mCherry-Atg8a
B
FLAG-dDORlong Line 2
mCherry-Atg8a
Hoechst
FED
FLAG-dDORlong2
Nuclei
mCherry-Atg8a
A'
FLAG-dDORlong Line 1
B'
FLAG-dDORlong Line 2
C
FED
FLAG-dDORlong3
Nuclei
mCherry-Atg8a
FLAG-dDORlong Line 3
mCherry-Atg8a
Hoechst
D
FED
FLAG-dDORFENNL1
Nuclei
mCherry-Atg8a
FLAG-dDORFENNL Line 1
mCherry-Atg8a
Hoechst
C'
FLAG-dDORlong Line 3
D'
FLAG-dDORFENNL Line 1

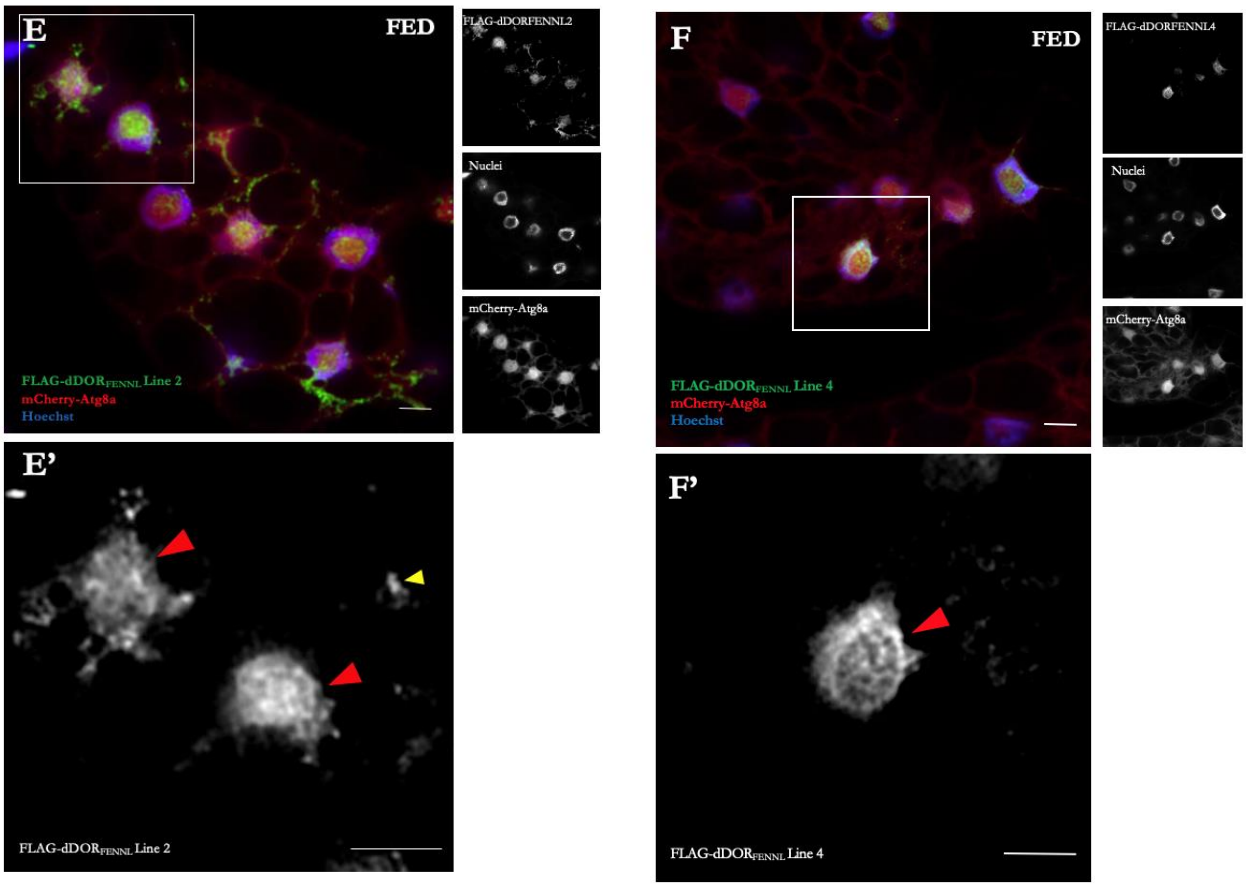

Figure 5.12 Localisation of dDOR in Newly Generated Transgenic Lines.

Confocal sections of fat body from pre-wandering third-instar larvae, clonally expressing mCherry-Atg8a and either (A-C) FLAG-dDOR$_{long}$ (lines 1-3) or (D-F) FLAG-dDOR$_{FENLL}$ (lines 1, 2 and 4), under fed conditions. The grayscale panels (A'-G') show the anti-FLAG stained (green) channels from an example area (box) in the merged picture. Yellow arrows indicate examples of the presence of cytosolic structures, and red arrows of staining concentrated to the nucleus. Scale: 10um. Genotypes: *yw hs-Flp;Ac > CD2 > GAL4/+;UAS-mCherry-GFP-Atg8a/UAS-3xFLAG-dDOR$_{long}$*, *yw hs-Flp;Ac > CD2 > GAL4/+;UAS-mCherry-GFP-Atg8a/UAS-3xFLAG-dDOR$_{FENLL}$*.

5.5.2.2 dDOR exits the nucleus in response to nutrient starvation

Given that dDOR$_{long}$ line 1 and dDOR$_{FENLL}$ line 1 produced larvae in higher abundance in comparison to other lines, these lines were used to investigate the localisation of dDOR in parallel starvation conditions. In cells exhibiting the induction of autophagy through the accumulation of Atg8a positive puncta in the cytoplasm, dDOR$_{long}$ and dDOR$_{FENLL}$ was observed to exit the nucleus and reside exclusively in the cytoplasm (Fig. 5.13 A-B). It must be noted that anti-FLAG staining may be somewhat diffused in certain regions of clones presented here,

however as observed in fed conditions, the presence of individual bright green spherical structures is indicative of dDOR specificity.

Interestingly, image analysis using 'co-loc2' indicated a moderate level of co-localisation between cytoplasmic Atg8a and $dDOR_{long}$ and $dDOR_{FENLL}$. Across both constructs, not all dDOR were seen to co-localise with Atg8a, indicating that perhaps dDOR is only able to interact with a subset of Atg8a structures. This was reflected in the modest Pearson coefficient values generated for each line, which considers points across the entire cytosolic compartment. The presence of overlapping fluorescent puncta between channels however (Fig. 5.13 A-B, yellow and white arrows), is indicative of protein co-residency at a specific point. Although co-localisation is not an indication of physical interaction, it does strengthen the possibility of a cytoplasmic interaction between the two proteins. No significant difference in Atg8a co-localisation between $dDOR_{long}$ and $dDOR_{FENLL}$ was observed.

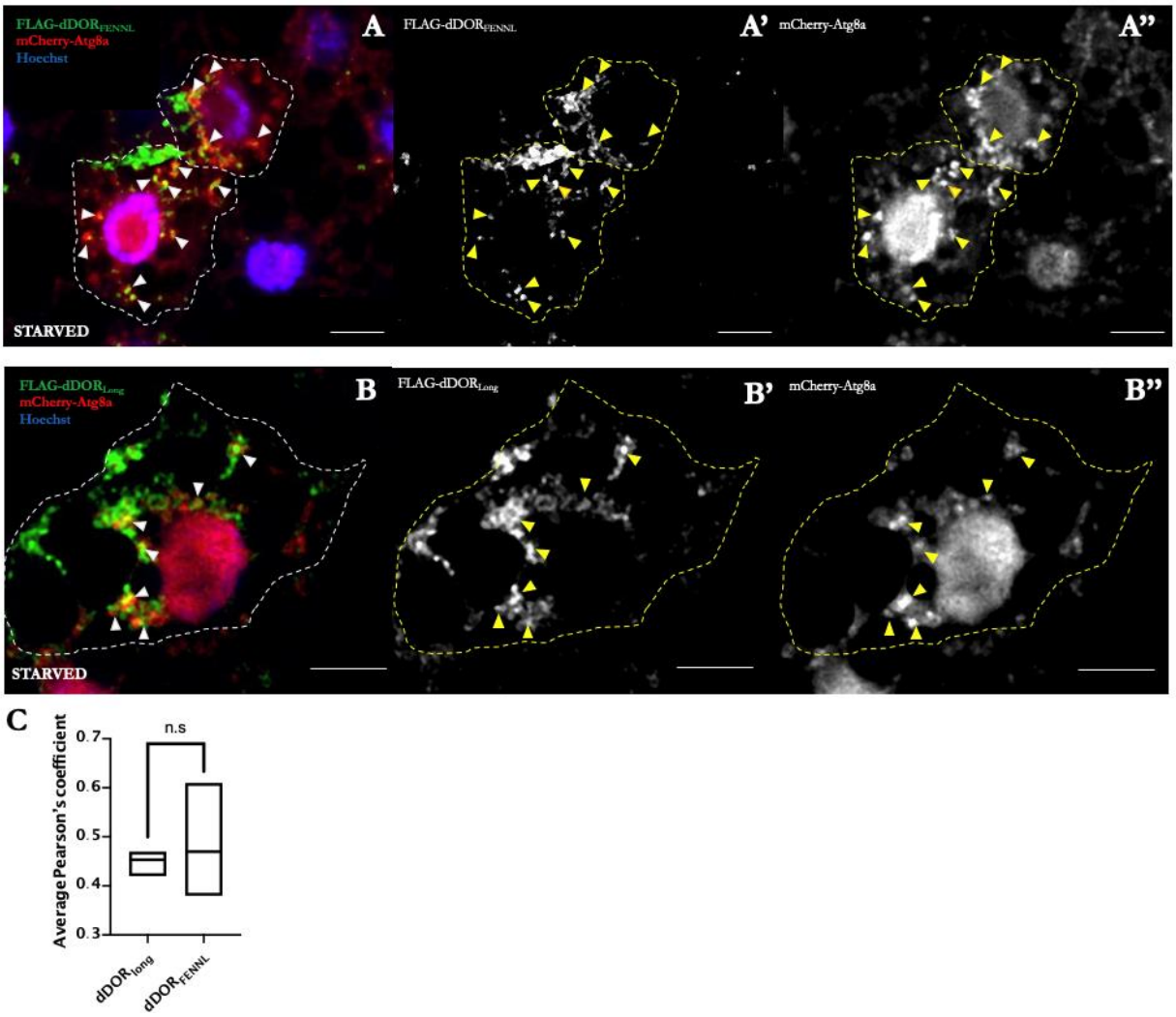

Figure 5.13 dDOR Exits the Nucleus with Atg8a During Starvation Induced Autophagy.

Confocal sections of fat body from starved pre-wandering third-instar larvae, clonally expressing mCherry-Atg8a and either (A) FLAG-dDOR$_{long}$ (line 1) or (B) FLAG-dDOR$_{FENLL}$ (line 1). The grayscale panels show split channels, with yellow arrows are indicative of overlapping regional points across channels. Scale: 10m. (C) Quantification of the Colocalisation of FLAG-dDOR and mCherry-Atg8a signals, using Pearson's correlation coefficient. Box plot denotes ± SD and average. Two-tailed Student's t-test showed p> 0.05. Genotype: *yw hs-Flp;Ac > CD2 > GAL4/+;UAS-mCherry-GFP-Atg8a/UAS-3xFLAG-dDOR$_{long}$, yw hs-Flp;Ac > CD2 > GAL4/+;UAS-mCherry-GFP-Atg8a/UAS-3xFLAG-dDOR$_{FENLL}$*.

5.6 End of Chapter Conclusions

In order to begin to uncover the mechanism by which Atg8a leaves the nucleus, our investigation turned its attention to diabetes- and obesity-regulated nuclear factor, DOR. In mammalian cells, DOR interacts with LC3/GABARAP, exits the nucleus, and targets to autophagosomes through mTOR[339]. Here we show similar results in *Drosophila*; where under full nutrients conditions dDOR predominantly localises to the nucleus (Fig. 5.12), with starvation

conditions causing dDOR to exit and localise to the cytoplasm (Fig. 5.13). Indications that dDOR co-localises with Atg8a in the cytoplasm (Fig. 5.13) and may degraded by autophagy (Fig. 5.7), hint towards its localisation to autophagosomes. Furthermore, dDOR is observed to interact with a subset of cytoplasmic Atg8a structures (Fig. 5.13), which is consistent to findings reported in mammalian cells[339]. As dDOR is observed to be present in small amounts in the cytoplasm during full nutrient conditions (Fig. 5.12), it is speculated that these structures may be representative of those which do not co-localise with Atg8a in the cytoplasm during starvation conditions. However the dDOR structures present in the cytoplasm may be as a result of basal autophagy in the cells.

Modifications at position K46 were confirmed to play a role in the induction of autophagy with results from mass spectrometry indicating this region to be acetylated in fed conditions, and de-acetylated in starved (Fig. 4.2). With acetylation at position K46 observed to moderately weaken the binding of Atg8a to dDOR, it is inferred that deacetylation of this region may play a role in the translocation of Atg8a-bound dDOR into the cytoplasm. This proposition is in accordance with results in mammalian cells, where the nuclear exit of LC3-DOR is dependent on the deacetylation of LC3 by SIRT1 at K49 and K51, and that the LC3 K49Q-K51Q mutant shows weaker interaction with mammalian DOR[158]. Results here also point towards the ability of dDOR to modulate the expression of *Atg8a* in fed conditions, given that dDOR was both detected at its promotor and its expression is upregulated in a *dor* deplete setting (Fig. 5.11).

CHAPTER 6. THESIS DISCUSSION

6.1 Screening with the iLIR tool

The bioinformatics-based screening presented in Chapter 3 represents the ongoing efforts of our lab to identify novel Atg8a-interacting proteins. The refinement of the canonical LIR motif and the development of the iLIR tool[215] has provided an excellent platform in identifying candidates; with previous work leading to the identification of the novel adaptor LIR-motif containing protein, Kenny[202].

6.1.1 The evolution of the LIR

The interaction between Sequoia's mammalian homolog KDM4A and GABARAP-L1 (the closest mammalian homolog to Atg8a) has been shown by Johansen's lab; however, the interaction does not depend on a functional LIR motif (Appendix paper A; S1 B,C)[376]. This may be related to the loss of the functionality of the LIR motif during evolution, as it has been shown for Kenny and its mammalian homolog, inhibitor of nuclear factor kB kinase (NF-kB) subunit g/NF-kB essential modulator (IKKg/NEMO)[202]. Sequence analysis of Sequoia in comparison to its homologues throughout the *Drosophila* genus, revealed that the motif is very well preserved (Fig 6.1 A). This trend is also apparent in more distant relatives in the fly family, where it is observed that both aliphatic and aromatic residues remain intact, with the composition of the LIR being very similar. Exploration outside of the fly family yielded no trace of a similar LIR in candidate homologues, however this it is hard to infer at which point the LIR motif begun to diverge given that there is not enough data available from species that may be of interest. Interestingly, sequence query of the Rph1 via the iLIR tool revealed a candidate xLIR motif with the sequence EEWLPI (Fig 6.1 B). The position of the key residues (EE**W**LP**I**) correspond to those found in Sequoia, suggesting that this LIR motif is conserved from yeast to *Drosophila*; however, its function remains to be explored experimentally in yeast.

As a prerequisite to large scale interaction- screening, the iLIR tool can be used to query the dependency of the motif in an already predicted interaction. This was the case when a yeast-2-hybrid screen revealed an interaction between Atg8a and dDOR. Querying the dependency of LIR motif in an interaction can be considered as a very useful and fruitful route in the preliminary investigations of a protein, especially given the tools, such as the Atg8a LDS mutant, which have been developed. Given the reports that the mammalian homolog of dDOR,

TP53INP2, depends on a functional LIR motif in order to interact with LC3[413], this may be indicative of a gain of functionality during LIR motif evolution from *Drosophila* to mammals.

A

```
Drosophila melanogaster   259  GDEEDDDENG----MLHVKYEEQSLEHDPENEHDAEQEHEYEEYQVIKAEVEAEAAELAA  314
Drosophila sechellia      256  GDEEDDDENG----LLHVKYEEQSLEHDPENEHDAEQEHEYEEYQVIKAEVEAEAAELAA  311
Drosophila simulans       195  GDEEDDDENG----LLHVKYEEQSLEHDPENEHDAEQEHEYEEYQVIKAEVEAEAAELAA  250
Drosophila pseudoobscura  843  DDEESGLQAKYDDDGLQVKYEEQEQDLDQ--------GQDYEEYQVIKAEVEAEAAEQAA  894
Drosophila persimilis     273  DDEESGLQAKYDDDGLQVKYEEQEQDLDQ--------GQDYEEYQVIKAEVEAEAAEQAA  324
Drosophila guanche        868  DDEESGLQAKYEDEGLQVKYEEQEQDLDQ--------GQEYEEYQVIKAEVEAEAAEQAA  919
Drosophila grumshawi      274  DEELLE-EDEEEESGLRVKYEEQSLEH-D--------DHDFEEYQVIKAEVEAEAAEQAA  323
Drosophila navojoa        315  DEEMLE-ED--EESGLQVKYEEQSMEH----------DHDFEEYQVIKAEVEAEAAEQAA  361
Drosophila willistoni     266  EEQEDDDEGGDEGAGLQVKYEEQSLDN----------DQYEEYQVIKAEVEAEAAEQAA  314
Sacrophage bullata        259  ---IHTQQPQNQQQDVVVKYEDQSLDD----------DSYEEFLSVSQSPQKEQ---QQ  301
Lucilia cuprina           868  ---QH-SQQQLQQQEVIVKYEDQSLDD----------DSYEEFQAVSQSPQKDQ---QQ  909
Musca domestica          1001  ---QQQQQQHHQQQEVIIKYEDQSLDD----------DSYEEFQSIAS-PQKDQQ-NGG 1044
                                     :       : :***:*. :             ..:**:  :    : :
```

B

> Rph1

Motif	Start	End	LIR Sequence	PSSM score	Similar LIRs	Anchor
xLIR	341	346	EEWLPI	19 (1.2e-02)	Q9SB64_ARATH 659-664	No

Figure 6.1 The Evolution of the LIR motif in Sequoia.

(A) Protein sequence alignment via COBALT revealed the LIR motif of Sequoia in *Drosophila Melanogaster* (orange) to be well conserved (*) throughout the *Drosophila* genus (yellow) or to be functionally similar (:) and in various members of the fly family (yellow). (B) Submission of the protein sequence of Rph1 into the iLIR tool revealed it to have a predicted xLIR motif (EEWLPI), at position 341-346, which is similar to that of Sequoia. A PSSM score of 19 is deemed as a high confidence level, however this motif has not been investigated experimentally.

6.2 Sequoia- A Master Transcriptional Regulator of Core Starvation *Atg* genes

Most LIR motif-containing proteins interact with Atg8-family proteins in the cytoplasm and relate to the formation of autophagosomes or to the recruitment of cargoes for degradation. However, Sequoia is maintained in the nucleus upon starvation, which first suggested that the interaction between Sequoia and Atg8a orchestrates the regulation of autophagy induction exclusively from this organelle.

A natural question to ask here would be: how does the level of *Atg* gene transcription regulate autophagy activity? Several *Atg* genes have been shown to have a higher expression after starvation[247,414], suggesting that this increase is required to support optimal autophagy activity.

Reports have highlighted ~20 *ATG* conserved genes, as 'absolutely required', for efficient autophagosome formation across species[10,99,135]. In the context of starvation induced autophagy, these include *Atg1*, *Atg5*, *Atg7*, *Atg8a*, *Atg9*, *Atg13* and *Atg14* in *Drosophila*[27,247,384]; all of which are shown here to be upregulated upon *sequoia* knock-down, and upon which Sequoia is enriched at the promotor. Well documented examples of the autophagic effects of these speculated genes in *Drosophila* include those surrounding *Atg7*, *Atg9* and *Atg8*. In fact, in many studies, including ours, *Atg7, Atg8*a and *Atg9* mutants are utilised in order to test an experimental setting in which autophagy is defective[27,116,202,279,328]. Interestingly, *Atg18a* and *Atg8a* showed particularly high levels of upregulation as a result of knockdown of *sequoia* (Fig. 3.10). Given that in *Drosophila* Atg18a appears to function upstream of Atg8a recruitment during the formation of phagophore, with Atg8a positive puncta localisation lost in *Atg18* mutants[116]; this highlights the potential importance of maintaining high levels of *Atg18a* transcription in an environmental setting in which Atg8a accumulation is needed at the site of autophagosome formation. It would therefore be interesting to determine whether Sequoia is directly involved in the transcriptional repression of *Atg18a* and to further explore the potential impact of this gene in the context of starvation induced autophagy. Further verification of the activation of autophagy in *sequoia*-depleted cells, is presented by colleagues who observed the post-transcriptional accumulation of Atg8a-II and Atg1 protein in *sequoia*-depleted larvae (Appendix paper A; Fig. S2 A-D)[376]. Taken together, it is postulated that, in the case of nutrient rich conditions, a concomitant downregulation of these aforementioned *Atg* genes contribute to a transcriptional repression in the magnitude of autophagy activity and thereby, to the efficient suppression of autophagosome formation.

It was also observed in a *sequoia*-depleted setting that the expression of *kenny* and *ref(2)p* is downregulated (Fig. 3.11). Interestingly, it has been reported that an upregulation in *ref(2)p* results in an extended life span in middle aged adult *Drosophila,* and has been linked to the induction of autophagy [415]. Given this, it appears contradictory for a down-regulation of *ref(2)P* to be observed given the repressive nature of Sequoia. One plausible explanation for the observed reduction in expression of *ref(2)p* and *kenny* in *sequoia*-depleted cells, may be linked to an inverse relationship to the up-regulatory trend seen in *Atg* genes, which is likely to account for autophagy constantly being 'on' in nutrient repleted conditions. Thereby, a reduction in the expression of *ref(2)p* and *kenny* may act as a counter-compensatory mechanism in order to limit the amount of cellular degradation, driven by the production of adaptor proteins Ref(2)P and Kenny, from reaching detrimental levels. This hypothesis is to some degree supported by the observation that the expression of *sequoia*-RNAi in the fat body results in a significantly smaller

larval body size, when compared to the control. It is postulated that this may be indicative of a 'hyper-active' level of autophagy in the absence of transcriptional repression, resulting in a hampered accumulation of body mass due to cellular breakdown. This however is purely speculative, and it must be emphasised that the implications and rationale behind the downregulated expression levels cannot be gauged without further investigation.

Very recently, the role in Rph1 in the context of nutrient stress was further characterised in yeast, where it was shown to dynamically regulate the transcription of ribosomal RNA and ribosomal protein gene transcription[416]. Ribosomes provide the basis for cell mass accumulation and protein production, which drives cell growth. A model is suggested by Shu *et al.,* in which the DNA binding of Rph1 provides a sensing system to adjust the production of ribosomes properly in response to nutrient starvation[416]. Furthermore, a direct interaction of Rph1 with the TORC1-mediated pathway is suggested. These results expand the potential levels of control for Sequoia by highlighting the integral role of its yeast homolog Rph1 in the cellular response to nutrient stress.

6.3 The Role of the LIR motif in the Interaction Between Atg8a and Sequoia

Following the confirmation of a LIR-dependant interaction between Sequoia and Atg8a; the LIR motif-deficient form of Sequoia, was observed to be less enriched at the promotor region of autophagy genes, correlating to their upregulation in fed conditions (Fig. 3.13). This led to the suggestion that perhaps the interaction between Sequoia and Atg8a was required for the repressive ability of Sequoia to remain in-tact under fed conditions. Interestingly however, during fed conditions the absence of *Atg8a* was seen to have no effect on the regulation of *Atg* genes (Fig 4.15 A), with Sequoia remaining enriched at their promotors (Fig. 4.19). This in fact seems logical since without the presence of Atg8a, autophagy cannot be initiated efficiently, hence the $Atg8a^{KG}$ line is characterised in having severe autophagy deficits[116]. Therefore, it seems logical for the transcriptional repression of *Atg* genes to function independently of the cellular presence of Atg8a. This suggests that the purpose of the LIR interaction between the two proteins may be that of retaining Atg8a within the nucleus, thus preventing it from entering the cytoplasm to take part in the formation of autophagosomes. This hypothesis is supported by the observation that mutation of the Sequoia LIR motif results in an increased accumulation of

Atg8a positive puncta in the fed condition (Fig. 3.6). Examples of this have been shown in mammalian cells, with an IRS-1-LC3 bound complex found to repress autophagy induced by amino acid starvation, in a process in which nuclear IRS-1 sequestered LC3 inside the nucleus[156]. These events possibly prevent the cytosolic translocation of LC3 and the formation of autophagosomes.

In the absence of a functional LIR, the inability of Sequoia to be retained at the promotor, and the subsequent translocation of Atg8a into the cytoplasm, also highlights another possible mode in which Sequoia is lifted off the promotor region of autophagy genes. This observation may be reflective of a two-way mechanism in which both the LIR governed interaction and the subsequent exit of Atg8a from the nucleus are both sufficient in elevating the repressive cap enforced by Sequoia. This possibility was strengthened by the observation that the LIR mutant is only enriched on the promotor region of all target *Atg* genes, in the absence of Atg8a (Fig 4.20).

6.4 The Mechanistic Role of Acetylation

Following from results presented in Chapter 4, a working model is proposed in which YL-1 plays a role in regulating the acetylation of Atg8a under fed conditions, which in turn contributes to the interaction between Atg8a and Sequoia at the promoter regions of *Atg* genes. In such conditions, the interaction between Sequoia and Atg8a contributes to the sequestration of Atg8a in the nucleus, resulting in its inability to translocate to the cytoplasm to take part in the formation of autophagosomes. Furthermore, the accumulation of Atg8a-positive puncta *in vivo* (Fig. 4.14) and the accumulation of lipidated Atg8a *in vitro* (Appendix paper A; S2 A, B)[376], in a *yl-1* depleted setting, further strengthens the suggestion that YL-1 is a negative regulator of autophagy, acting to maintain the acetylated status of Atg8a and its nuclear localisation. Given these results, the absence of free GFP *in vitro* under the same *yl-1*-depleted environment (Fig. 4.11) is unclear, however this could be reflective of the lack of reliability of the assay in the detection of autophagy induction in *Drosophila*. In yeast cells the accumulation of cleaved free GFP in the vacuole from GFP-Atg8 is a widely considered a reliable assay used to measure autophagy. However, it has been suggested that in mammalian cells this assay is far more complicated given that lysosomes have a lower pH and degrade free GFP more efficiently[414]. In mammalian cells, it has been reported that accumulation of free GFP from GFP-LC3 could either reflect increased delivery or reduced lysosomal activity[414]. Therefore, it is postulated here

that it may be also hard to distinguish whether the absence of free GFP is reflective of both increased autophagy and efficient lysosome activity, or reduced delivery of GFP-Atg8a to the lysosome. However this is very cell line dependant and it has yet to be fully explored in the context of *Drosophila* cells.

Due to the predicted conformational change upon the removal of acetyl-CoA by Sir2, it is proposed that deacetylated Atg8a interacts more strongly with Sequoia (Fig, 4.4). It is also proposed that the bound proteins cannot be maintained at the promoter regions of *Atg* genes, leading to the activation of their transcription. It is suggested that as a result of this, deacetylated Atg8a is able to translocate to the cytoplasm and contribute to the formation of autophagosomes. This proposed mechanism thus implies that deacetylation by Sir2 may have a crucial role in the ability of Atg8a to lift Sequoia off the promotor region of autophagy-related genes in nutrient scarce conditions (Fig. 6.2). However, this is yet to be tested from a transcriptional perspective.

Results presented in Chapter 4 support previous reports about the role of acetylation and deacetylation of LC3 in mammals[158,291,292,392,401] and the regulation of autophagy by acetylation[324,417]. Interestingly, YL-1 is expressed in higher eukaryotes and also harbours specific H2A.Z-binding properties, as shown in *Drosophila*[418]. Work conducted by our collaborators in the Johansen lab have already established an interaction human YL-1/VPS72 and GABARAP (Appendix paper A; Fig. S1 B)[376], therefore it would be interesting for others to assess its role in the acetylation of Atg8-family proteins in the induction of autophagy in mammalian cells. Nuclear SIRT1 has very recently been discovered to be recognised as an autophagy substrate during senescence, and that aging contributes to loss of SIRT1 via the autophagosome-lysosome pathway in many tissues related to the immune and haematopoietic system[419]. Therefore, understanding the function of nuclear SIRT1 in the control of autophagy may aid in understanding the implications of its depletion during aging, and may lead to potential strategies to help stabilise or promote its production.

It is hypothesised that the LIR-dependant interaction between Sequoia and Atg8a has a dual purpose; firstly, to retain acetylated Atg8a within the nucleus in the repression of autophagy in fed conditions. Secondly, in starvation conditions the LIR interaction enables deacetylated Atg8a to bind more strongly to Sequoia, enabling the former to "lift" the latter off its repressive residency and induce autophagy. Results in Chapter 4 suggest that genetic knockdown or

overexpression of YL-1 and Sir2, respectively affect Atg8a acetylation. It is also likely that the relocation of Atg8a to the cytoplasm also induces Sequoia to abandon its residency on the promotor region in a rally to magnitude autophagic activity.

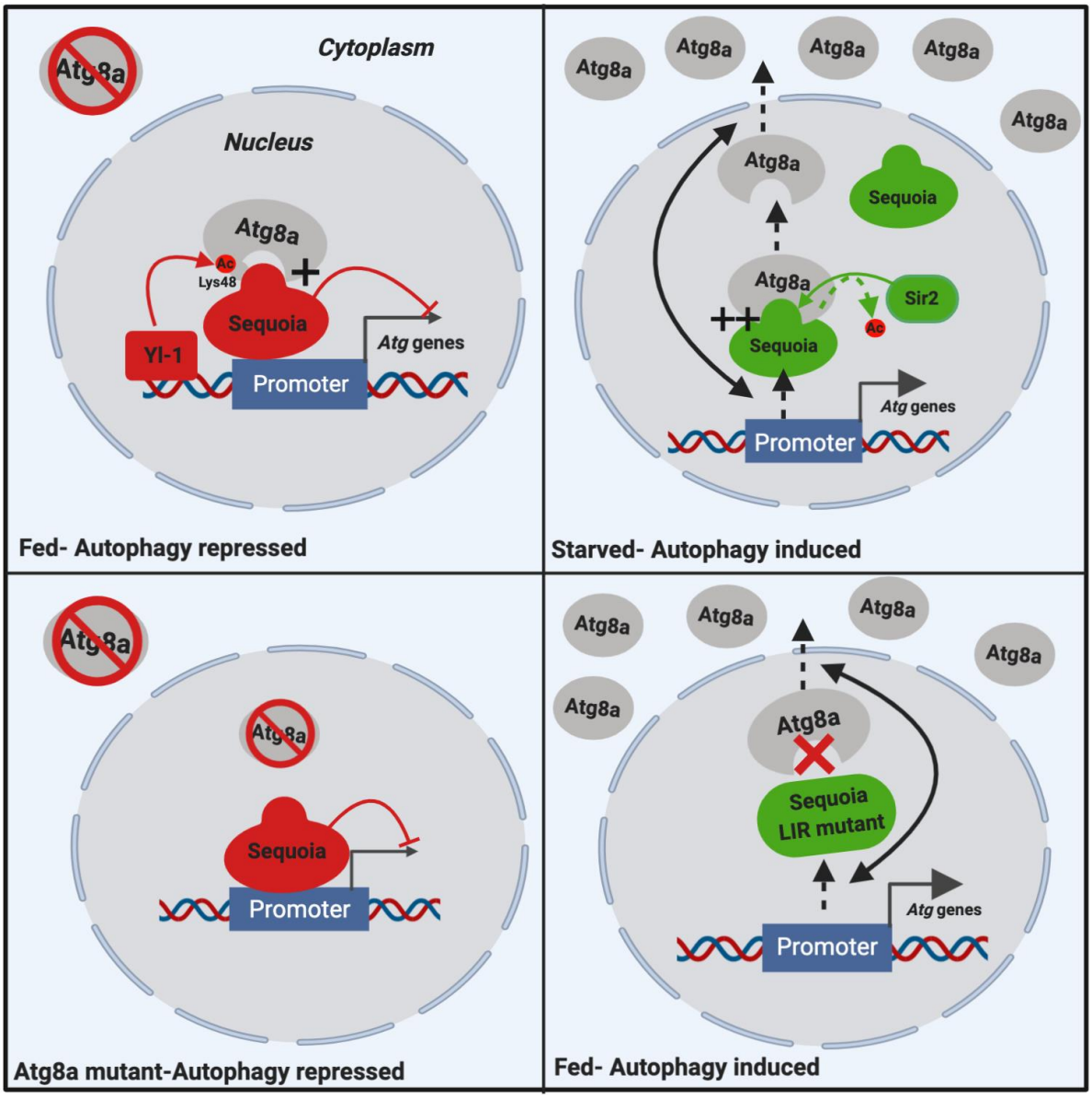

Figure 6.2 A Proposed Molecular Mechanism for Atg8a Binding Sequoia and the Induction of *Atg* genes. In nutrient-rich conditions, the transcription factor Sequoia interacts with Atg8a in a LIR motif dependent manner and localizes at the promoter regions of autophagy-related (Atg) genes to repress their expression. In such conditions, Atg8a acetylation at K46 is maintained by its interaction with an acetyltransferase complex via YL-1. Deletion of *Atg8a* does not affect the enrichment of Sequoia at the promotor. It is postulated that the LIR interaction between Atg8a and Sequoia is responsible for maintaining Atg8a in the nucleus, with mutation of the LIR shown to result in the relocation of Atg8a to the cytoplasm. It is predicted that translocation of Atg8a into the cytoplasm, signalling the induction of autophagy, also results in Sequoia (WT and LIR) being removed from the promotor to allow for transcriptionally elevated induction of autophagy, by an alternative mechanism. When nutrients are scarce, Atg8a is deacetylated by Sir2, resulting in a stronger binding to Sequoia **(++)**, which can be lifted from the autophagy gene promoters, leading to their transcriptional activation. Sequoia remains nuclear in both fed and starved conditions.

6.5 The Potential Role of dDOR and the UIM in *Drosophila*

The acetylation of K46 and K48 is speculated to modulate the respective binding of Atg8a to dDOR, and Sequoia, independently. It is postulated that acetylation of these regions could modulate in a similar fashion and with a similar strength. However, this would need to be investigated further with a more robust assay than that presented in Figure 5.10. With this hypothesis in mind however, it would be very interesting for future work to determine whether Atg8a functions to bind both proteins simultaneously. With mutations in the UDS of Atg8a hinting towards a potential weakened binding to dDOR (Fig. 5.5), and a mutation in the top candidate LIR motif (determined using the iLIR tool) in dDOR showing no indication of compromised binding to Atg8a (Fig. 5.4); the possibility of Atg8a binding both Sequoia and dDOR is of future interest especially given the potential dependence on different functional motifs (LIR and UIM) in each case. This leads to a proposed mechanism by which Atg8a binds both Sequoia and dDOR with more strength in starvation conditions, thus enabling the Atg8a-dDOR complex to relocate to the cytoplasm, and Sequoia to be removed from its promotor residency (Fig. 6.3). It would be interesting for future work to identify if dDOR exits the nucleus in *sequoia*-depleted cells, as has been shown for Atg8a (Fig. 3.8 and 3.9). This would provide more clarity to the mechanism in which it is postulated that Sequoia provides an anchor for retaining Atg8a-bound dDOR in the nucleus. The ability of KDM4A to bind GABARAP in a LIR-independent manner[376] and TP53INP2 in a LIR-dependant manner[413], hints at the potential for LC3-like proteins to bind both TP53INP2 and KDM4 simultaneously within the nucleus, as is proposed here in *Drosophila*. Theoretically this ability also provides a potential rationale to the evolutionarily loss of functionality in the LIR motif of KDM4A.

A natural focus for future work would be in the investigation of the autophagic role of dDOR in the cytoplasm, following the induction of autophagy by starvation conditions. In mammalian cells, upon-exiting the nucleus, LC3-associated TP53INP2 directly binds to ATG7, which facilitates the LC3-ATG7 interaction and promotes the formation of autophagosomes[413]. This mechanism is also dependent on LC3 deacetylation by SIRT1 in the nucleus. With an observed interaction between Atg8 and Atg7 in the yeast also affected by acetylation of Atg8[401], the idea that this mechanism is shared among eukaryotic organisms is well supported, and it would therefore be very interesting to see if Atg8a-bound dDOR directly binds Atg7, through the action of Sir2, in a similar fashion as in mammals.

The investigation of dDOR failed to shed any light onto the mechanism by which the interaction between Sequoia and Atg8a is disrupted, prior to the speculated cytoplasmic relocation of Atg8a-dDOR. A suggested line of future investigation would be in establishing the modifications, and thus the conformational changes which occur in Sequoia during the induction of autophagy. In the case of Rph1, phosphorylation by kinase Rim15 has been shown to be integral in the proper induction of autophagy upon starvation[247]. Rim15 had previously been shown to translocate into the nucleus upon nitrogen starvation[278]. A BLAST search revealed a *Drosophila* serine/threonine kinase called dop (drop out), to be a homolog of Rim15. Although dop has only been characterised in the cytoplasm[420], it has yet to be studied in the context of autophagy, and it would therefore be interesting to investigate if it plays a role in the induction of autophagy in relation to Sequoia.

The detected interaction between dDOR and Atg8a K46Q, though marginally weaker than its deacetylated form, is suggestive of an interaction in full nutrients conditions and therefore may reflect a requirement for basal autophagy. Results here point towards the ability of dDOR to modulate the expression of *Atg8a* in fed conditions, given that dDOR was both detected at its promotor and its expression is upregulated in a *dor* deplete setting. Following reports in mammalian cells, it is likely that the main role of dDOR from within the nucleus is to increase the efflux of Atg8a in starvation conditions[158,421], however results here may be a first insight into the potential role nuclear dDOR in the transcriptional regulation of *Atg8a* and thus a control in the production of the protein it facilitates to transport across the nuclear membrane. dDOR was not observed to be enriched at the promotor region of other *Atg* genes regulated by Sequoia, or to impact their expression, indicating it has no impact on the overall induction of autophagy. This also makes a possible interaction between Sequoia and dDOR at the promotors unlikely, given that a direct interaction between Atg8a and Sequoia was detected by association of Atg8a to all queried *Atg* promotor regions. Interestingly knock-down of *sequoia* and *dor* both independently resulted in an increase in *Atg8a* expression in fed conditions, suggesting they are both required to maintain a lowered expression levels in basal conditions. This is consistent with observations in yeast where multiple transcriptional regulators have also been identified across *ATG* genes, with Pho23, Ume6 and Rph1 all shown to regulate Atg8 expression[422]. In the case of *dor* knock-down, it is predicted that an increase in *Atg8a* expression is unlikely to result in an induction of autophagy processes; given that the primary role of dDOR in the promotion of autophagy is likely to facilitate the transport of the Atg8a protein across the nuclear membrane. This was highlighted in reports which have previously used the *dor- RNAi* line used in this study;

showing its failure to form autophagosomes during the induction of autophagy[339]. However, future work would need to confirm this experimentally under starvation conditions. Taken together, it is speculated that dDOR may contribute to maintaining a lowered transcriptional level of *Atg8a* in basal conditions, given that the demand of the cell for a nuclear efflux of Atg8a-bound dDOR is low. The exact mechanisms of this regulation would need to be investigated further, as findings presented here are only preliminary. Further rounds of ChIP could not complete as part of this study due to an insufficient anti-dDOR stock, however the generation of the FLAG-tagged dDOR transgenic lines provide the ideal environment for the future exploration of the transcriptional potential of dDOR using a verified ChIP grade antibody.

Atg8-binding UIM proteins are considered a new class of interactors which engage with the UIM-like sequence rather than the canonical LIR motif. To date, UIM-type autophagy adaptors and receptors have only been found in yeast, plants and humans[226]. However, here we uncover the first indications that the binding of Atg8a may involve a UIM in *Drosophila.* In order to verify this, future investigations must now be aimed at determining the UIM sequence in dDOR, and to explore whether a mutation in this region impacts Atg8a binding. Furthermore, it would be of interest to investigate how acetylation of K46 impacts the structural conformation of the interaction between Atg8a and dDOR.

Interestingly, it has been reported that mutation of the UIM in TP53INP2 does not affect its interaction with LC3/GABARAP, whereas deletion of its LIR motif compromises the interaction significantly[413,227]. Results here in *Drosophila* hint that the inverse may be the case for dDOR. This could be reflective on evolutionary changes seen in motifs based on the functionality of a protein. Interestingly, TP53INP2 has recently been shown to mediate autophagic degradation through its UIM, hinting that it may have a role as an autophagic adaptor through the recruitment of ubiquitinated substrates to autophagosomes for degradation[227]. It is therefore tempting to speculate that perhaps an evolutionary shift in the Atg8-family-binding motif of TP53INP2/DOR occurred in accordance with the development of its autophagic role which may have evolved in mammalian cells. It is further speculated that a protein in which contributes to autophagic processes in the cytoplasm may structurally evolve to utilise its UIM in order to bind LC3-family proteins. This is however purely speculative, especially given that function of dDOR in the context of autophagy remains to be fully characterised. Following sequence analysis presented in Chapter 5.3.3, it is suggested that the potential of dDOR$_{FENLL}$

could represent a more closely related *Drosophila* homolog of TP53INP2, so it is recommended that both $dDOR_{long}$ and $dDOR_{FENLL}$ are explored in future investigations.

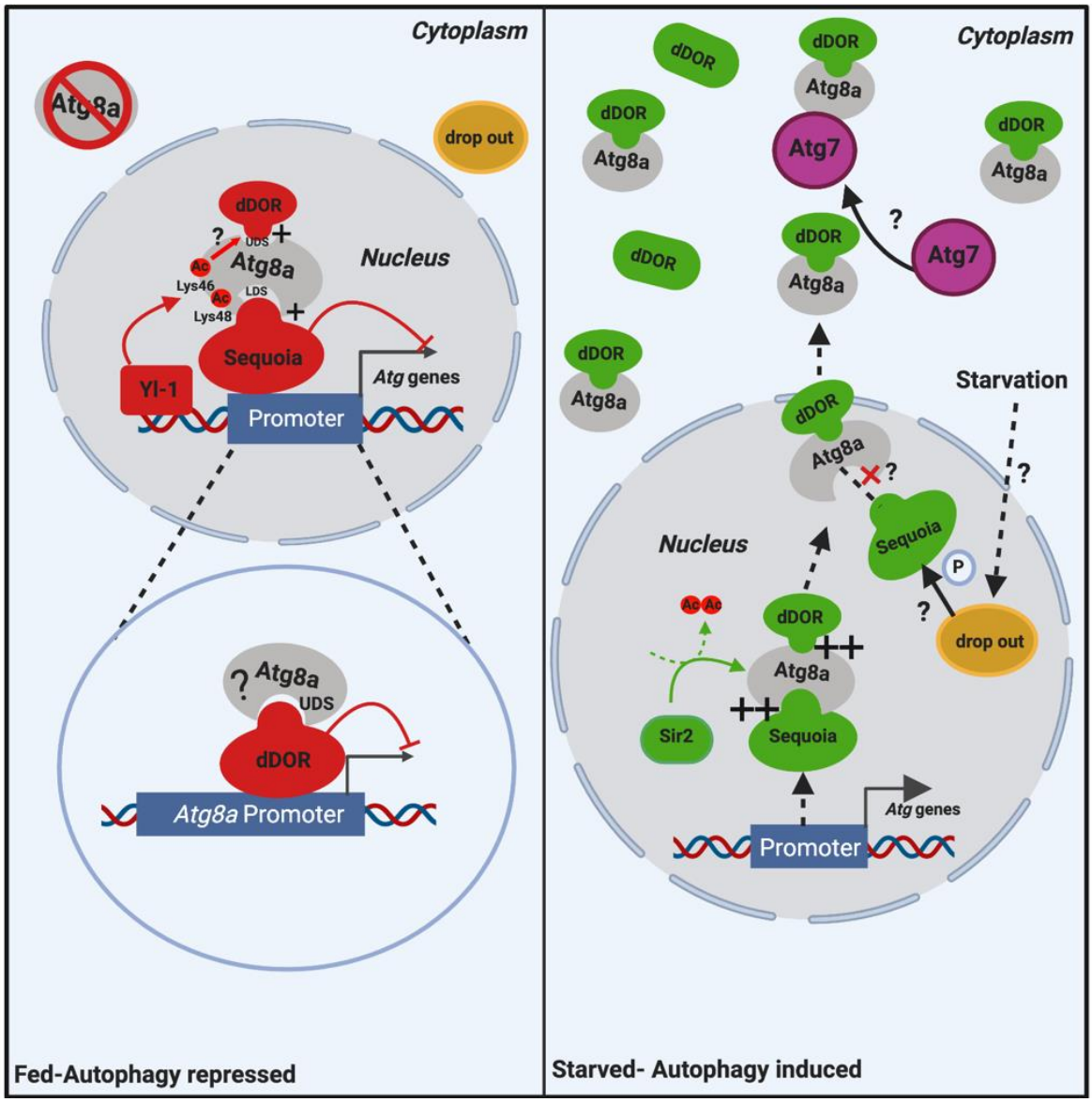

Figure 6.3 A Proposed Function of dDOR in Autophagy.

Under fed conditions, it is proposed that acetylated Atg8a functions to bind both Sequoia and dDOR simultaneously, through its UDS and UIM respectively. Atg8a is indirectly associated to the *Atg* promotors governed by Sequoia. dDOR is found to be exclusively enriched at the promotor of *Atg8a* hinting that it could have a role in the modulation of its expression in a nutrient replete setting. Whether *Atg8a* promotor enriched dDOR is able to bind Atg8a is unclear. Under these conditions, all three proteins remain nuclear and autophagy is repressed through the action of Sequoia. In starvation conditions, Atg8a is deacetylated by Sir2, which strengthens its interaction with dDOR and Sequoia. This results in Sequoia being unable to be maintained at the promotor of *Atg* genes, inducing their expression. Atg8a-bound dDOR functions to translocate to the cytoplasm under starvation conditions. A candidate factor for phosphorylating Sequoia, thus compromising its binding to Atg8a, is the serine-threonine kinase drop out; however, its nuclear localisation in the context of autophagy is unknown. Based on its mammalian homolog, dDOR is also predicted to mediate the binding of Atg8a to Atg7, thereby leading to the lipidation of Atg7 and the formation of autophagosomes.

6.6 Concluding remarks

Atg8-family proteins have been extensively described for their implications in autophagosome formation and cargo selection in the cytoplasm. Although Atg8 family proteins also localize in the nucleus, their role in this compartment remains largely unexplored. Here, the nuclear role of *Drosophila* Atg8a in the de-repression of autophagy gene expression, and induction of autophagy via a LIR motif-dependent interaction with transcription factor Sequoia was uncovered. The remarkable effects of Sequoia provide evidence of it being a master transcriptional repressor of starvation induced autophagy, which is also likely to function to sequester Atg8a in the nucleus for an additional hold on autophagic processes. We also highlight the importance of acetylation in the regulation of nuclear Atg8a through the roles of YL-1 and Sir2, in mechanisms that mirror those seen in higher eukaryotes. Taken together, this work brings into the spotlight the unanticipated role of a non-degradative LIR motif-dependent interaction in the nucleus, which functions to control cellular self-eating in the cytoplasm. Furthermore, the potential of another binding interface in governing the nuclear regulation and cytoplasmic re-location of Atg8a is uncovered through the investigation of dDOR. The potential of the UIM in mediating Atg8-interactors in *Drosophila* further highlight how work in this powerful model organism can continue to give a valuable insight into the regulation of starvation induced autophagy.

Bibliography

1. Deter, R. L. & De Duve, C. Influence of glucagon, an inducer of cellular autophagy, on some physical properties of rat liver lysosomes. *J. Cell Biol.* **33**, 437–449 (1967).
2. Axe, E. L. *et al.* Autophagosome formation from membrane compartments enriched in phosphatidylinositol 3-phosphate and dynamically connected to the endoplasmic reticulum. *Cell* **25**, 685–701 (2000).
3. Simonsen, A. & Tooze, S. A. Coordination of membrane events during autophagy by multiple class III PI3-kinase complexes. *J. Cell Biol.* **186**, 773–782 (2009).
4. Mizushima, N. Autophagy: Process and function. *Genes Dev.* **21**, 2861–2873 (2007).
5. Yorimitsu, T. & Klionsky, D. J. Autophagy: molecular machinery for self-eating. *Cell Death Differ.* **12**, 1542–1552 (2005).
6. Gukovsky, I., Li, N., Todoric, J., Gukovskaya, A. & Karin, M. Inflammation, Autophagy, and Obesity: Common Features in the Pathogenesis of Pancreatitis and Pancreatic Cancer. *Gastroenterology* **144**, 1199–209.e4 (2013).
7. Lamb, C. A., Yoshimori, T. & Tooze, S. A. The autophagosome: Origins unknown, biogenesis complex. *Nat. Rev. Mol. Cell Biol.* **14**, 759–774 (2013).
8. Klionsky, D. J. Autophagy revisited: A conversation with Christian de Duve. *Autophagy* **4**, 740–743 (2008).
9. Porter, T. A. and K. Cytoplasmic components in hepatic cell lysosomes.
10. Tsukada, M. Isofation and characterization of autophagy-defective mutants of. **333**, 169–174 (1993).
11. Suzuki, K. *et al.* The pre-autophagosomal structure organized by concerted functions of APG genes is essential for autophagosome formation. *EMBO J.* **20**, 5971–5981 (2001).
12. Mizushima, N., Yoshimori, T. & Ohsumi, Y. The Role of Atg Proteins in Autophagosome Formation. *Annu. Rev. Cell Dev. Biol.* **27**, 107–132 (2011).
13. McPhee, C. K. & Baehrecke, E. H. Autophagy in Drosophila melanogaster. *Biochim. Biophys. Acta - Mol. Cell Res.* **1793**, 1452–1460 (2009).
14. Adams, M. D. *et al.* The genome sequence of Drosophila melanogaster. *Science (80-.).* **287**, 2185–2195 (2000).
15. Venken, K. J. T. & Bellen, H. J. Transgenesis upgrades for Drosophila melanogaster. *Development* **134**, 3571–3584 (2007).
16. Bellen, H. J. *et al.* The BDGP gene disruption project: Single transposon insertions associated with 40% of Drosophila genes. *Genetics* **167**, 761–781 (2004).
17. Lőrincz, P., Mauvezin, C. & Juhász, G. Exploring Autophagy in Drosophila. *Cells* **6**, 22

(2017).

18. Zhou, J. & Tong, C. Design and Methods of Large-Scale RNA Interference Screens in Drosophila. in *High-Throughput RNAi Screening: Methods and Protocols* (eds. Azorsa, D. O. & Arora, S.) 163–169 (Springer New York, 2016). doi:10.1007/978-1-4939-6337-9_13.
19. Pandey, U. B. & Nichols, C. D. Human Disease Models in Drosophila melanogaster and the Role of the Fly in Therapeutic Drug Discovery. *Pharmacol. Rev.* **63**, 411–436 (2011).
20. Juhasz, G. & Neufeld, T. P. Experimental control and characterization of autophagy in Drosophila. *Methods Mol. Biol.* **445**, 125–133 (2008).
21. Mauvezin, C., Ayala, C., Braden, C. R., Kim, J. & Neufeld, T. P. Assays to monitor autophagy in Drosophila. *Methods* **68**, 134–139 (2014).
22. Klionsky, D. J. *et al.* Guidelines for the use and interpretation of assays for monitoring autophagy in higher eukaryotes. *Autophagy* **4**, 151–175 (2008).
23. Nagy, P., Varga, Á., Kovács, A. L., Takáts, S. & Juhász, G. How and why to study autophagy in Drosophila: It's more than just a garbage chute. *Methods* **75**, 151–161 (2015).
24. Rusten, T. E. *et al.* Programmed autophagy in the Drosophila fat body is induced by ecdysone through regulation of the PI3K Pathway. *Dev. Cell* **7**, 179–192 (2004).
25. Butterworth, F. M., Emerson, L. & Rasch, E. M. Maturation and degeneration of the fat body in the Drosophila larva and pupa as revealed by morphometric analysis. *Tissue Cell* **20**, 255–268 (1988).
26. Lee, C. Y., Cooksey, B. A. K. & Baehrecke, E. H. Steroid regulation of midgut cell death during Drosophila development. *Dev. Biol.* **250**, 101–111 (2002).
27. Scott, R. C., Schuldiner, O. & Neufeld, T. P. Role and regulation of starvation-induced autophagy in the Drosophila fat body. *Dev. Cell* **7**, 167–178 (2004).
28. Dikic, I. & Elazar, Z. Mechanism and medical implications of mammalian autophagy. *Nat. Rev. Mol. Cell Biol.* **19**, 349–364 (2018).
29. Johansen, T. & Lamark, T. Selective autophagy mediated by autophagic adapter proteins. *Autophagy* **7**, 279–296 (2011).
30. Glick, D., Barth, S. & Macleod, K. F. Autophagy : cellular and molecular mechanisms. *J. Pathol.* **221**, 3–12 (2010).
31. He, C. & Klionsky, D. J. Regulation Mechanisms and Signalling Pathways of Autophagy. *Annu. Rev. Genet.* **43**, 67 (2009).
32. Kaushik, S. & Cuervo, A. M. *The coming of age of chaperone-mediated autophagy*. vol. 19 (2019).
33. Tekirdag, K. & Cuervo, A. M. Chaperone-mediated autophagy and endosomal microautophagy: Joint by a chaperone. *J. Biol. Chem.* **293**, 5414–5424 (2018).

34. Dice, J. F. Altered degradation of proteins microinjected into senescent human fibroblasts. *J. Biol. Chem.* **257**, 14624–14627 (1982).
35. Chiang, H. L. & Dice, J. F. Peptide sequences that target proteins for enhanced degradation during serum withdrawal. *J. Biol. Chem.* **263**, 6797–6805 (1988).
36. Cuervo, A. M. & Dice, J. F. A Receptor for the Selective Uptake and Degradation of Proteins by Lysosomes. *Science (80-.).* **273**, 501 LP – 503 (1996).
37. Bandyopadhyay, U., Kaushik, S., Varticovski, L. & Cuervo, A. M. The Chaperone-Mediated Autophagy Receptor Organizes in Dynamic Protein Complexes at the Lysosomal Membrane. *Mol. Cell. Biol.* **28**, 5747–5763 (2008).
38. Agarraberes, F. A., Terlecky, S. R. & Dice, J. F. An intralysosomal hsp70 is required for a selective pathway of lysosomal protein degradation. *J. Cell Biol.* **137**, 825–834 (1997).
39. Gough, N. R. & Fambrough, D. M. Different steady state subcellular distributions of the three splice variants of lysosome-associated membrane protein LAMP-2 are determined largely by the COOH-terminal amino acid residue. *J. Cell Biol.* **137**, 1161–1169 (1997).
40. Aniento, F., Roche, E., Cuervo, A. M. & Knecht, E. Uptake and degradation of glyceraldehyde-3-phosphate dehydrogenase by rat liver lysosomes. *J. Biol. Chem.* **268**, 10463–10470 (1993).
41. Schneider, J. L., Suh, Y. & Cuervo, A. M. Deficient chaperone-mediated autophagy in liver leads to metabolic dysregulation. *Cell Metab.* **20**, 417–432 (2014).
42. Massey, A. C., Kaushik, S., Sovak, G., Kiffin, R. & Cuervo, A. M. Consequences of the selective blockage of chaperone-mediated autophagy. *Proc. Natl. Acad. Sci. U. S. A.* **103**, 5805–5810 (2006).
43. Rodríguez-Muela, N. *et al.* Balance between autophagic pathways preserves retinal homeostasis. *Aging Cell* **12**, 478–488 (2013).
44. Mijaljica, D., Prescott, M. & Devenish, R. J. Microautophagy in mammalian cells: Revisiting a 40-year-old conundrum. *Autophagy* **7**, 673–682 (2011).
45. De Duve, C. & Wattiaux, R. Functions of lysosomes. *Annu. Rev. Physiol.* (1966).
46. Mortimore, G. E., Lardeux, B. R. & Adams, C. E. Regulation of microautophagy and basal protein turnover in rat liver. Effects of short-term starvation. *J. Biol. Chem.* **263**, 2506–2512 (1988).
47. Chanoca, A., Burkel, B., Grotewold, E., Eliceiri, K. W. & Otegui, M. S. Imaging Vacuolar Anthocyanins with Fluorescence Lifetime Microscopy (FLIM). in *Plant Vacuolar Trafficking: Methods and Protocols* (ed. Pereira, C.) 131–141 (Springer New York, 2018). doi:10.1007/978-1-4939-7856-4_10.

48. Mizushima, N. *et al.* A protein conjugation system essential for autophagy. *Nature* **395**, 395–398 (1998).
49. Tuttle, D. L. & Dunn, W. A. Divergent modes of autophagy in the methylotrophic yeast Pichia pastoris. *J. Cell Sci.* **108**, 25–35 (1995).
50. Oku, M. & Sakai, Y. Three Distinct Types of Microautophagy Based on Membrane Dynamics and Molecular Machineries. *BioEssays* **40**, 1–6 (2018).
51. Müller, O. *et al.* Autophagic Tubes: Vacuolar Invaginations Involved in Lateral Membrane Sorting and Inverse Vesicle Budding. *J. Cell Biol.* **151**, 519–528 (2016).
52. Schuck, S., Gallagher, C. M. & Walter, P. ER-phagy mediates selective degradation of endoplasmic reticulum independently of the core autophagy machinery. *J. Cell Sci.* **127**, 4078–4088 (2014).
53. Roberts, P. *et al.* Piecemeal Microautophagy of Nucleus in Saccharomyces cerevisiae. *Mol. Biol. Cell* **13**, 4100–4109 (2002).
54. Kiššova, I. *et al.* Selective and non-selective autophagic degradation of mitochondria in yeast. *Autophagy* **3**, 329–336 (2007).
55. Moeller, C. H. & Thomson, W. W. Uptake of lipid bodies by the yeast vacuole involving areas of the tonoplast depleted of intramembranous particles. *J. Ultrasructure Res.* **68**, 38–45 (1979).
56. Sattler, T. & Mayer, A. Cell-free Reconstitution of Microautophagic Vacuole Invagination and Vesicle Formation Tanja. *J. Cell Biol.* **151**, 529–538 (2000).
57. Oku, M. *et al.* Evidence for ESC RT- and clathrin-dependent microautophagy. *J. Cell Biol.* **216**, 3263–3274 (2017).
58. Kawamura, N. *et al.* Delivery of endosomes to lysosomes via microautophagy in the visceral endoderm of mouse embryos. *Nat. Commun.* **3**, (2012).
59. Uytterhoeven, V. *et al.* Hsc70-4 Deforms Membranes to Promote Synaptic Protein Turnover by Endosomal Microautophagy. *Neuron* **88**, 735–748 (2015).
60. Mukherjee, A., Patel, B., Koga, H., Cuervo, A. M. & Jenny, A. Selective endosomal microautophagy is starvation-inducible in Drosophila. *Autophagy* **12**, 1984–1999 (2016).
61. Chang, Y. Y. & Neufeld, T. P. Autophagy takes flight in Drosophila. *FEBS Lett.* **584**, 1342–1349 (2010).
62. Hardie, D. G. AMP-activated / SNF1 protein kinases : conserved guardians of cellular energy. **8**, (2007).
63. Pan, D. & Hardie, G. A homologue of AMP-activated protein kinase in Drosophila melanogaster is sensitive to AMP and is activated by ATP depletion. *Biochem. J.* **186**, 179–

186 (2002).

64. Shaw, R. J. *et al.* The tumor suppressor LKB1 kinase directly activates AMP-activated kinase and regulates apoptosis in response to energy stress. **101**, 3329–3335 (2004).
65. Boudeau, J. *et al.* MO25α/β interact with STRADα/β enhancing their ability to bind, activate and localize LKB1 in the cytoplasm. *EMBO J.* **22**, 5102–5114 (2003).
66. Joseph, B. K. *et al.* Inhibition of AMP Kinase by the Protein Phosphatase 2A. **290**, 10588–10598 (2015).
67. Hardie, D. G., Salt, I. P., Hawley, S. A. & Davies, S. P. AMP-activated protein kinase: an ultrasensitive system for monitoring cellular energy charge. **722**, 717–722 (1999).
68. Chen, L. *et al.* AMP-activated protein kinase undergoes nucleotide-dependent conformational changes. *Nat. Struct. Mol. Biol.* **19**, 716–718 (2012).
69. Johnson, E. C. *et al.* Altered Metabolism and Persistent Starvation Behaviors Caused by Reduced AMPK Function in Drosophila. **5**, (2010).
70. Viollet, B. *et al.* AMPK inhibition in health and disease. *Crit. Rev. Biochem. Mol. Biol.* **45**, 276–295 (2010).
71. Li, X. *et al.* Nucleus-Translocated ACSS2 Promotes Gene Transcription for Lysosomal Biogenesis and Autophagy. *Mol. Cell* **66**, 684-697.e9 (2017).
72. Wullschleger, S., Loewith, R. & Hall, M. N. Review TOR Signaling in Growth and Metabolism. 471–484 (2006) doi:10.1016/j.cell.2006.01.016.
73. Saxton, R. A. & Sabatini, D. M. mTOR Signaling in Growth, Metabolism, and Disease. **168**, 960–976 (2018).
74. Kim, J., Kundu, M., Viollet, B. & Guan, K. L. AMPK and mTOR regulate autophagy through direct phosphorylation of Ulk1. *Nat. Cell Biol.* **13**, 132–141 (2011).
75. Noda, T. & Ohsumi, Y. Tor, a phosphatidylinositol kinase homologue, controls autophagy in yeast. *J. Biol. Chem.* **273**, 3963–3966 (1998).
76. Gwinn, D. M. *et al.* AMPK Phosphorylation of Raptor Mediates a Metabolic Checkpoint. *Mol. Cell* **30**, 214–226 (2008).
77. Manning, B. D. & Cantley, L. C. Rheb fills a GAP between TSC and TOR. *Trends Biochem. Sci.* **28**, 573–576 (2003).
78. Ghosh, H. S., McBurney, M. & Robbins, P. D. SIRT1 negatively regulates the mammalian target of rapamycin. *PLoS One* **5**, 1–8 (2010).
79. Inoki, K., Li, Y., Xu, T. & Guan, K. Rheb GTPase is a direct target of TSC2 GAP activity and regulates mTOR signaling. 1829–1834 (2003) doi:10.1101/gad.1110003.GENES.
80. Egan, D. *et al.* The autophagy initiating kinase ULK1 is regulated via opposing

phosphorylation by AMPK and mTOR. **8627**, (2011).

81. Dunlop, E. A., Hunt, D. K., Acosta-Jaquez, H. A., Fingar, D. C. & Tee, A. R. ULK1 inhibits mTORC1 signaling, promotes multisite Raptor phosphorylation and hinders substrate binding. *Autophagy* **7**, 737–747 (2011).
82. Egan, D. F. *et al.* Phosphorylation of ULK1 (hATG1) by AMP-Activated Protein Kinase Connects Energy Sensing to Mitophagy. *Science (80-.).* **331**, 456–461 (2010).
83. Wang, Z., Wilson, W. A., Fujino, M. A. & Roach, P. J. Antagonistic Controls of Autophagy and Glycogen Accumulation by Snf1p, the Yeast Homolog of AMP-Activated Protein Kinase, and the Cyclin-Dependent Kinase Pho85p. *Mol. Cell. Biol.* **21**, 5742–5752 (2001).
84. Mitchelhill, K. I. *et al.* Mammalian AMP-activated protein kinase shares structural and functional homology with the catalytic domain of yeast Snf1 protein kinase. *J. Biol. Chem.* **269**, 2361–2364 (1994).
85. Lippai, M. *et al.* SNF4Aγ, the Drosophila AMPK γ subunit is required for regulation of developmental and stress-induced autophagy. *Autophagy* **4**, 476–486 (2008).
86. Ulgherait, M., Rana, A., Rera, M., Graniel, J. & Walker, D. W. AMPK modulates tissue and organismal aging in a non-cell-autonomous manner. *Cell Rep.* **8**, 1767–1780 (2014).
87. Löffler, A. S. *et al.* Ulk1-mediated phosphorylation of AMPK constitutes a negative regulatory feedback loop. *Autophagy* **7**, 696–706 (2011).
88. Neufeld, T. P. TOR-dependent control of autophagy: Biting the hand that feeds. *Curr. Opin. Cell Biol.* **22**, 157–168 (2010).
89. Gao, X. *et al.* Tsc tumour suppressor proteins antagonize amino-acid-TOR signalling. *Nat. Cell Biol.* **4**, 699–704 (2002).
90. Kapahi, P. *et al.* Regulation of Lifespan in Drosophila by Modulation of Genes in the TOR Signaling Pathway. *Curr. Biol.* **14**, 1118 (2010).
91. Boily, G. *et al.* SirT1 regulates energy metabolism and response to caloric restriction in mice. *PLoS One* **3**, (2008).
92. Kaeberlein, M., McVey, M. & Guarente, L. The SIR2/3/4 complex and SIR2 alone promote longevity in Saccharomyces cerevisiae by two different mechanisms. *Genes Dev.* **13**, 2570–2580 (1999).
93. Rogina, B. & Helfand, S. L. Sir2 mediates longevity in the fly through a pathway related to calorie restriction. *Proc. Natl. Acad. Sci.* **101**, 15998–16003 (2004).
94. Bao, J. & Sack, M. N. Protein deacetylation by sirtuins: Delineating a post-translational regulatory program responsive to nutrient and redox stressors. *Cell. Mol. Life Sci.* **67**,

3073–3087 (2010).

95. Lan, F., Cacicedo, J. M., Ruderman, N. & Ido, Y. SIRT1 modulation of the acetylation status, cytosolic localization, and activity of LKB1: Possible role in AMP-activated protein kinase activation. *J. Biol. Chem.* **283**, 27628–27635 (2008).

96. Cantó, C. *et al.* AMPK regulates energy expenditure by modulating NAD+ metabolism and SIRT1 activity. *Nature* **458**, 1056–1060 (2013).

97. Narala, S. *et al.* SIRT1 Acts as a Nutrient-sensitive Growth Suppressor and Its Loss Is Associated with Increased AMPK and Telomerase Activity. *Mol. Biol. Cell* **18**, 3250–3263 (2007).

98. Zhao, Y. *et al.* Cytosolic FoxO1 is essential for the induction of autophagy and tumour suppressor activity. *Nat. Cell Biol.* **12**, 665–675 (2010).

99. Klionsky, D. J. *et al.* A unified nomenclature for yeast autophagy-related genes. *Dev. Cell* **5**, 539–545 (2003).

100. Yang, Q., Inoki, K., Kim, E. & Guan, K. L. TSC1/TSC2 and Rheb have different effects on TORC1 and TORC2 activity. *Proc. Natl. Acad. Sci. U. S. A.* **103**, 6811–6816 (2006).

101. Chang, Y.-Y. & Neufeld, T. P. An Atg1/Atg13 Complex with Multiple Roles in TOR-mediated Autophagy Regulation. *Mol. Biol. Cell* **20**, 2004–2014 (2009).

102. Nagy, P. *et al.* Atg17/FIP200 localizes to perilysosomal Ref(2)P aggregates and promotes autophagy by activation of Atg1 in Drosophila. *Autophagy* **10**, 453–467 (2014).

103. Guo, T. *et al.* The autophagy-related gene Atg101 in Drosophila regulates both neuron and midgut homeostasis. *J. Biol. Chem.* **294**, 5666–5676 (2019).

104. Galluzzi, L. *et al.* Molecular definitions of autophagy and related processes. *EMBO J.* **36**, 1811–1836 (2017).

105. Berry, D. L. & Baehrecke, E. H. Growth Arrest and Autophagy Are Required for Salivary Gland Cell Degradation in Drosophila. *Cell* **131**, 1137–1148 (2007).

106. Lrincz, P. *et al.* Atg6/UVRAG/Vps34-containing lipid kinase complex is required for receptor downregulation through endolysosomal degradation and epithelial polarity during drosophila wing development. *Biomed Res. Int.* **2014**, (2014).

107. Itakura, E. & Mizushima, N. Atg14 and UVRAG: Mutually exclusive subunits of mammalian Beclin 1-PI3K complexes. *Autophagy* **5**, 534–536 (2009).

108. Juhász, G. *et al.* The class III PI(3)K Vps34 promotes autophagy and endocytosis but not TOR signaling in Drosophila. *J. Cell Biol.* **181**, 655–666 (2008).

109. Nakamura, S. *et al.* Suppression of autophagic activity by Rubicon is a signature of aging. *Nat. Commun.* **10**, 1–11 (2019).

110. Thumm, M. & Kadowaki, T. The loss of Drosophila APG4/AUT2 function modifies the phenotypes of cut and Notch signaling pathway mutants. *Mol. Genet. Genomics* **266**, 657–663 (2001).
111. Scott, R. C., Juhász, G. & Neufeld, T. P. Direct Induction of Autophagy by Atg1 Inhibits Cell Growth and Induces Apoptotic Cell Death. *Curr. Biol.* **17**, 1–11 (2007).
112. Ichimura, Y. *et al.* A ubiquitin-like system mediates protein lipidation. *Nature* **408**, 488–492 (2000).
113. Nagy, P. *et al.* Drosophila atg16 promotes enteroendocrine cell differentiation via regulation of intestinal Slit/Robo signaling. *Dev.* **144**, 3990–4001 (2017).
114. Xiong, Q. *et al.* The Role of ATG16 in Autophagy and The Ubiquitin Proteasome System. *Cells* **8**, 2 (2018).
115. Reggiori, F., Tucker, K. A., Stromhaug, P. E. & Klionsky, D. J. The Atg1-Atg13 complex regulates Atg9 and Atg23 retrieval transport from the pre-autophagosomal structure. *Dev. Cell* **6**, 79–90 (2004).
116. Nagy, P., Hegedus, K., Pircs, K., Varga, Á. & Juhász, G. Different effects of Atg2 and Atg18 mutations on Atg8a and Atg9 trafficking during starvation in Drosophila. *FEBS Lett.* **588**, 408–413 (2014).
117. Karanasios, E. *et al.* Autophagy initiation by ULK complex assembly on ER tubulovesicular regions marked by ATG9 vesicles. *Nat. Commun.* **7**, 1–17 (2016).
118. Kim, M. *et al.* Drosophila Fip200 is an essential regulator of autophagy that attenuates both growth and aging. *Autophagy* **9**, 1201–1213 (2013).
119. Mizushima, N. The role of the Atg1/ULK1 complex in autophagy regulation. *Curr. Opin. Cell Biol.* **22**, 132–139 (2010).
120. Hegedus, K., Nagy, P., Gáspári, Z. & Juhász, G. The putative HORMA domain protein Atg101 dimerizes and is required for starvation-induced and selective autophagy in drosophila. *Biomed Res. Int.* **2014**, (2014).
121. Hosokawa, N. *et al.* Atg101, a novel mammalian autophagy protein interacting with Atg13. *Autophagy* **5**, 973–979 (2009).
122. Jung, C. H. ULK-Atg13-FIP200 Complexes Mediate mTOR Signaling to the Autophagy Machinery. *Mol. Biol. Cell* **20**, 2673–2683 (2009).
123. Neufeld, Y.-Y. C. and T. P. An Atg1/Atg13 Complex with Multiple Roles in TOR-mediated Autophagy Regulation. *Mol. Biol. Cell* **20**, 2673–2683 (2009).
124. Kamada, Y. *et al.* Tor-mediated induction of autophagy via an Apg1 protein kinase complex. *J. Cell Biol.* **150**, 1507–1513 (2000).

125. Kraft, C. *et al.* Binding of the Atg1/ULK1 kinase to the ubiquitin-like protein Atg8 regulates autophagy. *EMBO J.* **31**, 3691–3703 (2012).
126. Fujioka, Y. *et al.* Structural basis of starvation-induced assembly of the autophagy initiation complex. *Nat. Struct. Mol. Biol.* **21**, 513–521 (2014).
127. Papinski, D. & Kraft, C. Regulation of Autophagy by Signaling Through the Atg1/ULK1 Complex. *J. Mol. Biol.* **428**, 1725–1741 (2016).
128. Kawamata, T., Kamada, Y., Kabeya, Y., Sekito, T. & Ohsumi, Y. Organization of the Pre-autophagosomal Structure Responsible for Autophagosome Formation. *Mol. Biol. Cell* **18**, 3250–3263 (2008).
129. Ganley, I. G. *et al.* ULK1·ATG13·FIP200 complex mediates mTOR signaling and is essential for autophagy. *J. Biol. Chem.* **284**, 12297–12305 (2009).
130. Kim, B. W. *et al.* The C-terminal region of ATG101 bridges ULK1 and PtdIns3K complex in autophagy initiation. *Autophagy* **14**, 2104–2116 (2018).
131. Park, J. M. *et al.* The ULK1 complex mediates MTORC1 signaling to the autophagy initiation machinery via binding and phosphorylating ATG14. *Autophagy* **12**, 547–564 (2016).
132. Yu, L., Chen, Y. & Tooze, S. A. Autophagy pathway: Cellular and molecular mechanisms. *Autophagy* **14**, 207–215 (2018).
133. Suzuki, H., Kaizuka, T., Mizushima, N. & Noda, N. N. Structure of the Atg101-Atg13 complex reveals essential roles of Atg101 in autophagy initiation. *Nat. Struct. Mol. Biol.* **22**, 572–580 (2015).
134. Nishimura, T. *et al.* FIP200 regulates targeting of Atg16L1 to the isolation membrane. *EMBO Rep.* **14**, 284–291 (2013).
135. Suzuki, K., Kubota, Y., Sekito, T. & Ohsumi, Y. Hierarchy of Atg proteins in pre-autophagosomal structure organization. *Genes to Cells* **12**, 209–218 (2007).
136. Itakura, E. & Mizushima, N. Characterization of autophagosome formation site by a hierarchical analysis of mammalian Atg proteins. *Autophagy* **6**, 764–776 (2010).
137. Zhang, D. *et al.* AMPK regulates autophagy by phosphorylating BECN1 at threonine 388. *Autophagy* **12**, 1447–1459 (2016).
138. Kim, J. *et al.* Differential regulation of distinct Vps34 complexes by AMPK in nutrient stress and autophagy. *Cell* **152**, 290–303 (2013).
139. Di Bartolomeo, S. *et al.* The dynamic interaction of AMBRA1 with the dynein motor complex regulates mammalian autophagy. *J. Cell Biol.* **191**, 155–168 (2010).
140. Alemu, E. A. *et al.* ATG8 family proteins act as scaffolds for assembly of the ULK

complex: Sequence requirements for LC3-interacting region (LIR) motifs. *J. Biol. Chem.* **287**, 39275–39290 (2012).

141. Tang, H. W. *et al.* Atg1-mediated myosin II activation regulates autophagosome formation during starvation-induced autophagy. *EMBO J.* **30**, 636–651 (2011).
142. Sekito, T., Kawamata, T., Ichikawa, R., Suzuki, K. & Ohsumi, Y. Atg17 recruits Atg9 to organize the pre-autophagosomal structure. *Genes to Cells* **14**, 525–538 (2009).
143. Suzuki, S. W. *et al.* Atg13 HORMA domain recruits Atg9 vesicles during autophagosome formation. *Proc. Natl. Acad. Sci. U. S. A.* **112**, 3350–3355 (2015).
144. Pickart, C. M. & Eddins, M. J. Ubiquitin: Structures, functions, mechanisms. *Biochim. Biophys. Acta - Mol. Cell Res.* **1695**, 55–72 (2004).
145. Shpilka, T., Weidberg, H., Pietrokovski, S., Elazar, * and Zvulun & *. Atg8: an autophagy-related ubiquitin-like protein family. *Genome Biol.* **12**, 222–236 (2011).
146. Érdi, B. *et al.* Loss of the starvation-induced gene Rack1 leads to glycogen deficiency and impaired autophagic responses in Drosophila. *Autophagy* **8**, 1124–1135 (2012).
147. Mulakkal, N. C. *et al.* Autophagy in drosophila: From historical studies to current knowledge. *Biomed Res. Int.* **2014**, (2014).
148. Matsushita, M. *et al.* Structure of Atg5·Atg16, a complex essential for autophagy. *J. Biol. Chem.* **282**, 6763–6772 (2007).
149. Kabeya, Y. *et al.* Erratum: LC3, a mammalian homolog of yeast Apg8p, is localized in autophagosome membranes after processing (EMBO Journal (2000) 19 (5720-5728)). *EMBO J.* **22**, 4577 (2003).
150. Kirisako, T. *et al.* Formation process of autophagosome is traced with Apg8/Aut7p in yeast. *J. Cell Biol.* **147**, 435–446 (1999).
151. Wild, P., McEwan, D. G. & Dikic, I. The LC3 interactome at a glance. *J. Cell Sci.* **127**, 3–9 (2014).
152. Nguyen, T. N. *et al.* Atg8 family LC3/GAB ARAP proteins are crucial for autophagosome-lysosome fusion but not autophagosome formation during PINK1/Parkin mitophagy and starvation. *J. Cell Biol.* **215**, 857–874 (2016).
153. Tsuboyama, K. *et al.* The ATG conjugation systems are important for degradation of the inner autophagosomal membrane. *Science (80-.).* **354**, 1036–1041 (2016).
154. Zhiping Xie, Usha Nair, and D. J. K. Atg8 controls phagophore expansion during autophagosome formation. *Mol. Biol. Cell* **18**, 3250–3263 (2007).
155. Suzuki, K., Kubota, Y., Sekito, T. & Ohsumi, Y. Hierarchy of Atg proteins in pre-autophagosomal structure organization. *Genes to Cells* **12**, 209–218 (2007).

156. Lassak, A. *et al.* Molecular and structural traits of IRS-1/LC3 nuclear structures and their role in autophagy control and tumor cell survival. *Mol. Cell. Biol.* MCB.00608-17 (2018) doi:10.1128/MCB.00608-17.
157. Song, T., Su, H., Yin, W., Wang, L. & Huang, R. Acetylation modulates LC3 stability and cargo recognition. *FEBS Lett.* **593**, 414–422 (2019).
158. Huang, R. *et al.* Deacetylation of nuclear LC3 drives autophagy initiation under starvation. *Mol. Cell* **57**, 456–467 (2015).
159. Kraft, L. J., Manral, P., Dowler, J. & Kenworthy, A. K. Nuclear LC3 associates with slowly diffusing complexes that survey the nucleolus. *Traffic* **17**, 369–399 (2016).
160. Petiot, A., Ogier-Denis, E., Blommaart, E. F. C., Meijer, A. J. & Codogno, P. Erratum: Distinct classes of phosphatidylinositol 3'-kinases are involved in signaling pathways that control macro-autophagy in HT-29 cells (Journal of Biological Chemistry (2000) 275 (992-998)). *J. Biol. Chem.* **275**, 12360 (2000).
161. Xie, Y. *et al.* Posttranslational modification of autophagy-related proteins in macroautophagy. **11**, 28–45 (2015).
162. Matsunaga, K. *et al.* Two Beclin 1-binding proteins, Atg14L and Rubicon, reciprocally regulate autophagy at different stages. *Nat. Cell Biol.* **11**, 385–396 (2009).
163. Russell, R. C. *et al.* ULK1 induces autophagy by phosphorylating Beclin-1 and activating VPS34 lipid kinase. *Nat. Cell Biol.* **15**, 741–750 (2013).
164. Nobukuni, T. *et al.* Amino acids mediate mTOR/raptor signaling through activation of class 3 phosphatidylinositol 3OH-kinase. *Proc. Natl. Acad. Sci. U. S. A.* **102**, 14238–14243 (2005).
165. Lu, Q. *et al.* The WD40 Repeat PtdIns(3)P-Binding Protein EPG-6 Regulates Progression of Omegasomes to Autophagosomes. *Dev. Cell* **21**, 343–357 (2011).
166. Polson, H. E. J. *et al.* Mammalian Atg18 (WIPI2) localizes to omegasome-anchored phagophores and positively regulates LC3 lipidation. *Autophagy* **6**, 506–522 (2010).
167. Chowdhury, S. *et al.* Insights into autophagosome biogenesis from structural and biochemical analyses of the ATG2A-WIPI4 complex. *Proc. Natl. Acad. Sci. U. S. A.* **115**, E9792–E9801 (2018).
168. Rieter, E. *et al.* Atg18 function in autophagy is regulated by specific sites within its β-propeller. *J. Cell Sci.* **126**, 593–604 (2013).
169. Takáts, S. *et al.* Autophagosomal Syntaxin17-dependent lysosomal degradation maintains neuronal function in Drosophila. *J. Cell Biol.* **201**, 531–539 (2013).
170. Webber, J. L. & Tooze, S. A. Coordinated regulation of autophagy by p38a MAPK

through mAtg9 and p38IP. *EMBO J.* **29**, 27–40 (2010).

171. Orsi, A. *et al.* Dynamic and transient interactions of Atg9 with autophagosomes, but not membrane integration, are required for autophagy. *Mol. Biol. Cell* **23**, 1860–1873 (2012).
172. Weerasekara, V. K. *et al.* Metabolic-Stress-Induced Rearrangement of the 14-3-3 Interactome Promotes Autophagy via a ULK1- and AMPK-Regulated 14-3-3 Interaction with Phosphorylated Atg9. *Mol. Cell. Biol.* **34**, 4379–4388 (2014).
173. Rogov, V., Dötsch, V., Johansen, T. & Kirkin, V. Interactions between Autophagy Receptors and Ubiquitin-like Proteins Form the Molecular Basis for Selective Autophagy. *Mol. Cell* **53**, 167–178 (2014).
174. Geng, J. & Klionsky, D. J. The Atg8 and Atg12 ubiquitin-like conjugation systems in macroautophagy. 'Protein Modifications: Beyond the Usual Suspects' Review Series. *EMBO Rep.* **9**, 859–864 (2008).
175. Mizushima, N. *et al.* Mouse Apg16L, a novel WD-repeat protein, targets to the autophagic isolation membrane with the Apg12-Apg5 conjugate. *J. Cell Sci.* **116**, 1679–1688 (2003).
176. Nakatogawa, H., Ichimura, Y. & Ohsumi, Y. Atg8, a Ubiquitin-like Protein Required for Autophagosome Formation, Mediates Membrane Tethering and Hemifusion. *Cell* **130**, 165–178 (2007).
177. Lőrincz, P. & Juhász, G. Autophagosome-Lysosome Fusion. *J. Mol. Biol.* 1–21 (2019) doi:10.1016/j.jmb.2019.10.028.
178. Itakura, E., Kishi-Itakura, C. & Mizushima, N. The hairpin-type tail-anchored SNARE syntaxin 17 targets to autophagosomes for fusion with endosomes/lysosomes. *Cell* **151**, 1256–1269 (2012).
179. Rusten, T. E. *et al.* ESCRTs and Fab1 Regulate Distinct Steps of Autophagy. *Curr. Biol.* **17**, 1817–1825 (2007).
180. Mindell, J. A. Lysosomal Acidification Mechanisms. *Annu. Rev. Physiol.* **74**, 69–86 (2012).
181. Tanida, I. Lysosomal Turnover, but Not a Cellular Level, of Endogenous LC3 is a Marker for Autophagy. *Autophagy* **1**, 84–91 (2005).
182. Novak, I. *et al.* Nix is a selective autophagy receptor for mitochondrial clearance. *EMBO Rep.* **11**, 45 LP – 51 (2010).
183. Deosaran, E. *et al.* NBR1 acts as an autophagy receptor for peroxisomes. *J. Cell Sci.* **126**, 939–952 (2013).
184. Zheng, Y. T. *et al.* The Adaptor Protein p62/SQSTM1 Targets Invading Bacteria to the Autophagy Pathway. *J. Immunol.* **183**, 5909–5916 (2009).
185. Dupont, N. *et al.* Shigella Phagocytic Vacuolar Membrane Remnants Participate in the

Cellular Response to Pathogen Invasion and Are Regulated by Autophagy. *Cell Host Microbe* **6**, 137–149 (2009).

186. Kraft, C., Deplazes, A., Sohrmann, M. & Peter, M. Mature ribosomes are selectively degraded upon starvation by an autophagy pathway requiring the Ubp3p/Bre5p ubiquitin protease. *Nat. Cell Biol.* **10**, 602–610 (2008).
187. Pankiv, S. *et al.* p62/SQSTM1 binds directly to Atg8/LC3 to facilitate degradation of ubiquitinated protein aggregates by autophagy*[S]. *J. Biol. Chem.* **282**, 24131–24145 (2007).
188. Schreiber, A. & Peter, M. Substrate recognition in selective autophagy and the ubiquitin-proteasome system. *Biochim. Biophys. Acta - Mol. Cell Res.* **1843**, 163–181 (2014).
189. Shaid, S., Brandts, C. H., Serve, H. & Dikic, I. Ubiquitination and selective autophagy. *Cell Death Differ.* **20**, 21–30 (2013).
190. Pant, S. *et al.* Landscape of the PARKIN-dependent ubiquitylome in response to mitochondrial depolarization Shireen. *Nature* **496**, 372–376 (2013).
191. Kanki, T., Wang, K., Cao, Y., Baba, M. & Klionsky, D. J. Atg32 is a mitochondrial protein that confers selectivity duringmitophagy. **17**, 98–109 (2010).
192. Thurston, T. L. M., Wandel, M. P., Von Muhlinen, N., Foeglein, Á. & Randow, F. Galectin 8 targets damaged vesicles for autophagy to defend cells against bacterial invasion. *Nature* **482**, 414–418 (2012).
193. Khaminets, A. *et al.* Regulation of endoplasmic reticulum turnover by selective autophagy. *Nature* **522**, 354–358 (2015).
194. Mochida, K. *et al.* Receptor-mediated selective autophagy degrades the endoplasmic reticulum and the nucleus. *Nature* **522**, 359–362 (2015).
195. Jiang, S., Wells, C. & Roach, P. J. Starch-binding domain-containing protein 1 (Stbd1) and glycogen metabolism: Identification of the Atg8 family interacting motif (AIM) in Stbd1 required for interaction with GABARAPL1. *Biochem. Biophys. Res. Commun.* **413**, 420–425 (2011).
196. Korac, J. *et al.* Ubiquitin-independent function of optineurin in autophagic clearance of protein aggregates. *J. Cell Sci.* **126**, 580–592 (2013).
197. Grasso, D. *et al.* Zymophagy, a novel selective autophagy pathway mediated by VMP1-USP9x-p62, prevents pancreatic cell death. *J. Biol. Chem.* **286**, 8308–8324 (2011).
198. Pohl, C. & Jentsch, S. Midbody ring disposal by autophagy is a post-abscission event of cytokinesis. *Nat. Cell Biol.* **11**, 65–70 (2009).
199. Watson, R. O., Manzanillo, P. S. & Cox, J. S. Extracellular M. tuberculosis DNA targets bacteria for autophagy by activating the host DNA-sensing pathway. *Cell* **150**, 803–815

(2012).

200. Nezis, I. P. *et al.* Ref(2)P, the Drosophila melanogaster homologue of mammalian p62, is required for the formation of protein aggregates in adult brain. *J. Cell Biol.* **180**, 1065–1071 (2008).

201. Nezis, I. P. & Stenmark, H. p62 at the interface of autophagy, oxidative stress signaling, and cancer. *Antioxid. Redox Signal.* **17**, 786–793 (2012).

202. Tusco, R. *et al.* Kenny mediates selective autophagic degradation of the IKK complex to control innate immune responses. *Nat. Commun.* **8**, 1–15 (2017).

203. Finley, K. D. *et al.* Blue cheese mutations define a novel, conserved gene involved in progressive neural degeneration. *J. Neurosci.* **23**, 1254–1264 (2003).

204. Chang, C.-Y. & Huang, W.-P. Atg19 Mediates a Dual Interaction Cargo Sorting Mechanism in Selective Autophagy. *Mol. Biol. Cell* **18**, 919–929 (2006).

205. Kraft, C., Peter, M. & Hofmann, K. Selective autophagy: ubiquitin-mediated recognition and beyond. *Nat. Cell Biol.* **12**, 836–841 (2010).

206. Birgisdottir, A. B., Lamark, T. & Johansen, T. The LIR motif – crucial for selective autophagy. *J. Cell Sci.* **126**, 3552–3562 (2013).

207. Birgisdottir, A. B., Lamark, T. & Johansen, T. The LIR motif - crucial for selective autophagy. *J. Cell Sci.* **126**, 3237–3247 (2013).

208. Suzuki, H. *et al.* Structural Basis of the Autophagy-Related LC3/Atg13 LIR Complex: Recognition and Interaction Mechanism. *Structure* **22**, 47–58 (2014).

209. Noda, N. N., Ohsumi, Y. & Inagaki, F. Atg8-family interacting motif crucial for selective autophagy. *FEBS Lett.* **584**, 1379–1385 (2010).

210. Schreiber, A. & Peter, M. Substrate recognition in selective autophagy and the ubiquitin-proteasome system. *Biochim. Biophys. Acta - Mol. Cell Res.* **1843**, 163–181 (2014).

211. Noda, N. N. *et al.* Structural basis of target recognition by Atg8/LC3 during selective autophagy. *Genes to Cells* **13**, 1211–1218 (2008).

212. Jain, A. *et al.* P62/sequestosome-1, autophagy-related gene 8, and autophagy in Drosophila are regulated by nuclear factor erythroid 2-related factor 2(NRF2), independent of transcription factor TFEB. *J. Biol. Chem.* **290**, 14945–14962 (2015).

213. Popelka, H. & Klionsky, D. J. Structural basis for extremely strong binding affinity of giant ankyrins to LC3 / GABARAP and its application in the inhibition of autophagy GABARAP and its application in the inhibition of autophagy. *Autophagy* **14**, 1847–1849 (2018).

214. Alemu, E. A. *et al.* ATG8 family proteins act as scaffolds for assembly of the ULK

complex: Sequence requirements for LC3-interacting region (LIR) motifs. *J. Biol. Chem.* **287**, 39275–39290 (2012).

215. Kalvari, I. *et al.* iLIR: A web resource for prediction of Atg8-family interacting proteins. *Autophagy* **10**, 913–925 (2014).
216. McEwan, D. G. *et al.* PLEKHM1 regulates autophagosome-lysosome fusion through HOPS complex and LC3/GABARAP proteins. *Mol. Cell* **57**, 39–54 (2015).
217. Pankiv, S. *et al.* FYCO1 is a Rab7 effector that binds to LC3 and PI3P to mediate microtubule plus end - Directed vesicle transport. *J. Cell Biol.* **188**, 253–269 (2010).
218. Satoo, K. *et al.* The structure of Atg4B-LC3 complex reveals the mechanism of LC3 processing and delipidation during autophagy. *EMBO J.* **28**, 1341–1350 (2009).
219. Ichimura, Y. *et al.* Structural basis for sorting mechanism of p62 in selective autophagy. *J. Biol. Chem.* **283**, 22847–22857 (2008).
220. Thurston, T. L. M., Ryzhakov, G., Bloor, S., von Muhlinen, N. & Randow, F. The TBK1 adaptor and autophagy receptor NDP52 restricts the proliferation of ubiquitin-coated bacteria. *Nat. Immunol.* **10**, 1215–1221 (2009).
221. Schwarten, M. *et al.* Nix directly binds to GABARAP: a possible crosstalk between apoptosis and autophagy. *Autophagy* **5**, 690–698 (2009).
222. Wild, P. *et al.* Phosphorylation of the autophagy receptor optineurin restricts Salmonella growth. *Science* **333**, 228–233 (2011).
223. Behrends, C. & Fulda, S. Receptor proteins in selective autophagy. *Int. J. Cell Biol.* **2012**, (2012).
224. Marshall, R. S., Li, F., Gemperline, D. C., Book, A. J. & Vierstra, R. D. Autophagic Degradation of the 26S Proteasome Is Mediated by the Dual ATG8/Ubiquitin Receptor RPN10 in Arabidopsis. *Mol. Cell* **58**, 1053–1066 (2015).
225. Marshall, R. S., Hua, Z., Mali, S., McLoughlin, F. & Vierstra, R. D. ATG8-Binding UIM Proteins Define a New Class of Autophagy Adaptors and Receptors. *Cell* **177**, 766-781.e24 (2019).
226. Marshall, R. S., Hua, Z., Mali, S., McLoughlin, F. & Vierstra, R. D. ATG8-Binding UIM Proteins Define a New Class of Autophagy Adaptors and Receptors. *Cell* **177**, 766-781.e24 (2019).
227. Xu, Y. & Wan, W. TP53INP2 mediates autophagic degradation of ubiquitinated proteins through its ubiquitin-interacting motif. *FEBS Lett.* **593**, 1974–1982 (2019).
228. Lei, Y. & Klionsky, D. J. UIM-UDS: a new interface between ATG8 and its interactors. *Cell Res.* **29**, 507–508 (2019).

229. Settembre, C. *et al.* TFEB links autophagy to lysosomal biogenesis. *Science (80-.).* **332**, 1429–1433 (2011).
230. Morselli, E. *et al.* Caloric restriction and resveratrol promote longevity through the Sirtuin-1-dependent induction of autophagy. *Cell Death Dis.* **1**, 1–10 (2010).
231. He, C. *et al.* Exercise-induced BCL2-regulated autophagy is required for muscle glucose homeostasis. *Nature* **481**, 511–515 (2012).
232. Rouschop, K. M. A. *et al.* The unfolded protein response protects human tumor cells during hypoxia through regulation of the autophagy genes MAP1LC3B and ATG5. *J. Clin. Invest.* **120**, 127–141 (2010).
233. Palmieri, M. *et al.* Characterization of the CLEAR network reveals an integrated control of cellular clearance pathways. *Hum. Mol. Genet.* **20**, 3852–3866 (2011).
234. Mammucari, C. *et al.* FoxO3 Controls Autophagy in Skeletal Muscle In Vivo. *Cell Metab.* **6**, 458–471 (2007).
235. Zhao, J. *et al.* FoxO3 Coordinately Activates Protein Degradation by the Autophagic/Lysosomal and Proteasomal Pathways in Atrophying Muscle Cells. *Cell Metab.* **6**, 472–483 (2007).
236. Sanchez, A. M. J. *et al.* AMPK promotes skeletal muscle autophagy through activation of forkhead FoxO3a and interaction with Ulk1. *J. Cell. Biochem.* **113**, 695–710 (2012).
237. Xu, P., Das, M., Reilly, J. & Davis, R. J. JNK regulates FoxO-dependent autophagy in neurons. *Genes Dev.* **25**, 310–322 (2011).
238. Xiong, X., Tao, R., DePinho, R. A. & Dong, X. C. The autophagy-related gene 14 (Atg14) is regulated by forkhead box O transcription factors and circadian rhythms and plays a critical role in hepatic autophagy and lipid metabolism. *J. Biol. Chem.* **287**, 39107–39114 (2012).
239. Liu, H. Y. *et al.* Hepatic autophagy is suppressed in the presence of insulin resistance and hyperinsulinemia. Inhibition of FoxO1-dependent expression of key autophagy genes by insulin. *J. Biol. Chem.* **284**, 31484–31492 (2009).
240. Budanov, A. V. & Karin, M. p53 Target Genes Sestrin1 and Sestrin2 Connect Genotoxic Stress and mTOR Signaling. *Cell* **134**, 451–460 (2008).
241. Chantranupong, L. *et al.* The sestrins interact with gator2 to negatively regulate the amino-acid-sensing pathway upstream of mTORC1. *Cell Rep.* **9**, 1–8 (2014).
242. Crighton, D. *et al.* DRAM, a p53-Induced Modulator of Autophagy, Is Critical for Apoptosis. *Cell* vol. 126 121–134 (2006).
243. Tasdemir, E. *et al.* Regulation of autophagy by cytoplasmic p53. *Nat. Cell Biol.* **10**, 676–687

(2008).

244. Kenselmann, D. B. *et al.* Global genomic profiling reveals an extensive p53-regulated autophagy program contributing to key p53 responses. *J. Appl. Psychol.* **100**, 917–934 (2015).

245. Chauhan, S. *et al.* ZKSCAN3 Is a Master Transcriptional Repressor of Autophagy. *Mol. Cell* **50**, 16–28 (2013).

246. Bowman, C. J., Ayer, D. E. & Dynlacht, B. D. Foxk proteins repress the initiation of starvation-induced atrophy and autophagy programs. *Nat. Cell Biol.* **16**, 1202–1214 (2014).

247. Bernard, A. *et al.* Rph1/KDM4 mediates nutrient-limitation signaling that leads to the transcriptional induction of autophagy. **36**, 1011–1014 (2015).

248. Hemesath, T. J. *et al.* in Melanocyte Development , Defines a Discrete Transcription Factor Family. 2770–2780 (1994).

249. Steingrímsson, E. *et al.* Mitf and Tfe3, two members of the Mitf-Tfe family of bHLH-Zip transcription factors, have important but functionally redundant roles in osteoclast development. *Proc. Natl. Acad. Sci. U. S. A.* **99**, 4477–4482 (2002).

250. Toh, P. P. C. *et al.* Myc inhibition impairs autophagosome formation. *Hum. Mol. Genet.* **22**, 5237–5248 (2013).

251. Nagy, P., Varga, Á., Pircs, K., Hegedus, K. & Juhász, G. Myc-Driven Overgrowth Requires Unfolded Protein Response-Mediated Induction of Autophagy and Antioxidant Responses in Drosophila melanogaster. *PLoS Genet.* **9**, (2013).

252. Sardiello, M. A Gene Network Regulating Lysosomal Biogenesis and Function. 473–478 (2009).

253. Peña-Llopis, S. *et al.* Regulation of TFEB and V-ATPases by mTORC1. *EMBO J.* **30**, 3242–3258 (2011).

254. Martina, J. A., Chen, Y., Gucek, M. & Puertollano, R. MTORC1 functions as a transcriptional regulator of autophagy by preventing nuclear transport of TFEB. *Autophagy* **8**, 903–914 (2012).

255. Shin, H.-J. *et al.* AMPK–SKP2–CARM1 signalling cascade in transcriptional regulation of autophagy. *Nature* **534**, 553–557 (2016).

256. Martina, J. A. *et al.* The nutrient-responsive transcription factor TFE3 promotes autophagy, lysosomal biogenesis, and clearance of cellular debris. *Sci. Signal.* **7**, 1–16 (2014).

257. Ploper, D. *et al.* MITF drives endolysosomal biogenesis and potentiates Wnt signaling in melanoma cells. *Proc. Natl. Acad. Sci. U. S. A.* **112**, E420–E429 (2015).

258. Hallsson, J. H. *et al.* The basic helix-loop-helix leucine zipper transcription factor Mitf is conserved in Drosophila and functions in eye development. *Genetics* **167**, 233–241 (2004).
259. Bouché, V. *et al.* Drosophila Mitf regulates the V-ATPase and the lysosomal-autophagic pathway. *Autophagy* **12**, 484–498 (2016).
260. Sun, X., Chen, W. D. & Wang, Y. D. DAF-16/FOXO transcription factor in aging and longevity. *Front. Pharmacol.* **8**, 1–8 (2017).
261. Juhász, G. *et al.* Gene expression profiling identifies FKBP39 as an inhibitor of autophagy in larval Drosophila fat body. *Cell Death Differ.* **14**, 1181–1190 (2007).
262. Lin, X. X. *et al.* DAF-16/FOXO and HLH-30/TFEB function as combinatorial transcription factors to promote stress resistance and longevity. *Nat. Commun.* **9**, (2018).
263. Füllgrabe, J., Ghislat, G., Cho, D. H. & Rubinsztein, D. C. Transcriptional regulation of mammalian autophagy at a glance. *J. Cell Sci.* **129**, 3059–3066 (2016).
264. Robin, M. *et al.* Drosophila p53 integrates the antagonism between autophagy and apoptosis in response to stress. *Autophagy* **15**, 771–784 (2019).
265. You, H. *et al.* p53-dependent inhibition of FKHRL1 in response to DNA damage through protein kinase SGK1. *Proc. Natl. Acad. Sci. U. S. A.* **101**, 14057–14062 (2004).
266. Brady, O. A. *et al.* The transcription factors TFE3 and TFEB amplify p53 dependent transcriptional programs in response to DNA damage. *Elife* **7**, 1–34 (2018).
267. Urrutia, R. Protein family review KRAB-containing zinc-finger repressor proteins. *Genome Biol.* **4**, 231 (2003).
268. Initial sequencing and analysis of the human genome. *Nature* **412**, 565–566 (2001).
269. Emerson, R. O. & Thomas, J. H. Adaptive evolution in zinc finger transcription factors. *PLoS Genet.* **5**, (2009).
270. Sakamaki, J. *et al.* Emerging roles of transcriptional programs in autophagy regulation. *Transcription* **0**, 00–00 (2017).
271. Li, Y. *et al.* Protein kinase C controls lysosome biogenesis independently of mTORC1. *Nat. Cell Biol.* **18**, 1065–1077 (2016).
272. Bartholomew, C. R. *et al.* Ume6 transcription factor is part of a signaling cascade that regulates autophagy. *Proc. Natl. Acad. Sci. U. S. A.* **109**, 11206–11210 (2012).
273. Banreti, A., Hudry, B., Sass, M., Saurin, A. J. & Graba, Y. Hox Proteins Mediate Developmental and Environmental Control of Autophagy. *Dev. Cell* **28**, 56–69 (2014).
274. Duffraisse, M. *et al.* Role of a versatile peptide motif in controlling Hox nuclear export and autophagy in the Drosophila fat body. *bioRxiv* 843383 (2019) doi:10.1101/843383.
275. Dard, A. *et al.* Human HOX Proteins Use Diverse and Context-Dependent Motifs to

Interact with TALE Class Cofactors. *Cell Rep.* **22**, 3058–3071 (2018).

276. Devenish, R. J. & Prescott, M. Autophagy: Starvation relieves transcriptional repression of ATG genes. *Curr. Biol.* **25**, R238–R240 (2015).
277. Tu, S. *et al.* Identification of histone demethylases in Saccharomyces cerevisiae. *J. Biol. Chem.* **282**, 14262–14271 (2007).
278. Pedruzzi, I. *et al.* TOR and PKA Signaling Pathways Converge on the Protein Kinase Rim15 to Control Entry into G0. *Mol. Cell* **12**, 1607–1613 (2003).
279. Juhász, G., Érdi, B., Sass, M. & Neufeld, T. P. Atg7-dependent autophagy promotes neuronal health, stress tolerance, and longevity but is dispensable for metamorphosis in Drosophila. *Genes Dev.* **21**, 3061–3066 (2007).
280. Howe, F. S., Fischl, H., Murray, S. C. & Mellor, J. Is H3K4me3 instructive for transcription activation? *BioEssays* **39**, 1–12 (2017).
281. Gan, Q. *et al.* Monovalent and unpoised status of most genes in undifferentiated cell-enriched Drosophila testis. *Genome Biol.* **11**, (2010).
282. Sakamaki, J. ichi *et al.* Bromodomain Protein BRD4 Is a Transcriptional Repressor of Autophagy and Lysosomal Function. *Mol. Cell* **66**, 517-532.e9 (2017).
283. Bánréti, Á., Sass, M. & Graba, Y. The emerging role of acetylation in the regulation of autophagy. *Autophagy* **9**, 819–829 (2013).
284. Füllgrabe, J. *et al.* The histone H4 lysine 16 acetyltransferase hMOF regulates the outcome of autophagy. *Nature* **500**, 468–471 (2013).
285. Hale, C. M. *et al.* Identification of modulators of autophagic flux in an image-based high content siRNA screen. *Autophagy* **12**, 713–726 (2016).
286. Yang, X. J. & Seto, E. Lysine Acetylation: Codified Crosstalk with Other Posttranslational Modifications. *Mol. Cell* **31**, 449–461 (2008).
287. Sadoul, K., Wang, J., Diagouraga, B. & Khochbin, S. The tale of protein lysine acetylation in the cytoplasm. *J. Biomed. Biotechnol.* **2011**, (2011).
288. Matsuzaki, H. *et al.* Acetylation of Foxo1 alters its DNA-binding ability and sensitivity to phosphorylation. *Proc. Natl. Acad. Sci. U. S. A.* **102**, 11278–11283 (2005).
289. Shen, Q. *et al.* Acetylation of STX17 (syntaxin 17) controls autophagosome maturation. *Autophagy* **0**, 1 (2020).
290. In, H. L. *et al.* A role for the NAD-dependent deacetylase Sirt1 in the regulation of autophagy. *Proc. Natl. Acad. Sci. U. S. A.* **105**, 3374–3379 (2008).
291. Lee, I. H. & Finkel, T. Regulation of autophagy by the p300 acetyltransferase. *J. Biol. Chem.* **284**, 6322–6328 (2009).

292. Song, T., Su, H., Yin, W., Wang, L. & Huang, R. Acetylation modulates LC3 stability and cargo recognition. *FEBS Lett.* (2019) doi:10.1002/1873-3468.13327.

293. Hariharan, N. *et al.* Deacetylation of FoxO by Sirt1 plays an essential role in mediating starvation-induced autophagy in cardiac myocytes. *Circ. Res.* **107**, 1470–1482 (2010).

294. Lin, S.-Y. *et al.* GSK3-TIP60-ULK1 Signaling Pathway Links Growth Factor Deprivation to Autophagy. *Science (80-.).* **336**, 477 LP – 481 (2012).

295. Yi, C. *et al.* Function and molecular mechanism of acetylation in autophagy regulation. *Science (80-.).* **336**, 474–477 (2012).

296. Cheng, X. *et al.* Pacer Is a Mediator of mTORC1 and GSK3-TIP60 Signaling in Regulation of Autophagosome Maturation and Lipid Metabolism. *Mol. Cell* **73**, 788-802.e7 (2019).

297. Moresi, V. *et al.* Histone deacetylases 1 and 2 regulate autophagy flux and skeletal muscle homeostasis in mice. *Proc. Natl. Acad. Sci. U. S. A.* **109**, 1649–1654 (2012).

298. Oh, M., Choi, I. K. & Kwon, H. J. Inhibition of histone deacetylase1 induces autophagy. *Biochem. Biophys. Res. Commun.* **369**, 1179–1183 (2008).

299. Yi, C. *et al.* Function and Molecular Mechanism of Acetylation in Autophagy Regulation. *Science (80-.).* **336**, 474–477 (2012).

300. Roccaro, A. M. *et al.* microRNA-dependent modulation of histone acetylation in Waldenstrom macroglobulinemia. *Blood* **116**, 1506–1514 (2010).

301. Hrzenjak, A. *et al.* SAHA induces caspase-independent, autophagic cell death of endometrial stromal sarcoma cells by influencing the mTOR pathway. *J. Pathol.* **216**, 495–504 (2008).

302. Zhang, X. *et al.* HDAC6 Modulates Cell Motility by Altering the Acetylation Level of Cortactin. *Mol. Cell* **27**, 197–213 (2007).

303. Kume, S. *et al.* Calorie restriction enhances cell adaptation to hypoxia through Sirt1-dependent mitochondrial autophagy in mouse aged kidney. *J. Clin. Investig.* **120**, 1043–1055 (2010).

304. Sathyanarayan, A., Mashek, M. T. & Mashek, D. G. ATGL Promotes Autophagy/Lipophagy via SIRT1 to Control Hepatic Lipid Droplet Catabolism. *Cell Rep.* **19**, 1–9 (2017).

305. Latifkar, A. *et al.* Loss of Sirtuin 1 Alters the Secretome of Breast Cancer Cells by Impairing Lysosomal Integrity. *Dev. Cell* **49**, 393-408.e7 (2019).

306. Mukherjee, S. *et al.* Effects of longevinex (modified resveratrol) on cardioprotection and its mechanisms of action. *Can. J. Physiol. Pharmacol.* **88**, 1017–1025 (2010).

307. Guarente, L. & Picard, F. Calorie restriction - The SIR2 connection. *Cell* **120**, 473–482 (2005).

308. Nemoto, S., Fergusson, M. M. & Finkel, T. Nutrient availability regulates SIRT1 through a forkhead-dependent pathway. *Science (80-.).* **306**, 2105–2108 (2004).

309. Cohen, H. Y. *et al.* Calorie restriction promotes mammalian cell survival by inducing the SIRT1 deacetylase. *Science (80-.).* **305**, 390–392 (2004).

310. Ebrahimi, A. *et al.* Bromodomain inhibition of the coactivators CBP/EP300 facilitate cellular reprogramming. *Nat. Chem. Biol.* **15**, 519–528 (2019).

311. Morselli, E. *et al.* Spermidine and resveratrol induce autophagy by distinct pathways converging on the acetylproteome. *J. Cell Biol.* **192**, 615–629 (2011).

312. Black, J. C., Mosley, A., Kitada, T., Washburn, M. & Carey, M. The SIRT2 Deacetylase Regulates Autoacetylation of p300. *Mol. Cell* **32**, 449–455 (2008).

313. Han, Y. *et al.* Acetylation of Sirt2 by p300 attenuates its deacetylase activity. *Biochem. Biophys. Res. Commun.* **375**, 576–580 (2008).

314. Sapountzi, V. & Côté, J. MYST-family histone acetyltransferases: Beyond chromatin. *Cell. Mol. Life Sci.* **68**, 1147–1156 (2011).

315. Cai, Y. *et al.* Identification of New Subunits of the Multiprotein Mammalian TRRAP/TIP60-containing Histone Acetyltransferase Complex. *J. Biol. Chem.* **278**, 42733–42736 (2003).

316. Kusch, T. *et al.* Acetylation by Tip60 is required for selective histone variant exchange at DNA lesions. *Science (80-.).* **306**, 2084–2087 (2004).

317. Lee, J. Y. *et al.* HDAC6 controls autophagosome maturation essential for ubiquitin-selective quality-control autophagy. *EMBO J.* **29**, 969–980 (2010).

318. Dou, Z. *et al.* Autophagy mediates degradation of nuclear lamina. *Nature* **527**, 105–109 (2015).

319. Kraft, L. J., Dowler, J., Manral, P. & Kenworthy, A. K. Size, organization, and dynamics of soluble SQSTM1 and LC3-SQSTM1 complexes in living cells. *Autophagy* **12**, 1660–1674 (2016).

320. Drake, K. R., Kang, M. & Kenworthy, A. K. Nucleocytoplasmic distribution and dynamics of the autophagosome marker EGFP-LC3. *PLoS One* **5**, (2010).

321. Huang, R. & Liu, W. Identifying an essential role of nuclear LC3 for autophagy. *Autophagy* **11**, 852–853 (2015).

322. Gao, F. B., Brenman, J. E., Lily Yeh Jan & Yuh Nung Jan. Genes regulating dendritic outgrowth, branching, and routing in Drosophila (. *Genes Dev.* **13**, 3170 (1999).

323. Cai, Y. *et al.* The mammalian YL1 protein is a shared subunit of the TRRAP/TIP60 histone acetyltransferase and SRCAP complexes. *J. Biol. Chem.* **280**, 13665–13670 (2005).
324. Flegel, K., Grushko, O., Bolin, K., Griggs, E. & Buttitta, L. Roles for the histone modifying and exchange complex Nua4 in cell cycle progression in Drosophila melanogaster. *Genetics* **203**, 1265–1281 (2016).
325. Latrick, C. M. *et al.* Molecular basis and specificity of H2A.Z-H2B recognition and deposition by the histone chaperone YL1. *Nat. Struct. Mol. Biol.* **23**, 309–316 (2016).
326. Liang, X. *et al.* Structural basis of H2A.Z recognition by SRCAP chromatin-remodeling subunit YL1. *Nat. Struct. Mol. Biol.* **23**, 317–323 (2016).
327. Furuyama, T., Banerjee, R. & Breen, thomas, Harte, P. SIR2 Is Required for Polycomb Silencing and Is Associated with an E(Z) Histone Methyltransferase Complex. *Artif. Intell. Med.* **14**, 1118 (2010).
328. Kiss, V. *et al.* Drosophila Atg9 regulates the actin cytoskeleton via interactions with profilin and Ena. *Cell Death Differ.* **27**, 1677–1692 (2020).
329. Brand, A. H. & Perrimon, N. Targeted gene expression as a means of altering cell fates and generating dominant phenotypes. *Development* **118**, 401 LP – 415 (1993).
330. Neckameyer, W. S. & Argue, K. J. Comparative approaches to the study of physiology: Drosophila as a physiological tool. *Am. J. Physiol. Regul. Integr. Comp. Physiol.* **304**, R177–R188 (2013).
331. Sethi, S. & Wang, J. W. A versatile genetic tool for post-translational control of gene expression in Drosophila melanogaster. *Elife* **6**, 1–17 (2017).
332. Lee, J., Cranna, N., Chahal, A. & Quinn, L. Genetic Systems to Investigate Regulation of Oncogenes and Tumour Suppressor Genes in Drosophila. *Cells* **1**, 1182–1196 (2012).
333. Ajjuri, R. R., Hall, M., Reiter, L. T. & O'Donnell, J. M. Drosophila. *Mov. Disord.* 77–96 (2015) doi:10.1016/B978-0-12-405195-9.00005-6.
334. Dietzl, G. *et al.* A genome-wide transgenic RNAi library for conditional gene inactivation in Drosophila. *Nature* **448**, 151–156 (2007).
335. Nezis, L. P. *et al.* Cell death during Drosophila melanogaster early oogenesis is mediated through autophagy. *Autophagy* **5**, 298–302 (2009).
336. Kimura, S., Noda, T. & Yoshimori, T. Dissection of the autophagosome maturation process by a novel reporter protein, tandem fluorescent-tagged LC3. *Autophagy* **3**, 452–460 (2007).
337. Nezis, I. P. *et al.* Autophagic degradation of dBruce controls DNA fragmentation in nurse cells during late Drosophila melanogaster oogenesis. *J. Cell Biol.* **190**, 523–531 (2010).

338. Jacomin, A.-C. & Nezis, I. P. Using Fluorescent Reporters to Monitor Autophagy in the Female Germline Cells in Drosophila melanogaster. in *Oogenesis: Methods and Protocols* (ed. Nezis, I. P.) 69–78 (Springer New York, 2016). doi:10.1007/978-1-4939-3795-0_5.

339. Mauvezin, C. *et al.* The nuclear cofactor DOR regulates autophagy in mammalian and Drosophila cells. *EMBO Rep.* **11**, 37–44 (2010).

340. Teleman, A. A. dDOR Is an EcR Coactivator that Forms a Feed-Forward Loop Connecting Insulin and Ecdysone Signaling. *J. Am. Acad. Child Psychiatry* **24**, 239 (1985).

341. Laemmli, U. K. Cleavage of structural proteins during the assembly of the head of bacteriophage T4. *Nature* **227**, 680–685 (1970).

342. Nesvizhskii, A. I., Keller, A., Kolker, E. & Aebersold, R. A statistical model for identifying proteins by tandem mass spectrometry. *Anal. Chem.* **75**, 4646–4658 (2003).

343. Nitzsche, A., Steinhausser, C., Mucke, K., Paulus, C. & Nevels, M. Histone H3 Lysine 4 Methylation Marks Postreplicative Human Cytomegalovirus Chromatin. *J. Virol.* **86**, 9817–9827 (2012).

344. Letunic, I., Doerks, T. & Bork, P. SMART: Recent updates, new developments and status in 2015. *Nucleic Acids Res.* **43**, D257–D260 (2015).

345. Schultz, J., Milpetz, F., Bork, P. & Ponting, C. P. SMART, a simple modular architecture research tool: Identification of signaling domains. *Proc. Natl. Acad. Sci. U. S. A.* **95**, 5857–5864 (1998).

346. Papadopoulos, J. S. & Agarwala, R. COBALT: Constraint-based alignment tool for multiple protein sequences. *Bioinformatics* **23**, 1073–1079 (2007).

347. Smith, T. F. & Wateran, M. S. Identification of Common Molecular Subsequences. *J. molec* 195–197 (1981).

348. R. R: A language and environment for statistical computing. R Foundation for Statistical Computing. URL http://www.R-project.org/ (2013).

349. Bailey, T. L. *et al.* MEME SUITE : tools for motif discovery and searching. **37**, 202–208 (2009).

350. Frith, M. C., Saunders, N. F. W., Kobe, B. & Bailey, T. L. Discovering sequence motifs with arbitrary insertions and deletions. *PLoS Comput. Biol.* **4**, (2008).

351. Mathelier, A. & Wasserman, W. W. The Next Generation of Transcription Factor Binding Site Prediction. *PLoS Comput. Biol.* **9**, (2013).

352. Holm, S. A Simple Sequentially Rejective Multiple Test Procedure. *Scand. J. Stat.* **6**, 65–70 (1979).

353. Husnjak, K. & Dikic, I. Ubiquitin-Binding Proteins: Decoders of Ubiquitin-Mediated

Cellular Functions. *Annu. Rev. Biochem.* **81**, 291–322 (2012).

354. Tusco, R. Molecular mechanisms of selective autophagy in innate immunity. *Thesis* (2017).
355. Mulakkal, N. C. Molecular mechanisms of selective autophagy in Drosophila Melanogaster. *Thesis* (2016).
356. Jacomin, A. C., Samavedam, S., Charles, H. & Nezis, I. P. iLIR databases: A web resource for LIR motif-containing proteins in eukaryotes. *Autophagy* **13**, 1782–1789 (2017).
357. Wiesner, C. *et al.* Prediction of Protein Binding Regions in Disordered Proteins. *PLoS One* **7**, 1–10 (2012).
358. Mei, Y. *et al.* Intrinsically disordered regions in autophagy proteins. *Proteins Struct. Funct. Bioinforma.* **82**, 565–578 (2014).
359. Popelka, H. & Klionsky, D. J. Analysis of the native conformation of the LIR/AIM motif in the Atg8/LC3/GABARAP-binding proteins. *Autophagy* **11**, 2153–2159 (2015).
360. Brenman, J. E., Gao, F. B., Jan, L. Y. & Jan, Y. N. Sequoia, a Tramtrack-Related Zinc Finger Protein, Functions as a Pan-Neural Regulator for Dendrite and Axon Morphogenesis in Drosophila. *Dev. Cell* **1**, 667–677 (2001).
361. Xiong, W. C. & Montell, C. tramtrack is a transcriptional repressor required for cell fate determination in the Drosophila eye. *Genes Dev.* **7**, 1085–1096 (1993).
362. Petrovic, M. & Hummel, T. Temporal identity in axonal target layer recognition. *Nature* **456**, 800–804 (2008).
363. Andrews, H. K., Giagtzoglou, N., Yamamoto, S., Schulze, K. L. & Bellen, H. J. Sequoia regulates cell fate decisions in the external sensory organs of adult Drosophila. *EMBO Rep.* **10**, 636–641 (2009).
364. Araújo, S. J. & Casanova, J. Sequoia establishes tip-cell number in drosophila trachea by regulating FGF levels. *Development* **138**, 2335–2340 (2011).
365. Gunnar, E., Bivik, C., Starkenberg, A. & Thor, S. Sequoia controls the type I>0 daughter proliferation switch in the developing drosophila nervous system. *Dev.* **143**, 3774–3784 (2016).
366. Li, Z. *et al.* A Switch in Tissue Stem Cell Identity Causes Neuroendocrine Tumors in Drosophila Gut. *Cell Rep.* **30**, 1724-1734.e4 (2020).
367. Jain, A. *et al.* P62/sequestosome-1, autophagy-related gene 8, and autophagy in Drosophila are regulated by nuclear factor erythroid 2-related factor 2(NRF2), independent of transcription factor TFEB. *J. Biol. Chem.* **290**, 14945–14962 (2015).
368. Gu, Y. *et al.* Mammalian Atg8 proteins regulate lysosome and autolysosome biogenesis through SNARE s . *EMBO J.* **38**, 1–22 (2019).

369. Skytte Rasmussen, M. *et al.* ATG4B contains a C-terminal LIR motif important for binding and efficient cleavage of mammalian orthologs of yeast Atg8. *Autophagy* **13**, 834–853 (2017).
370. Wirth, M. *et al.* Molecular determinants regulating selective binding of autophagy adapters and receptors to ATG8 proteins. *Nat. Commun.* **10**, (2019).
371. Clissold, P. M. & Ponting, C. P. JmjC: cupin metalloenzyme-like domains in jumonji, hairless and phospholipase A2beta. *Trends Biochem. Sci.* **26**, 7–9 (2001).
372. Shalaby, N. A. *et al.* Systematic discovery of genetic modulation by Jumonji histone demethylases in Drosophila. *Sci. Rep.* **7**, 1–12 (2017).
373. Aasland, R., Gibson, T. J. & Stewart, A. F. The PHD finger: Implications for chromatin-mediated transcriptional regulation. *Trends Biochem. Sci.* **20**, 56–59 (1995).
374. Harrison, S. D. & Travers, A. A. The tramtrack gene encodes a Drosophila finger protein that interacts with the ftz transcriptional regulatory region and shows a novel embryonic expression pattern. *EMBO J.* **9**, 207–216 (1990).
375. Pagans, S. The Drosophila transcription factor tramtrack (TTK) interacts with Trithorax-like (GAGA) and represses GAGA-mediated activation. *Nucleic Acids Res.* **30**, 4406–4413 (2002).
376. Jacomin, A. C. *et al.* Regulation of Expression of Autophagy Genes by Atg8a-Interacting Partners Sequoia, YL-1, and Sir2 in Drosophila. *Cell Rep.* **31**, 107695 (2020).
377. Shiga, Y., Tanaka-Matakatsu, M. & Hayashi, S. A nuclear GFP/B-galactosidase fusion protein as a marker for morphogenesis in living Drosophila. (1996).
378. Schindelin, J. *et al.* Fiji: An open-source platform for biological-image analysis. *Nat. Methods* **9**, 676–682 (2012).
379. Dunn, K. W., Kamocka, M. M. & McDonald, J. H. A practical guide to evaluating colocalization in biological microscopy. *Am. J. Physiol. Cell Physiol.* **300**, C723–C742 (2011).
380. Adler, J. & Parmryd, I. Quantifying colocalization by correlation: The pearson correlation coefficient is superior to the Mander's overlap coefficient. *Cytom. Part A* **77**, 733–742 (2010).
381. Day, R. N. & Davidson, M. W. Fluorescent proteins for FRET microscopy: monitoring protein interactions in living cells. *Bioessays* **34**, 341–350 (2013).
382. Boda, A. *et al.* Drosophila Arl8 is a general positive regulator of lysosomal fusion events. *Biochim. Biophys. Acta - Mol. Cell Res.* **1866**, 533–544 (2019).
383. Lakatos, Z. & L, P. Sec20 Is Required for Autophagic and Endocytic. (2019).
384. Bali, A. & Shravage, B. V. Characterization of the autophagy related gene-8a (Atg8a)

promoter in drosophila melanogaster. *Int. J. Dev. Biol.* **61**, 551–555 (2017).

385. Porter, K., Nallathambi, J., Lin, Y. & Liton, P. B. Lysosomal basification and decreased autophagic flux in oxidatively stressed trabecular meshwork cells Implications for glaucoma pathogenesis. *Autophagy* **9**, 581–594 (2013).
386. Touzet, H. & Varré, J. S. Efficient and accurate P-value computation for position weight matrices. *Algorithms Mol. Biol.* **2**, 1–12 (2007).
387. Baglivo, I. *et al.* The structural role of the zinc ion can be dispensable in prokaryotic zinc-finger domains. *Proc. Natl. Acad. Sci. U. S. A.* **106**, 6933–6938 (2009).
388. Bailey, T. L. & Elkan, C. The value of prior knowledge in discovering motifs with MEME. *Proc. Int. Conf. Intell. Syst. Mol. Biol.* **3**, 21–29 (1995).
389. Liu, J. S., Neuwald, A. F. & Lawrence, C. E. Bayesian Models for Multiple Local Sequence Alignment and Gibbs Sampling Strategies. *J. Am. Stat. Assoc.* **90**, 1156–1170 (1995).
390. Wunderlich, Z. & Mirny, L. Different gene regulation strategies revealed by analysis of binding motifs. *Trends Genet.* **25**, 429–434 (2009).
391. Hooghe, B., Broos, S., Van Roy, F. & De Bleser, P. A flexible integrative approach based on random forest improves prediction of transcription factor binding sites. *Nucleic Acids Res.* **40**, (2012).
392. Xu, P. *et al.* The NuA4 Core Complex Acetylates Nucleosomal Histone H4 through a Double Recognition Mechanism. *Mol. Cell* **63**, 965–975 (2016).
393. Palu, R. A. S. & Thummel, C. S. Sir2 Acts through Hepatocyte Nuclear Factor 4 to maintain insulin Signaling and Metabolic Homeostasis in Drosophila. *PLoS Genet.* **12**, 1–18 (2016).
394. Reis, T., Gilst, M. R. Van & Hariharan, I. K. A Buoyancy-Based Screen of Drosophila Larvae for Fat- Storage Mutants Reveals a Role for Sir2 in Coupling Fat Storage to Nutrient Availability. **6**, (2010).
395. Banerjee, K. K., Deshpande, R. S., Koppula, P., Ayyub, C. & Kolthur-seetharam, U. Central metabolic sensing remotely controls nutrient-sensitive endocrine response in Drosophila via Sir2 / Sirt1 – upd2 – IIS axis. **106**, 1187–1191 (2017).
396. Ali, I. *et al.* Lysine Acetylation Goes Global: From Epigenetics to Metabolism and Therapeutics. *Chem. Rev.* **118**, 1216–1252 (2019).
397. Burnett, C. *et al.* Absence of effects of Sir2 over-expression on lifespan in C.elegans and Drosophila. **477**, 482–485 (2012).
398. Tang, H. W. *et al.* Atg9 interacts with dTRAF2/TRAF6 to regulate oxidative stress-induced JNK activation and autophagy induction. *Dev. Cell* **27**, 489–503 (2013).

399. Pircs, K. *et al.* Advantages and Limitations of Different p62-Based Assays for Estimating Autophagic Activity in Drosophila. *PLoS One* **7**, (2012).
400. Shokri, L. *et al.* A Comprehensive Drosophila melanogaster Transcription Factor Interactome. *Cell Rep.* **27**, 955-970.e7 (2019).
401. Lee, I. H. *et al.* A role for the NAD-dependent deacetylase Sirt1 in the regulation of autophagy. 1–6 (2008).
402. Baumgartner, B. G. *et al.* Identification of a novel modulator of thyroid hormone receptor-mediated action. *PLoS One* **2**, 1–13 (2007).
403. Sancho, A. *et al.* Dor/tp53inp2 and tp53inp1 constitute a metazoan gene family encoding dual regulators of autophagy and transcription. *PLoS One* **7**, (2012).
404. Nowak, J. *et al.* The TP53INP2 Protein Is Required for Autophagy in Mammalian Cells. **20**, 870–881 (2009).
405. Giot, L. *et al.* A protein interaction map of Drosophila melanogaster. *Science* **302**, 1727–36 (2003).
406. Thurmond, J. *et al.* FlyBase 2.0: The next generation. *Nucleic Acids Res.* **47**, D759–D765 (2019).
407. Francis, A. & Zorzano, A. Article dDOR Is an EcR Coactivator that Forms a Feed-Forward Loop Connecting Insulin and Ecdysone Signaling. 1799–1808 (2010) doi:10.1016/j.cub.2010.08.055.
408. Fields, S. & Song, O. A novel genetic system to detect protein-protein interactions. *Nature* **340**, 245–246 (1989).
409. Brooks, D. *et al. Drosophila NUAK functions with Starvin/BAG3 in autophagic protein turnover. PLoS Genetics* vol. 16 (2020).
410. Johansen, T. & Lamark, T. Selective Autophagy: ATG8 Family Proteins, LIR Motifs and Cargo Receptors. *J. Mol. Biol.* **432**, 80–103 (2020).
411. Verheugd, P. *et al.* Regulation of NF-κB signalling by the mono-ADP-ribosyltransferase ARTD10. *Nat. Commun.* **4**, (2013).
412. O'Hare, K. & Rubin, G. M. Structures of P transposable elements and their sites of insertion and excision in the Drosophila melanogaster genome. *Cell* **34**, 25–35 (1983).
413. You, Z. *et al.* TP53INP2 contributes to autophagosome formation by promoting LC3-ATG7 interaction. *Autophagy* **0**, 15548627.2019.1580510 (2019).
414. Jin, M. *et al.* Transcriptional Regulation by Pho23 Modulates the Frequency of Autophagosome Formation. *Curr. Biol.* **24**, 1314–1322 (2014).
415. Aparicio, R., Rana, A. & Walker, D. W. Upregulation of the Autophagy Adaptor

p62/SQSTM1 Prolongs Health and Lifespan in Middle-Aged Drosophila Ricardo. *Physiol. Behav.* **176**, 139–148 (2016).

416. Shu, W. *et al.* Rph1 coordinates transcription of ribosomal protein genes and ribosomal RNAs to control cell growth under nutrient stress conditions. *Nucleic Acids Res.* **48**, 8360–8373 (2020).
417. Li, F. *et al.* Gcn5-mediated Rph1 acetylation regulates its autophagic degradation under DNA damage stress. *Nucleic Acids Res.* **45**, 5183–5197 (2017).
418. Liang, X. *et al.* Structural basis of H2A.Z recognition by SRCAP chromatin-remodeling subunit YL1. *Nat. Struct. Mol. Biol.* **23**, 317–323 (2016).
419. Xu, C. *et al.* SIRT1 is downregulated by autophagy in senescence and ageing. *Nat. Cell Biol.* (2020) doi:10.1038/s41556-020-00579-5.
420. Hain, D. *et al.* The Drosophila MAST kinase drop out is required to initiate membrane compartmentalisation during cellularisation and regulates dynein-based transport. *Dev.* **141**, 2119–2130 (2014).
421. Liu, X. & Klionsky, D. J. TP53INP2/DOR protein chaperones deacetylated nuclear LC3 to the cytoplasm to promote macroautophagy. *Autophagy* **11**, 1441–1442 (2015).
422. Delorme-Axford, E. & Klionsky, D. J. Transcriptional and post-transcriptional regulation of autophagy in the yeast Saccharomyces cerevisiae. *J. Biol. Chem.* **293**, 5396–5403 (2018).
414. Hong-Min, Ni. *et al.* Dissecting the dynamic turnover of GFP-LC3 in the autolysosome. *Autophagy* **7:2**, 188-204 (2011).

APPENDIX-PUBLICATIONS

A 'Regulation of Expression of Autophagy Genes by Atg8a-Interacting Partners Sequoia, YL-1, and Sir2 in *Drosophila*'

B 'A nuclear role for Atg8-family proteins'

Cell Reports

Report

Regulation of Expression of Autophagy Genes by Atg8a-Interacting Partners Sequoia, YL-1, and Sir2 in *Drosophila*

Graphical Abstract

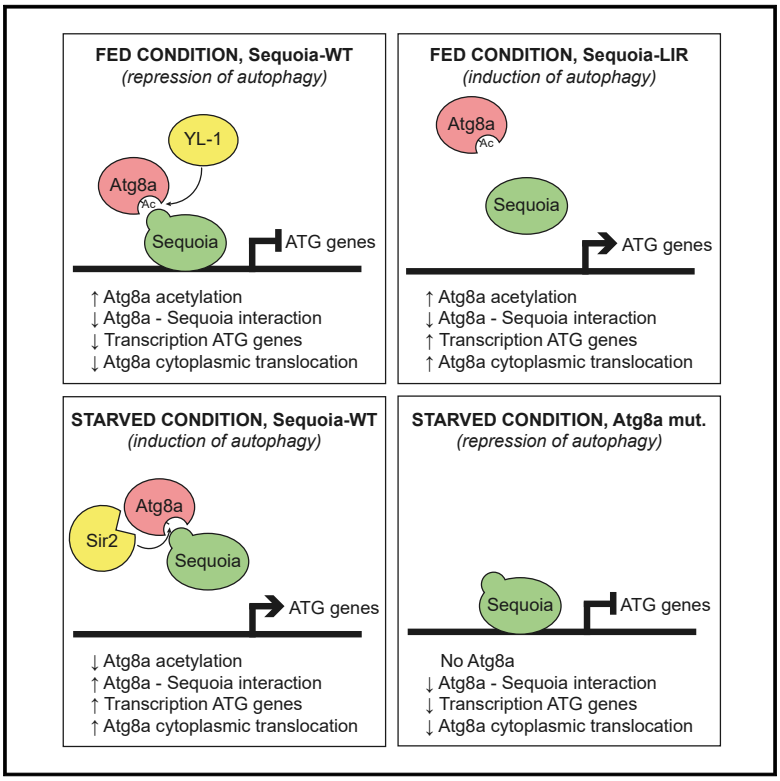

Highlights

- Transcription factor Sequoia is a negative regulator of autophagy
- Sequoia interacts with Atg8a via a LIR motif
- Atg8a interacts with YL-1, a subunit of a nuclear acetyltransferase complex
- Sir2 interacts with and deacetylates Atg8a during starvation

Authors

Anne-Claire Jacomin, Stavroula Petridi, Marisa Di Monaco, ..., Alexander Cameron, Terje Johansen, Ioannis P. Nezis

Correspondence

i.nezis@warwick.ac.uk

In Brief

Jacomin et al. show that Atg8a interacts with transcription factor Sequoia. Depletion of Sequoia induces autophagy through enhanced expression of autophagy genes. Atg8a also interacts with YL-1, a component of a nuclear acetyltransferase complex, and deacetylase Sir2. Sir2 deacetylates Atg8a during starvation to activate autophagy.

Jacomin et al., 2020, Cell Reports *31*, 107695
May 26, 2020
https://doi.org/10.1016/j.celrep.2020.107695

CellPress

Cell Reports

CellPress
OPEN ACCESS

Report

Regulation of Expression of Autophagy Genes by Atg8a-Interacting Partners Sequoia, YL-1, and Sir2 in *Drosophila*

Anne-Claire Jacomin,[1,5] Stavroula Petridi,[1,5] Marisa Di Monaco,[1,5] Zambarlal Bhujabal,[2] Ashish Jain,[2,3,4] Nitha C. Mulakkal,[1] Anthimi Palara,[1,2] Emma L. Powell,[1] Bonita Chung,[1] Cleidiane Zampronio,[1] Alexandra Jones,[1] Alexander Cameron,[1] Terje Johansen,[2] and Ioannis P. Nezis[1,6,*]

[1]School of Life Sciences, University of Warwick, CV4 7AL Coventry, UK

[2]Molecular Cancer Research Group, Institute of Medical Biology, University of Tromsø–The Arctic University of Norway, 9037 Tromsø, Norway

[3]Department of Molecular Cell Biology, Institute for Cancer Research, Oslo University Hospital, Montebello, 0379 Oslo, Norway

[4]Centre for Cancer Cell Reprogramming, Institute of Clinical Medicine, Faculty of Medicine, University of Oslo, Montebello, 0379 Oslo, Norway

[5]These authors contributed equally

[6]Lead Contact

*Correspondence: i.nezis@warwick.ac.uk

https://doi.org/10.1016/j.celrep.2020.107695

SUMMARY

Autophagy is the degradation of cytoplasmic material through the lysosomal pathway. One of the most studied autophagy-related proteins is LC3. Despite growing evidence that LC3 is enriched in the nucleus, its nuclear role is poorly understood. Here, we show that *Drosophila* Atg8a protein, homologous to mammalian LC3, interacts with the transcription factor Sequoia in a LIR motif-dependent manner. We show that Sequoia depletion induces autophagy in nutrient-rich conditions through the enhanced expression of autophagy genes. We show that Atg8a interacts with YL-1, a component of a nuclear acetyltransferase complex, and that it is acetylated in nutrient-rich conditions. We also show that Atg8a interacts with the deacetylase Sir2, which deacetylates Atg8a during starvation to activate autophagy. Our results suggest a mechanism of regulation of the expression of autophagy genes by Atg8a, which is linked to its acetylation status and its interaction with Sequoia, YL-1, and Sir2.

INTRODUCTION

Autophagy is a fundamental, evolutionary conserved process in which cytoplasmic material is degraded through the lysosomal pathway. It is a cellular response during nutrient starvation; yet, it is also responsible in basal conditions for the removal of aggregated proteins and damaged organelles and therefore plays an important role in the maintenance of cellular homeostasis (Ambrosio et al., 2019; Dikic and Elazar, 2018; Füllgrabe et al., 2014; Gatica et al., 2018; Lamb et al., 2013; Sakamaki et al., 2017, 2018). There are three main types of autophagy: macroautophagy, microautophagy, and chaperone-mediated autophagy (Dikic and Elazar, 2018; Gatica et al., 2018; Lamb et al., 2013). Macroautophagy, referred to as autophagy, is the best-described type of autophagy. During macroautophagy, cytoplasmic material is isolated into double-membrane vesicles called autophagosomes. Autophagosomes eventually fuse with lysosomes, allowing for the degradation of cargoes by lysosomal hydrolases. The products of degradation are transported back into the cytoplasm through lysosomal membrane permeases and can be reused by the cell (Dikic and Elazar, 2018; Gatica et al., 2018; Lamb et al., 2013).

One of the most important and well-studied autophagy-related proteins is LC3 (microtubule-associated protein 1 light chain 3, called Atg8 in yeast and *Drosophila*), which participates in autophagosome formation. LC3 interacts with LIR (LC3-interacting region) motifs also known as AIM (Atg8-interacting motifs) on selective autophagy receptors that carry cargo for degradation, and is one of the most widely used markers of autophagy (Gatica et al., 2018; Kabeya et al., 2000). Despite growing evidence that LC3 is enriched in the nucleus, little is known about the mechanisms involved in targeting LC3 to the nucleus and the nuclear components with which it interacts (Dou et al., 2015; Guo et al., 2018; Huang et al., 2015; Kabeya et al., 2000; Klionsky et al., 2016; Kraft et al., 2016).

Here, we show that *Drosophila* Atg8a protein, homologous to mammalian LC3 and yeast Atg8, interacts with the transcription factor Sequoia in a LIR motif-dependent manner that is not responsible for the degradation of Sequoia. We show that Sequoia depletion induces autophagy in nutrient-rich conditions through the enhanced expression of autophagy genes. We also found that Atg8a is acetylated and interacts with YL-1, a component of the NuA4/Tip60 nuclear acetyltransferase complex. We show that Atg8a interacts with the deacetylase

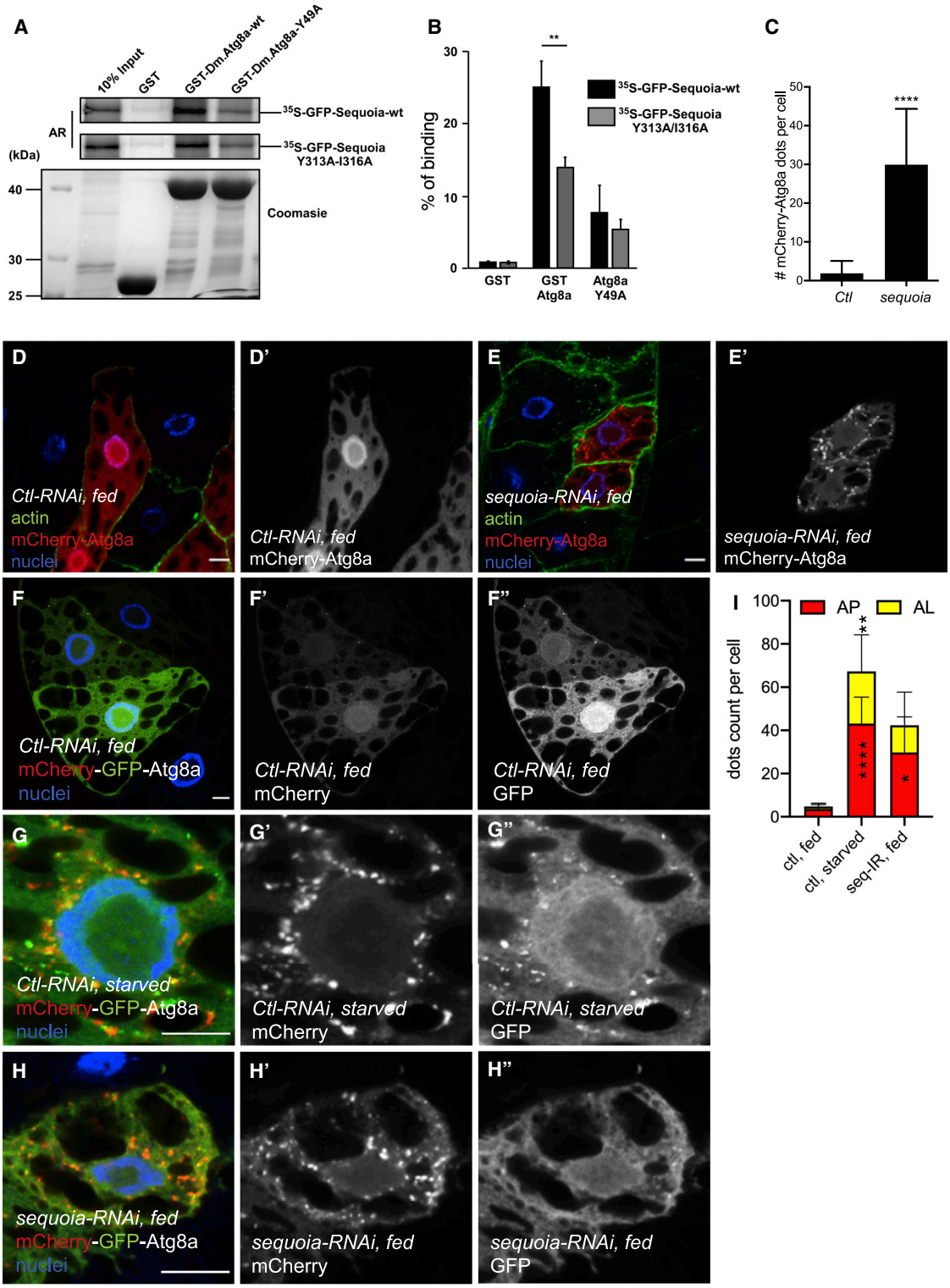

Figure 1. Sequoia Binds to Atg8a via a LIR Motif and Negatively Regulates Autophagy

(A and B) Sequoia interacts with Atg8a in a LIR motif-dependent manner. (A) GST-pull-down assay between GST-tagged Atg8a-WT or Atg8a-LDS mutant (Y49A), and radiolabeled GFP-Sequoia-WT or GFP-Sequoia-LIR mutant (Y313A/316A). GST was used as negative control. Quantification of the binding is shown in (B). Statistical significance was determined using Student's t test; **p < 0.01.

(legend continued on next page)

Sir2, which deacetylates Atg8a during starvation to activate autophagy. Our results suggest a novel mechanism of regulation of autophagy gene expression by Atg8a, which is linked to its acetylation status and its interaction with Sequoia, YL-1, and Sir2.

RESULTS

Transcription Factor Sequoia Is an Atg8a-Interacting Protein

To identify novel Atg8a-interacting proteins in *Drosophila*, we screened the *Drosophila* proteome for LIR motif-containing proteins using the iLIR software that we developed (Jacomin et al., 2016; Kalvari et al., 2014). We found that the transcription factor Sequoia (CG32904) has a predicted LIR motif at position 311–316 with the sequence EEYQVI (Figure S1A) (Jacomin et al., 2016; Kalvari et al., 2014; Popelka and Klionsky, 2015). Sequoia contains two zinc-finger domains that are homologous to the DNA-binding domain of Tramtrack and has been shown to regulate neuronal morphogenesis (Brenman et al., 2001). We confirmed the direct interaction between Sequoia and Atg8a using glutathione S-transferase (GST)-pull-down binding assays (Figures 1A and 1B). This interaction was significantly reduced when we used a mutant of Atg8a in which the LIR motif docking site (LDS) (Y49A) was impaired, indicating that the interaction between Sequoia and Atg8a is LIR motif dependent (Birgisdottir et al., 2013; Ichimura et al., 2008; Jain et al., 2015). Furthermore, point mutations of the Sequoia LIR motif in positions 313 and 316 by alanine substitutions of the aromatic and hydrophobic residues (Y313A and I316A) reduced its binding to Atg8a (Figures 1A and 1B). Using GST-pull-down assays, we also observed that the mammalian homolog of Sequoia, KDM4A, interacts with GABARAP and GABARAP-L1 (the closest mammalian homologs to Atg8a), suggesting evolutionary conservation of the interaction (Figures S1B and S1C). However, mutation of the putative LIR motifs of KDM4A did not abrogate its interaction with GABARAP-L1 (Figure S1C).

Given the observed interaction between Sequoia and Atg8a, we examined whether Sequoia is degraded by autophagy. Western blot analysis showed that endogenous Sequoia is not accumulated in *Atg8a* and *Atg7* mutants compared to wild-type (WT) flies (Figure S1D). These results indicate that Sequoia is an Atg8a-interacting protein and that this interaction is LIR motif dependent. In spite of its interaction with Atg8a, Sequoia is not a substrate for autophagic degradation.

Sequoia Is a Negative Transcriptional Regulator of Autophagy

To examine the role of Sequoia in autophagy, we silenced *sequoia* using RNAi alongside the expression of the autophagic marker mCherry-Atg8a (Chang and Neufeld, 2009; Nezis et al., 2009). We observed a significant increase in the number of mCherry-Atg8a puncta in Sequoia-depleted fat body cells in fed conditions compared to control cells (Figures 1C–1E). An accumulation of $Atg8a^{+}$ puncta in the cell can result either from an induction or a blockade of the autophagic flux. To make the distinction between these two possibilities, we made use of a tandem-tagged Atg8a (GFP-mCherry-Atg8a) (Nezis et al., 2010). In cells expressing RNAi against *sequoia*, we noticed an increased accumulation of red puncta that lack GFP fluorescence compared to the control, suggesting an induction of autophagic flux (Figures 1F–1I). To further test the activation of autophagy in Sequoia-depleted cells, we used western blotting and examined the presence of lipidated Atg8a (Atg8a-II). We observed that Atg8a-II accumulates more in Sequoia-depleted larvae compared to controls (Figures S2A and S2B).

We next examined whether the expression of autophagy genes was affected upon *Sequoia* knockdown. Real-time quantitative PCR (qPCR) analysis showed that the expression of numerous autophagy genes was increased when *sequoia* was silenced (Figure 2A). As Sequoia is a transcription factor and contains C2H2 zinc-finger domains involved in DNA binding, we performed a chromatin immunoprecipitation (ChIP) assay to test the ability of Sequoia to bind the promoter region of autophagy genes (promoter regions shown in Table S1). We found that Sequoia is enriched on the promoters of several autophagy genes, suggesting that Sequoia is acting as a repressor to negatively regulate autophagy (Figure 2B). These results show that Sequoia is a negative transcriptional regulator of autophagy.

The Repressive Activity of Sequoia on Autophagy Depends on Its LIR Motif

To evaluate whether the role of Sequoia in the negative transcriptional regulation of autophagy depends on its interaction with Atg8a via its LIR motif, we created transgenic flies allowing for the expression of GFP-tagged WT (GFP-Sequoia-WT) or LIR mutant (GFP-Sequoia-Y313A/I316A) Sequoia under the control of a UAS region. Expression of the Sequoia LIR mutant demonstrated the reduced presence of Sequoia on the promoter regions of autophagy genes and that correlates with a higher expression level of those genes (Figures 2C–2E). Both GFP-Sequoia-WT and GFP-Sequoia-Y313A/I316A proteins localized

(C–E) Confocal sections of larval fat bodies clonally expressing the autophagy marker mCherry-Atg8a (red) in combination with a control RNAi (D) or a *sequoia* RNAi (E). Fixed fat bodies where stained for cortical actin (green) and nuclei (blue). Scale bar: 10 μm.

(C) Quantification of the number of mCherry-Atg8a dots per cell. Bars denote means ± SDs. Statistical significance was determined using Student's t test; ****$p < 0.0001$.

(F–I) Confocal sections of larval fat bodies clonally expressing the autophagy flux marker GFP-mCherry-Atg8a (red and green) in combination with a control-RNAi in fed (F) or starved (G) or *sequoia*-RNAi in fed larvae. Sequoia depletion induces accumulation of autolysosomes. (H). Fixed fat bodies where stained for nuclei (blue). Scale bar: 10 μm. Quantification of the yellow (AP, autophagosome) and red only (AL, autolysosomes) puncta per cell. Statistical significance was determined using 1-way ANOVA test; *$p < 0.05$, **$p < 0.01$, ****$p < 0.001$.

Genotypes for D: yw hs-Flp;Ac > CD2 > GAL4/+;UAS-mCherry-Atg8a/UAS-luc-RNAi. (E) yw hs-Flp;Ac > CD2 > GAL4/+; UAS-mCherry-Atg8a/UAS-sequoia-RNAi. (F and G) ctl: Cg-GAL4/+;UAS-luc-RNAi/+, seq-RNAi: Cg-GAL4/+; UAS-sequoia-RNAi/+. (H) yw hs-Flp;Ac > CD2 > GAL4/+;UAS-mCherry-GFP-Atg8a/UAS-sequoia-RNAi.

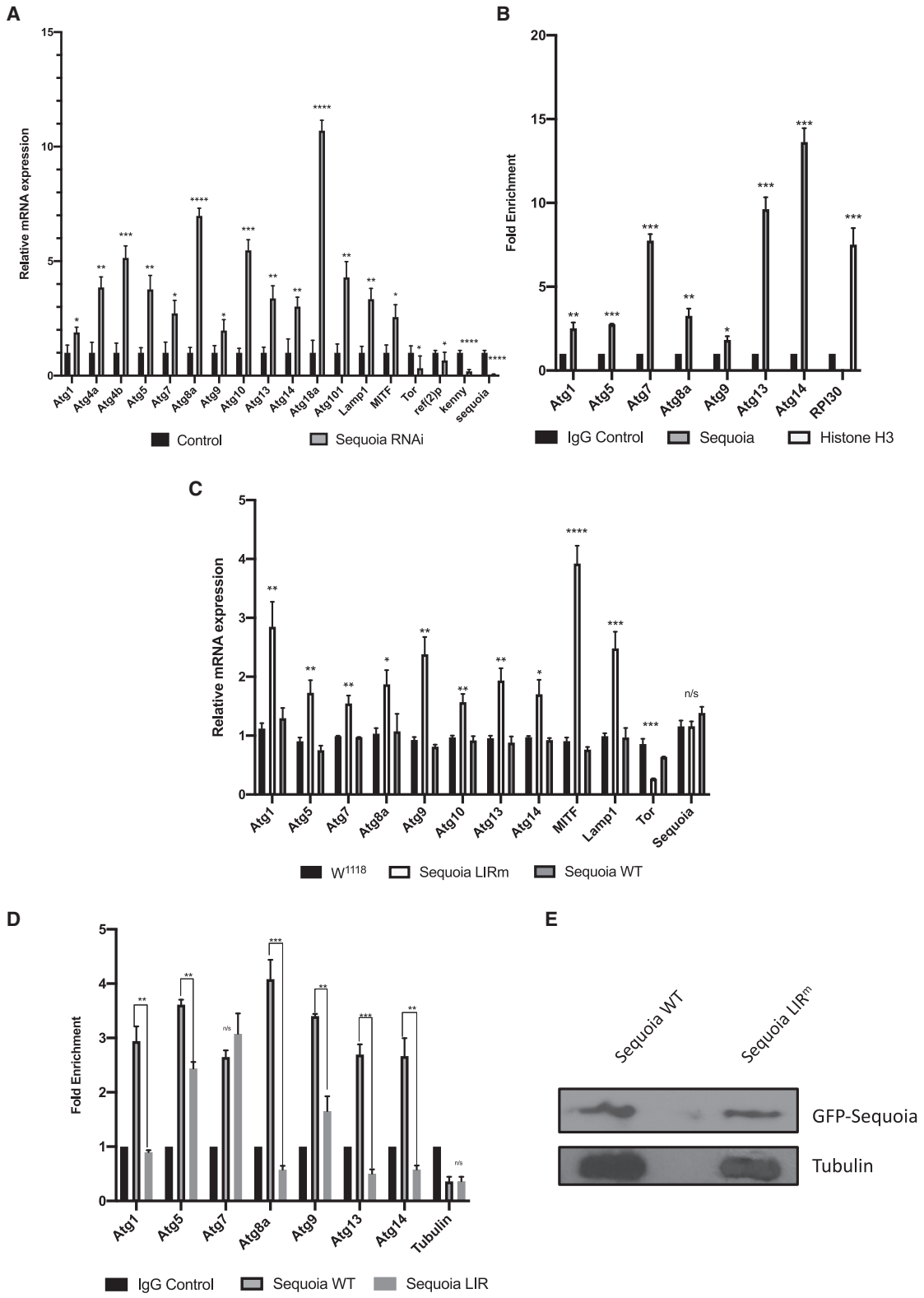

Figure 2. Sequoia Negatively Regulates Autophagy Genes

(A) Analysis of the mRNA levels of autophagy-associated genes, sequoia, and autophagy receptors (Kenny and Ref(2)P) in control (luciferase RNAi) and Sequoia-depleted fat bodies in fed conditions, using real-time qPCR.

(legend continued on next page)

exclusively in the nucleus of fat body cells (Figures 3A and 3C). GFP-Sequoia-WT localized in the nucleus in both fed and starved conditions (Figures 3A and 3B). The expression of GFP-Sequoia-Y313A/I316A resulted in a significant increase in mCherry-Atg8a puncta in the cytoplasm in fed conditions, while the expression of WT Sequoia had no effect (Figures 3A, 3C, 3D, and 3G). In addition, mosaic analysis revealed that only cells expressing LIR-mutated Sequoia had an increase in the lysosomal marker cathepsin L (Figures 3E and 3F). These results suggest that Sequoia negatively regulates autophagy through its LIR motif-dependent interaction with Atg8a.

Atg8a Interacts with YL-1, a Subunit of a Nuclear Acetyltransferase Complex, and Is Acetylated in Nutrient-Rich Conditions

In a bioinformatics screening for Atg8-interacting proteins, we identified YL-1 (CG4621), a subunit of a nuclear acetyltransferase complex, as a putative interactor of Atg8a. YL-1 belongs to the multi-subunit chromatin-remodeling complexes called SWR1 in yeast and the related SRCAP and NuA4/Tip60 complexes in mammals that have been shown to control histone acetylation (Cai et al., 2005; Flegel et al., 2016; Kusch et al., 2004; Latrick et al., 2016; Liang et al., 2016) and have been previously shown to regulate acetylation of autophagy-related proteins Atg3 and ULK1 in yeast and mammals (Lin et al., 2012; Yi et al., 2012). Tip60 has acetyltransferase activity, whereas YL-1 has a regulatory role (Cai et al., 2005; Flegel et al., 2016; Kusch et al., 2004; Latrick et al., 2016; Liang et al., 2016). We therefore sought to explore the role of YL-1 in autophagy in *Drosophila*. *In vitro* translated YL-1 (^{35}S-Myc-YL-1) bound very strongly and directly to the N-terminal half (amino acid residues 1–71) of recombinant GST-Atg8a (Figures 4A and 4B). However, mutation of either the LDS of Atg8a (Figures 4A and 4B) or the putative LIR motifs of YL-1 (Figure S2E) did not abrogate significantly the interaction between Atg8a and YL-1, suggesting that this interaction is likely to be LIR motif independent. Since constructs of Atg8a harboring residues 26–121 or only residues 1–26 do not bind to YL-1 (Figure 4B), the N-terminal 26 amino acids of Atg8a are required for binding but are not sufficient. In addition, transgenic flies expressing GFP-YL-1 exhibit nuclear localization, confirming a nuclear role for YL-1 (Figure S2F). We also found that human YL-1/VPS72 interacts with GABARAP (Figure S1B). Since YL-1 is a component of the NuA4/Tip60 acetyltransferase complex, we examined whether YL-1 regulates the acetylation of Atg8a. To examine this, we immunoprecipitated GFP-Atg8a and used an anti-acetyl-lysine antibody to reveal Atg8a acetylation by western blotting. We found that GFP-Atg8a is acetylated in fed conditions and that its acetylation is reduced after starvation and when YL-1 is depleted using RNAi (Figures 4C, 4D, and S2G). These data show that YL-1 is a novel Atg8a-interacting protein and regulates the acetylation of Atg8a.

Sir2 Interacts with and Deacetylates Atg8a during Starvation

To further investigate the impact of acetylated Atg8a on the activation of autophagy, we focused on the deacetylase Sir2, a homolog of mammalian Sirtuin-1, that has been shown to play a role in lipid metabolism and insulin resistance (Banerjee et al., 2012; Palu and Thummel, 2016; Reis et al., 2010). The Sir2 homolog in mice has been shown to directly deacetylate autophagy machinery components, so we sought to investigate its role in *Drosophila* (Lee et al., 2008). Using a fly line for the expression of myc-tagged Sir2 (Sir2-myc), we found that Sir2 localizes in the nucleus of fat body cells in both fed and starved larvae (Figures S3A and S3B). Fat bodies clonally overexpressing Sir2-myc and stained for acetylated lysine revealed a reduction in nuclear staining for acetylated protein in clonal cells compared to their WT neighbors (Figures S3C–S3E). This suggests that dSir2 is required for deacetylation in the nucleus.

Staining fat bodies from *Sir2* mutant starved larvae for endogenous Atg8a or LysoTracker Red failed to show an accumulation of autophagosomes and autolysosomes in fat body cells (Figures 4E–4G and S3F). Furthermore, Sir2 mutants showed a decrease in Atg8a lipidation during starvation (Figures S4A and S4B). In addition, the overexpression of Sir2-myc resulted in a reduction in GFP-Atg8a acetylation and an increase in Atg8a lipidation in fed and starved larvae (Figures 4C, 4D, S4C, and S4D). GFP-Atg8a cleavage was also increased in starved larvae (Figure 4C). In the same settings, YL-1 depletion using RNAi showed a moderate increase in Atg8a lipidation (Figures S2A and S2B). Moreover, we observed that Sir2-myc interacted preferentially with GFP-Atg8a in starved conditions (Figures 4H and 4I). Using an *in vitro* GST-pull-down assay, we showed that Sir2 interacted preferentially with WT Atg8a compared to an Atg8a-LDS mutant (Figures 4J and 4K). These results suggest that deacetylation of Atg8a by Sir2 is required for the activation of autophagy during starvation.

Effect of Acetylation of Atg8a on Binding to Sequoia

We next investigated whether the interaction of Atg8a with Sequoia is regulated by the acetylation status of Atg8a in fed conditions (when Atg8a is acetylated) and in starved conditions (when Atg8a is deacetylated). To test this, we examined the binding of WT and acetylation mimic forms of Atg8a to Sequoia. LC3

(B) Analyses of Sequoia binding to the promoter of autophagy genes in fed conditions, as detected by ChIP (chromatin immunoprecipitation) using a Sequoia antibody. ChIP DNA values were normalized to input DNA using the 2-ΔΔCt method. Fold enrichment values are shown relative to the immunoglobulin G (IgG) control. Histone H3 enrichment to *RPL30* was used as a positive control.
(C) Analysis of the mRNA level of autophagy-associated genes in W^{1118}, Sequoia LIR mutant, and Sequoia WT fat bodies in fed conditions, using real-time qPCR.
(D) Analyses of Sequoia binding to the promoter of autophagy genes in fed conditions, as detected by ChIP using a GFP antibody. ChIP DNA values were normalized to input DNA using the 2-ΔΔCt method. Fold enrichment values are shown relative to the IgG control. Tubulin was used as a non-autophagy-related gene control.
(E) Expression of GFP-Sequoia protein in Sequoia WT and Sequoia LIR mutant following heat shock. All data shown as means ± SDs, n = 3 independent experiments. Statistical significance was determined using Student's t test; *$p < 0.05$ and ***$p < 0.005$.
Genotypes for A: ctl: Cg-GAL4/+;UAS-luc-RNAi/+, seq-RNAi: Cg-GAL4/+;UAS-sequoia-RNAi/+. (B): Cg-GAL4/+;W^{1118}. (C—E) hs::Gal4/UAS-GFP-Sequoia-WT,hs::Gal4/UAS-GFP-Sequoia-LIRm.

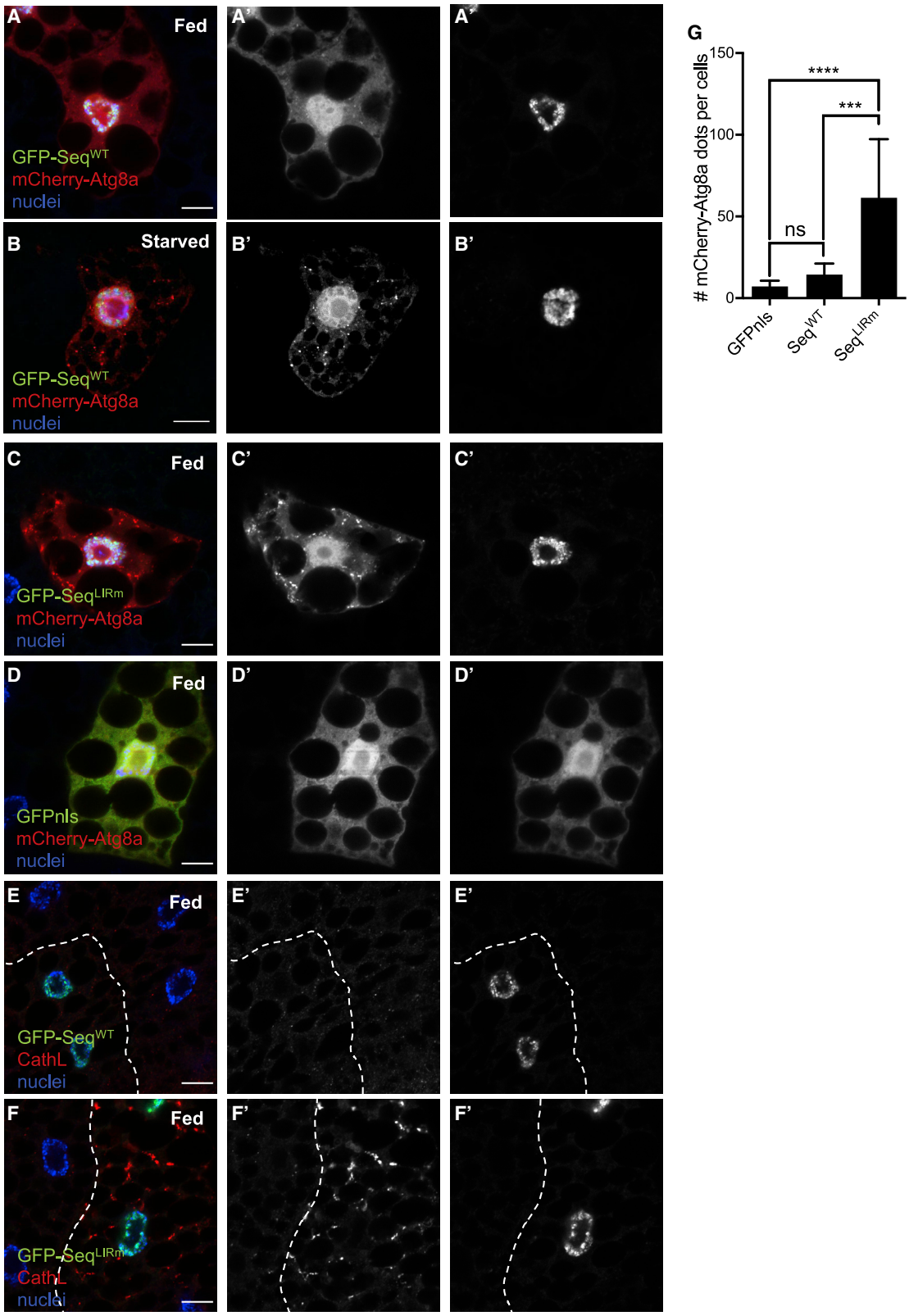

(legend on next page)

has been shown to be acetylated at residues K49 and K51 in fed conditions (Huang et al., 2015). Therefore, we tested the homologous residues K46 and K48 in *Drosophila* Atg8a. We found that only acetylation mimic mutation Atg8a K48Q showed a significant decrease in its binding to Sequoia (Figures 4L and 4M). To examine the effect of K48 acetylation on binding to Sequoia, we also created a homology model of the LIR peptide of Sequoia binding to *Drosophila* Atg8a based on the structure of GABARAP-L1 ATG4B LIR complex (PDB: 5LXI) (Figures S4E and S4F). The residues Y313 and I316 of the LIR peptide of Sequoia are likely to bind in the HP1 and HP2 pockets, respectively. The negatively charged glutamates (E) will interact with the positively charged lysine (K) residues of the 44-LDKKKYLVP-52 motif (shown as sticks under the surface). Upon acetylation, the K48 residue will become bulkier, will lose the positive charge, and the potential salt-bridge interaction between K48 and E309 will be removed by acetylation. These data suggest that deacetylated Atg8a during starvation binds more strongly to Sequoia.

Atg8a Regulates the Expression of Autophagy Genes during Starvation

All of the above results show a role for Atg8a-interacting proteins Sequoia, YL-1, and Sir2 in the expression of autophagy genes. To examine the direct role of Atg8a on autophagy gene expression, we performed real-time qPCR experiments in Atg8a mutants in which the Atg8a protein is not present. We observed that the absence of Atg8a has a significant negative impact on the expression of other autophagy genes during starvation (Figure S5A). However, lack of Atg9, which is part of a different complex of autophagy proteins required for the initiation of autophagosome formation, demonstrated very little or no impact on the expression of autophagy genes (Figure S5B). Furthermore, using a ChIP assay, we observed that Atg8a is associated with the promoter region of autophagy genes (Figure S5C). These results suggest a role for Atg8a in the regulation of the expression of autophagy genes during starvation.

DISCUSSION

Atg8 family proteins have been extensively described for their implications in autophagosome formation and cargo selection in the cytoplasm. Although Atg8 family proteins also localize in the nucleus, their role in this compartment remains largely unexplored. Here, we uncovered a nuclear role for *Drosophila* Atg8a in the regulation of autophagy gene expression and induction of autophagy via a LIR motif-dependent mechanism, regulated by Atg8a acetylation. We demonstrated that the transcription factor Sequoia interacts with Atg8a in the nucleus to control the transcriptional activation of autophagy genes. We suggest that the acetylation status of Atg8a at position K48 contributes to the modulation of the interaction between Sequoia and Atg8a in the nucleus. We also identified that YL-1, a component of a nuclear acetyltransferase complex, and deacetylase Sir2 interact with Atg8a, and that they act as regulators of Atg8a acetylation.

We propose a working model in which in fed conditions, histone-interacting protein YL-1 contributes to the acetylation of Atg8a, while Sequoia resides at the promoter regions of autophagy genes to repress their expression (Figure S5D). In such conditions, the interaction between Sequoia and Atg8a contributes to the sequestration of Atg8a in the nucleus. Atg8a cannot therefore translocate to the cytoplasm to take part in the formation of autophagosomes. This hypothesis is supported by the observation that mutation of the Sequoia LIR motif results in an increased accumulation of autophagosomes and autolysosomes in the fed condition (Figure S5D). This is observed alongside a reduction in the enrichment of Sequoia at the promoter region of autophagy genes, resulting in their increased expression. Hence, in the absence of an interaction between Atg8a and Sequoia, the subsequent translocation of Atg8a to the cytoplasm may also play a key role in relieving the repressive abilities of Sequoia at the promoter regions of autophagy genes. Upon starvation, Sir2 interacts with and deacetylates Atg8a. Deacetylated Atg8a interacts more strongly with Sequoia, which cannot be maintained at the promoter regions of autophagy genes, leading to the activation of their transcription. Deacetylated Atg8a is then able to translocate to the cytoplasm and contribute to the formation of autophagosomes (Figure S5D). We propose that Atg8a plays an essential role in relieving Sequoia from the promoter regions of autophagy genes specifically during starvation-induced autophagy as Atg8a loss of function results in the repression of the expression of autophagy genes (Figure S5D).

Our results support previous findings about the yeast and mammalian homologs of Sequoia, Rph1, and KDM4A, respectively, which have been shown to negatively regulate the transcription of autophagy genes (Bernard et al., 2015). Here, we elucidate how the LIR-dependent interaction between Sequoia and Atg8a is involved in modulating the expression of autophagy genes during starvation. Mammalian KDM4A also directly interacts with GABARAP-L1; however, the interaction does not require a functional LIR motif. This may be related to the loss of the functionality of the LIR motif during evolution, as it has been shown for Kenny, another LIR-motif containing protein in *Drosophila*, and its mammalian homolog inhibitor of nuclear factor κB kinase (NF-κB) subunit γ/NF-κB essential modulator (IKKγ/NEMO) (Tusco et al., 2017). Our study also

Figure 3. The LIR Motif of Sequoia Is Required to Repress Autophagy

(A–D) Confocal sections of larval fat bodies clonally expressing the autophagy marker mCherry-Atg8a (red) in combination with GFP-Sequoia WT (A and B), GFP-Sequoia LIRm (C), or GFP-nls (D) (green). Larvae were well fed (A, C, and D) or starved for 4 h (B). Fixed fat bodies were stained for nuclei (blue). Scale bar: 10 μm.
(E and F) Confocal sections of larval fat bodies clonally expressing GFP-Sequoia WT (E) and GFP-Sequoia LIRm (F) (green) and stained for cathepsin L (red).
(G) Quantification of the number of mCherry-Atg8a dots per cell. Bars denote means ± SDs. Statistical significance was determined using 1-way ANOVA; ***$p < 0.001$ and ****$p < 0.0001$.

Genotypes for A and B: yw hs-Flp;Ac > CD2 > GAL4/UAS-GFP-Sequoia-WT;UAS-mCherry-Atg8a/+. (C) yw hs-Flp;Ac > CD2 > GAL4/UAS-GFP-Sequoia-LIRm;UAS-mCherry-Atg8a/+. (D) yw hs-Flp;Ac > CD2 > GAL4/+;UAS-mCherry-Atg8a/UAS-GFPnls. (E) yw hs-Flp;Ac > CD2 > GAL4/UAS-GFP-Sequoia-WT. (F) yw hs-Flp;Ac > CD2 > GAL4/UAS-GFP-Sequoia-LIRm.

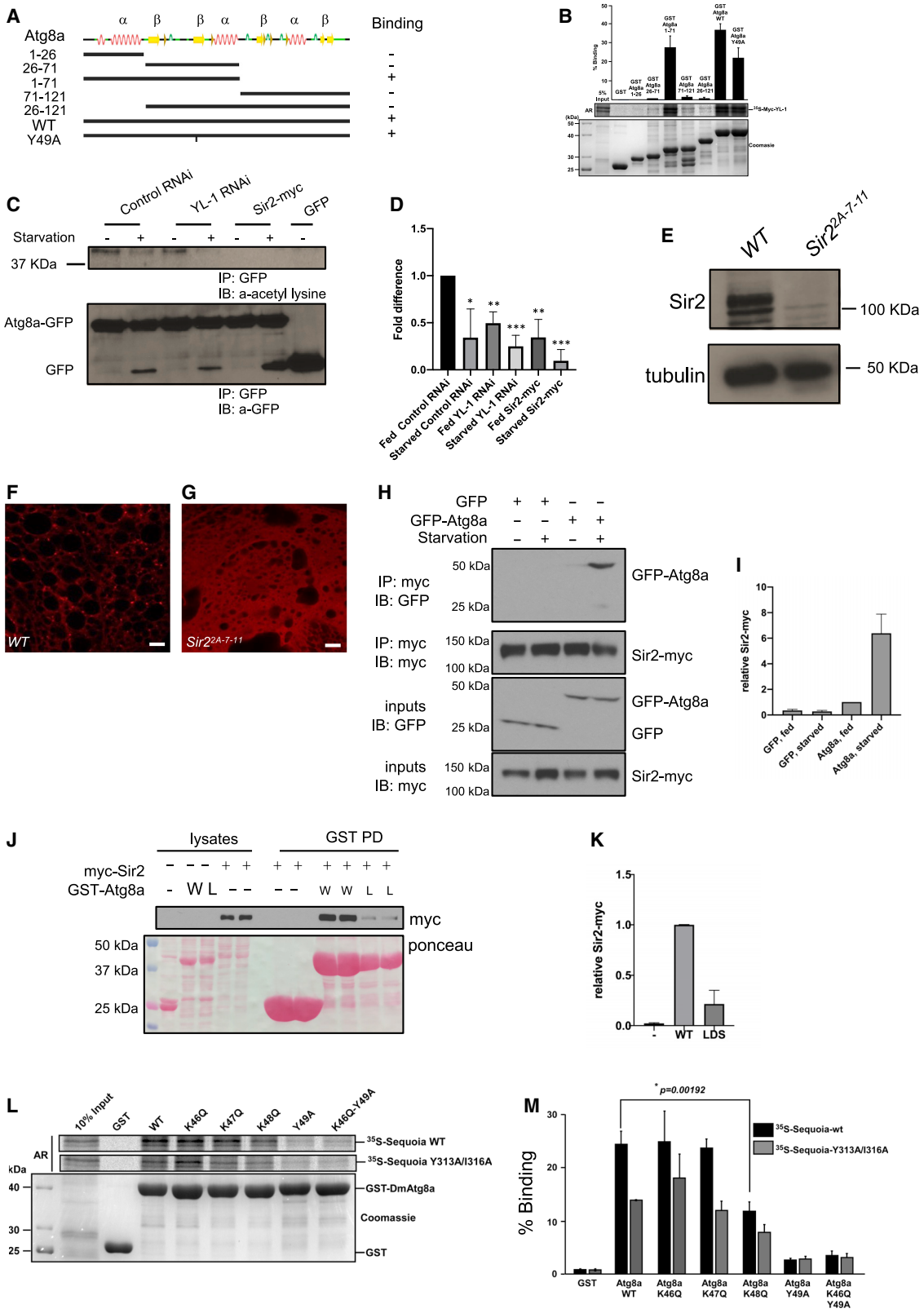

(legend on next page)

supports previous reports about the role of acetylation and deacetylation of LC3 in mammals (Huang et al., 2015; Lee et al., 2008; Lee and Finkel, 2009; Li et al., 2016; Song et al., 2019) and the regulation of autophagy by acetylation (Flegel et al., 2016; Li et al., 2017).

Higher eukaryotes express YL-1, a highly conserved Swc2 homolog, which has specific H2A.Z-binding properties. *Drosophila* YL-1 has been shown to have a H2A.Z-binding domain that binds H2A.Z-H2B dimer (Liang et al., 2016). Here, we report a novel role for YL-1 in the regulation of acetylation of non-histone proteins and the regulation of autophagy induction.

In conclusion, our results unveil a novel nuclear role for Atg8a in the regulation of autophagy gene expression in *Drosophila*, which is linked to its acetylation status and its ability to interact with transcription factor Sequoia. Our study highlights the physiological importance of the non-degradative role of LIR motif-dependent interactions of Atg8a with a transcription factor and provide novel mechanistic insights on an unanticipated nuclear role of a protein that controls cytoplasmic cellular self-eating.

STAR★METHODS

Detailed methods are provided in the online version of this paper and include the following:

- KEY RESOURCES TABLE
- RESOURCE AVAILABILITY
  - Lead Contact
  - Materials Availability
  - Data and Code Availability
- EXPERIMENTAL MODEL AND SUBJECT DETAILS
  - Fly Husbandry and Generation of Transgenic Lines
- METHOD DETAILS
  - Protein Extraction, Immunoprecipitation, and Western Blotting
  - Immunohistochemistry
  - Real-Time qPCR
  - Plasmid Constructs
  - GST Pull-Down Assays
  - Chromatin Immunoprecipitation Assay
  - Structural Modeling
- QUANTIFICATION AND STATISTICAL ANALYSIS
  - Quantification of mCherry-Atg8a Puncta
  - Quantification of Binding Interaction Assays
  - Statistical Analysis

SUPPLEMENTAL INFORMATION

Supplemental Information can be found online at https://doi.org/10.1016/j.celrep.2020.107695.

ACKNOWLEDGMENTS

This work was supported by BBSRC grant BB/P007856/1 and Leverhulme Trust project grant RPG-2017-023, to I.P.N., and a Toppforsk (grant no. 249884) from the Research Council of Norway, to T.J. M.D.M. has a PhD studentship funded by the Midlands Integrative Biosciences Training Partnership. We thank Prof. J. Yan (University of California) and Prof. Gabor Juhasz (Eotvos Lorand University) for the Sequoia and Atg1 antibodies and Atg9 and Atg7 mutants. We thank the Bloomington *Drosophila* Stock Center and the Vienna *Drosophila* Resource Center for the flies. We thank Mark Ward for preparing the fly food.

AUTHOR CONTRIBUTIONS

A.-C.J., S.P., M.D.M., A. Jain, Z.B., N.C.M., A.P., E.L.P., B.C., C.Z., A. Jones, A.C., T.J., and I.P.N. performed the experiments and/or analyzed the data. I.P.N. designed and supervised the study. A.-C.J., S.P., M.D.M., and I.P.N.

Figure 4. YL-1 and Sir2 Interact with Atg8a, Regulating Its Acetylation Status

(A and B) YL-1 interacts with Atg8a in a non-LIR-dependent manner. (A) Overview of the secondary structure of Atg8a with deletion mutants and the Y49A LDS mutant of Atg8a used in GST-pull-down assays in (B).

(B) GST-pull-down assays between GST-tagged WT Atg8a, Atg8a deletion mutants, and the LDS mutant (Y49A) and radiolabeled myc-YL-1.

(C) Knockdown of the YL-1 acetyltransferase reduces the acetylation of Atg8a. Flies that were constitutively expressing GFP-Atg8a in their fat bodies were crossed with the control luciferase RNAi, the YL-1 RNAi line, and the Sir2-Myc line and their offspring were collected. Protein acetylation was determined by immunoprecipitation (IP) with a GFP antibody followed by western blotting (WB) for an antibody recognizing acetyl-lysine residues. IP was performed with 1 mg protein lysate from full larvae both in fed and starved (4 h in 20% sucrose) conditions.

(D) Quantification of the quantity of Atg8a protein normalized to GFP. Bar chart shows means ± SDs. Statistical significance was determined using 2-tailed Student's t test; *$p < 0.05$, **$p < 0.01$, and ***$p < 0.001$.

(E) Sir2 WB on protein lysates prepared from 7-day-old w1118 and the Sir2[2A- 7-11] mutant. Tubulin was used as a loading control.

(F and G) Confocal sections of fat bodies from w1118 (F) and the Sir22A-7-11 (G) larvae stained with LysoTracker Red after 4 h of starvation. Scale bar: 10 μm.

(H) CoIP of Sir2-myc and GFP-Atg8a from extracts of fed and starved larvae. Sir2-myc was immunoprecipitated from larva lysates and subjected to SDS-PAGE.

(I) Quantification of the relative quantity of GFP-Atg8a co-precipitated with Sir2-myc. Bars denote means ± SDs. Statistical significance was determined using 1-way ANOVA; ***$p < 0.001$.

(J) *In vitro* interaction between recombinant GST-Atg8a and Sir2-myc expressed in larvae. GST, GST-Atg8a-WT (W, wild-type) or GST-Atg8a-LDS (L, LDS mutated) were pulled down and incubated with larval lysate expressing Sir2-myc. Eluates were subjected to SDS-PAGE. Membrane was stained with Ponceau S for total protein staining and immunoblotted with anti-myc antibody for Sir2-myc.

(K) Quantification of the relative quantity of Sir2-myc co-precipitated with GST recombinant proteins. Bars denote means ± SDs. Statistical significance was determined using 1-way ANOVA; ****$p < 0.0001$.

(L) GST-pull-down assay between GST-tagged Atg8a-WT; the acetylation mutants K46Q, K47Q, and K48Q; the LDS mutant (Y49A); and radiolabeled ^{35}S-labeled Sequoia-WT or ^{35}S-labeled Sequoia-LIR mutant.

(M) Quantifications of the binding of radiolabeled myc-Sequoia-WT or LIR mutant (Y313A/I316A) to GST-ATG8a-WT or the respective mutants represented as percentage binding relative to 10% of the input. The bars represent the mean values with SDs from 3 independent experiments. The statistical significance of the Sequoia binding with Atg8a-WT compared to its mutation K48Q was determined with Student's t test; $p = 0.00192$.

Genotypes for C and D: Control RNAi: Cg-GAL4 UAS-GFP-Atg8a/+;UAS-luc-RNAi/+, YL-1-RNAi: Cg-GAL4 UAS-GFP-Atg8a/+;UAS-YL-1-RNAi/+, Sir2-myc: Cg-GAL4 UAS-GFP-Atg8a/+;UAS-Sir2-myc/+, GFP: Cg-GAL4/+;UAS-GFP/+.

drafted the manuscript. All of the authors read and contributed to the manuscript.

DECLARATION OF INTERESTS

The authors declare no competing interests.

Received: November 15, 2019
Revised: April 7, 2020
Accepted: May 6, 2020
Published: May 26, 2020

REFERENCES

Ambrosio, S., Ballabio, A., and Majello, B. (2019). Histone methyl-transferases and demethylases in the autophagy regulatory network: the emerging role of KDM1A/LSD1 demethylase. Autophagy *15*, 187–196.

Banerjee, K.K., Ayyub, C., Sengupta, S., and Kolthur-Seetharam, U. (2012). dSir2 deficiency in the fatbody, but not muscles, affects systemic insulin signaling, fat mobilization and starvation survival in flies. Aging (Albany NY) *4*, 206–223.

Bernard, A., Jin, M., González-Rodríguez, P., Füllgrabe, J., Delorme-Axford, E., Backues, S.K., Joseph, B., and Klionsky, D.J. (2015). Rph1/KDM4 mediates nutrient-limitation signaling that leads to the transcriptional induction of autophagy. Curr. Biol. *25*, 546–555.

Birgisdottir, A.B., Lamark, T., and Johansen, T. (2013). The LIR motif - crucial for selective autophagy. J. Cell Sci. *126*, 3237–3247.

Brenman, J.E., Gao, F.B., Jan, L.Y., and Jan, Y.N. (2001). Sequoia, a tramtrack-related zinc finger protein, functions as a pan-neural regulator for dendrite and axon morphogenesis in Drosophila. Dev. Cell *1*, 667–677.

Cai, Y., Jin, J., Florens, L., Swanson, S.K., Kusch, T., Li, B., Workman, J.L., Washburn, M.P., Conaway, R.C., and Conaway, J.W. (2005). The mammalian YL1 protein is a shared subunit of the TRRAP/TIP60 histone acetyltransferase and SRCAP complexes. J. Biol. Chem. *280*, 13665–13670.

Chang, Y.Y., and Neufeld, T.P. (2009). An Atg1/Atg13 complex with multiple roles in TOR-mediated autophagy regulation. Mol. Biol. Cell *20*, 2004–2014.

Dikic, I., and Elazar, Z. (2018). Mechanism and medical implications of mammalian autophagy. Nat. Rev. Mol. Cell Biol. *19*, 349–364.

Dou, Z., Xu, C., Donahue, G., Shimi, T., Pan, J.A., Zhu, J., Ivanov, A., Capell, B.C., Drake, A.M., Shah, P.P., et al. (2015). Autophagy mediates degradation of nuclear lamina. Nature *527*, 105–109.

Flegel, K., Grushko, O., Bolin, K., Griggs, E., and Buttitta, L. (2016). Roles for the Histone Modifying and Exchange Complex NuA4 in Cell Cycle Progression in Drosophila melanogaster. Genetics *203*, 1265–1281.

Füllgrabe, J., Klionsky, D.J., and Joseph, B. (2014). The return of the nucleus: transcriptional and epigenetic control of autophagy. Nat. Rev. Mol. Cell Biol. *15*, 65–74.

Gatica, D., Lahiri, V., and Klionsky, D.J. (2018). Cargo recognition and degradation by selective autophagy. Nat. Cell Biol. *20*, 233–242.

Guo, W., Jin, J., Pan, J., Yao, R., Li, X., Huang, X., Ma, Z., Huang, S., Yan, X., Jin, J., and Dong, A. (2018). The change of nuclear LC3 distribution in acute myeloid leukemia cells. Exp. Cell Res. *369*, 69–79.

Huang, R., Xu, Y., Wan, W., Shou, X., Qian, J., You, Z., Liu, B., Chang, C., Zhou, T., Lippincott-Schwartz, J., and Liu, W. (2015). Deacetylation of nuclear LC3 drives autophagy initiation under starvation. Mol. Cell *57*, 456–466.

Ichimura, Y., Kumanomidou, T., Sou, Y.S., Mizushima, T., Ezaki, J., Ueno, T., Kominami, E., Yamane, T., Tanaka, K., and Komatsu, M. (2008). Structural basis for sorting mechanism of p62 in selective autophagy. J. Biol. Chem. *283*, 22847–22857.

Jacomin, A.C., and Nezis, I.P. (2016). Using Fluorescent Reporters to Monitor Autophagy in the Female Germline Cells in Drosophila melanogaster. Methods Mol. Biol. *1457*, 69–78.

Jacomin, A.C., Samavedam, S., Promponas, V., and Nezis, I.P. (2016). iLIR database: a web resource for LIR motif-containing proteins in eukaryotes. Autophagy *12*, 1945–1953.

Jain, A., Rusten, T.E., Katheder, N., Elvenes, J., Bruun, J.A., Sjøttem, E., Lamark, T., and Johansen, T. (2015). p62/Sequestosome-1, Autophagy-related Gene 8, and Autophagy in Drosophila Are Regulated by Nuclear Factor Erythroid 2-related Factor 2 (NRF2), Independent of Transcription Factor TFEB. J. Biol. Chem. *290*, 14945–14962.

Juhász, G., Erdi, B., Sass, M., and Neufeld, T.P. (2007). Atg7-dependent autophagy promotes neuronal health, stress tolerance, and longevity but is dispensable for metamorphosis in Drosophila. Genes Dev. *21*, 3061–3066.

Kabeya, Y., Mizushima, N., Ueno, T., Yamamoto, A., Kirisako, T., Noda, T., Kominami, E., Ohsumi, Y., and Yoshimori, T. (2000). LC3, a mammalian homologue of yeast Apg8p, is localized in autophagosome membranes after processing. EMBO J. *19*, 5720–5728.

Kalvari, I., Tsompanis, S., Mulakkal, N.C., Osgood, R., Johansen, T., Nezis, I.P., and Promponas, V.J. (2014). iLIR: a web resource for prediction of Atg8-family interacting proteins. Autophagy *10*, 913–925.

Kiss, V., Jipa, A., Varga, K., Takáts, S., Maruzs, T., Lőrincz, P., Simon-Vecsei, Z., Szikora, S., Földi, I., Bajusz, C., et al. (2020). Drosophila Atg9 regulates the actin cytoskeleton via interactions with profilin and Ena. Cell Death Differ. *27*, 1677–1692.

Klionsky, D.J., Abdelmohsen, K., Abe, A., Abedin, M.J., Abeliovich, H., Acevedo Arozena, A., Adachi, H., Adams, C.M., Adams, P.D., Adeli, K., et al. (2016). Guidelines for the use and interpretation of assays for monitoring autophagy (3rd edition). Autophagy *12*, 1–222.

Kraft, L.J., Manral, P., Dowler, J., and Kenworthy, A.K. (2016). Nuclear LC3 Associates with Slowly Diffusing Complexes that Survey the Nucleolus. Traffic *17*, 369–399.

Kusch, T., Florens, L., Macdonald, W.H., Swanson, S.K., Glaser, R.L., Yates, J.R., 3rd, Abmayr, S.M., Washburn, M.P., and Workman, J.L. (2004). Acetylation by Tip60 is required for selective histone variant exchange at DNA lesions. Science *306*, 2084–2087.

Lamb, C.A., Yoshimori, T., and Tooze, S.A. (2013). The autophagosome: origins unknown, biogenesis complex. Nat. Rev. Mol. Cell Biol. *14*, 759–774.

Latrick, C.M., Marek, M., Ouararhni, K., Papin, C., Stoll, I., Ignatyeva, M., Obri, A., Ennifar, E., Dimitrov, S., Romier, C., and Hamiche, A. (2016). Molecular basis and specificity of H2A.Z-H2B recognition and deposition by the histone chaperone YL1. Nat. Struct. Mol. Biol. *23*, 309–316.

Lee, I.H., and Finkel, T. (2009). Regulation of autophagy by the p300 acetyltransferase. J. Biol. Chem. *284*, 6322–6328.

Lee, I.H., Cao, L., Mostoslavsky, R., Lombard, D.B., Liu, J., Bruns, N.E., Tsokos, M., Alt, F.W., and Finkel, T. (2008). A role for the NAD-dependent deacetylase Sirt1 in the regulation of autophagy. Proc. Natl. Acad. Sci. USA *105*, 3374–3379.

Li, X., Wang, Y., Xiong, Y., Wu, J., Ding, H., Chen, X., Lan, L., and Zhang, H. (2016). Galangin Induces Autophagy via Deacetylation of LC3 by SIRT1 in HepG2 Cells. Sci. Rep. *6*, 30496.

Li, Y.T., Yi, C., Chen, C.C., Lan, H., Pan, M., Zhang, S.J., Huang, Y.C., Guan, C.J., Li, Y.M., Yu, L., and Liu, L. (2017). A semisynthetic Atg3 reveals that acetylation promotes Atg3 membrane binding and Atg8 lipidation. Nat. Commun. *8*, 14846.

Liang, X., Shan, S., Pan, L., Zhao, J., Ranjan, A., Wang, F., Zhang, Z., Huang, Y., Feng, H., Wei, D., et al. (2016). Structural basis of H2A.Z recognition by SRCAP chromatin-remodeling subunit YL1. Nat. Struct. Mol. Biol. *23*, 317–323.

Lin, S.Y., Li, T.Y., Liu, Q., Zhang, C., Li, X., Chen, Y., Zhang, S.M., Lian, G., Liu, Q., Ruan, K., et al. (2012). GSK3-TIP60-ULK1 signaling pathway links growth factor deprivation to autophagy. Science *336*, 477–481.

Nagy, P., Kárpáti, M., Varga, A., Pircs, K., Venkei, Z., Takáts, S., Varga, K., Erdi, B., Hegedűs, K., and Juhász, G. (2014). Atg17/FIP200 localizes to perilysosomal Ref(2)P aggregates and promotes autophagy by activation of Atg1 in Drosophila. Autophagy *10*, 453–467.

Nezis, I.P., Lamark, T., Velentzas, A.D., Rusten, T.E., Bjørkøy, G., Johansen, T., Papassideri, I.S., Stravopodis, D.J., Margaritis, L.H., Stenmark, H., and Brech, A. (2009). Cell death during Drosophila melanogaster early oogenesis is mediated through autophagy. Autophagy *5*, 298–302.

Nezis, I.P., Shravage, B.V., Sagona, A.P., Lamark, T., Bjørkøy, G., Johansen, T., Rusten, T.E., Brech, A., Baehrecke, E.H., and Stenmark, H. (2010). Autophagic degradation of dBruce controls DNA fragmentation in nurse cells during late Drosophila melanogaster oogenesis. J. Cell Biol. *190*, 523–531.

Palu, R.A., and Thummel, C.S. (2016). Sir2 Acts through Hepatocyte Nuclear Factor 4 to maintain insulin Signaling and Metabolic Homeostasis in Drosophila. PLoS Genet. *12*, e1005978.

Popelka, H., and Klionsky, D.J. (2015). Analysis of the native conformation of the LIR/AIM motif in the Atg8/LC3/GABARAP-binding proteins. Autophagy *11*, 2153–2159.

Reis, T., Van Gilst, M.R., and Hariharan, I.K. (2010). A buoyancy-based screen of Drosophila larvae for fat-storage mutants reveals a role for Sir2 in coupling fat storage to nutrient availability. PLoS Genet. *6*, e1001206.

Sakamaki, J.I., Wilkinson, S., Hahn, M., Tasdemir, N., O'Prey, J., Clark, W., Hedley, A., Nixon, C., Long, J.S., New, M., et al. (2017). Bromodomain Protein BRD4 Is a Transcriptional Repressor of Autophagy and Lysosomal Function. Mol. Cell *66*, 517–532.e9.

Sakamaki, J.I., Long, J.S., New, M., Van Acker, T., Tooze, S.A., and Ryan, K.M. (2018). Emerging roles of transcriptional programs in autophagy regulation. Transcription *9*, 131–136.

Scott, R.C., Juhász, G., and Neufeld, T.P. (2007). Direct induction of autophagy by Atg1 inhibits cell growth and induces apoptotic cell death. Curr. Biol. *17*, 1–11.

Song, T., Su, H., Yin, W., Wang, L., and Huang, R. (2019). Acetylation modulates LC3 stability and cargo recognition. FEBS Lett. *593*, 414–422.

Tusco, R., Jacomin, A.C., Jain, A., Penman, B.S., Larsen, K.B., Johansen, T., and Nezis, I.P. (2017). Kenny mediates selective autophagic degradation of the IKK complex to control innate immune responses. Nat. Commun. *8*, 1264.

Yi, C., Ma, M., Ran, L., Zheng, J., Tong, J., Zhu, J., Ma, C., Sun, Y., Zhang, S., Feng, W., et al. (2012). Function and molecular mechanism of acetylation in autophagy regulation. Science *336*, 474–477.

STAR★METHODS

KEY RESOURCES TABLE

REAGENT or RESOURCE	SOURCE	IDENTIFIER
Antibodies		
anti-GFP	Abcam	ab290; RRID:AB_303395
anti-myc	Cell Signaling Technology	#2276; RRID:AB_331783
anti-mCherry	Novus NBP1	#96752; RRID:AB_11034849
anti-alpha tubulin	Sigma-Aldrich	T5168; RRID:AB_477579
anti-acetyl lysine	Cell Signaling	#9441; RRID:AB_331805
anti-dSir2	DSHB	p4A10; RRID:AB_1553778
anti-mouse HRP	Thermo Scientific	#31450, #31460; RRID:AB_228341
Veriblot HRP-coupled for IP detection	Abcam	ab131366
anti-Cathepsin-L	Abcam	ab58991; RRID:AB_940826
Normal Rabbit IgG	Cell Signaling	#2729; RRID:AB_1031062
anti-Sequoia	Gift from Prof. Y Jan	N/A
Histone H3 Antibody	Cell Signaling	#9715; RRID:AB_331563
anti-GABARAP	Abcam	ab109364; RRID:AB_10861928
anti-Atg1	Gift from Gabor Juhasz, Eotvos Lorand University, Budapest. (Nagy et al., 2014)	N/A
a-actin	Abcam	ab8227; RRID:AB_2305186
Bacterial and Virus Strains		
BL21(DE3) Competent *E.Coli*	New England Biolabs	Cat#C2527I
SoluBL21™ Competent *E.Coli*	Ambio	C700200
Rosetta2(DEM3) Singles Competent Cells	Novagen	71400
Chemicals, Peptides, and Recombinant Proteins		
EDTA-free protease inhibitor cocktails	Roche	5892791001
Deactylation inhibitors	Santa Cruz	sc-362323
Sepharose-coupled G-beads	Sigma-Aldrich	Cat#28-9670-66
LysoTracker™ Deep Red	Thermo Fisher Scientific	L12492
Glutathione-Sepharose 4 Fast Flow beads	Amersham Biosciences	Cat#17513201
Formaldehyde	Sigma-Aldrich	Cat#F8775
Protein A beads	GE Healthcare	28967062
GoTaq qPCR Master Mix	Promega	A6002
Critical Commercial Assays		
PureLink™ RNA mini kit	Life Technologies	Cat#12183025
RevertAid Kit	Thermo Scientific	Cat#K1622
QuickChange site-directed mutagenesis	Stratagene	200523
Phusion High-Fidelity DNA Polymerase	Thermo Scientific	Cat#F-530XL
EasyTag™ L-[35S]-methionine	PerkinElmer Life Sciences	NEG709A500UC
Experimental Models: Organisms/Strains		
w^{1118}	Bloomington *Drosophila* stock center	#3605
Cg-GAL4	Bloomington *Drosophila* stock center	#7011
UAS-YL-1-RNAi	Bloomington *Drosophila* stock center	#31938
UAS-Sir2-myc	Bloomington *Drosophila* stock center	#44216
UAS-Sequoia-RNAi	Vienna Drosophila Resource Centre	#50146
$Atg7^{\Delta 77}$	Gift from Gabor Juhasz, Eotvos Lorand University, Budapest. (Juhász et al., 2007)	N/A

(*Continued on next page*)

Continued

REAGENT or RESOURCE	SOURCE	IDENTIFIER
Atg7$^{\Delta 14}$	Gift from Gabor Juhasz, Eotvos Lorand University, Budapest. Juhász et al., 2007)	N/A
Sir2$^{2A-7-11}$	Bloomington *Drosophila* stock center	#8838
yw hs-flp; UAS-mCherry-Atg8a;Ac > CD2 > GAL4	Tusco et al. (2017)	N/A
UAS-GFP-Sequoia-WT	This paper; generated by P-element-mediated transformation (BestGene Inc)	N/A
UAS-GFP-Sequoia-LIRm (Y313A/316A)	This paper; generated by P-element-mediated transformation (BestGene Inc)	N/A
UAS-GFP-YL-1	This paper; generated by P-element-mediated transformation (BestGene Inc)	N/A
Atg9^{B5}/CyO	Gift from Gabor Juhasz, Eotvos Lorand University, Budapest. (Kiss et al., 2020)	N/A
Atg9$^{DF(ED2487)}$/GFP twi CyO	Gift from Gabor Juhasz, Eotvos Lorand University, Budapest. (Kiss et al., 2020)	N/A
Atg8a [KG07569]	(Scott et al., 2007)	N/A
UAS-Sequoia-RNAi	Bloomington *Drosophila* stock center	#51923
Oligonucleotides		
Primers for mRNA Atg expression, see Table S1	This paper	N/A
Primers for Atg promotor region, see Table S1	This paper	N/A
Recombinant DNA		
Plasmid: pPGW	*Drosophila* Genomics Resource Centre	1077
Gateway pDONR221 Vector	Thermo Scientific	Cat#12536017
Gateway^{TM} pENTR^{TM}	Thermo Scientific	SKU#A10467
Software and Algorithms		
iLIR database	Kalvari et al. (2014)	http://repeat.biol.ucy.ac.cy/iLIR
AtgCOUNTER (ImageJ/Fiji macro)	Jacomin and Nezis (2016)	https://imagej.nih.gov/ij/
PyMol	The PyMOL Molecular Graphics System, Version 2.0 Schrödinger, LLC.	https://pymol.org/2/

RESOURCE AVAILABILITY

Lead Contact

Additional information and requests for reagents and protocols should be directed to and will be fulfilled by the Lead Contact, Ioannis Nezis (I.Nezis@warwick.ac.uk).

Materials Availability

All materials are publicly available. Please contact Dr Ioannis Nezis.

Data and Code Availability

The published report includes all data generated or analyzed during this study. No code was used or generated during this study.

EXPERIMENTAL MODEL AND SUBJECT DETAILS

Fly Husbandry and Generation of Transgenic Lines

Flies used in experiments were kept at 25°C and 70% humidity raised on cornmeal-based feed. The following fly stocks were obtained from the Bloomington *Drosophila* stock center: *w^{1118}* (#3605), *Cg-GAL4* (#7011) and *UAS-YL-1-RNAi* (#31938), *UAS-Sir2-myc (#44216)*, *UAS-Sequoia-RNAi* (#51923). *UAS-Sequoia-RNAi* (#50146) was obtained from the Vienna *Drosophila* Resource Center. The following mutant lines have been used: *Atg7$^{\Delta 77}$*, and *Atg7$^{\Delta 14}$/CyO-GFP* (Juhász et al., 2007), *Atg9^{B5}/CyO* and *Atg9$^{DF(ED2487)}$/GFP twi CyO* (Kiss et al., 2020), Atg8a [KG07569] (Scott et al., 2007), *Sir2$^{2A-7-11}$* from Bloomington (#8838). The clonal

analysis using the FLPout system has been performed with the following lines: *yw hs-flp; UAS-mCherry-Atg8a;Ac > CD2 > GAL4*. The transgenic lines UAS-GFP-Sequoia-WT, UAS-GFP-Sequoia-LIRm (Y313A/316A) and UAS-GFP-YL-1 have been generated by cloning the cDNA of *sequoia* or *YL-1* respectively into the pPGW plasmid (DGRC). Transgenic flies were generated by P-element-mediated transformation (BestGene Inc). Early third-instar larvae were collected either fed or starved for 4 hours in 20% sucrose solution in PBS.

METHOD DETAILS

Protein Extraction, Immunoprecipitation, and Western Blotting

Protein content was extracted from larvae in Nuclear lysis buffer (20 mM Tris pH 7.5, 137 mM NaCl, 1mM $MgCl_2$, 1mM $CaCl_2$, 1% Igepal, 10% Glycerol, 1mM Na_3VO_4, 15mM $Na_4P_2O_7$, 5mM Sodium butyrate supplemented with EDTA-free proteases inhibitors cocktail (Roche, 5892791001) and deacetylase inhibitors (Santa Cruz, sc-362323) using a motorized mortar and pestle. Co-immunoprecipitations were performed on lysates from flies expressing GFP alone, GFP-Atg8a or Sir2-myc along with mCherry-Atg8a. After a 30 min pre-clear of the lysates (1 mg total proteins) with Sepharose-coupled G-beads (Sigma), the co-immunoprecipitations were performed for 2 h at 4°C using an anti-GFP antibody (Abcam, Ab290) or anti-myc (Cell Signaling Technology, #2276) and fresh Sepharose-coupled G-beads. Four consecutive washes with the lysis buffer were performed before suspension of the beads in 60 μL 2X Laemmli loading buffer. All protein samples (whole fly lysates and co-immunoprecipitation eluates) were boiled for 5-10 min at 95°C. Quantity of 10–40 μg of proteins (whole lysates) or 20 μL (co-immunoprecipitation eluates) were loaded on polyacrylamide gels and were transferred onto either nitrocellulose or PVDF membranes (cold wet transfer in 10%–20% ethanol for 1h at 100V). Membranes were blocked in 5% BSA or non-fat milk in TBST (0.1% Tween-20 in TBS) for 1 h. Primary antibodies diluted in TBST were incubated overnight at 4°C or for 2 h at room temperature with gentle agitation. HRP-coupled secondary antibodies binding was done at room temperature (RT) for 45 min in 1% BSA or non-fat milk dissolved in TBST and ECL mix incubation for 2 min. All washes were performed for 10 min in TBST at RT. The following primary antibodies were used: anti-GFP (Santa Cruz sc-9996, 1:1000), anti-mCherry (Novus NBP1 #96752, 1:1000), anti-alpha tubulin (Sigma-Aldrich T5168, 1:50,000), anti-acetyl lysine (Cell Signaling #9441, 1:1000), anti-dSir2 (DSHB p4A10, 1:50), anti-Atg1 (Nagy et al., 2014). HRP-coupled secondary antibodies were from Thermo Scientific (anti-mouse HRP #31450; anti-rabbit HRP #31460). Following co-immunoprecipitation, Veriblot HRP-coupled IP secondary antibody was used (Abcam ab131366, 1:5000).

Immunohistochemistry

Larva tissues were dissected in PBS and fixed for 30 min in 4% formaldehyde in PBS. Blocking and antibody incubations were performed in PBT (0.3% BSA, 0.3% Triton X-100 in PBS). Primary and secondary antibodies were incubated overnight at 4°C in PBT. The following primary antibody was used: anti-Cathepsin-L (Abcam ab58991, 1:400). Washes were performed in PBW (0.1% Tween-20 in PBS). All images were acquired using Carl Zeiss LSM710 or LSM880 confocal microscopes, using a × 63 Apochromat objective. Staining with LysoTracker was performed by incubating the non-fixed larval fat body in LysoTracker Red in PBS (1:1,000) for 10 min followed by mounting in 75% glycerol in PBS.

Real-Time qPCR

RNA extraction was performed with a Life Technologies Ambion PureLinkTM RNA Mini kit according to the manufacturer protocol. Fat bodies from 20 L3 larvae were used per extract. Subsequent steps were performed using 1 μg of total RNA. ThermoScientific DNase I was used in order to digest genomic DNA. The ThermoScientific RevertAid Kit was subsequently used to synthesize cDNA. RT-qPCR was performed using the Promega GoTaq qPCR Master Mix (ref. A6002). Primer sequences are available in Table S2.

Plasmid Constructs

Sequences of the genes of interest were amplified by PCR and inserted in desired plasmid using either Gateway recombination system or restriction enzyme cloning. PCR products were amplified from cDNA using Phusion high fidelity DNA polymerase with primers containing the Gateway recombination site or restriction enzyme sites for Gateway entry vector and cloned into pDONR221 or pENTR using Gateway recombination cloning. Point mutants were generated using the QuikChange site-directed mutagenesis (Stratagene, 200523). Plasmid constructs were verified by conventional restriction enzyme digestion and/or by DNA sequencing.

GST Pull-Down Assays

GST-fusion proteins were expressed in *Escherichia coli* BL21(DE3), SoluBL21 or Rosetta2. GST-fusion proteins were purified on glutathione-Sepharose 4 Fast Flow beads (Amersham Biosciences). GST pull-down assays were performed using either recombinant proteins produced in bacteria or *in vitro* translated ^{35}S-methionine-labeled proteins. L-[35S]-methionine was obtained from PerkinElmer Life Sciences. A volume of 10 μL of the *in vitro* translation reaction products (0.5 μg of plasmid in a 25 μL reaction volume) were incubated with 1–10 μg of GST-recombinant protein in 200 μL of NETN buffer (50 mM Tris, pH 8.0, 150 mM NaCl, 1 mM EDTA, 0.5% Nonidet P-40, 1 mM dithiothreitol supplemented with Complete Mini EDTA-free protease inhibitor cocktail (Roche Applied Science)) for 2 h at 4°C, washed six times with 1 mL of NETN buffer, boiled with 2X SDS gel loading buffer, and subjected to SDS-PAGE.

Gels were stained with Coomassie Blue and vacuum- dried. ^{35}S-Labeled proteins were detected on a Fujifilm bio-imaging analyzer BAS- 5000 (Fuji).

Chromatin Immunoprecipitation Assay

Approximately 200 whole larvae from wild-type (WT) flies were fixed with 1% Formaldehyde (Sigma-Aldrich, Cat#: F8775) at 37°C for 15 min followed by incubation on ice for 2 min. For the supernatant preparation 200 μl of lysis buffer was added (50 mM Tris-HCl, pH 7.6, 1 mM $CaCl_2$, 0.2% Triton X-100 or NP-40, 5 mM butyrate, and 1X proteinase inhibitor cocktail). The lysates were subjected to sonication to shear DNA to the length of approximately between 150 and 900 bp using an Epishear^{TM} Probe Sonicator (Active motif). The sample was then diluted by adding RIPA buffer (10 mM Tris-HCl, pH 7.6, 1 mM EDTA, 0.1% SDS, 0.1% Na-Deoxycholate, 1% Triton X-100, supplemented with protease inhibitors and PMSF). For the input samples 40 μl were saved and supplemented with 2 μl 5M NaCl and were incubated at 65°C O/N to reverse crosslink. The rest of the lysate was then incubated with control IgG (Cell Signaling Technology, Cat#: 2729S) or primary antibody against Sequoia (gift from Prof Y Jan) together with 40 μl of Protein A beads (GE Healthcare, 28967062) at 4°C O/N. The beads were washed sequentially with the following buffers: RIPA buffer, RIPA buffer supplemented with 0.3M NaCl, LiCl buffer (0.25 M LiCl, 0.5% NP40, 0.5% NaDOC), TE buffer supplemented with 0.2% Triton X-100 and TE buffer. To reverse crosslink, the beads were resuspended in 100 μl TE buffer (supplemented with 10% SDS and Proteinase K (20 mg/ml) and were incubated at 65°C O/N. The DNA was purified by phenol-chloroform extraction followed by qPCR analysis. Primers are listed in Table S2, promotor region sequences are listed in Table S1.

Structural Modeling

The model of the peptide of Sequoia binding to *Drosophila* ATG8a was derived from the structure of GABARAP-L1 ATG4B LIR Complex (PDB code 5LXI). Essentially all residues in the structure were mutated to the correct sequence. No energy minimization was carried out. The structures and electrostatic surfaces were displayed in PyMol. As an approximation the electrostatic surface associated with the acetylated protein was calculated with a methionine as a mimic of the acetylated K48.

QUANTIFICATION AND STATISTICAL ANALYSIS

Quantification of mCherry-Atg8a Puncta

Fiji/ImageJ was used to quantify the mCherry-Atg8a dots using the macro AtgCOUNTER (Jacomin and Nezis, 2016).

Quantification of Binding Interaction Assays

Signals from ^{35}S-labeled proteins were measured in terms of unit of photostimulated luminescent (PSL) and quantitated in comparison with 10% of the *in vitro*-translated lysate using the Image Gauge software (Fuji).

Statistical Analysis

Statistical analysis was performed as described in figure legends. All statistical analysis was performed with GraphPad Prism7, along with graph generation.

Autophagy

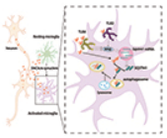

Autophagy

ISSN: (Print) (Online) Journal homepage: https://www.tandfonline.com/loi/kaup20

A nuclear role for Atg8-family proteins

Anne-Claire Jacomin , Stavroula Petridi , Marisa Di Monaco & Ioannis P. Nezis

To cite this article: Anne-Claire Jacomin , Stavroula Petridi , Marisa Di Monaco & Ioannis P. Nezis (2020) A nuclear role for Atg8-family proteins, Autophagy, 16:9, 1721-1723, DOI: 10.1080/15548627.2020.1794356

To link to this article: https://doi.org/10.1080/15548627.2020.1794356

Published online: 18 Jul 2020.

AUTOPHAGY
2020, VOL. 16, NO. 9, 1721–1723
https://doi.org/10.1080/15548627.2020.1794356

Taylor & Francis
Taylor & Francis Group

AUTOPHAGIC PUNCTUM

A nuclear role for Atg8-family proteins

Anne-Claire Jacomin*, Stavroula Petridi*, Marisa Di Monaco*, and Ioannis P. Nezis#

School of Life Sciences, University of Warwick, Coventry, UK

ABSTRACT

Despite the growing evidence that the macroautophagy/autophagy-related protein LC3 is localized in the nucleus, why and how it is targeted to the nucleus are poorly understood. In our recent study, we found that transcription factor seq (sequoia) interacts via its LIR motif with Atg8a, the *Drosophila* homolog of LC3, to negatively regulate the transcription of autophagy genes. Atg8a was found to also interact with the nuclear acetyltransferase complex subunit YL-1 and deacetylase Sirt2. Modulation of the acetylation status of Atg8a by YL-1 and Sirt2 affects the interaction between seq and Atg8a, and controls the induction of autophagy. Our work revealed a novel nuclear role for Atg8a, which is linked with the transcriptional regulation of autophagy genes.

ARTICLE HISTORY
Received 15 June 2020
Revised 18 June 2020
Accepted 26 June 2020

KEYWORDS
Acetylation; autophagy; LIR motif; nucleus; transcription; LC3/Atg8

Macroautophagy is a type of autophagy where double-membrane compartments – phagophores – are being formed to engulf part of the cytoplasm, enclosing it within an autophagosome and targeting it for lysosomal degradation. Atg8-family proteins play an essential role in the regulation of autophagy as they enable the formation of the autophagosomes, as well as mediate the degradation of cargoes. As basal-level autophagy is very low, an efficient mechanism is required to induce autophagy in organisms that are put under stress by extracellular cues, such as nutrient deprivation. Although there is a body of evidence that indicates that Atg8-family proteins are enriched in the nucleus in nutrient-replete conditions, the machinery by which they are targeted to the nucleus, and thus the nuclear components with which they interact, remain largely uncharacterized. Uncovering these components may therefore be key in advancing our understanding of how autophagy-related proteins govern cellular responses to starvation.

A hallmark of most Atg8-interacting proteins is the presence of an LC3-interacting region (LIR) motif, which is required for their interaction with the Atg8-family proteins. The requirement for LIR motifs to convey the ability of autophagy-related proteins to interact with Atg8-family members is conserved across eukaryotes. The *Drosophila* Atg8a protein interacts with autophagy machinery components and selective autophagy receptors, through a LIR motif. We used an *in silico* approach for the identification of putative nuclear Atg8-family protein interactors based on a predicted LIR motif. This resulted in the identification of putative LIR motif-containing proteins susceptible to interact with Atg8a and to be involved in acetylation modulation: the transcription regulator seq (sequoia) and a subunit of the NuA4-Tip60 acetyltransferase complex, YL-1 [1].

The direct interaction between these proteins and Atg8a was validated, with a LIR motif-dependent interaction between seq and Atg8a confirmed. Moreover, we showed that the lack of *seq* in *Drosophila* larvae fat body cells – a larval tissue well-known for its ability to activate autophagy upon starvation – leads to the induction of autophagy through the generation of autophagosomes and their fusion with lysosomes [1]. This exceptional effect is observed notably in nutrient-rich conditions when autophagy activity is low and only maintained to the basal level. Our data support previous findings about Rph1 and KDM4A, yeast and mammalian homologs of seq, and the negative transcriptional regulation of autophagy.

Most LIR motif-containing proteins interact with Atg8-family proteins in the cytoplasm and relate to the formation of autophagosomes or to the recruitment of cargoes for degradation. However, seq is maintained in the nucleus upon starvation, suggesting that the interaction between seq and Atg8a orchestrates the regulation of autophagy induction exclusively from this organelle.

seq is a transcription factor, and its involvement in the repression of autophagy was uncovered when it was observed to bind to the promoter regions of autophagy genes in fed conditions, thereby reducing their transcription. This is exemplified by an observed induction in the expression of autophagy genes in *seq*-depleted larvae. Further to this, the LIR motif-deficient form of seq, which exhibits a reduced ability to bind to Atg8a, is less enriched at the promotor region of autophagy genes, which correlates to their upregulation when compared to wild-type seq. Interestingly, we observed that the absence of Atg8a has a significant negative impact on the expression of the same set of autophagy genes during starvation; however, a lack of Atg9 (a non-nuclear protein, which is part of a different

CONTACT Ioannis P. Nezis I.Nezis@warwick.ac.uk School of Life Sciences, University of Warwick, CV4 7AL Coventry, UK
*These authors contributed equally.
#Lead contact.

complex required for the initiation of autophagosome formation) demonstrates no impact on their expression. This highlights the transcriptional importance of the nuclear interaction between Atg8a and seq in the expression of autophagy genes in starvation conditions. This is further emphasized in the observed association of Atg8a with the promoter region of autophagy genes, which is assumed to be by virtue of its interaction with seq [1].

The interaction between seq and Atg8a may contribute to the sequestration of Atg8a in the nucleus. Hence, in the absence of an interaction between Atg8a and seq (as showcased in the LIR mutant), the "releasing" of Atg8a by seq and its subsequent translocation into the cytoplasm, may also play a key role in lifting seq off the promotor region of autophagy genes; thereby elevating the repressive cap enforced upon these regions and initiating the induction of autophagy (Figure 1).

In mammalian cells, nuclear LC3 protein is acetylated in nutrient-rich conditions, and its deacetylation is associated with its ability to translocate from the nucleus to the cytoplasm. We showed that *Drosophila* Atg8a is also acetylated and that starvation induces its deacetylation. We found that the YL-1 and the deacetylase Sirt2 are involved in the modulation of the acetylated status of Atg8a [1]. YL-1 protein is a subunit of a nuclear acetyltransferase complex known as SWR1 in yeast and the related SRCAP and NuA4-KAT5 /Tip60 complexes in mammals, that control histone acetylation. We showed that the interaction between Atg8a and YL-1 is direct and does not depend on a functional LIR motif. Depletion of YL-1 by using an RNAi line, results in a reduced level of acetylated Atg8a in both fed and starved conditions. We showed that the acetylation status of Atg8a governed by YL-1 contributes to the modulation of the interaction between seq and Atg8a in the nucleus. Therefore, our data suggest that YL-1 is a negative regulator of autophagy, acting to maintain the acetylated status of Atg8a and its nuclear localization [1].

Acetylation of Atg8a by YL-1 is counter-balanced by the deacetylase Sirt2, which is the *Drosophila* homolog of the mammalian SIRT1 (sirtuin 1). The lack of autophagy induction in *Drosophila* larvae fat body cells upon starvation that we observed in Sirt2 mutants, confirms previous reports that this deacetylase is a positive regulator of autophagy. We showed that Sirt2 mutants exhibit reduced Atg8a lipidation during starvation, whereas overexpression of Sirt2 results in increased lipidation of Atg8a, both in fed and starved

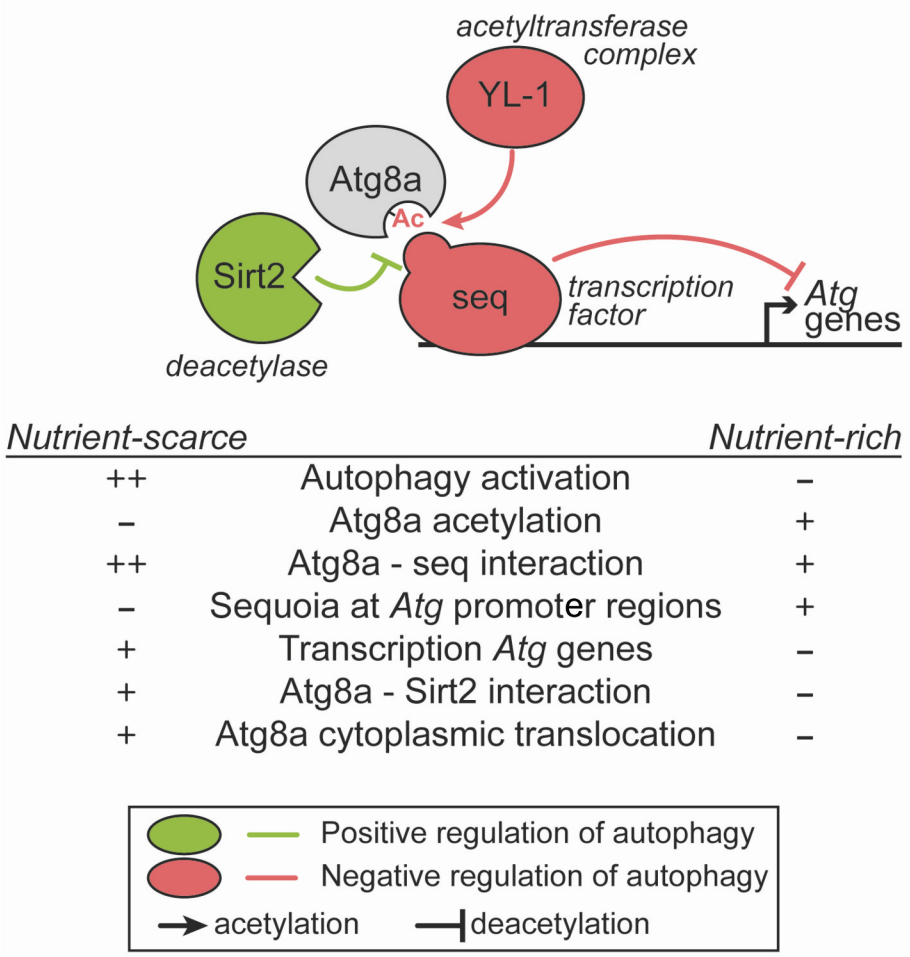

Figure 1. Role of Atg8a and seq in the negative regulation of autophagy. In nutrient-rich conditions, the transcription factor seq interacts with Atg8a in a LIR motif-dependent manner, and localizes at the promoter regions of autophagy-related (*Atg*) genes to repress their expression. In such conditions, Atg8a acetylation is maintained by its interaction with an acetyltransferase complex via YL-1. When nutrients are scarce, Atg8a is deacetylated by Sirt2, resulting in a stronger binding to seq, which can be lifted from the autophagy gene promoters, leading to their transcriptional activation.

conditions. Furthermore, we showed that Sirt2 overexpression leads to decreased acetylation of Atg8a both in fed and starved conditions and that Sirt2 preferentially interacts with Atg8a when larvae are starved. This observation suggests that the binding of Sirt2 to Atg8a may contribute to Atg8a deacetylation and export to the cytoplasm. Furthermore, we suggest that in the event of deacetylation of Atg8a, due to its conformational change, its interaction with seq strengthens. This thus implies that deacetylation by Sirt2 may have a crucial role in the ability of Atg8a to lift seq off the promotor region of autophagy-related genes in nutrient-scarce conditions [1].

Taken all together, we uncovered a novel nuclear role for *Drosophila* Atg8a which is governed by its ability to bind a LIR motif-containing transcription factor, and its acetylation status, and determines its nuclear localization and the regulation of expression of autophagy-related genes (Figure 1). This brings into the spotlight the unanticipated role of a non-degradative LIR motif-dependent interaction in the nucleus, which functions to control cellular self-eating in the cytoplasm.

Disclosure statement

No potential conflict of interest was reported by the authors.

Funding

This work was supported by BBSRC grant BB/P007856/1 and Leverhulme Trust project grant [RPG-2017-023] to I.P.N. M.D.M. has a PhD studentship funded by the Midlands Integrative Biosciences Training Partnership.

Reference

[1] Jacomin AC, Petridi S, Di Monaco M, et al. Regulation of expression of autophagy genes by Atg8a-interacting partners sequoia, YL-1, and Sir2 in *Drosophila*. Cell Rep. 2020;31(8):107695.